ОБЩЕСТВО НА ТРИБОЛОЗИТЕ В БЪЛГАРИЯ

SOCIETY OF BULGARIAN TRIBOLOGISTS

ТЕХНИЧЕСКИ УНИВЕРСИТЕТ – СОФИЯ

TECHNICAL UNIVERSITY OF SOFIA

ТРИБОЛОГИЧЕН ЖУРНАЛ БУЛТРИБ

Доклади от

10-та Международна конференция БУЛТРИБ '13

и

проект CEEPUS III-BG-0703-02-1314

”Съвременни тенденции в образованието и изследванията на механични системи - създаване на мост между надеждност, качество и трибология”

TRIBOLOGICAL JOURNAL BULTRIB

Papers from

the 10th International Conference BULTRIB '13

and

The Project CEEPUS III-BG-0703-02-1314

”Modern Trends in Education and Research on Mechanical Systems - Bridging Reliability, Quality and Tribology”

24-26 октомври 2013, София **Година IV, 2014**

October 24-26, 2013, Sofia ***Volume IV, 2014***

Трибологичният журнал БУЛТРИБ се издава със средствата на проект, финансиран от субсидията за „Дни на науката на ТУ - София – 2013”.

Tribological journal BULTRIB is published by the resources of a project funded by the grant for "Days of Science of TU - Sofia - 2013."

Трибологичен журнал БУЛТРИБ

Доклади от 10-та Международна конференция по Трибология BULTRIB'13, 24-26 октомври, 2013, София,

Tribological Journal BULTRIB

Papers from the 10th International Conference BULTRIB '13
October 24-26, 2013, Sofia

Издателство ТУ-София
София 2014

Publ. House TU - Sofia
Sofia 2014

ISSN: 1313-9878

Том IV, 2014

ТРИБОЛОГИЧЕН ЖУРНАЛ БУЛТРИБ

Списание на Общество на триболозите в България

www.bultrib.com

Vol. 4, 2014

TRIBOLOGICAL JOURNAL BULTRIB

Journal of the Society of Bulgarian Tribologists

Editor in Chief:

Mara Kandeva, Technical University - Sofia

Associate Editors:

Emilia Assenova, Society of Bulgarian Tribologists, Sofia

Juliana Javorova, University of Chemical Technology and Metallurgy - Sofia

Editorial Board:

Vyara Pozhidaeva, *University of Mining and Geology „St Ivan Rilsky"- Sofia*
Georgi Mishev, *Technical University – Sofia, Branch Plovdiv*
Ivan Kralov, *Technical University – Sofia*
Anna Andonova, *Technical University – Sofia*
Nikolay Nikolov, *Technical University – Sofia*
Kiril Stanulov, *University of Chemical Technology and Metallurgy - Sofia*
Georgi Cholakov, *University of Chemical Technology and Metallurgy - Sofia*
Ivan Mitov, *Institute of Catalysis, Bulgarian Academy of Sciences*
Manahil Tongov, *Technical University – Sofia*
Nikolay Tonchev, *Higher Technical Education School „T. Kableshkov" - Sofia*
Dimitar Karastoyanov, *Institute of Information and Communication Technologies – Bulgarian Academy of Sciences*

Cover design:

Petar Hristov, *Interdisciplinary Civic Academy, Sofia*
Agop Erdeklyan, *Interdisciplinary Civic Academy, Sofia*

Tribological Journal BULTRIB, **Vol. IV, 2014**
Papers from the International Conference **BULTRIB '13**
October 24-26, 2013, Sofia
Society of Bulgarian Tribologists
Technical University of Sofia

CONTENTS

Kandeva Mara, *President of Society of Bulgarian Tribologists*
Opening Speech 7

***Jost H. P.**, President of International Tribology Council, UK*
Greeting address to BULTRIB'13 and CEEPUS workshop 9

Manolov N., The global crisis in a tribological cross-section
Plenary paper 12

Kandeva M., Vencl A., Assenova E., Influence of "Valena" metal-plating additive on the friction properties of ball bearings 18

Vencl A., Vučetić F., Bobić I.,The influence of strontium addition on the tribological properties of Zn25Al1Si alloy in boundary lubricated condition 25

Kandeva M., Proposal for the opening of MSc specialty „Triboengineering" 31

Ripeanu R. G., Studies above erosion behavior of rotor turbine materials 34

Ripeanu R. G., Ispas V., Ispas D., Studies regarding improving sealing at three cone bits bearings 40

Radovanovic M., Investigation on surface roughness of carbon steel machined by abrasive water jet using Taguchi method 47

Kostova N. G., Eliyas A., Fabian M., Dutkova E., Balaz P., Photocatalytic degradation of methyl orange using mechanochemucally prepared Fe_2O_3-ZnO mixed oxides doped with silver 55

Sinanoğlu C., Yilmaz E., Topal E.S., Canbulut F., Experımental research of the effects of slipper bearing geometry and working conditions on the system rigidity in axial piston pumps 60

Mishev G., Rupetsov V., Simov M., Possibilities for improvement the resource of extrusion instruments 69

Zhivkovich K. D., ***Požidajeva V.,*** Charles Coulomb and his contribution to tribology 75

Fedorov S. V., Generalized energy model for sliding friction coefficient and evolution of tribosystems 82

Zaharieva K., Cherkezova-Zheleva Z., Kunev B., Dimova S., Tsvetkov M., Mitov I., Milanova M., Phase changes in nanodimensional cobalt ferrite-type material activated by mechanochemical treatment 89

Yordanova I., Paneva D., Cherkezova-Zheleva Z., Kunev B., Mitov I., Mechanochemical synthesis and properties of $LaMnO_3$ 95

Capitanu L.*, *Florescu V., Bursuc D. C., A solution for improving seizure resistance in metal on metal total hip prostheses with self directed balls 99

Rus D., Florescu V., Capitanu L., Modelling possibilities of very high temperatures and pressures at friction contact plastics filled with glass fibres on steel 113

***Rus D., Florescu V., Capitanu L., Badita L.-L.*.,** Qualitative correlation between friction coefficient and metal surface wear in the case of linear friction dry contact with reinforced polymers with glass fibre 124

Abdullah O. I., Schlattmann J., Akhtar M. J., Effect of the thickness of the frictional lining on the thermoelastic behaviour in the dry clutches 137

Mishev G., Dishliev S., Rupetsov V., Increase the wear resistance of injection molds using PVD coatings 147

Kozhoukharova E., The behavior of rolling garnet porphyroblasts in tribozones 155

Penyashki T., Study of the influence of temperature on the structure of the deposited electrospark coatings 159

Teletin C., Spânu C., Bîrsan I. G., Ciortan S., 3D surface layer characterization for hydrogenated X65 steel samples 169

Yankova I., Quality of electron beam welded Charpy specimens 175

Simeonova T., Characterization of ceramic layers produced by plasma transferred arc process 181

***Kandeva M., Blaskov V., Stambolova I., Kostova N. G., Vassilev S., Balashev K., Shipochka M*.** Tribological properties of Ni doped TiO_2 coatings 187

Yordanova I., Cherkezova-Zheleva Z., Paneva D., Kunev B., Mitov I., Mechanochemical preparation of perovskite type materials 193

Radulescu A., Radulescu I. Advanced technologies used in education and training for lubrication processes 197

Miteva A. Functionally graded materials in tribology 203

Ташева Е., В. Гайдаров, П. Ташев, Г. Замфирова, С. Вълканов. Изследване на структурата и микротвърдостта на заварени образци от стомана WELDOX 700 218

Tashev P., R. Lazarova. Study of layer built-up with adding TiN nanoparticles 227

Tribological Journal BULTRIB, **Vol. IV, 2014**
Papers from the International Conference **BULTRIB '13**
October 24-26, 2013, Sofia
Society of Bulgarian Tribologists
Technical University of Sofia

ВСТЪПИТЕЛНО СЛОВО

Мара КАНДЕВА

Председател на Обществото на триболозите в България

Скъпи колеги и гости на 10-тата международна конференция БУЛТРИБ 2013,

От името на Обществото на триболозите в България Ви приветствам с Добре дошли в София на територията на Техническия университет-София!

БУЛТРИБ 2013 се провежда във време на много интензивно развитие на трибологията в света и на Балканите. Преди малко повече от месец се проведе мащабно събитие на световната трибология – Петият световен конгрес по трибология в Торино под председателството на Международния съвет по трибология и домакинството на Обществото на триболозите в Италия. Българската делегация от 6 души представи постиженията си в 5 доклада.

През 2014 г. през месец октомври ще се проведе 8 –мата международна конференция БАЛКАНТРИБ 2014 на Балканската трибологична асоциация. Събитието ще се състои в Синая, Румъния, където Румънската трибологична асоциация ще поеме мандата на ръководство на Балканската трибологична асоциация от Гърция.

Уважаеми триболози, на настоящата конференция БУЛТРИБ 2013 в качеството си на председател на ОТБ си позволявам да поставя на Вашето внимание един много съществен въпрос, свързан с развитието на трибологичните знания в университетското образование в България. А именно обсъждане на възможностите за разкриване на магистърска специалност за обучаване на магистри-триболози с наименование „ТРИБОИНЖЕНЕРИНГ” в Машинно - Технологичен факултет при ТУ-София.

В обем от 1 страница предлагам кратко описание на предпоставките и възможностите за осъществяване това предложение в нашата страна. Предложението беше обсъдено и намери подкрепа от Управителния съвет на ОТБ.

Моля да изразите Вашите мнения, препоръки и подкрепа по времето, отделено в програмата на това предложение.

Пожелавам приятна и ползотворна работа на конференцията!

Доц. д-р Мара Кандева

Tribological Journal BULTRIB, **Vol. IV, 2014**
Papers from the International Conference **BULTRIB '13**
October 24-26, 2013, Sofia
Society of Bulgarian Tribologists
Technical University of Sofia

OPENING SPEECH

*by **Mara Kandeva***

President of the Society of Bulgarian Tribologists

Dear colleagues and guests of the 10th International Conference BULTRIB'13,

In the name of the Society of Bulgarian tribologists, I would like to welcome you in Sofia and in the area of the Technical University of Sofia.

The Conference BULTRIB 2013 hits the time of highly intensive development of tribology worldwide and in our region. A month ago the most important tribological forum – the 5th World Tribology Congress – took place in Torino. It was organized by the International Tribology Council and the Italian Ttribology Association. Bulgaria had 6 delegates presenting 5 papers.

In October 2014 in Sinaia, Romania, the 8th International Conference BALKANTRIB'14 will be chaired by the Balkan Tribological Association and hosted by the Romanian Tribology Association (RTA). Then the RTA will obtain the mandate of the Balkan Tribological Association from Greece.

Dear colleagues tribologists, being president of the Society of Bulgarian Tribologists, I would like to call your attention to a highly important question related to the development of the tribological knowledge in the university education in Bulgaria, particularly, thinking about the possibilities for opening a MSc discipline for tribologists named „TRIBOENGINEERING" at the Faculty of Industrial Technology of the Technical University - Sofia.

I propose a short description of the conditions for accomplishment of this proposal in our country. The proposal was discussed and approved by the Managing Committee of the Society of Bulgarian Tribologists.

I would like to ask you to express your opinion, recommendations and possible approval during the presentation of the proposal in BULTRIB Program.

I wish you pleasant and fruitful work during the Conference!

Mara Kandeva, Assoc. Prof. Dr.

International Tribology Council
President: Professor H. Peter Jost CBE DSc DTech DEng

Administered by:
University of Central Lancashire
Jost Institute for Tribotechnology
Preston, Lancashire PR1 2HE
Tel: +44 (0) 1772 893312
Fax: +44 (0) 1772 892915
Email: isherrington@uclan.ac.uk

President's Office:
Angel Lodge Chambers
57 London Road, Enfield,
Middlesex EN2 6DU
Tel: +44 (0) 203 213 1030
Fax: +44 (0) 203 213 1040
Email: itcpresident@btconnect.com

Please visit website: ***www.itctribology.org***

October 2013

MESSAGE TO BULTRIB '13 and CEEPUS WORKSHOP

24 – 26 October 2013

by

PROFESSOR H PETER JOST CBE DSc DTech DEng

Greetings to the Chairman, Members of the Organising Committee and all participants of the BULTRIB Conference.

We all know that Technology and Engineering are moving at a rate faster than ever and so is Tribology. Since last you met at this Conference, there have been many developments. Some of these were demonstrated by over 800 scientific and technological papers presented at last month's Fifth World Tribology Congress in Turino at which were present participants of 74 nations.

Judging by the scientific and engineering papers to be presented at this conference, many of the developments described, of value to the economy and the environment, have already been recognised.

Indeed if the papers and discussions of BULTRIB '13 will contribute to moving towards the goal of saving materials and energy and of enhancing the environment and the quality of life, the Conference will have served a valuable purpose, not only for tribology but, in its field, for the maintenance of life as we know it. Tribology is a worthy cause to pursue and to play its rightful part for the benefit of science, technology and ultimately, mankind.

With this I wish you an informative and enjoyable BULTRIB '13 enabling you to return to your place of occupation strengthened in mind and having made new friends and acquaintances.

H Peter Jost
President

PLENARY AND SECTIONAL PAPERS

Tribological Journal BULTRIB, **Vol. IV, 2014**
Papers from the International Conference **BULTRIB '13**
October 24-26, 2013, Sofia
Society of Bulgarian Tribologists
Technical University of Sofia

Пленарен доклад

ГЛОБАЛНАТА КРИЗА В ТРИБОЛОГИЧЕН СРЕЗ

Нягол Манолов

С тази обща по характера си тема си поставям три задачи:

Първо: да обявя и обясня пенсионирането си във функционалното пространство на ОТБ.

Второ: да облека духът на трибологията в парадигмален модел.

Трето: да направя трибологична интерпретация на бушуващата в света глобална криза.

По първата задача:

Административно се пенсионирах в ТУ-София през 2000-та година. Функционално се пенсионирах в ТУ-София през 2012 г. на 80 годишна възраст.

През 2013 г. на конференцията „БУЛТРИБ13" избирам да се пенсионирам административно и функционално в пространството на ОТБ. Общият ми трудов стаж като учител, университетски преподавател и триболог дотук възлиза на 61 години. От тях като изследовател, ръководител и организатор съм посветил 45 години.

Кои са трайните следи, които предавам в наследство на ОТБ, оставени през тези 45 години:

- разкриване на номенклатурна специалност по трибология;
- научно-приложна лаборатория по трибология – ТУ-София;
- гражданско сдружение Общество на триболозите в България;
- Балканска трибологична асоциация (БТА);
- Интердисциплинна гражданска академия (ИНГА);
- Национална концепция по трибология;
- личен малък и голям докторат по трибология;
- ученици и последователи: професори, доценти, доктори и инженери;
- списания по трибология: Списание на Балканската трибологична асоциация, на ИНГА и на ОТБ;
- 300 научни публикации, 20 научно-образователни монографии и учебници, 40 изобретения;

Основните ми сътрудници и последователи по трибология, взели активно участие в осъществяването на тези следи са: доц. д-р Мара Кандева, доц. д-р Емилия Асенова, проф. д-р Васко Тенчев, доц. д-р Александър Янков, доц. д-р Маруся Антова, доц. д-р Станчо Кавалджиев, д-р Любомир Йорданов, проф. дтн София Карапетрова, доц. д-р Димитър Пиперков, доц. д-р Христо Илиев, проф. дхн Слави Иванов, проф. дтн Митко Миховски, проф. д-р Васил Александров, доц. д-р Вяра Пожидаева, проф. дсн Ивайло Кусев, доц. д-р Пенко Гюров, проф. д-р Юлика Симеонова, проф. д-р Симеон Панев и др.

В резюме с тази моя научно-преподавателска и организационна дейност са поставени основите на българската школа по трибология.

Позволете ми накрая по тази задача да Ви кажа сбогом и с Ваше позволение да премина в заключителния етап на своя живот като Ви заявявам, че вратите на моя дом, на моето семейство и на моето сърце остават широко отворени за Вас.

По втора задача:

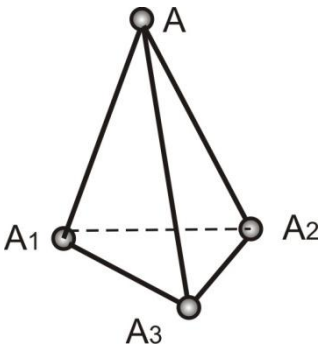
Основната парадигма на човешките чувства, мисли и поведение в нашата действителност се основава на двуполюсен онтологичен модел. Израз на този модел са формулите: нищо-нещо; истина-лъжа; макро-микро; добро-зло; материално-духовно и т.н. Двуполюсното начало предполага две опорни точки като дуалистичен модел, поради което то е неустойчиво. Тази е причината най-често то да се редуцира до еднополюсно начало чрез абсолютизиране на едното от тях. Например, диадата „материално-духовно" се редуцира само

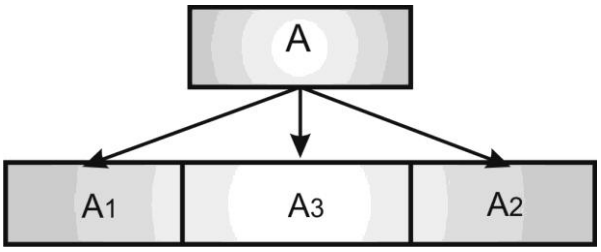
до материално или само до духовно както е при Маркс и Хегел, във връзка с което възникна презумцията за основния въпрос на философията за първичност на материята или на духа.

Трибологията като модел на своите елементарни контактни съединения включва между алтернативите на двуполюсния модел трето начало под формата на функционално тяло, наречено „контакт”. По такъв начин диадите се превръщат в триади. Например, диадата „тяло-противотяло” се трансформира в триада „тяло-контакт-противотяло”; диадата „плъзгач-направляваща” се трансформира в триада „плъзгач-контакт-направляваща”. Последната се обозначава като едно цяло с името „плъзгащ лагер”.

С въвеждане на контакта като трето начало всяко нещо като контактна система се идентифицира с три начала: форма, структура и съдържание. Контактите превръщат всяко цяло от двуединно в триединно. Дуализмът за всяко цяло от света по Аристотел и Декарт като онтологичен модел се превръща в триализъм. С други думи всичко, което битува в света като цяло, съдържа минимум три елемента – две алтернативи и трети функционален елемент между тях, наречен „контакт”.

Така се достига до идеята за представянето на всяко цяло *(A)* под формата на функционален атом (ФА), състоящ се от две алтернативи *(A_1)* и *(A_2)* с контакт *(A_3)* между тях чрез моделите на фиг. 1 и фиг. 2.



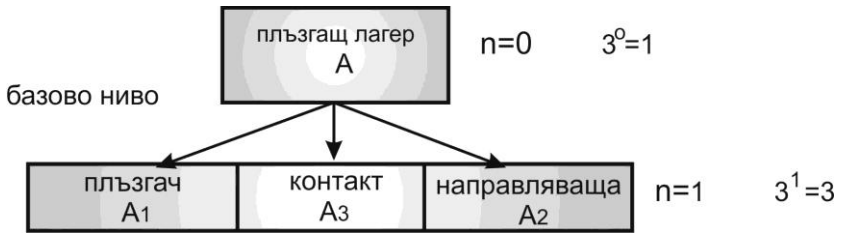


Фиг. 1: *Пространствен модел на ФА* **фиг. 2:** *Равнинен модел на ФА*

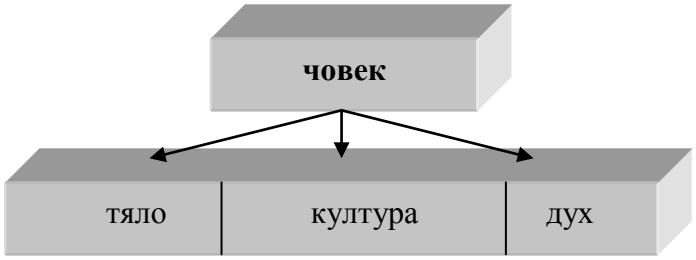
Всяко цяло независимо от неговото естество и сложност може да се представи като система от функционални атоми, разположени на различни равнища и срезове, така че теорията на контактните системи да се сведе до теорията на функционални атоми. Ето няколко примера за функционалните атоми на различни понятия: плъзгащ лагер, човек, семейство, светът (фиг.3).

Триализъм – това е философията на триединния святм триалектика – това е диалектиката на триединния свят и триология – това е науката за триединството на света.

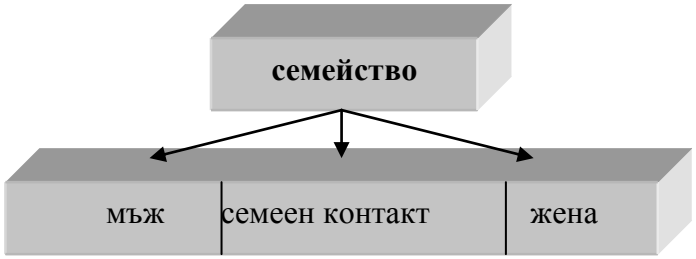
В пространството на триологията се намират всички науки, в това число и трибологията като наука за контактите и контактните взаимодействия на техническите системи.



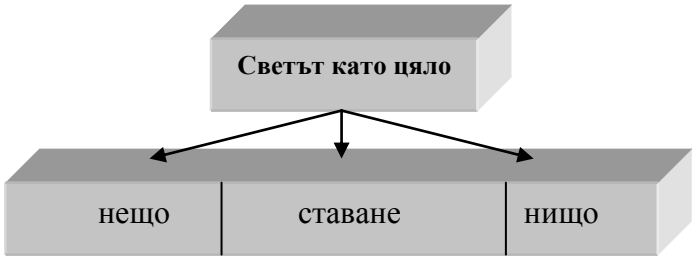
ФА на плъзгащ лагер



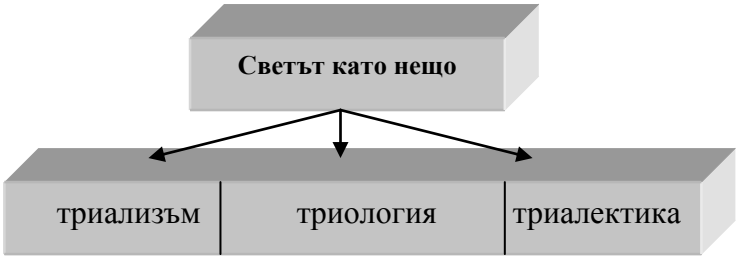
Функционален атом на човека



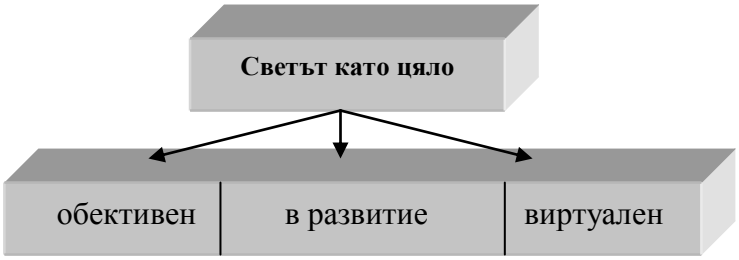
Функционален атом на семейството



Функционален атом на света в пространствен срез



Функционален атом на света в научно-методологичен срез



Функционален атом на света във времеви срез

Фиг. 3

По трета задача:

Контактните системи са системи от функционални атоми, обединени в единство чрез система от контактни мрежи. Последните са тези, които чрез силови, енергетични и материални потоци поддържат устойчиво битието на всяко цяло в света.

По метафоричната представа на Гьоте „Между две крайности не се намира истината, а проблемите”, по представата на Нютон „Бог не се намира в нещата, а между тях”. Айнщайн констатира „Не зарядите и частиците в твърдите тела, а полето между тях е съществено за протичане на физическите процеси” и по-нататък „Не можеш да решаваш проблеми със същото мислене, с което си ги създавал”, а според Никсън „Ако от две злини не можеш да направиш едно добро, опитай с три”.

От фиг. 3 се вижда, че текущия свят, в който живеем, се явява контакт между обективния и виртуален свят. Проблемите, които трябва да се решават, се намират в текущия свят в съответствие с формулата на Гьоте. Глобалната криза по модела на ФА е контактната криза на света, съдържаща се в текущия свят, който е замърсен с нерешени проблеми. Тази е причината светът да е несигурен и неустойчив. Източникът на тази неустойчивост се явява дефицитът на човешкото съзнание спрямо реалното съдържание и структури на контактните системи.

В триологията и в частност в трибологията като наука за контактите в техническите системи се съдържа формулата за изход от кризисната ситуация.

Заключение

Българската школа по трибология се идентифицира с усилията, изследванията и резултатите, получени в областта на контактните взаимодействия като централни и водещи във формирането на теорията на контактните системи.

Литература

1. Манолов, Н. Акустический метод исследования контакта твердых тел. Автореферат диссертации – ктн., Москва, 1970.
2. Манолов, Н. Пневмохидравличният метод в трибологията. Автореферат на дисертация – дтн. С., 1984.
3. Манолов, Н. Ситуацията. ОТБ, кн. I, С., 1995.
4. Манолов, Н. Третото начало, кн. II, изд. Темто, С., 2000.
5. Манолов, Н. Контактен подход, кн. III, изд. Темто, С., 2007.
6. Манолов, Н. Трибология и интердисциплинност, изд. Темто, 2003.
7. Манолов, Н., Е. Асенова, М. Кандева. Концепция за развитието на трибологията в Р. България, Св. Ив. Рилски, С., 2005.
8. Манолов, Н., М. Кандева. Обща трибология. Св. Ив. Рилски, С., 2004.
9. Манолов, Н., М. Кандева. Механика в интердисциплинен стил. С., 2004.
10. Кандева, М. Контактният подход в инженерната трибология. ТУ-София, 2012.

Plenary paper (summarized)

THE GLOBAL CRISIS IN A TRIBOLOGICAL CROSS-SECTION

N. Manolov

Prof. Manolov follows three lines in his exposé:
First: The traces he has personally left in the development and history of Bulgarian Tribology;
Second: The tribological paradigm model he has proposed;
Third: Interpretation of the global crisis.

The first task: Development and history of Bulgarian Tribology

Prof. Manolov has 61 years of work as teacher and lecturer; 45 of them as researcher, leader and organizer of Tribology, including:

- Opening the nomenclature specialty of Tribology;
- Interdisciplinary Civil Academy Development of the Laboratory of Tribology at the Technical University - Sofia;
- Founding the civil Society of Bulgarian Tribology;
- Founding the Balkan Tribological;
- Founding the Interdisciplinary Civil Academy;
- Development of the National Conception of tribology;
- Defense of PhD and DSc theses in tribology;
- Followers and learners: professors, associate professors, doctors and engineers;
- Tribological Journals: Journals of the Balkan Tribological Association, of the Interdisciplinary Civil Academy and the Society of Bulgarian Tribologists;
- 300 scientific publications, 20 monographs and textbooks in tribology, 40 patents.

Summarized: his scientific, teaching and organizational work has put the foundations of Bulgarian Tribology

The second task: The tribological paradigm model

Tribology as a model of the contact pair includes between the alternatives of the two-pole model (the dyad of the dualism) the third body – a functional body called “contact”. The contacts transform every entity from dyad to triad. So, the idea emerges, that every entity can be presented as a Functional Atom FA consisting of minimum two alternatives and one contact.

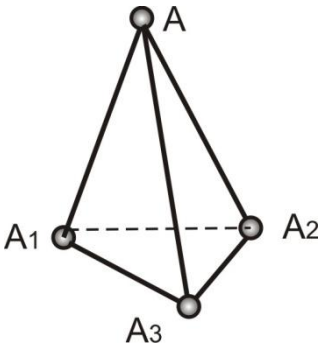


Fig. 1: *Spatial model of FA*

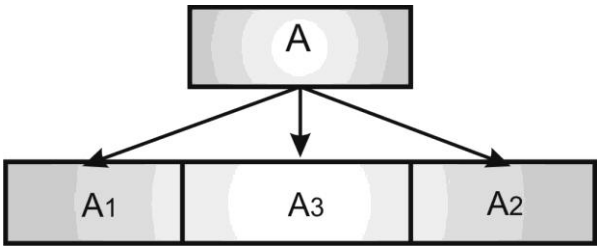


Fig. 2: *Plane model of FA*

The third task: Interpretation of the global crisis

Contact systems are systems of functional atoms gathered in unity through contact networks.

The global crisis according to the model of the functional atom is a contact crisis of our world, which is polluted by the non-solved problems. This is the reason why our world is non-safe and non-sustainable. The source of the lack of sustainability is the deficiency of human knowledge about the real contents and structure of the contact systems.

Prof. Manolov believes that through Tribology as science of the contact systems solution and way out of the crisis could be found.

Tribological Journal BULTRIB, **Vol. IV, 2014**
Papers from the International Conference **BULTRIB '13**
October 24-26, 2013, Sofia
Society of Bulgarian Tribologists
Technical University of Sofia

INFLUENCE OF "VALENA" METAL-PLATING ADDITIVE ON THE FRICTION PROPERTIES OF BALL BEARINGS

Mara KANDEVA, Aleksandar VENCL, Emilia ASSENOVA

Abstract: *The repair-regeneration oil additives are new generation additives with important place in the application of lubricants. Added to oils or greases they assure partial regeneration of worn surfaces and, at the same time, decrease the moment of friction and the coefficient of friction in the contact pairs of machines. Most common are the organic oil-soluble additives. The paper exposes results of the study of the oil-soluble metal-plating composite additive "Valena". The influence of this additive on the friction parameters of ball bearing lubricated by motor oil M-63/14 (SAE 15W-40, API SF/CC) and transmission oil TM-5-18 (SAE 80W-90, API GL-5) has been investigated.*

Key Words: *Friction properties, additives, ball bearings*

1. INTRODUCTION

The continuous improvement and advance technology of machines necessitate higher quality of lubricants and lubrication technologies, which influences equipment life and environment [1,2]. Being a working medium in the contact systems, lubricants reduce friction and wear replacing the external dry friction between surfaces by internal friction between lubricant molecules.

The repair-regeneration oil additives are new generation additives and have an important place in the application of lubricants. Added to oils or greases they assure partial regeneration of worn surfaces under special dynamic friction conditions. At the same time they decrease the moment of friction and the coefficient of friction in the contact pairs of machines. Different names were given to these additives, depending on their composition and condition. Most common are the organic oil-soluble additives. The hard non-soluble non-organic materials are habitually called *antifriction additives*, and the composites based on polymers – *modifiers*.

The metal-plating composite additives are also named *remetallizers*. Their development is based on:

- the theory of system self-organization as per I. Prigogine, W. Ebeling, D.N. Garkunov, G. Polzer, etc. [3,4];
- the scientific discovery and the application of the selective transfer of materials between contacting surfaces and the no-wear effect originating with the work of D.N. Garkunov, I.V. Kragelskii, G. Polzer, V. Babel, etc. [5,6]

This paper exposes results of the study of one of the newest additives, the oil-soluble metal-plating composite additive called "Valena", manufactured by the company "Rudservice" from Kazakhstan. The influence of this additive on the friction parameters of ball bearing lubricated by motor oil M-63/14 (SAE 15W-40, API SF/CC) and transmission oil TM-5-18 (SAE 80W-90, API GL-5) has been investigated.

2. MATERIALS

2.1. Metal-plating composite additive "Valena"

"Valena" additive is a metal containing oil-soluble composite lubricant additive registered as patent in 2005 in Russia by V. Babel, D. Garkunov, S. Mamikin and P. Kornik [5]. It is designed for improvement of the tribological properties of lubricants, namely the decrease of friction, normal wear and seizure. The additive is a dense dark-green liquid with good solubility in oils and greases, in which it forms a solution, with the metal in the form of ions. The solubility of this additive is due to its particular composition; it contains metal salts of non-organic and organic acids. The non-organic acid

salts are salts of Cu, Co, Pb, Sn, Ni (chlorides, bromides, and iodides). The organic acid salts belong to metals of variable valence with carbon atoms C_{15}….C_{18}.

Improvement of the tribological properties by use of “Valena” additive is achieved through the selective transfer of material between the frictional surfaces and the effect of no-wear during friction process. The essence is in the forming of 1 to 4 μm thick protective layer on the real contact area of the friction surfaces called by D.N. Garkunov “servotite” metal-plating layer. This layer compensates the wear and screens the infiltration of hydrogen in the surfaces, reducing thus the hydrogen wear. The recommendations of the manufacturer for the percent contents of “Valena” additive in the lubricant depend on the state of the tribological pair, as given in Table 1.

Table 1: *Recommended percent contents of “Valena” additive*

Condition of the tribological pair	% of Valena additive	
	Grease	Oil
new	1 %	1 %
in-service	5 %	3 %
worn-out	9 %	9 %

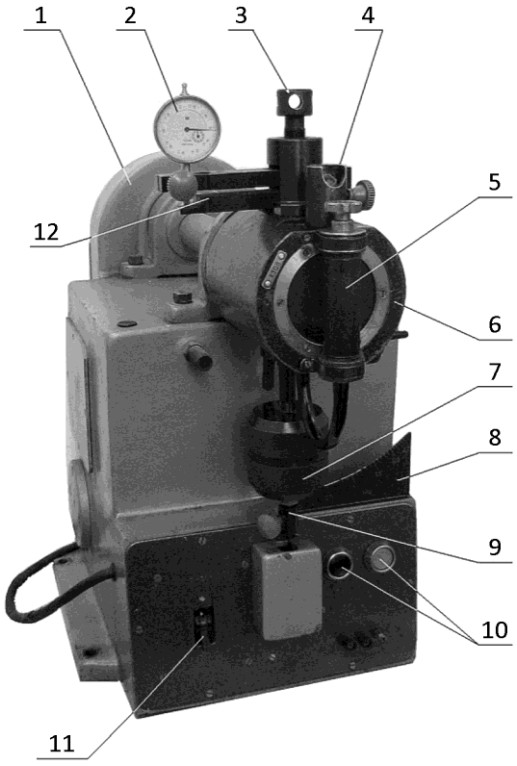
2.2. Motor oil M-63/14 and transmission oil TM-5-18

The motor oil M-63/14 is a multigrade mineral oil designated as SAE 15W-40, API SF/CC. It is designed mainly for petrol engines, but it can be used in Diesel engines as well.

The transmission oil TM-5-18 is a universal multigrade mineral oil designated as SAE 80W-90, API GL-5. It is designed for mechanical gear boxes and, transmission gears of petrol and Diesel engines.

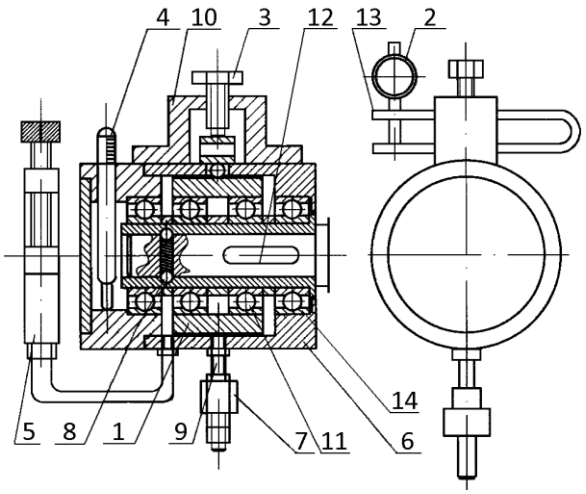
3. EXPERIMENTAL PROCEDURE

The tribological parameters: moment of friction and coefficient of friction have been studied under lubricated conditions, with motor and transmission oil at various normal loads. Device “DM 28M” used for measurement of moment of friction in ball bearings is shown in Figs. 1 and 2. The device consists of casted housing with mounted driving shaft. A bearing (measuring) box is connected to the end of the shaft, where the four ball bearings (two in the middle and two at the end), which are tested, are located. Single-row steel ball bearings (Designation 308, GOST 8338-57) were used, with bore diameter of 40 mm, outside diameter of 90 mm and width of 23 mm.



1 – belt-drive in housing
2 – indicator
3 – loading screw for the bearing
4 – location for the thermometer
5 – injector for regulation of oil level
6 – bearing box
7 – load of the pendulum
8 – dial for moment of friction reading
9 – pendulum
10 – on and off buttons of the motor
11 – switch on for the circuit
12 – dynamometric beam

Fig. 1: *View of the device “DM 28M”*



1 – external housing;
2 – indicator;
3 – loading screw for the bearing;
4 – thermometer;
5 – injector;
6 – cased housing;
7 – load of the pendulum;
8 – ball;
9 – pendulum;
10 – clamp;
11 – middle bearings;
12 – driving shaft;
13 – dynamometric beam;
14 – end bearings

Fig. 2: *Bearing box (detail from the Fig. 1)*

The outer rings of the two middle bearings are located in common chamber, and the outer rings of the two end bearings are fixed tightly in the housing of the bearing box, so that they form tight contact. The inner rings of the bearings are connected tightly on the driving shaft. In this manner the motion of the driving shaft is transmitted to the inner rings of the bearings and to the outer rings of the bearings by means of the rolling balls. The outer rings of the bearings transmit the motion to the housing of the bearing pair, and the bearing box tends to rotate in the direction of shaft rotation. As a result, the appearing moment of friction sweeps along the bearing box. A pendulum is connected to the bearing box. The deflecting angle of the pendulum against the vertical position corresponds to the value of the moment of friction.

The bearing are externally loaded by means of the loading screw. The load is read on the loading indicator dial, graduated in accordance with the reference characteristic of the dynamometric beam. Oil is put into the bearing box through the casted housing and its level is regulated by means of piston displacement. All experiments are done at one, same for all tests, oil level, measured near the center of the bearing balls in order to ensure equal lubrication conditions in the bearing box. During the lubricant change, the bearing box is cleaned with benzene and dried by hot air. Bearing temperature is measured by the thermometer immersed in the oil. Appropriate limiters inhibit bearing head rotation during engine start. The number of revolutions (1880 min^{-1}) was constant, set through the regulation of the belt-drive, and controlled by the remote revolution counter.

Moment of friction and temperature is measured in the regime without load (unloaded conditions) and under four different loads (1130, 1635, 2725 and 5650 N). Test durations were the same for each load, i.e. 10 minutes, with data readings on every 2 minutes. The reduced (arbitrarily brought to one of the four bearings in the box) coefficient of friction in a bearing is determined by the formula:

$$\mu_r = \frac{2M}{P \cdot d},$$

where: M is moment of friction, P is normal load and d = 0.04 m is inner (bore) diameter of the bearing.

4. EXPERIMENTAL RESULTS AND DISSCUSION

4.1. Study of friction in bearings, lubricated by motor oil M-63/14 without and with additive

Experimental results show the variation of the moment of friction with the temperature of oil in the bearing, in regime without normal load, for motor oil M-63/14 without and with additive. The values are measured every 2 min with overall duration of 10 min. Figure 3 shows the variation of temperature and Fig. 4 shows the variation of moment of friction during the period of 10 min. For both variants (without and with additive) moment of friction reached steady-state values after 8 to 10 minutes (Fig. 4). This is the reason why time interval of 10 minutes was chosen as test duration in loaded bearings studies. The temperature of oil with additive is slightly lower than that of oil without additive (Fig. 3).

Four different loads are applied in tests with loaded bearings, with test duration of 10 minutes for each load. Oil temperature and moment of friction are measured for each load and are presented in Figs. 5 and 6. Calculated values of the corresponding coefficient of friction, for each load, are shown in Fig. 7.

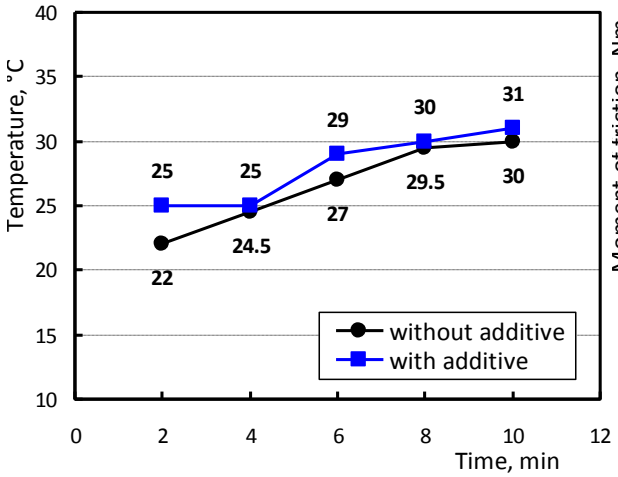


Fig. 3: *Variation of temperature of M-63/14 oil in bearing during friction without loading*

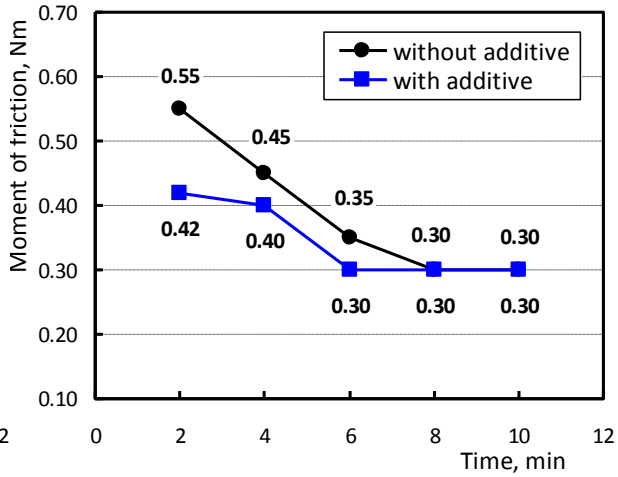


Fig. 4: *Variation of moment of friction during friction without loading*

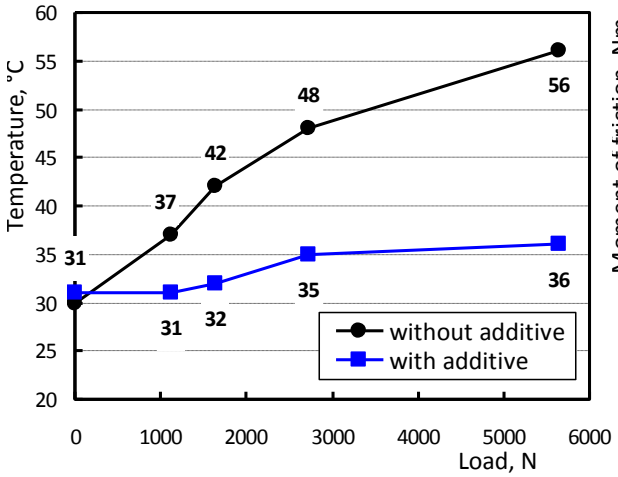


Fig. 5*: Variation of temperature of M-63/14 oil in bearing during friction with different loads*

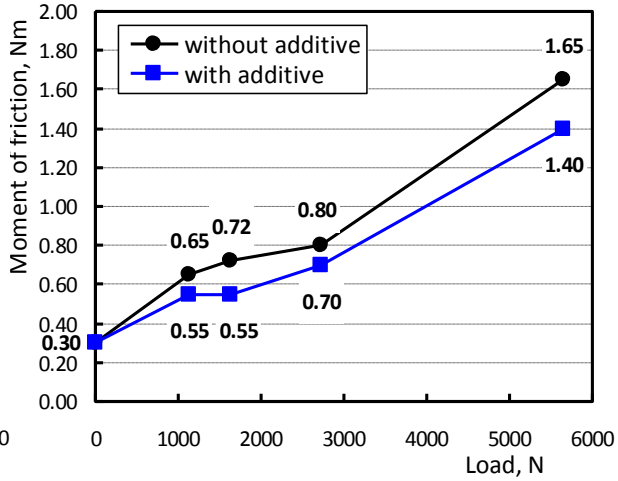


Fig. 6: *Variation of moment of friction in bearing during friction with different loads*

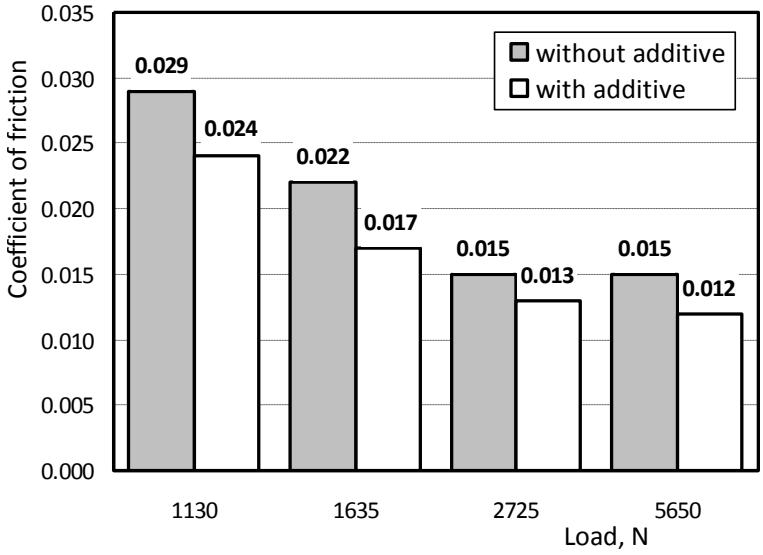


Fig. 7: *Dependence of the coefficient of friction on load for motor oil M-63/14 without and with additive*

From Figs. 6 and 7 it is obvious that the values of the moment of friction and coefficient of friction are for each load lower in the case of motor oil that contain “Valena” additive. Fig. 6 shows that the

moment of friction increases with the increment of the normal load, and the relationship is non-linear. The differences between moments increase with the augmentation of load. The reduction of the coefficient of friction by using “Valena” additive differs (from 13 to 23 %) with the applied load, and the average reduction is 18.3 %.

The results for oil temperature measurement (Fig. 5) show that in the case of motor oil with additive the temperature increases only 5 °C from unloaded to fully loaded conditions, while in the case of motor oil without additive temperature increases 25 °C for the same load increase. This suggests that the decrease of moment friction and coefficient of friction in the case of motor oil with “Valena” additive is not due to oil viscosity reduction at higher temperature, but due to the physic-chemical surface effects in the contact region during friction. Although it was not measured the wear of the balls and rings might be also diminished by the presence of additive, since its positive effect on friction properties.

After dismantling, the presence of thin reddish film on shaft surface was observed. The composition, structure and thickness of this film were not exanimate in this investigation, but it seems logical to suggest that this film has been formed during friction, due to physic-chemical and mechanical processes of selective transfer of copper on the steel shaft surface. The metal-plating additive “Valena” contains copper ions which are possibly transferred on the shaft under the specific conditions of the experiment. The formed film compensates the roughness on the surface, and due to the small tangential resistance it makes the plastic deformations during friction in the surface layers easier.

4.2. Study of friction in bearings, lubricated by transmission oil TM-5-18 without and with additive

Experimental results show the variation of the moment of friction with the temperature of oil in the bearing, in regime without normal load, for transmission oil TM-5-18 without and with additive. The values are measured every 2 min with overall duration of 10 min. Figure 8 shows the variation of temperature and Fig. 9 shows the variation of moment of friction during the period of 10 min. In case of transmission oil lubrication (without and with additive), moment of friction reached steady-state values after 4 to 6 minutes (Fig. 9). This time interval is shorter than it is in the case of motor oil lubrication (see Fig. 4), but the same time interval of 10 minutes was chosen as test duration in loaded bearings studies with transmission oil.

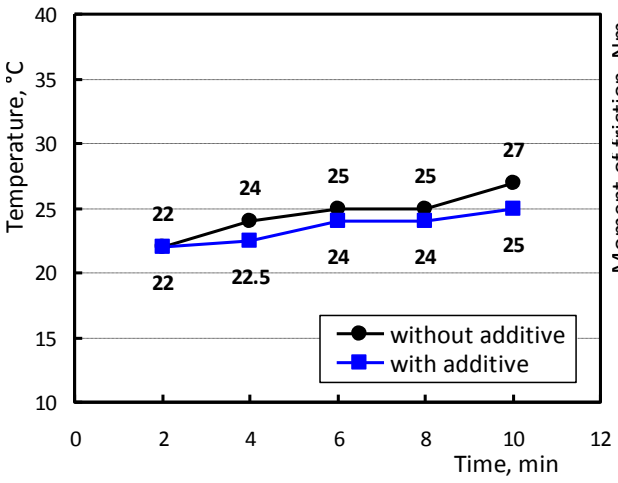


Fig. 8: *Variation of temperature of TM-5-18 oil in bearing during friction without loading*

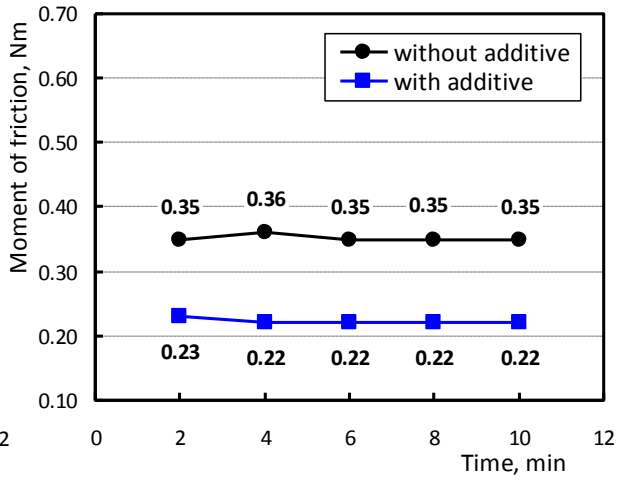


Fig. 9: *Variation of moment of friction during friction without loading*

Figure 8 shows that the temperature of oil with additive is slightly lower than that of oil without additive (as it was in the case of motor oil lubrication, see. Fig. 3). The moment of friction (Fig. 9) is almost constant in time for both transmission oil variant (without and with additive), being significantly lower for oil with additive. This difference in the moment of friction for oil without and with additive is much bigger in the case of transmission oil compared with the motor oil (see Fig. 6).

As in the case of motor oil test, four different loads are applied in transmission oil tests with loaded bearings. The duration of the test for each load is also 10 minutes. Oil temperature and moment of friction are measured for each load and are presented in Figs. 10 and 11. Calculated values of the corresponding coefficient of friction, for each load, are shown in Fig. 12.

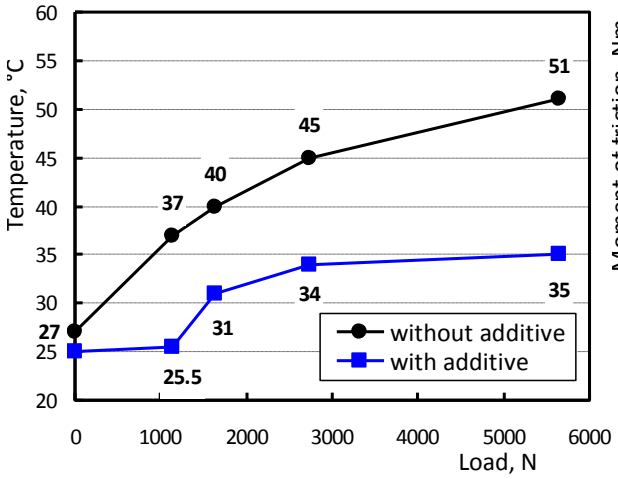


Fig. 10*: Variation of temperature of oil TM-5-18 in bearing during friction with different loads*

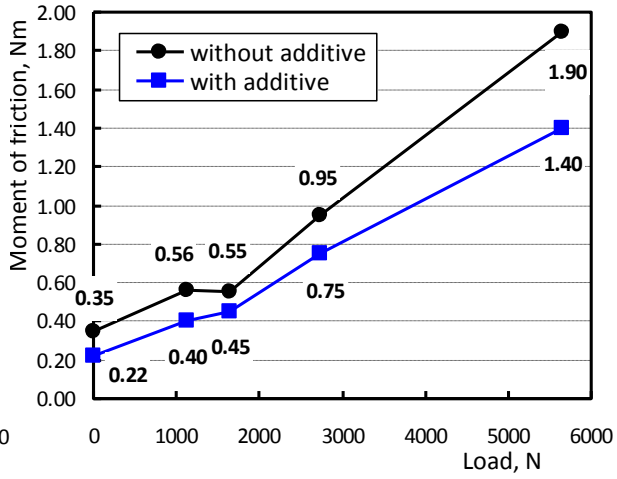


Fig. 11: *Variation of moment of friction in bearing during friction with different loads*

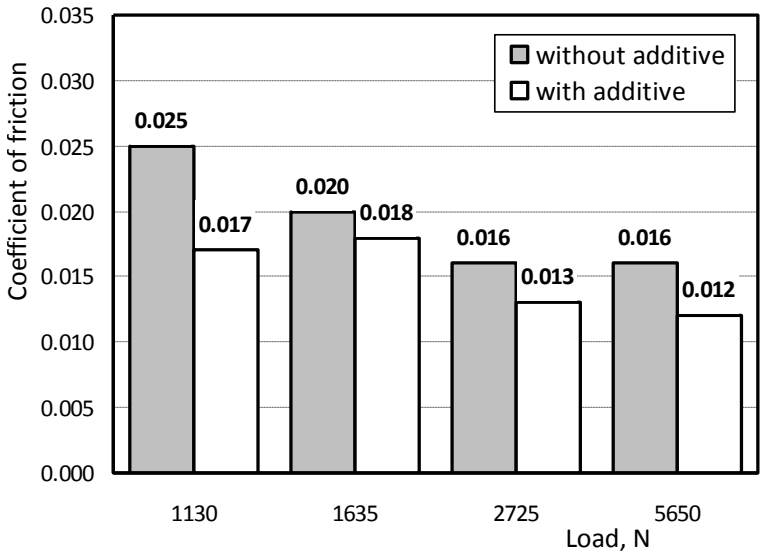


Fig. 12: *Dependence of the coefficient of friction on load for transmission oil TM-5-18 without and with additive*

From Figs. 11 and 12 it is obvious that the values of the moment of friction and coefficient of friction are for each load lower in the case of transmission oil that contain “Valena” additive. Fig. 11 shows that the moment of friction increases with the increment of the normal load, and the relationship is non-linear. The differences between moments increase with the augmentation of load. The reduction of the coefficient of friction by using “Valena” additive differs (from 10 to 32 %) with the applied load, and the average reduction is 21.4 %.

The results for oil temperature measurement (Fig. 10) show that in the case of transmission oil with additive the temperature increases only 10 °C from unloaded to fully loaded conditions, while in the case of transmission oil without additive temperature increases 24 °C for the same load increase. This suggests that the decrease of moment friction and coefficient of friction in the case of transmission oil with “Valena” additive, similar to the case of motor oil with “Valena” additive, is not due to oil viscosity reduction at higher temperature, but due to the physic-chemical surface effects in the contact region during friction. Although it was not measured the wear of the balls and rings might be also decreased by the presence of additive, because of the positive effect of the additive on friction properties.

After dismantling, the presence of thin reddish film on shaft surfaces was observed. The composition, structure and thickness of this film were not exanimate in this investigation, but it seems logical to suggest that this film has been formed during friction, due to physic-chemical and mechanical processes of selective transfer of copper on the steel shaft surface. The metal-plating additive “Valena” contains copper ions which are possibly transferred on the shaft under the specific conditions of the experiment. The formed film compensates the roughness on the surface, and due to

the small tangential resistance it makes the plastic deformations during friction in the surface layers easier.

5. CONCLUSION

The influence of “Valena” metal-plating additive on friction properties of ball bearings is studied in two cases, i.e. with motor oil and with transmission oil lubrication.

In both cases the values of the moment of friction and coefficient of friction are for each load lower in the case of oil that contain “Valena” additive.

The reduction of the coefficient of friction in the case of motor oil was app. 18 %, and in the case of transmission oil app. 21 %.

The results for oil temperature measurement confirmed that the decrease of moment friction and coefficient of friction in the case of oil with “Valena” additive is not due to oil viscosity reduction at higher temperature, but due to the physic-chemical surface effects in the contact region during friction.

The obtained results stimulate a future systematic study of the influence of “Valena” additive on friction, wear and other tribological process in tribosystems operating under various conditions and various characteristics, i.e. additive concentration, composition and structure of the contacting surfaces; the parameters of friction regime: loads, sliding speeds, presence of particles, vibrations, temperatures, lubricant availability (lubricity) in different friction regimes, etc.

ACKNOWLEDGMENTS

This study embraces the completion of tasks under the following projects: (a) Program for scientific-technological collaboration of the Tribology center in TU-Sofia and the company “Rudservice” from Gezkazgan, Kazakhstan; (b) Stage 2 of the first tribological network under CEEPUS project CIII-BG-0703-02-1314 “Modern Trends in Education and Research on Mechanical Systems – Bridging Reliability, Quality and Tribology”; (c) International cooperation agreement between the Faculty of Industrial Technology at TU-Sofia and the Faculty of Mechanical Engineering at the University of Belgrade.

REFERENCES

1. MORTIER, R.M., FOX, M.F., ORSZULIK, S.T. (Eds.), Chemistry and Technology of Lubricants, 3rd ed., Springer, Dordrecht, 2010.
2. BHUSHAN, B. (Ed.), Modern Tribology Handbook, CRC Press, Boca Raton, 2001.
3. NICOLIS, G., PRIGOGINE, I., Self-organization in Nonequilibrium Systems, John Willey & Sons, New York, 1977.
4. ASSENOVA, E., KANDEVA, M., Self-organization in tribology: The role of synergism and selective transfer, in Proceedings of the 7th International Conference on Tribology – BALKANTRIB ’11, October 3 – 5, 2011, Thessaloniki, Greece, pp.305 – 310.
5. GARKUNOV, D.N., No-wear Effect Under Friction: Hydrogen Wear of Metals, MAA Publishing House, Moscow, 2007.
6. POLZER, G., Der Erfahrungsaustausch: Reibbeschichten und selective Uebertragung, Publ. Bezirks-Neuerer-Zentrum, Gera, 1988.

CORRESPONDENCE

Mara Kandeva
Technical University-Sofia, Faculty of Industrial Engineering, Tribology Center,
8, Blvd Kl. Ohridski,1156 Sofia, Bulgaria,
e-mail: kandeva@tu-sofia.bg

Aleksandar Vencl
University of Belgrade, Faculty of Mechanical Engineering, Tribology Laboratory,
Kraljice Marije 16, 11120 Belgrade 35, Serbia,
e-mail: avencl@mas.bg.ac.rs

Emilia Assenova
Society of Bulgarian Tribologists, 74B, G. Sofiiski St., 1606 Sofia, Bulgaria,
e-mail: emiass@abv.bg

Tribological Journal BULTRIB, **Vol. IV, 2014**
Papers from the International Conference **BULTRIB '13**
October 24-26, 2013, Sofia
Society of Bulgarian Tribologists
Technical University of Sofia

THE INFLUENCE OF STRONTIUM ADDITION ON THE TRIBOLOGICAL PROPERTIES OF Zn25Al1Si ALLOY IN BOUNDARY LUBRICATED CONDITION

Aleksandar VENCL, Ilija BOBIĆ, Filip VUČETIĆ, Biljana BOBIĆ

Abstract: *The zinc-aluminium based casting alloy ZA-27 is well-established alloy and is frequently used materials for sleeves of plain bearings. It has good physical, mechanical and tribological properties. However, one of the major disadvantages is its dimensional instability over a period of time (ageing). To overcome this, the copper in the alloy may be replaced by silicon. Coarsening of the silicon particles is controlled by suitable additions of strontium. The influence of the strontium addition on friction and wear properties in boundary lubricated conditions was done on block-on-disc tribometer. The tests were carried-out for three Zn25Al1Si alloys with variable strontium content (0 wt. %, 0.03 wt. % and 0.05 wt. %), and, for the purpose of comparison, for standard ZA-27 alloy. Tests have confirmed that the wear rate of zinc-aluminium alloys with silicon is lower than the standard ZA-27, and have shown that the strontium addition lowers that rate additionally, with the slight increase of the coefficient of friction.*

Key Words: *Zn-Al alloys, strontium addition, sliding, boundary lubrication, friction, wear*

1. INTRODUCTION

The zinc-aluminium based casting alloy ZA-27 is well-established alloy and has widely been used in a variety of tribological applications as cost and energy effective substitutes to bronzes, cast irons and aluminium alloys [1,2]. It major disadvantages, like all conventional zinc-aluminium alloys containing 8 to 28 wt. % Al and 0.5 to 2.5 wt. % Cu, are inferior mechanical properties at temperatures above 100 °C [1,3] or 120 °C [2,4] and long-term dimensional instability (irreversible change of dimensions over a period of time) [1,2,5]. Heat treatment of the conventional zinc-aluminium alloys reduces the extent of dimensional changes but also deteriorates their hardness and tensile strength while ductility and sliding wear behaviour improve after the treatment [1,6].

Another approach, to overcome dimensional instability, is to replace the copper with silicon. The silicon not only improves the dimensional stability of zinc-aluminium alloys but also the wear properties [2,3,6]. However, too high silicon content can deteriorate the wear characteristics, and for each Al content there exists an optimum Si content [7]. This appears to be due to a coarsening of the silicon particles. Modification of the alloy melt with strontium addition prior to solidification refines the silicon structure, and improves the wear resistance [8].

The idea of this paper was to investigate the influence of strontium addition on the tribological properties of Zn25Al1Si alloy, since its addition already improved alloy structure. The tests were carried-out for three Zn25Al1Si alloys with variable strontium content (0, 0.03 and 0.05 wt. %), and, for the purpose of comparison, for standard ZA-27 alloy.

2. EXPERIMENTAL DETAILS

2.1. Materials

The investigated materials were made in the Department of Materials Science of the “Vinca” institute. The chemical composition of the alloys is given in Table 1. Technically pure zinc and aluminium were used to obtain these alloys, with the addition of master alloys Al7Si and Al18Si for achieving the desired content of silicon. Strontium was added in the alloys using the master alloy Al10Sr. The alloys were melted in the laboratory electric resistance furnace. The molten alloys (570 °C) were poured in the steel moulds preheated to 200 °C. Immediately before pouring the melts were intensively mixed by hand. In addition, for the purpose of comparison, a commercial ZA-27 alloy [9] was used (designated as ZA-27). The alloy was supplied from the RAR® foundry, Batajnica.

The alloy was also casted following the procedure identical to that for Zn-Al-Si and Zn-Al-Si-Sr alloys.

Table 1. Chemical composition of Zn-Al-Si and Zn-Al-Si-Sr alloys (wt. %)

Alloy designation	Al	Si	Sr	Zn
Zn25Al1Si	25	1	0	Balance
Zn25Al1Si-0.03Sr			0.03	
Zn25Al1Si-0.05Sr			0.05	

The microstructures of the tested materials were examined on the samples prepared in the standard metallurgical way and etched with 9 vol. % water solution of HNO_3 (Fig. 1). The microstructure of the conventional ZA-27 alloy (Fig. 1a) consists of complex dendrites with the core (α phase), the periphery (a mixture of α and η phase) and the interdendritic space (η phase). The elements of the structure are indicated in Fig. 1a. The α phase is rich in aluminium and the η phase contain about 93 wt. % zinc [10]. The morphology of the dendrites is a consequence of the peritectic reactions during the solidification of the alloy [11].

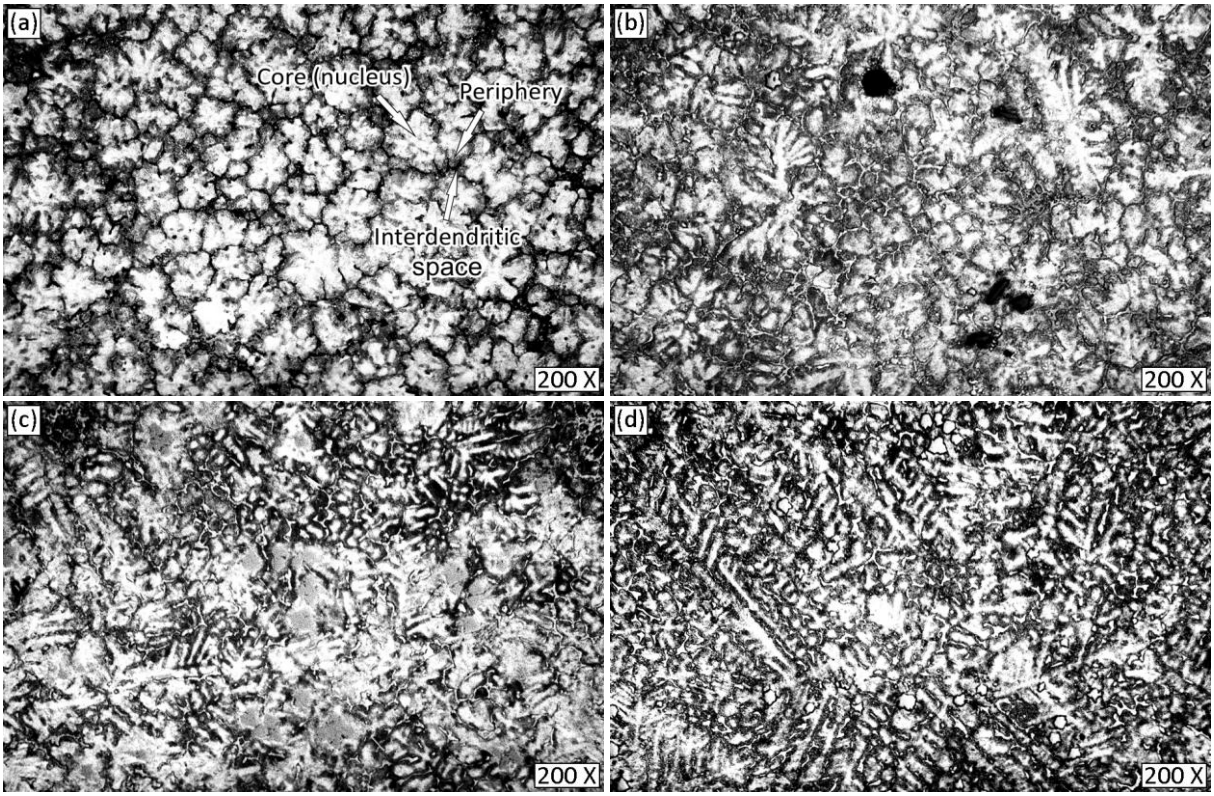


Fig. 1. Microstructures of tested materials: (a) ZA-27 alloy, (b) Zn25Al1Si alloy, (c) Zn25Al1Si-0.03Sr alloy and (d) Zn25Al1Si-0.05Sr alloy

Due to the content of zinc and aluminium in Zn25Al alloy, it can be considered that solidification of this alloy with 1 wt. % Si occurs analogously to solidification of the conventional ZA-27 alloy, so it can be followed using the phase diagram aluminium-zinc [12]. The basic micro-constituents in the structure of Zn25Al1Si alloy (Fig. 1b) are the same as in the conventional ZA-27 alloy (Fig. 1a). The addition of silicon has resulted with some reduction in the fraction of α phase in the structure of Zn25Al1Si alloy, as well as with finer dendritic structure. Silicon particles, which differ in size, are located within the dendrites of α phase as well as in the interdendritic phase. Cavities (black regions in Fig. 1b) occurred due to the fallout of large silicon particles during metallographic preparation of samples. The addition of 0.03 or 0.05 wt. % strontium has no significant effect on the morphology of α phase, but it affects the size and distribution of silicon particles in the alloy structure (Figs. 1c and d). The silicon particles now are approximately equal in size. With an increase of the content of strontium from 0.03 to 0.05 wt. %, the size of silicon particles was reduced, while their distribution became more uniform.

Hardness measurements were performed in the Department of Materials Science of the “Vinca” institute. Five hardness readings were taken for each sample at different locations. The results of the Vickers hardness (HV5) are as follows: ZA-27 alloy (119.0); Zn25Al1Si (114.7); Zn25Al1Si-0.03Sr

(113.3); Zn25Al1Si-0.05Sr (114.0). The measured hardness of the ZA-27 alloy is in accordance with the value prescribed in the standard [9]. Alloys with silicon content (Zn25Al1Si, Zn25Al1Si-0.03Sr and Zn25Al1Si-0.05Sr alloy) show a slightly lower hardness values compared to the hardness of ZA-27 alloy. This was expected considering that ZA-27 alloy contains copper (2 to 3 wt. %) and magnesium (0.01 to 0.02 wt. %) that favourably affect hardness of the alloy. Addition of strontium had no effect on the hardness of alloys with 1 wt. % silicon.

2.2. Tribological testing

Tribological test were performed in the Tribology Laboratory at the Faculty of Mechanical Engineering in Belgrade, on the block-on-disc tribometer. The environmental conditions were: lubricated sliding and ambient air at room temperature (≈ 28 °C). A schematic diagram of tribometer is presented in Fig. 2a. Rectangular blocks of tested materials having 6 mm width and 16 mm length were used as wear test samples. Disc (hereafter referred to as counter body) of 44 mm diameter and 10 mm thickness was made of steel C60E (46 to 48 HRC). Lubrication was provided by revolving of the disc which was sunk into oil container (Fig. 2a). Lubricant was mineral engine oil (SAE 15W-40, ACEA E3). Lubricant temperature during the tests was more or less constant, and at the end of test it was ≈ 30.9 °C.

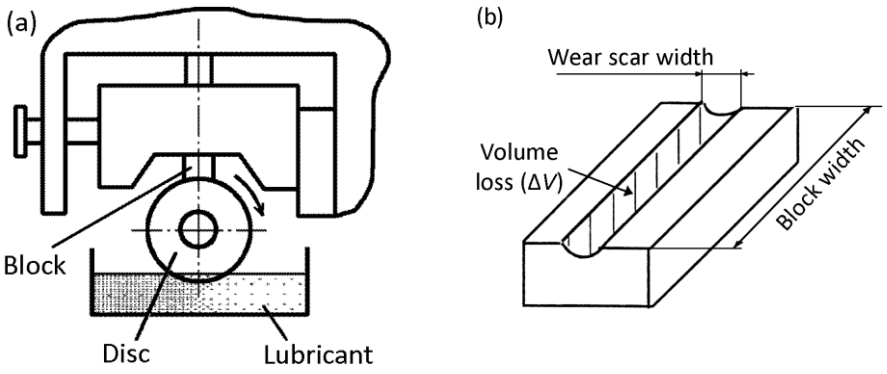


Fig. 2. Tribological testing: (a) schematic diagram of the block-on-disc tribometer and (b) block wear scar measurements

Before and after testing, both the block and the counter body were degreased and cleaned with benzene. Wear scars on pins were measured in accordance with ASTM G77 [13] with accuracy of 0.05 mm, after each test to calculate the volume loss ΔV (Fig. 2b). The values of oil temperature, friction coefficient, normal and friction force were monitored during the test and through data acquisition system stored in the PC. Tests were carried out at selected test conditions: sliding speed of 0.5 m/s, sliding distance of 1000 m and normal load of 100 N. Calculated pressure at the end of tests it was app. 5 MPa for ZA-27 alloy and app. 10 MPa for the other alloys. After testing, worn surfaces of blocks were examined by scanning electron microscope (SEM).

3. RESULTS AND DISCUSSION

This tribological investigation was just an initial one, with preliminary results and some more experiments to be done to completely understand tribological behaviour of these materials. In order to achieve a higher confidence level in evaluating test results, three to five replicate tests were run for all the tested materials. The values of the coefficient of friction are presented in Fig. 3.

Coefficients of friction were from 0.05 to 0.08, which suggest that the sliding was performed in boundary lubrication regime, since the approximate values for the boundary lubrication are from 0.05 to 0.15 [14,15]. Since the tests were performed in lubricated conditions the hardness of the materials did not have noticeable influence on friction values. Conventional ZA-27 alloy shows the highest value of the coefficient of friction of 0.07. Risdon et al. [16] tested differently obtained ZA-27 alloys and for permanent mould casted alloy the obtained coefficient of friction was between 0.03 and 0.07, but the used oil had lower viscosity and higher working temperature. In addition the sliding speed was lower and normal load differ as well.

The replacement of copper with silicon (Zn25Al1Si alloy) significantly lowers the values of the coefficient of friction (from 0.07 to 0.047). On the other hand, addition of strontium has negative effect on the coefficient of friction, i.e. with increase of Sr content coefficient of friction also increase. Similar dependence in dry sliding conditions was noticed for the Al20Si alloy modified with Sr, when Sr content exceeds some optimal value [17].

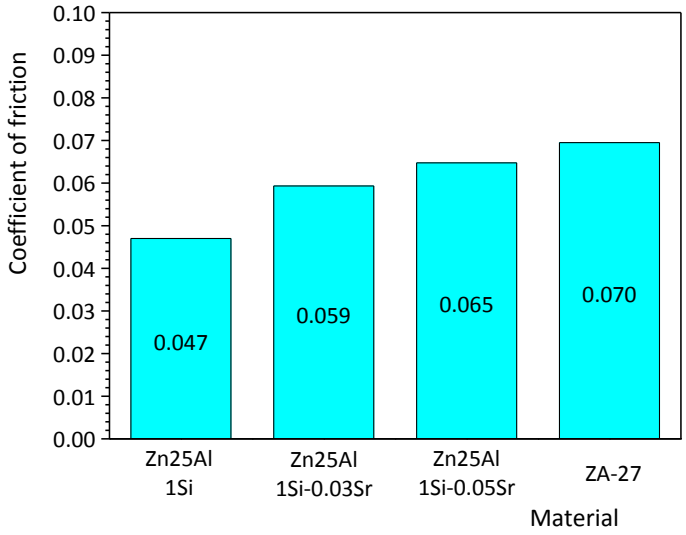


Fig. 3. Steady-state averaged values of the coefficient of friction

According to the SEM analysis (which is not presented in this paper), the dominant wear mechanism is a combination of adhesion and abrasion. Adhesive wear occur in highly-loaded, poorly lubricated sliding contacts, and was noticed at all sliding pairs. Abrasive wear was mostly pronounced at ZA-27 alloy, and this is the reason why this material showed the worse wear resistance (highest wear rate). The obtained value of the wear rate for this material of 1.41 × 10–3 mm3/m (Fig. 4) is in accordance with the data from the literature for the permanent mould casted ZA-27 alloy [16]. It should be noted that the wear process was not tracked during the tests, so the results in Fig. 4 present total wear rates.

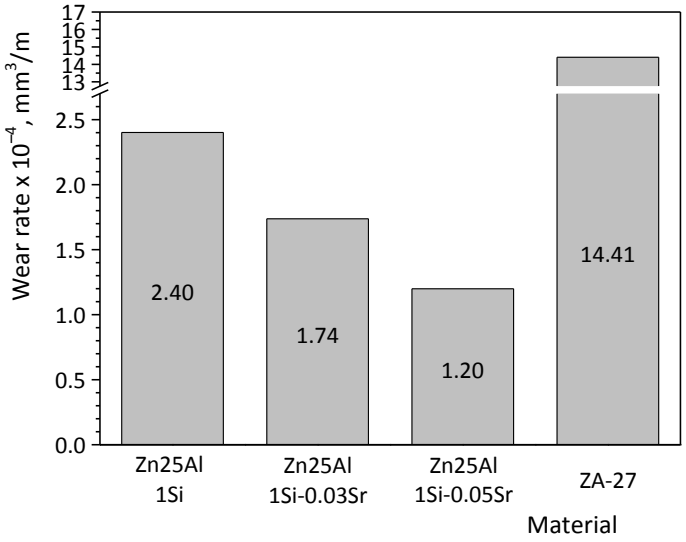


Fig. 4. Total wear rates for the tested materials

The wear rate of ZA-27 alloy was almost one order of magnitude higher than the rest of tested materials (Fig. 4), which suggests that the addition of Si instead of Cu in conventional ZA-27 alloy significantly improves its wear resistance.

Similar dependence was obtained by Savaskan and Murphy [6], who tested several Zn25Al based alloys with silicon and copper addition. The alloys were produced by gravity casting in the preheated (250 °C) steel mould. The testing conditions were as follows: block-on-disk tribometer (with conformed geometry of the block); normal load of 329 N (7.1 MPa); sliding speed of 1.73 m/s and motor oil (SAE 30) as a lubricant. The authors showed that the as-cast Zn25Al alloy containing 2.7 wt. % Si wear resistance was 4.5 to 12 times (after 1495 km and after 150 km sliding distance) higher than the same alloy containing 3.1 wt. % Cu. It is interesting to note that the wear rates of these two alloys were unproportional to its hardness, i.e. Zn25Al-2.7Si alloy showed higher wear resistance despite the fact that its hardness (81.6 HRF) were lower than the hardness of Zn25Al-3.1Cu alloy (93.7 HRF). The

same unproportion was in this study, i.e. hardness of all alloys containing Si was lower slightly than ZA-27 alloy.

In the study conducted by Jian et al. [8] alloys containing Si instead of Cu also showed wear resistance one order of magnitude higher than the alloy containing Cu. All tested materials (Zn27Al, Zn27Al-2Si, Zn27Al-2Si-0.05Sr and Zn27Al-2Si-0.5Sr alloy) were sand casted. They used block-on-disk tribometer (with conformed geometry of the block); normal load of 8 MPa; sliding speed of 0.21 m/s and grease as a lubricant. The authors also showed that the modification with strontium additionally improves the wear resistance by reducing the silicon particle size. The alloy containing 0.05 % Sr showed the highest wear resistance. At the same time the alloy containing 0.5 % Sr showed wear resistance lower than the alloy that was not modified with Sr (Zn27-2Si alloy), suggesting that over modification with Sr is possible situation. Nevertheless, with further testing, by continuously increasing normal load from 4 to 18 MPa, the influence of strontium addition on wear rate becomes lower and insignificant.

In this study the influence of strontium addition in Zn25Al1Si alloy was also beneficial to wear resistance, as the Fig. 4 shows. Addition of strontium decreases the wear rate, and in case of 0.05 wt. % Sr it is twice lower. This is in accordance with the data obtained by Jian et al. [8]. The fact that the addition of 0.05 wt. % Sr decreased wear rate more than addition of 0.03 wt. % Sr suggests that the further addition of strontium may decrease the wear rate even more, which should be investigated.

4. CONCLUSION

The microstructure of the Zn25Al1Si alloy was improved with addition of strontium. The morphology of α phase was not affected, but the addition of strontium affected size and distribution of silicon particles in the alloy. With addition of strontium (0.03 wt. %) the size of silicon particle become more uniform, and with further increase of strontium content (0.05 wt. %), the size of silicon particles was reduced, while their distribution became more uniform.

The hardness of the alloys with silicon content showed slightly lower values compared to the hardness of ZA-27 alloy. Addition of strontium had no effect on the hardness of alloys with 1 wt. % silicon.

Tribological tests have confirmed that the replacement of copper with silicon in the ZA-27 alloy gave greatly improved wear resistance, and even lowers the coefficient of friction value. Strontium modification of Zn25Al1Si alloy improved wear resistance additionally, and the improvement was higher in the case of 0.05 than in the case of 0.03 wt. Sr. The coefficient of friction value was higher as strontium content increase.

ACKNOWLEDGMENTS

This work has been performed as a part of activities within the projects TR 34028 and TR 35021. These projects are supported by the Republic of Serbia, Ministry of Education, Science and Technological Development, whose financial help is gratefully acknowledged.

REFERENCES

1. PRASAD, B.K., Effect of microstructure on the sliding wear performance of a Zn-Al-Ni alloy, Wear, 240, 1-2, 2000, 100-112.
2. LEE, P.P. Lee, SAVASKAN, T., LAUFER, E., Wear resistance and microstructure of Zn-Al-Si and Zn-Al-Cu Alloys, Wear, 117, 1, 1987, 79-89.
3. ZYSKA, A., KONOPKA, Z., ŁĄGIEWKA, M., NADOLSKI, M., Structure and selected properties of high-aluminium Zn alloy with silicon addition, Archives of Foundry Engineering, 11, Special Issue 3, 2011, 261-264.
4. PRASAD, B.K., MODI, O.P. Slurry wear characteristics of zinc-based alloys: Effects of sand content of slurry, silicon addition to alloy system and traversal distance, Transactions of Nonferrous Metals Society of China, 19, 2, 2009, 277-286.
5. SAVAŞKAN, T., PÜRÇEK, G., MURPHY, S., Sliding wear of cast zinc-based alloy bearings under static and dynamic loading conditions, Wear, 252, 9-10, 2002, 693-703.
6. SAVASKAN, T., MURPHY, S., Mechanical properties and lubricated wear of Zn-25Al-based alloys, Wear, 116, 2, 1987, 211-224.
7. SEGAWA, T., SATO, T., KIMURA, Y., Effects of Al and Si of zinc alloys on the bearing performance under conditions of boundary lubrication, Journal of the Japan Institute of Metals and Materials, 47, 6, 1983, 515-520 (in Japanese).
8. JIAN, L., LAUFER, E.E., MASOUNAVE, J., Wear in Zn-Al-Si alloys, Wear, 165, 1, 1993, 51-56.

9. EN 12844:1998 Zinc and zinc alloys - Castings - Specifications.
10. LEHUY, H., Mechanical properties of zinc-aluminium alloys extruded in the liquid-solid state, Journal of Materials Science, 23, 8, 1988, 2943-2950.
11. MURPHY, S., SAVASKAN, T., Metallography of zinc-25% Al based alloys in the as-cast and aged conditions, Practical Metallography, 24, 5, 1987, 204-221.
12. GERVAIS, E., BARNHURST, R.J., LOONG, C.A., A. An analysis of selected properties of ZA alloys, Journal of Metals (JOM), 37, 11, 1985, 43-47.
13. ASTM G77-98 Standard test method for ranking resistance of materials to sliding wear using block-on-ring wear test.
14. RAC, A., Basics of Tribology, Faculty of Mechanical Engineering, University of Belgrade, Belgrade, Serbia, 1991, pp. 7-23 (in Serbian).
15. HAMROCK, B.J., SCHMID, S.R., JACOBSON, B.O., Fundamental of Fluid Film Lubrication, Marcel Dekker, Inc., New York, USA, 2004, Ch. 1.
16. RISDON, T.J., BARNHURST, R.J., MIHAICHUK, W.M., Comparative wear rate evaluation of zinc aluminum (ZA) and bronze alloys through block on ring testing and field application, SAE Technical Paper 860064, 1986.
17. LIU, G., LI, G., CAI, A., CHEN, Z., The influence of Strontium addition on wear properties of Al-20 wt% Si alloys under dry reciprocating sliding condition, Materials and Design, 32, 1, 2011, 121-126.

CORRESPONDENCE

Aleksandar VENCL
Faculty of Mechanical Engineering, University of Belgrade
Kraljice Marije 16, 11120 Belgrade 35, Serbia
e-mail: avencl@mas.bg.ac.rs

Ilija BOBIĆ
Institute of Nuclear Sciences “Vinca”, University of Belgrade
Mike Petrovića Alasa 12-14, 11001 Belgrade, Serbia
ilijab@vinca.rs

Filip VUČETIĆ
Faculty of Mechanical Engineering, University of Belgrade
Kraljice Marije 16, 11120 Belgrade 35, Serbia
vucetic_filip90@yahoo.com

Biljana BOBIĆ
Institute of Chemistry, Technology and Metallurgy, University of Belgrade
Njegoševa 12, 11000 Belgrade, Serbia
biljanabobic@gmail.com

Tribological Journal BULTRIB, **Vol. IV, 2014**
Papers from the International Conference **BULTRIB '13**
October 24-26, 2013, Sofia
Society of Bulgarian Tribologists
Technical University of Sofia

ПРЕДЛОЖЕНИЕ ЗА РАЗКРИВАНЕ НА МАГИСТЪРСКА СПЕЦИАЛНОСТ „ТРИБОИНЖЕНЕРИНГ”

Мара Кандева
Председател на Обществото на триболозите в България

Предвид на кризата в университетското образование в страна, липсата на функционални контакти между инженерните университети и проблемите на бизнеса намираме, че е необходимо обогатяване на знанията и културата на инженерите със съвременните постиженията на трибологичните знания и технологии в техническите системи.

I. Предпоставки

1.Организационни:
- Концепция за развитие на трибологията в България, одобрена на национално ниво;
- Национален Координационен център по трибология;
- Национално гражданско сдружение „Общество на триболозите в България”;
- Балканска трибологична асоциация

2. Теоретико-методологични:
-наличие на учебно-методични пособия: Обща трибология, Интердисциплинната парадигма на трибологията, Контактният подход в инженерната трибология, Контактен подход и др.;
- Разработени са теоретико-методологични въпроси, свързани с приложение на нова интердисциплинна парадигма и контактен подход в инженерната трибология.

3. Учебно-методични:
- наличие на действащи учебни програми по трибология в образователна степен „магистър” - „Динамика и трибология на машините” и „Инженерна трибоекология” в три специалности на МТФ. Предстои разработване на нова програма по „Нанотрибология” по европейски проект на ТУ-София за нова магистърска специалност „Микро и нанотехнологии”.
- наличие на специализирано фирмено обучение по трибология;
-кадрови потенциал: защитени малки и големи докторати, професори, доценти, докторанти по трибология;
- учебно-изследователски лаборатории по трибология

4. Разработване на образователни, изследователски и технологични проекти, свързани с трибологията:
- Проект CEEPUS по първата трибологична мрежа на CIII-BG-0703-02-1314 ”Modern Trends in Education and Research on Mechanical Systems - Bridging Reliability, Quality and Tribology” – етап 2
- Междууниверситетски проект „Подобряване на висшето техническо образование на основата на интердисциплинен подход”, финансиран от Световната банка;
- Проект BG051PO001-4.3.04-0045 “Развитие на електронни форми за дистанционно обучение в областта на съвременни индустриални технологии за нуждите на учебния процес на МТФ при ТУ-София”
- Проект BG051PO001-3.1.07-0048 “Актуализиране на учебните планове и програми на специалностите във ФЕТТ, ФТК и МТФ на ТУ-София и създаване на нова съвместна магистърска специалност в съответствие с потребностите на пазара на труда“
- Триботехнологии и триботехника TREFA за регенерация на въздушни автомобилни филтри за нуждите на корпорация „Казахмыс“, Република Казахстан;

5. Информационно-издателска дейност:
- провеждане и участие в национални и международни конференции „БУЛТРИБ” и „БАЛКАНТРИБ”;
- издаване на 3 списания по требология: „Трибологичен журнал БУЛТРИБ”, „Списание на Балканската трибологична асоциация” и „Контакти”;
- издаване на сборници, статии и монографични трудове.

II. Аргументация
1. Необходимост от инженерни кадри по проблемите на трибологията в образованието, индустрията и управлението:
2. Повишаване на интердисциплинната култура на инженера за решаване на комплексни проблеми:
3. Задоволяване на потребностите на обществото от експерти и изследователи в областта на контактните взаимодействия в стопанската сфера.

III. Възможности
1. Наличие на предварително съгласие между триболозите в университетите на страната.
2. Наличие на необходимата материална база
3. Наличие на кадрови преподавателски състав
4. Наличие на проекти, свързани с усъвършенстване на университетското образование
5. Подкрепа от фирми в страната.

Въз основа на изложените предпоставки, аргументи и възможности предлагам да се започне работа по разкриване на нова магистърска специалност „ТРИБОИНЖЕНЕРИНГ”.

PROPOSAL
FOR THE OPENING OF MSC SPECIALTY „TRIBOENGINEERING”

Mara Kandeva, Assoc. Prof. Dr.
President of the Society of Bulgarian Tribologists

Having in view the crisis in the engineering education in our country, the lack of functional contacts between the engineering universities and the problems of the business, we are facing the necessity of improvement of the knowledge and culture of engineers by the modern tribological knowledge and technology about technical systems.

I. Background as availability of necessary condition
1. Organizational:
- Conception of the development of tribology in Bulgaria, accepted on national level;
- National Coordination Center of Tribology;
- National civil organization „Society of Bulgarian Tribologists”;
- Balkan Tribological Association.

2. Theoretical and methodological:
- Availability of teaching and methodological literature: Overall Tribology; Interdisciplinary Paradigm of tribology; The contact approach of engineering tribology, The contact approach, etc.;
- Development of theoretical and methodological problems related to the application of the new interdisciplinary paradigm and the contact approach in the engineering tribology.

3. Teaching and training:
- Availability of active syllabuses in Tribology for the educational Master degree - „Dynamics and tribology of machines” and „Engineering triboecology” for three specialties of the Faculty of Industrial Technology at the Technical University - Sofia. We are preparing a new syllabus „Nanotribology” under the European Project of the Technical University - Sofia for the new Master specialty „Micro- and nanotechnologies”.
- Availability of specialized company teaching in tribology;
- Personnel of experts: defended PhD and DSc dissertations, professors, associate professors, PhD students;
- Training and research laboratories in tribology.

4. Development and design of educational, research and technological projects related to tribology:
- Project CEEPUS in the first tribological network CIII-BG-0703-02-1314 ”Modern Trends in Education and Research on Mechanical Systems - Bridging Reliability, Quality and Tribology” – stage 2;

- Interuniversity project „Improvement of the higher technical education based on the interdisciplinary approach", funded by the World Bank;
- Project BG051PO001-4.3.04-0045 "Development of electronic forms for remote teaching in the field of modern industrial technologies for the educational needs the Faculty of Industrial Technology at the Technical University - Sofia"
- Project BG051PO001-3.1.07-0048 "Updating the syllabuses for the specialties in three of the faculties of the Technical University - Sofia and opening of a new common MSc specialty meeting the needs of the labor market"
- Tribotechnology and tribotechnique TREFA for regeneration of air automotive filters for the needs of the corporation „Kazakhmis", the Republic of Kazakhstan;

5. Informational and publishing activities:

- Organizing and participation in national and international conferences BULTRIB and BALKANTRIB;
- Publishing of three tribological journals: „Tribological Journal BULTRIB", „Journal of the Balkan Tribological Association" and „Contacts";
- Publishing of articles, papers, monographs.

II. Justification

1. Necessity of engineering specialists in the field of tribology in education, industry and management;
2. Improvement of the interdisciplinary culture of the engineering staff aiming complex problems solution;
3. Satisfying the social needs in experts and researchers in the field of the contact interactions in business.

III. Potential: availability of:

1. Preliminary agreement between the tribologists in the universities of the country;
2. Appropriate equipment;
3. Teachers and lecturers resource;
4. Projects in the field of advance of university education;
5. Support of companies from the country.

Based on above argumentation, I propose beginning of the preparation of the new MSc specialty "TRIBOENGINEERING".

Tribological Journal BULTRIB, **Vol. IV, 2014**
Papers from the International Conference **BULTRIB '13**
October 24-26, 2013, Sofia
Society of Bulgarian Tribologists
Technical University of Sofia

STUDIES ABOVE EROSION BEHAVIOR OF ROTOR TURBINE MATERIALS

Razvan George RIPEANU

Abstract: *Erosion and corrosion are the main wear mechanisms of rotor turbine surface. To reduce corrosion the stainless steels are used, but the hardness of these materials could not avoid erosion. Paper presents the tests made by author in order to characterize the erosion and corrosion behavior of hard thin layers obtained on stainless steels materials.*

Key Words: *Erosion, rotor, stainless steels, roughness*

1. INTRODUCTION

Gas turbine rotors works in works in special conditions, rotor blades being exposed at erosion, fatigue, tension stresses due to important centrifugal forces. When working medium are hot gases, appear also hot corrosion and thermal stresses. Materials used for blade manufacturing are special alloys, designed to resist at hot corrosion, thermal and mechanical fatigue stresses in conditions erosion wear due to small solid particles contained in gases, [1, 2, 3]. Erosion wear due to these fine solid particles generate craters on blades surfaces. The microgeometry modification due to erosion and corrosion modify flow conditions and also diminish blade fatigue resistance, [3, 4].

To diminish destructive effect of erosion and corrosion wear, hard thin coatings with good adherence and with good behavior at micro-fatigue could be used, [1, 4].

Paper presents the test made in order to evaluate erosion wear behavior of thin layers applied on AISI 316L base materials.

2. EXPERIMENTS

Abrasive erosion wear depends of fluid speed, solid particles geometry, hardness and mass, and of surface hardness and of impingement angle. At tensile materials with low hardness the critical impingement angle is between 15^0 and 30^0.and at hard materials the maximum wear is obtained at normal impingement, [2, 3, 4].

Erosion tests were conducted on sand blasting equipment type PR-50 adapted for this purpose. As erosive particles was used siliceous sand with dimensions smaller than 63 μm. These dimensions are closed of particles contained in turbine gas working medium. The gas turbine rotor blades have angles between 55^0 and 65^0 and at experimental tests was used an impingement angle of 60^0. In figure 1 it is presented the erosion testing device, [5].

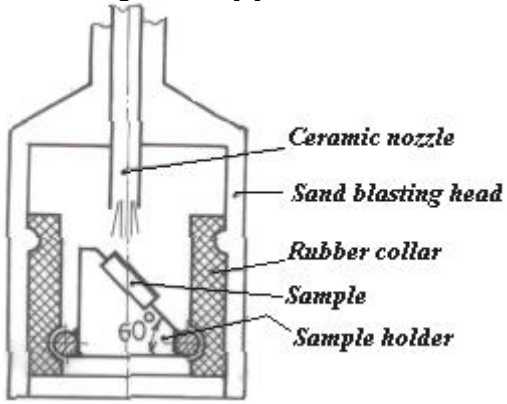


Fig.1. Erosion testing device

In figure 2 it is shown the constructive dimensions of the sample holder and in figure 3 the tested sample dimensions, [5].

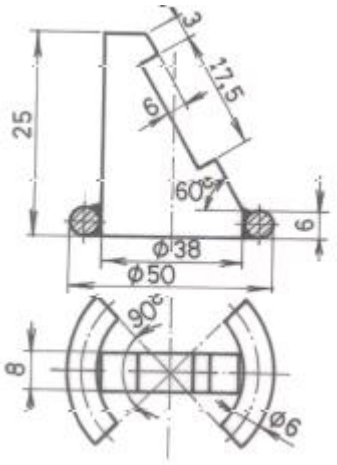


Fig.2. Sample holder

Were tested 5 sample types. Sample type 1 was base material AISI 316L coated on active surface with TiN, sample 2 was base material AISI 316L coated on active surface with ZrN, sample 3 was base material AISI 316L coated on active surface with TiN and ZrN in two stratums, sample 4 was base material AISI 316L coated on active surface with multilayer's of TiN / ZrN and sample 5 was AISI 316L not coated.

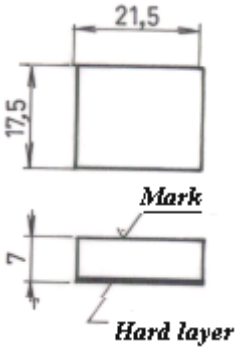


Fig.3. Sample dimensions

Tests were made at ambient temperature of 20^0C. Compressed air was passed threw two filters before siliceous sand admission in order to avoid contamination with oil the sand or the active sample surface.

Testing conditions were, [5]:

- air pressure p = 0.4 MPa;
- nozzle diameter d = 10 mm;
- distance between nozzle and sample l =50 mm;
- testing time for each sample t =10 minutes;
- siliceous sand mass consumption for each sample m =7 kg;
- grain sand size $g \leq 63$ μm;
- impingement angle $\alpha = 60^0$;
- 5 sample types:
    - sample type 1 was base material AISI 316L coated on active surface with TiN;
    - sample 2 was base material AISI 316L coated on active surface with ZrN;
    - sample 3 was base material AISI 316L coated on active surface with TiN and ZrN in two stratums;
    - sample 4 was base material AISI 316L coated on active surface with multilayer's of TiN / ZrN;
    - sample 5 was AISI 316L not coated.

To evaluate erosion wear was used roughness modification values and surface profiles. To measure micro-geometry parameters a Surtronic 3+ device was used and parameters were calculated with Tally ProfileLite soft [2, 3, 4]. In table 1 are presented the roughness values obtained.

Table 1. Initial and final roughness values

Sample type	Initial values for roughness parameters, [μm]			Final values for roughness parameters, [μm]		
	Ra	*Rz*	*Rt*	*Ra*	*Rz*	*Rt*
1	0.175	1.76	1.97	0.310	4.46	6.68
2	0.247	1.43	1.61	0.532	4.30	5.32
3	0.751	6.20	7.05	0.442	4.00	4.26
4	0.289	2.92	3.21	0.527	3.55	4.51
5	0.339	2.06	2.52	0.475	3.73	4.24

To calculate parameters a microroughness filtering is used, with a ratio of 2.5 μm. In tab1. The *Ra*, *Rz* and *Rt* were calculated were:

Ra means arithmetic mean deviation of the roughness profile;

Rz: - maximum height of roughness profile;

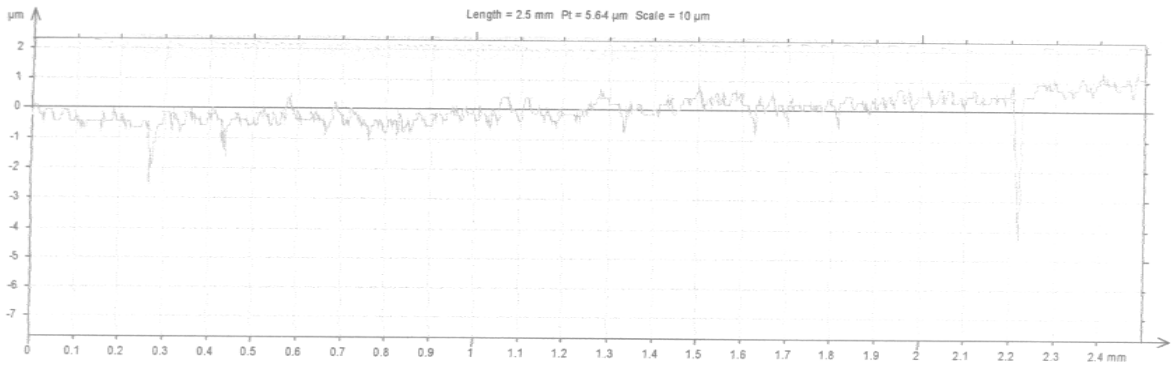
Rt - total height of roughness profile.

In table 2 are presented the roughness increasing values obtained.

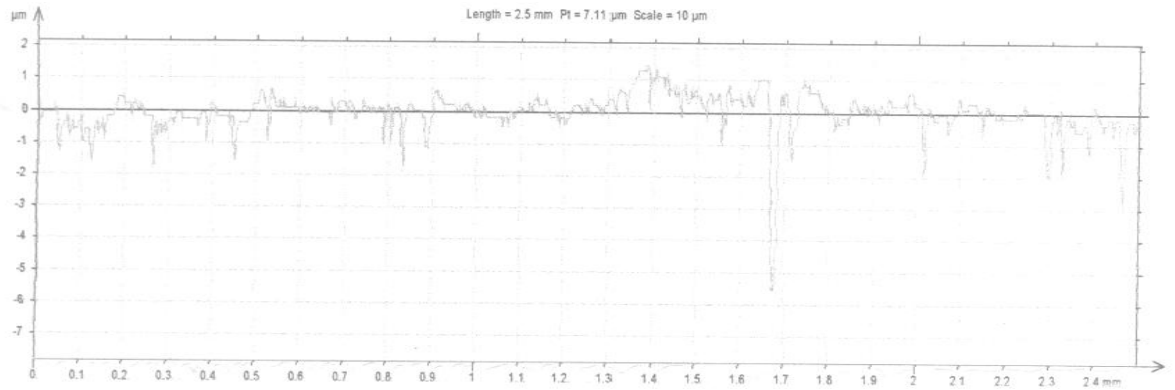
Table 2. Roughness increasing values due to erosion

Sample type	Increasing of the roughness parameter, [μm]		
	ΔRa	*ΔRz*	*ΔRt*
1	0.235	2.88	4.71
2	0.285	2.87	3.71
3	- 0.309	- 2.20	- 2.79
4	0.238	0.63	1.30
5	0.136	1.67	1.72

In figure 4 it is shown the profile graphs for sample 1.



a) Initial profile graph for sample 1

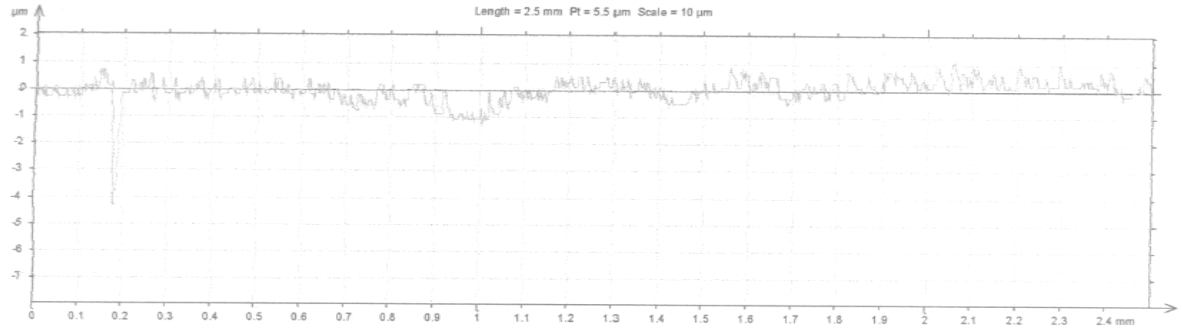


b) ***Final profile graph for sample 1***

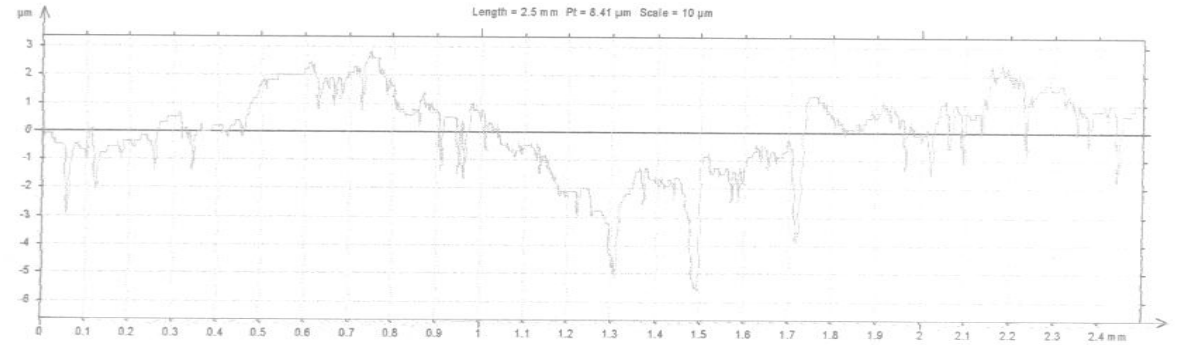
Fig.4. Profile graphs for sample 1

From fig.4 we could observe that surface profile after erosion test is similar with initial profile but presents holes more sharped and more frequent which indicate local detaching of the TiN stratum.

In figure 5 it is presented the profile graphs for sample 2.



a) Initial profile graph for sample 2

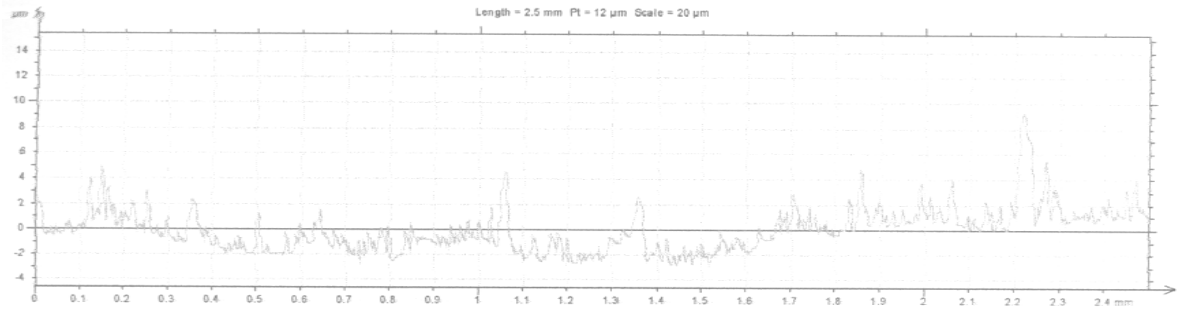


b) Final profile graph for sample 2

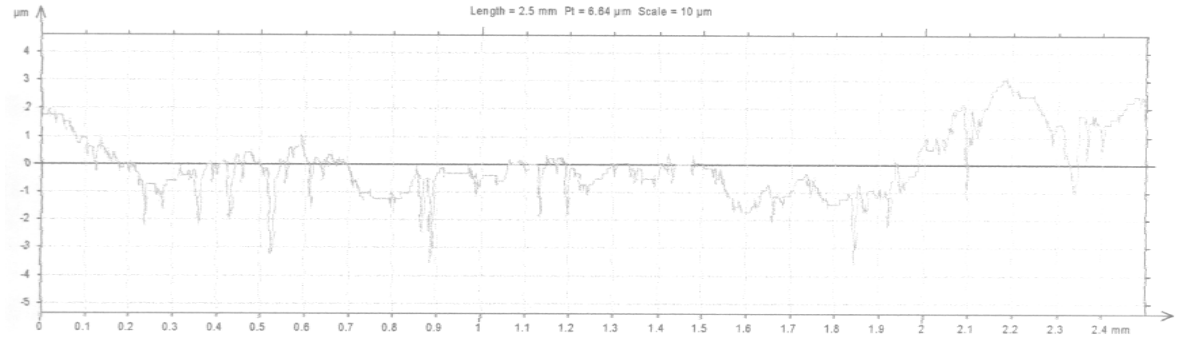
Fig.5. Profile graphs for sample 2

From fig. 5 we could observe that profile after erosion test is fundamentally different from the initial situation, on surface could be observed great deeps which pass the layer thickness.

In figure 6 it is shown the profile graphs for sample 3.



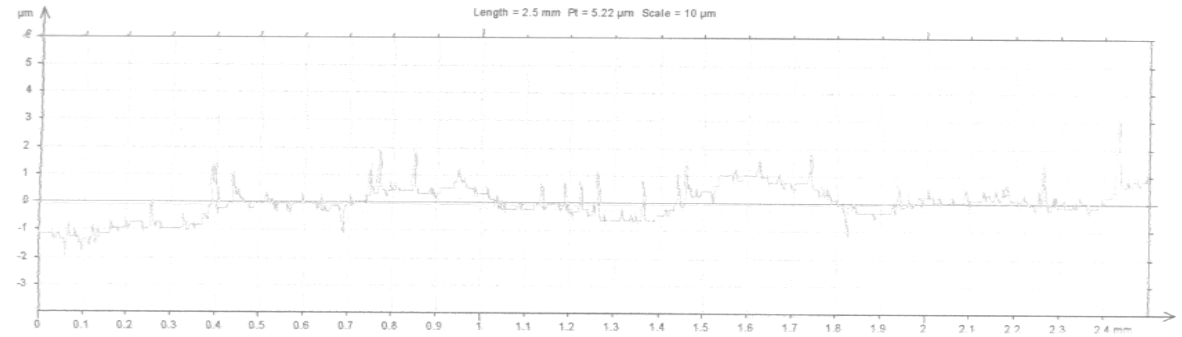
a) Initial profile graph for sample 3



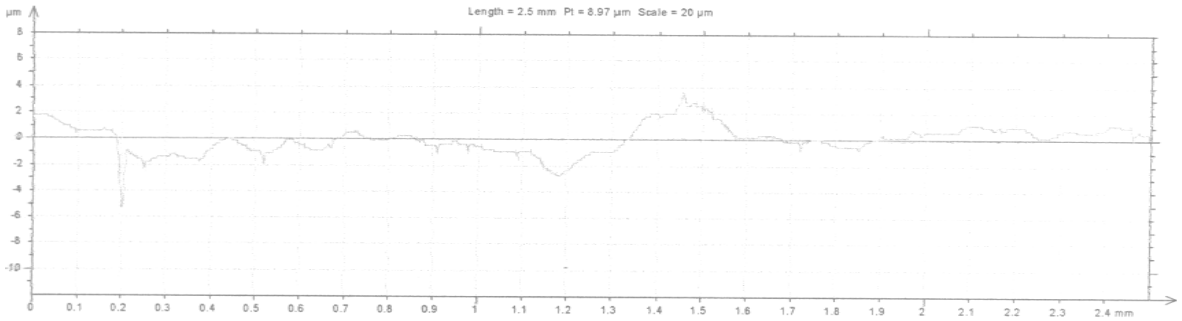
b) Final profile graph for sample 3

Fig.6. Profile graphs for sample 3

The profile graphs for sample 4 it is presented in figure 7.



a) Initial profile graph for sample 4

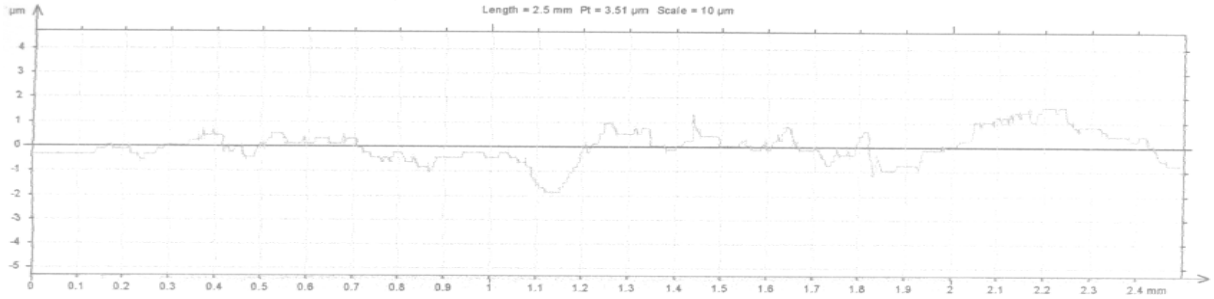


b) Final profile graph for sample 4

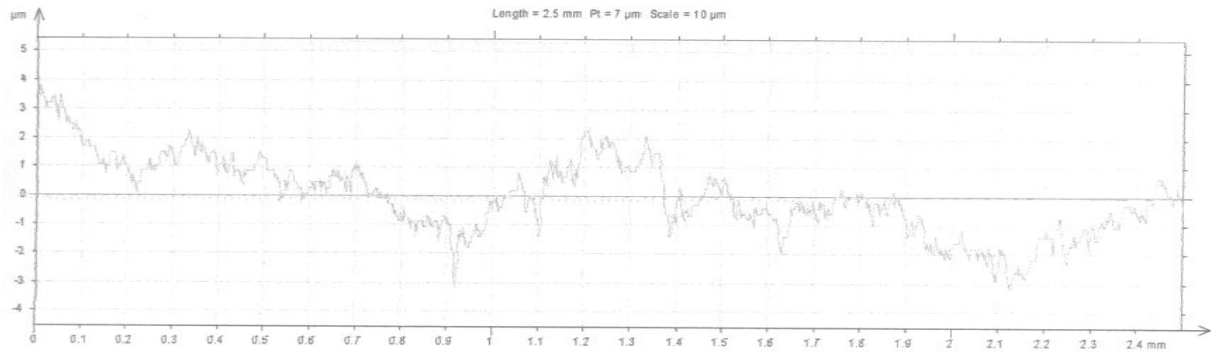
Fig.7. Profile graphs for sample 4

At sample 4 the peak after erosion tests are rounded as we could observe from fig.7 which indicate a good erosion behavior.

In figure 8 it is presented the profile graphs for sample 5 not coated.



a) Initial profile graph for sample 5



b) Final profile graph for sample 5

Fig.8. Profile graphs for sample 5

An important deterioration of roughness after erosion is observed from fig.8, asperities profile presenting sharp peaks and holes.

3. CONCLUSIONS

From profile graphs presented in fig. 4 to 8 and the dates from tab.1 and 2 we could conclude:

- For initial status:
  - roughness of layers reported at non coated sample is smaller at samples labeled 1, 2 and 4 and greater at sample 3;
  - the smallest roughness was obtained at sample labeled 1.
- After erosion tests:
  - asperities of the profiles were different depending of each layer type;
  - at sample 1 asperities profile after erosion is similar with initial one but presents many and more than initial sharp holes, which indicate the layer dislocation;
  - at sample 2 profile asperities after erosion is significant modified related to the initial profile, on surface being observed important holes greater than layer thickness:
  - at sample 3 the very sharp peaks were removed, but were created after erosion tests many cavities with sharp holes with dimensions greater than layer thickness;
  - at sample 4 the peak after erosion tests are rounded which indicate a good erosion behavior;
  - at non coated sample labeled 5 was observed an important deterioration of surface, profile roughness presenting sharp peaks and holes.

As a conclusion, the best erosion behavior presents sample 4 with base material AISI 316L coated on active surface with multilayer's of TiN / ZrN;

ACKNOWLEDGMENTS

We are gratefully to INOE 2000 Magurele for realizing the hard layers.

REFERENCES

1. SCHILKE, P.E., Advanced Gas Turbine Materials and Coatings, General Electric Company GER-3569G, New York, 2004
2. ONITIU, O., RIPEANU, R.G., TUDOR, I., Nitriding Treatments Influence Above Tribologic Behavior of Austenitic Stainless Steels, Bulletin of the Polytechnic Institute of Iasi, Vol. **LVII(LXI)** (2), 2011, 53-58;
3. RIPEANU, R.G., ISPAS, V., ISPAS, D., Austenitic stainless steel type AISI 316L corrosive behavior in hair shampoo medium, Journal of the Balkan Tribological Association, **18** (1), 2012, 36-43;
4. RIPEANU, R.G., TUDOR, I., DINU, F., Research about the efficiency of active anode protection at centrifugal pumps, Journal of the Balkan Tribological Association, **15** (.2), 2009, 193-201;
5. TUDOR, I., RIPEANU, R.G., TANASE, R., Microstructure researches above materials which will be used for coating turbine rotor surfaces, (in Romanian), Research contract no.7, Petroleum-Gas University of Ploiesti. 2003,

CORRESPONDENCE

Razvan George RIPEANU
Petroleum-Gas University of Ploiesti, Blvd. Bucuresti, no.39, 100680, ROMANIA
e-mail: rrapeanu@upg-ploiesti.ro

Tribological Journal BULTRIB, **Vol. IV, 2014**
Papers from the International Conference **BULTRIB '13**
October 24-26, 2013, Sofia
Society of Bulgarian Tribologists
Technical University of Sofia

STUDIES REGARDING IMPROVING SEALING AT THREE CONE BITS BEARINGS

Razvan George RIPEANU, Vasile ISPAS, Dorina ISPAS

Abstract: *Sliding bearings at three cone bits are lubricated in heavy conditions. To improve bearing durability the sealing must avoid drilling mud to enter in the bearing. Sealing material, as VITON, NBR and HNBR, behavior with temperature, with different compression loads and also O-ring seat dimensions were studied in order to improve the durability of bearings.*

Key Words: *bearing, O-ring, plastic deformation, temperature*

1. INTRODUCTION

At three cone drill bearing active surfaces we have abrasive, erosive, corrosive, adhesive and impact wear at variable loads. These working heavy conditions are rarely meet in surface industry, so construction, materials and technology used at drill bits manufacturing have to solve many problems.

As shown in figure 1, [1, 2], sealing's at three cone bits bearings consist of two radial sliding bearings (*6*), one axial sliding bearing, and a radial and axial ball bearing (*4,5*). This entire are inside a conic surface sealed with O-ring placed at cone base. During the drilling radial and axial sliding bearings must realize loads compensation. Each bearing load depends of radial clearance and of relative surfaces positions. At the start of drilling the axial-radial ball bearing must be discharged and the cone base surface must be not in contact with drill button, this two surfaces being not designated to commentate axial loads. During bore hole correcting, axial load is compensated by ball bearing. Durability of three cone bearings depends by sealing capacity of O-ring. In figure 1 we could see that sliding bearings *5* and *6* is close of sealing *3*. It's very important that lubricant to not be contaminated with drilling fluid. Because properties of rubber used at sealing are maintained till 80^0C the temperature in sliding bearings must not exceed this temperature. When drilling mud enter in the bearings appear an intense abrasive and corrosive wear. Paper presents the results and the solutions to raise the durability at three cone bits sliding bearings. Grease lubricant type is also important above wear and friction behavior.

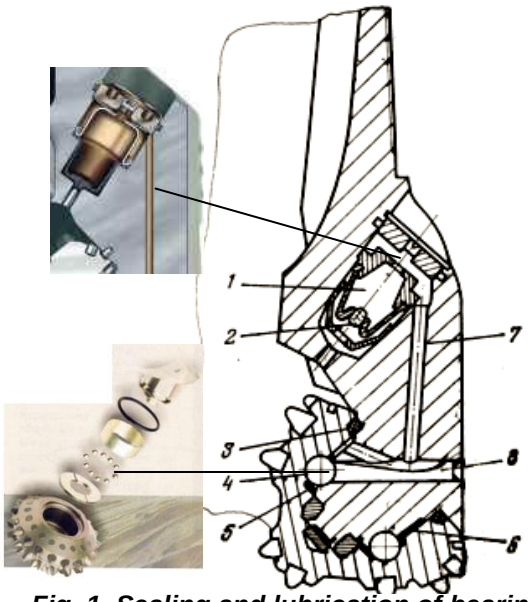
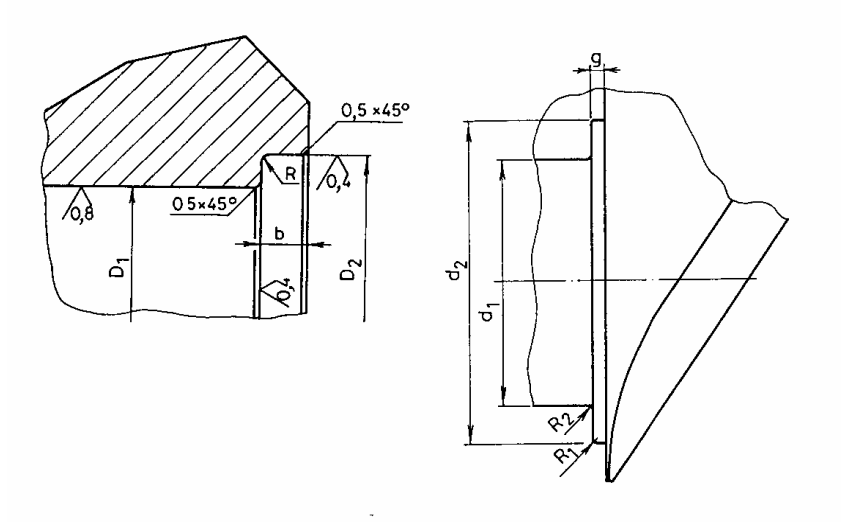


Fig. 1. Sealing and lubrication of bearings

1- lubricant reservoir; 2- ball valve; 3- O-ring: 4,5-axial-radial ball bearing;6- radial sliding bearing; 7,8 channels

1.1 Dimensions of O-ring seat

Characteristics surfaces which delimitate the O-ring seat are presented in figure 2 and table 1, [3].



a- cone *b- button*

Fig. 2. Dimensions for O ring seat

Nominal dimensions of seat where are placed rubber O-ring it is shown in figure 3 and the tightening of elastic ring in table 2, [3].

Table 1. Dimensions of seat sealing with O-ring at drill cone

Type and drill dimensions	Cone				Button				
	D_1	D_2	b	R	d_1	d_2	g	R_1	R_2
S – 8 3/8 GJ SM – 8 3/8 KGJ MA – 8 3/8 DGJ MTA – 8 3/8 DGJ TEA – 8 3/8 KGJ	60 C8 +0,186 +0,140	69,6 H8 +0,046 0	8 js13 +0,110 -0,110	1,6	60 h8 0 -0,046	69,4 h10 0 -0,120	0,5	0,2	2

Starting with drill assembling rubber O-ring presents important tightens.

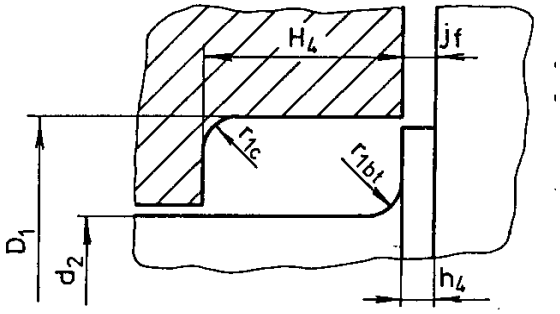


Fig.3. Nominal dimensions of seat where are placed rubber O-ring

We could observe that seat length $L = b - j_f$, [mm] and seat width $H = \frac{D_1 - d_2}{2}$,[mm]

Table 2. Tightening of elastic ring

Type and drill dimensions	L	H	$j_{rb\ min}$	d_i	S_{max}	
	mm	mm	mm	mm	mm	%
S – 8 3/8 GJ SM – 8 3/8 KGJ MA – 8 3/8 DGJ MTA – 8 3/8 DGJ TEA – 8 3/8 KGJ	7,5	4,8	0,070	5,7 ± 0,15	0,9	15,8

The recommendation for internal diameter of O-ring is to be increased with 6% and for external O-ring diameter to be reduced with 3% [3, 6]. Taking account of these recommendations the dimensions for:

-diameter of shaft surface at assembling:

$d=1.06 \cdot d_0$;

-diameter of bore surface at assembling:

$D=0.97 \cdot (d_0 + d_i)$

were d_0 is the internal nominal diameter of toroid ring;

d_i - the transversal diameter of toroid ring.

Plastic deformation depends mainly of rubber type, shape and quality, value and time of tightening, temperature and working medium. Paper presents the results obtained above different rubber types tested in different mediums with different tightening in order to improve three cone bits bearing sealing.

2. EXPERIMENTS

Tests were made in order to establish the plastic compression deformation obtained at different temperatures of 20^0C and 50^0C and with different tightening of 10, 20 and 30% in the presence of grease drill lubricant with respecting Romanian standard STAS 12043/2-81, [3, 4, 5].

In figure 4 it is shown the dimensions of rubber O-ring.

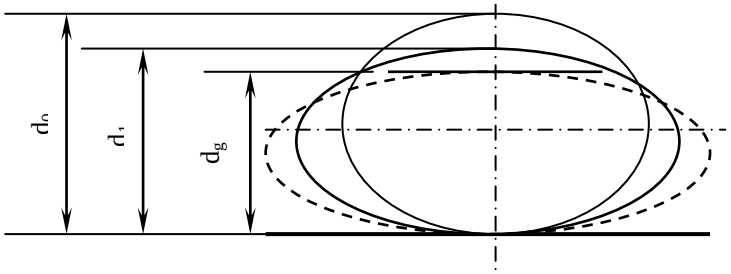


Fig.4. Dimensions of rubber O ring

d_0 – O-ring diameter before deformation; d_g – O-ring diameter in time of deformation with load applied; d_1 – O-ring diameter after deformation and without load.

The device used it is shown in figure 5.

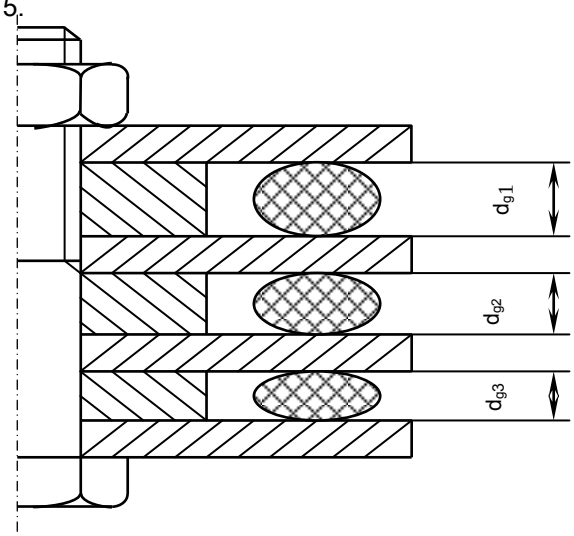


Fig.5. Device used for tests

Testing conditions were:

- ring with initial cross section nominal diameter *do* =5.7 mm;
- internal initial ring diameter $\phi = 59.2$ mm;
- rubber materials VITON, HNBR, NBR;
- d_{g1}=5.19 mm, d_{g2}=4.62 mm, d_{g3}=4.04 mm corresponding for 10. 20. 30% tightening;
- working medium- grease type UM 185 Li 2
- tempearature: 20^0C and 50^0C
- time for maintained at temperature 22 hours;
- 30 minutes relaxing time before measuring d_1.

In figure 6 it is presented the plastic deformation D_c % function of initial deformation for VITON rubber, in figure 7 for NBR rubber and in figure 8 for HNBR rubber, [3, 4].

$$D_c = \frac{d_0 - d_1}{d_0 - d_g} \cdot 100\%$$

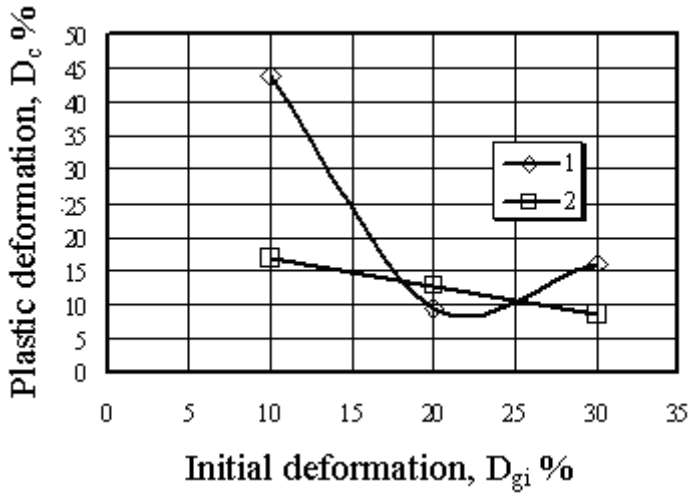


Fig.6. Plastic deformation vs. initial deformation at 1-50^{0}C, 2-20^{0}C for VITON rubber O-ring

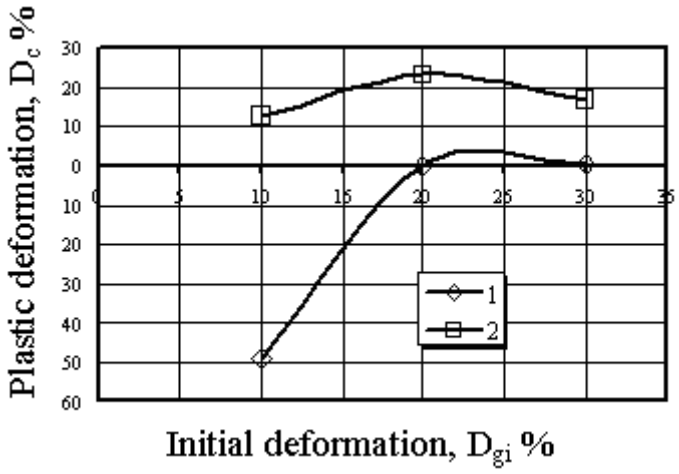


Fig.7. Plastic deformation vs. initial deformation at 1-50^{0}C, 2-20^{0}C for NBR rubber O-ring

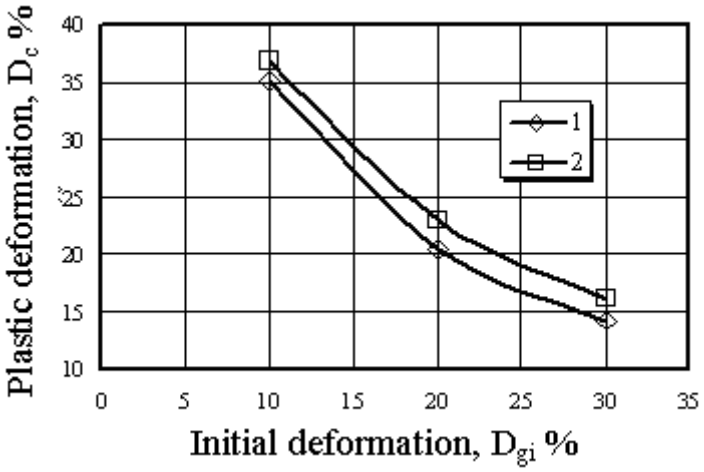


Fig.8. Plastic deformation vs. initial deformation at 1-50^{0}C, 2-20^{0}C for HNBR rubber O-ring

We could observe from figures 6, 7 and 8 as a general behavior for tested rubber O-rings that plastic deformation rise with temperature. Meanwhile between different rubber types appear differences. At NBR rubber O-ring especially at 50^{0}C O-ring diameters is greater that the initial one (fig.7). HNBR O-ring diameters were smallest influenced by initial deformation and by the temperatures.

In figure 9, 10 and 11 are presented the reduction of initial cross diameters of O-rings due to initial deformation and temperatures for O-rings made of VITON, NBR and HNBR rubber types, [3, 5].

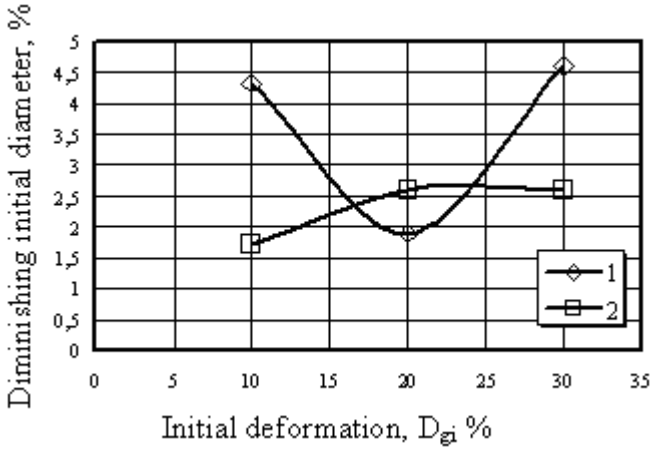


Fig.9. Reducing initial diameter vs.initial deformation at 1-50^{0}C, 2-20^{0}C for VITON rubber O-ring

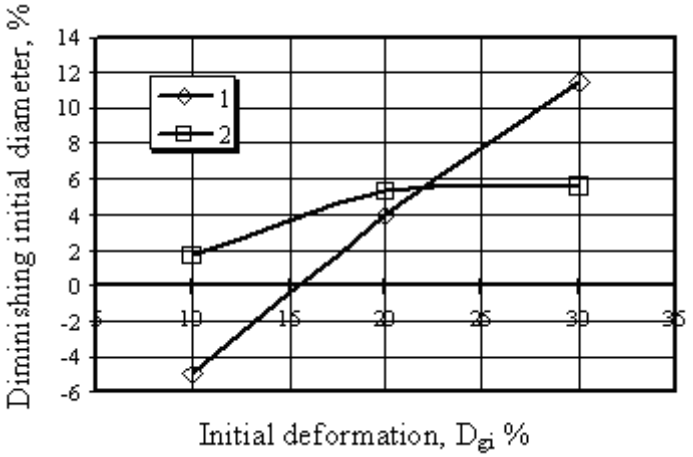


Fig.10. Reducing initial diameter vs.initial deformation at 1-50^{0}C, 2-20^{0}C for NBR rubber O-ring

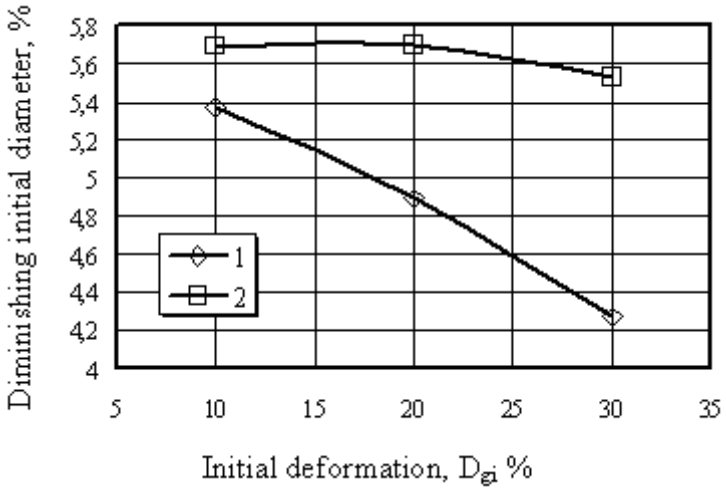


Fig.11. Reducing initial diameter vs.initial deformation at 1-50^{0}C, 2-20^{0}C for HNBR rubber O-ring

The less influenced by temperature and initial tightness are O-rings made of HNBR rubber (fig.11) were we could observe also a diminishing of plastic deformation vs. temperature and initial deformation. At VITON O-ring (fig.9) at 50^{0}C was observed a diameters diminishing with 20% and at NBR (fig.10) at 50^{0}C a diameters diminishing with 10%, [3].

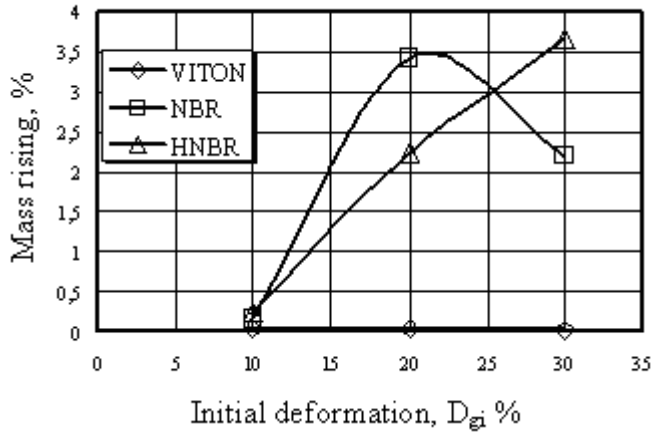


Fig.12. Mass rising vs. initial deformation at 1-50^{0}C, 2-20^{0}C for rubber O ring at 20^{0}C

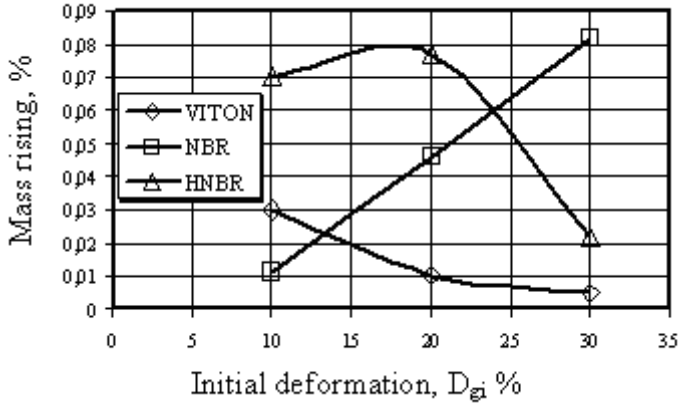


Fig.13. Mass rising vs. initial deformation at 1-50^{0}C, 2-20^{0}C for rubber O ring at 50^{0}C

From figures 12 and 13 could be observed for all O-rings rubber types tested that mass rising is diminished with temperature, [3]. The smallest mass risings were observed at VITON rubber.

At NBR rubber at initial deformation of 20% a maximum of mass rising was observed.

3. CONCLUSIONS

Based on theoretical –experimental researches we could conclude:

- Plastic deformation measured immediate after removing from testing device at all rubber types O-rings rise with temperature:
- O-rings of VITON rubber plastic deformation is sensible influenced by temperature;
- O-rings of NBR rubber at 50^0C at 20% initial deformation has a plastic deformation negative which indicate a tendency of absorption of oil from grease;
- O-rings of HNBR rubber were small influenced by initial deformation and temperature and are considered the most stabile materials.
- Plastic deformation after a period of relaxing at ambient temperature was different depending temperature and initial deformation:
- O-rings of VITON rubber at 50^0C presents a critical deformation of 20% with a maximum reduction of initial diameter;
- O-rings of NBR rubber at 50^0C and initial deformation smaller of 15% have a greater final diameter;
- O-ring of HNBR rubber at 50 ^{0}C presents the smallest tendency of diminishing initial diameter.
- Oil absorption from grease depends of temperature:
- VITON rubber has the smallest absorption tendency at 20 ^{0}C and at 50 ^{0}C;
- NBR and HNBR rubber at 20 ^{0}C absorption is greater than at 50 ^{0}C;

REFERENCES

1. RIPEANU R.G., TUDOR I., DRUMEANU A.C., Research above rising durability at three cone drill bits (in Romanian), Research contract no.45, Petroleum-Gas University of Ploiesti, 2008.
2. ZIDARU I., RIPEANU R.G., TUDOR I., DRUMEANU A.C., Research regarding the improvements of tribological behavior in three cone bits bearings, FME Transactions, **37**, (2), 2009, 99-102,.
3. TUDOR, I., ISPAS, V., ISPAS, D., RIPEANU R.G., Research theoretical and experimental above improving bits bearings (in Romanian), Research contract no.17, Petroleum-Gas University of Ploiesti, 2003.
4. ZIDARU, I., DRUMEANU, A. C., TUDOR, I. Some considerations concerning the friction moment of three-cone bits sealing rings. Journal of the Balkan Tribological Association, **11**, (4), 2005, 529 – 534.
5. Drumeanu, A. C., Zidaru, I.,, Tudor, I., Some consideration concerning the oversteain of the O rings used at bits bearing sealing, Petroleum-Gas University of Ploiesti Bulletin, Technical Series, **62**, (2), 2010, 189-193.
6. . XXX Joints toriques de precision et joints toriques vulcanises Kubo-Tech. www.kubotech.at

CORRESPONDENCE

Razvan George RIPEANU
Petroleum-Gas University of Ploiesti, Blvd. Bucuresti, no.39, 100680, ROMANIA
e-mail: rrapeanu@upg-ploiesti.ro

Tribological Journal BULTRIB, **Vol. IV, 2014**
Papers from the International Conference **BULTRIB '13**
October 24-26, 2013, Sofia
Society of Bulgarian Tribologists
Technical University of Sofia

INVESTIGATION ON SURFACE ROUGHNESS OF CARBON STEEL MACHINED BY ABRASIVE WATER JET USING TAGUCHI METHOD

Miroslav RADOVANOVIC

Abstract: *Taguchi method is employed to investigate surface roughness of carbon steel machined by abrasive water jet. Design of experiment was conducted using L_8 orthogonal array with four factors (water pressure, abrasive flow rate, traverse rate and standoff distance) and two levels. Analysis of means, analysis of variance and signal-to-noise ratios are employed to determine influence of factors on surface roughness and to determine optimal factor levels. Regression analysis was used to find correlation between surface roughness and factors.*

Key Words: *Abrasive water jet machining, surface roughness, Taguchi method*

1. INTRODUCTION

Abrasive water jet (AWJ) machining is an advance non-conventional technology. AWJ machining is like grinding, except that abrasive particles are moved through the material by water jet rather than by a solid wheel. Almost any material can be cut. Mix high pressure water jet with abrasives gives an effective cutting tool. AWJ can cut a wide range of thickness. Maximum thickness is 100 mm for stainless steel, 120 mm for aluminum, 140 mm for stone, 100 mm for glass, but not limited. AWJ makes it possible to cut random contours, very fine tabs and filigree structures. Tolerances of ±0.1 mm can be realized in metal cutting. There is no thermal effect on the workpiece. AWJ produces very little lateral force. Scheme of abrasive water jet machining is shown in Fig. 1.

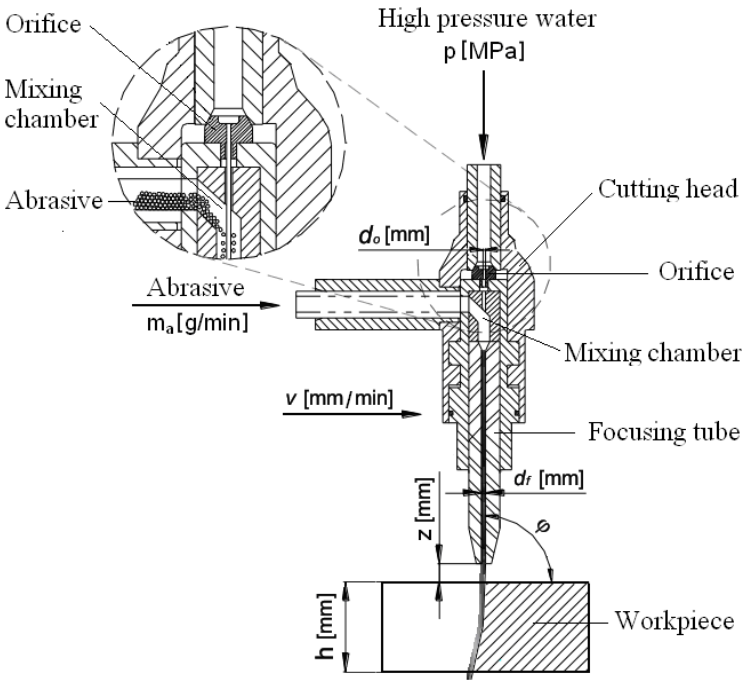


Fig. 1. Abrasive water jet machining

When cutting with AWJ high pressure pump produces water pressure up to 600 MPa. High pressure supply line directs the pressurized water from the pump via accumulator to the cutting head. Cutting head consists of orifice, mixing chamber and focusing tube. Orifice is made of sapphire, ruby or diamond. Orifice is with diameter of 0.15 to 0.35 mm. Focusing tube is made of hard metal. Focusing tube is with diameter of 0.54 to 1.1 mm and length of 50 to 100 mm. Water is pressed out of the orifice in form of jet at a speed of approximately 900 m/s – nearly three times the speed of sound. Result is a very thin, extremely high velocity water jet. Solid abrasive particles are added and mixed with the water jet in the mixing chamber of the cutting head and then focused by a focusing tube. High speed of the water jet creates a partial vacuum in the mixing chamber so that abrasive particles are sucked in and flushed away by the water jet. Focusing tube focuses and directs the abrasive water jet to the workpiece. Abrasive water jet cuts workpiece along the contour guided by NC programme.

Many factors affect on abrasive water jet machining. AWJ machining factors can be classified into categories that relate to: workpiece (material type, thickness, chemical structure, hardness, toughness, grain size), high pressure pump (pump pressure, water flow rate, water purity, accumulator volume), abrasive (material type, hardness, particle diameter, particle shape, particle size distribution, humidity), cutting head (orifice diameter, orifice material, focusing tube diameter, focusing tube length, focusing tube material), motion system (precision, accuracy, stiffness, working conditions) and process (water pressure, traverse rate, abrasive flow rate, standoff distance, impact angle, traverse direction). AWJ machining performances can be classified into categories that relate to: process (orifice wear, focusing tube wear, temperature, noise, vibration), quality (form deviations, dimension deviations, cut quality: surface roughness, burr, depth of cut, kerf width, kerf taper), productivity (machining time, productivity), and economy (machining cost, power consumption, abrasive consumptions).

There are some studies regarding investigation of surface roughness in AWJ machining using Taguchi method. Babu et al. in [1] were presented a study on the use of single mesh size abrasives in AWJ machining of aluminum 6063 T6. L_9 orthogonal array with four factors (single mesh size abrasives, water pressure, traverse rate and abrasive flow rate) and three levels is employed to investigate depth of cut, kerf width, kerf taper and surface roughness. Azmir et al. in [2] were presented an investigation on AWJ machining of aramid fibre reinforced plastics composite using Taguchi approach. L_{81} orthogonal array with four factors (water pressure, abrasive flow rate, standoff distance and traverse rate) and three levels is employed to investigate surface roughness and kerf taper. Kechagias et al. in [4] were presented a study of the influence of sheet thickness, focusing tube diameter, standoff distance and traverse rate on surface quality characteristics in AWJ machining of transformation-induced plasticity sheet steels. L_{18} orthogonal array with four factors and three levels is employed for investigation. Aydin et al. in [5] were presented an investigation on surface roughness of granite machined by AWJ using Taguchi method. L_{16} orthogonal array with five factors (traverse rate, abrasive flow rate, standoff distance, water pressure and abrasive size) and four levels is employed to investigate surface roughness.

2. DESIGN OF EXPERIMENT AND RESULTS

Experimental investigation was conducted in order to study the influence of factors on surface roughness in abrasive water jet machining of carbon steel. The equipment used for machining the samples was abrasive water jet cutting machine Hydro Jet Eco 0615 with pump pressure of 150 MPa, power of 7.5 kW and water flow rate of 2.4 l/min. Cutting head is with orifice diameter of 0.35 mm and a focusing tube diameter of 1.02 mm. Focusing tube length is 76 mm. All experiments were conducted with water pressure of 150 MPa. Abrasive material was Garnet with mesh size of 80. Workpiece material used in experimental tests was carbon steel EN S235, thickness of 6.5 mm. Chemical and mechanical characteristics of EN S235 are shown in Table 1.

Table 1. Chemical and mechanical characteristics of S235

C %	Si %	Mn %	P %	S %	N %	Cu %	Cr %	Ni %	Mo %	Al %	V %	$R_{p0.2}$ N/mm^2	R_m N/mm^2	A %
0.13	0.25	0.58	0.013	0.008	0.01	0.32	0.08	0.10	0.013	0.033	0.001	240	360-440	25

Design of experiment was conducted using Taguchi method. Taguchi method [7] is a relatively simple and powerful tool for design of experiment, analysis and optimization of the process. Taguchi method includes experimental design, conducting an experiment, data analysis, selection of factors, determining the optimal factor levels, and verification. Taguchi method uses a special design of orthogonal arrays where the experimental results are transformed into signal-to-noise (S/N) ratios as the measure of the quality characteristic. Orthogonal array and signal to noise (S/N) ratios are two

major tools used in Taguchi method. Depending on the criterion for the quality characteristic to be optimized, the S/N ratio characteristics can be divided into three stages: smaller-the-better, larger-the-better, and nominal-the-better. Larger S/N ratio corresponds to the better performance characteristic. Influence of factors on process performance can be determined using the analysis of means (ANOM) and analysis of variance (ANOVA). Optimal level of the factor is the level with the highest S/N ratio. A confirmation experiment is the final step in Taguchi method and is used to verify the optimal combination of the factor settings.

Control factors (independent variables) selected for the present investigation are: water pressure (p), abrasive flow rate (m_a), traverse rate (v) and standoff distance (h). Investigated performance (depended variable) is surface roughness (R_a). The Hommel Tester T500 was used to measure the surface roughness. Control factors and their levels are shown in Table 2.

Table 2. Control factors and levels

Code	Control factors	Levels	
		1	2
A	Water pressure, p (MPa)	130	150
B	Abrasive flow rate, m_a (g/min)	500	700
C	Traverse rate, v (mm/min)	50	100
D	Standoff distance, h (mm)	1	3

Four control factors with two levels are arranged in L_8 (2^4) orthogonal array. Table 3 shows standard L_8 orthogonal array and results. Left side of the table includes coding values of the control factors. Right side of the table includes the responses of the surface roughness (R_a), and S/N ratios (η).

Table 3. Orthogonal array and reponses

No	Control factors				Ra	η
	A	B	C	D	μm	dB
1	1	1	1	1	4.72	-13.4788
2	1	1	2	2	4.77	-13.5704
3	1	2	1	2	4.56	-13.1793
4	1	2	2	1	4.64	-13.3304
5	2	1	1	2	4.47	-13.0062
6	2	1	2	1	5.02	-14.0141
7	2	2	1	1	4.50	-13.0643
8	2	2	2	2	4.76	-13.5521
					$\overline{\eta}$ =	-13.3994

3. ANALYSIS OF RESULTS, OPTIMIZATION AND CONFIRMATION TEST

To analyze the effect type of factors on surface roughness Normal plot and Pareto chart were generated. In Fig. 2 and Fig. 3 are shown normal plot of the standardized effects and Pareto chart.

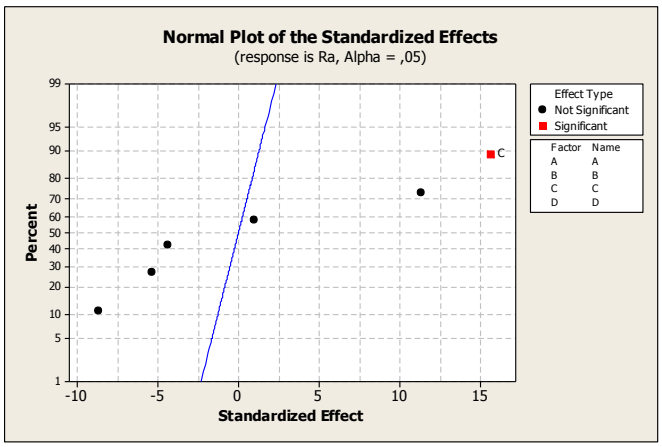


Fig. 2. Normal plot

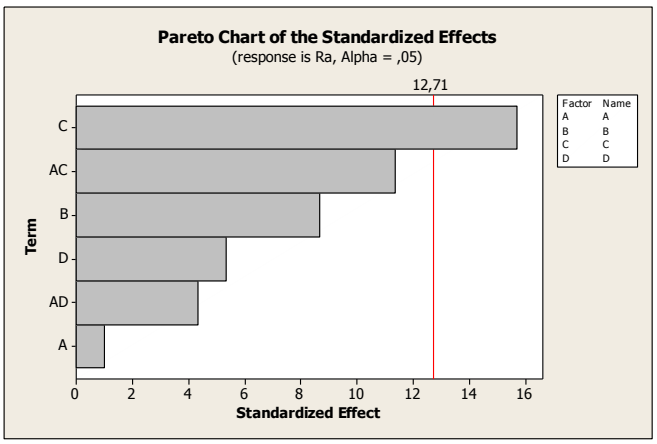


Fig. 3. Pareto chart

From Fig. 2 and Fig. 3 it is seen the effect type of factors and interactions (significant and not significant). Traverse rate is significant factor on surface roughness. Water pressure, abrasive flow rate and standoff distance are not significant factors. Interactions are not significant on surface roughness. Influence of factors on surface roughness was analyzed using the analysis of means and analysis of variance. Main effects plot for surface roughness (Ra) is presented in Fig. 4. The verticality of the line indicates the effect of factors.

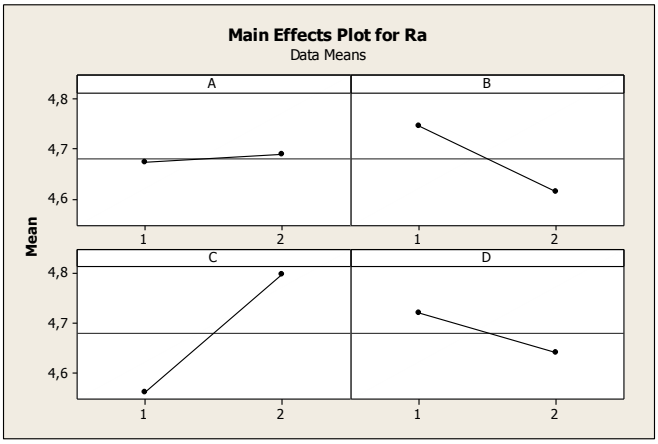


Fig. 4. Main effects plot for surface roughness

From Fig. 4 it is seen that as the water pressure and traverse rate increase the surface roughness increases. If the abrasive flow rate and standoff distance increase the surface roughness decreases. Fig. 4 indicates that the traverse rate is more significant factor as the slope gradient is big.

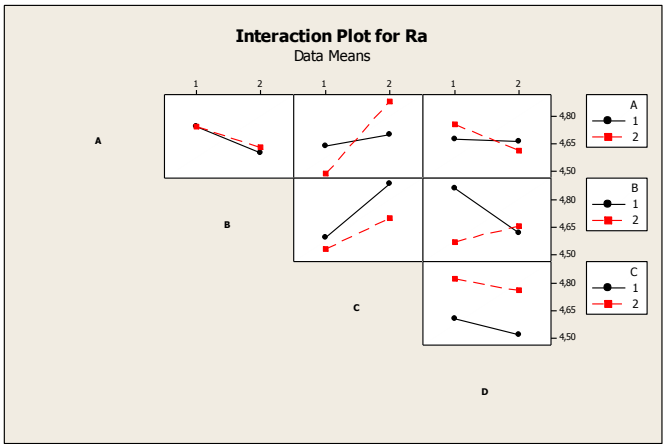


Fig. 5. Interaction plot for surface roughness

Interaction plot for surface roughness (Ra) is presented in Fig. 5. Parallel lines indicate that the interactions are not significant factors, such as interaction CD.

Objective of the experiment is to optimize the cutting conditions for AWJ machining with regard to the minimum surface roughness. For this purpose was used smaller-the-better characteristic defined as:

$$\eta = -10\log_{10}\left(\frac{1}{n}\sum_{i=1}^{n} y_i^2\right), \tag{1}$$

where is: η-signal to noise (S/N) ratio, n-number of repetitions of the experiment, y_i-measured values of the quality characteristic.

High S/N ratios are always preferred in a Taguchi's experiment. For smaller-the-better characteristic, this translates into lower process average.

Analysis of means (ANOM) is a statistical approach of estimating the mean S/N ratios for each parameters and each of its levels. The mean S/N ratios smaller-the-better for each level of the control factors is shown in Table 4.

Table 4. Response table for S/N ratios

Code	Control factors	Level		Max-Min	Rank
		1	2		
A	Water pressure, p (MPa)	-13.39*	-13.41	0.02	4
B	Abrasive flow rate, m_a (g/min)	-13.52	-13.28*	0.24	2
C	Traverse rate, v (mm/min)	-13.18*	-13.62	0.43	1
D	Standoff distance, h (mm)	-13.47	-13.33*	0.14	3

* Optimum level

Table 4 shows the rank of factors. In the first place is traverse rate, in the second place is abrasive flow rate, in the third place is standoff distance, and in the fourth place is water pressure. Results from Table 4 suggest that the optimum values of control factors within the tested range are given by $A_1B_2C_1D_2$, i.e. the optimal combination of the process factors could be achieved by using a water pressure of 130 MPa, abrasive flow rate of 700 g/min, traverse rate of 50 mm/min, and standoff distance of 3mm.

Analysis of variance (ANOVA) is used to estimate the relative significance of each factor. In ANOVA, the ratio between the variance of factor and the variance of error is called Fisher's ratio (F). It is used to determine whether the factor has a significant effect on the quality characteristic by comparing the F table value (F_α) at the α significance level. Greater the F-ratio more significant is the factor. ANOVA was carried out to find the relative effect of factors on the surface roughness. Table 5 shows analysis of variance for S/N ratios.

Table 5. Analysis of variance (ANOVA) for S/N ratios

Code	DF	SS	MS	F	p	%
A	1	0,000756	0,000756	0,33	0,669	0.10
B	1	0,111247	0,111247	48,32	0,091	14.70
C	1	0,377756	0,377756	164,07	0,050	49.91
D	1	0,041988	0,041988	18,24	0,146	5.55
AC	1	0,196321	0,196321	85,27	0,069	25.94
AD	1	0,026508	0,026508	11,51	0,182	3.50
Error	1	0,002302	0,002302	-	-	0.30
Total	7	0,756877	-	-	-	100
DF - degree of freedom, SS - sum of square, MS - mean square, F - variance ratio, p – value, and % - percent contribution						

Standard F table value at 95% confidence level is $F_{0.05,1,1}$=161.45. From Table 5 it can be seen that process factors water pressure, abrasive flow rate, traverse rate and standoff distance have effect on the surface roughness with contribution of 69.51%. Traverse rate is significant factor with strong (clearly statistically significant) effect on the surface roughness and effects on surface roughness with contribution of 49.91%. Water pressure, abrasive flow rate and standoff distance are not significant factors. Water pressure effects on surface roughness with contribution of 0.10%, abrasive flow rate effects with contribution of 14.70% and standoff distance effects with contribution of 5.55%. From

Table 5 it can be seen that the interactions are not significant factors. Interaction water pressure-traverse rate effects on surface roughness with contribution of 25.94%, and interaction water pressure-standoff distance effects with contribution of 3.50%.

Regression analysis (RA) was used to find correlation between surface roughness and factors. Regression analysis is a powerful tool for mathematical modeling real process. RA includes the experimental data, mathematical methods and statistical analysis. For mathematical model was selected the quasi-linear model:

$$Y = Y_e - \varepsilon = \beta_0 + \sum_{i=1}^{k} \beta_i X_i + \sum_{i=1}^{k-1} \sum_{j=i+1}^{k} \beta_{ij} X_i X_j \ , \tag{2}$$

where Y is the estimated response, Y_e is the measured response, X_i are the factors, ε is the experimental error, k is number of factors, β_0 is the free term, β_i is the linear effect and β_{ij} is the interaction effect.

Quasi-linear regression equation representing the surface roughness (Ra) can be expressed as a function of AWJ factors such as water pressure (p), abrasive flow rate (m_a), traverse rate (v) and standoff distance (h). The following regression equation, with coefficient of determination of R^2=99.8%, was obtained:

$$R_a = 4.68 - 0.0075p + 0.065m_a - 0.1175v + 0.04h + 0.085pv - 0.0325ph \ , \tag{3}$$

Surface plot of surface roughness (Ra) versus abrasive flow rate (m_a) and traverse rate (v), according equation (3), is shown in Fig. 6.

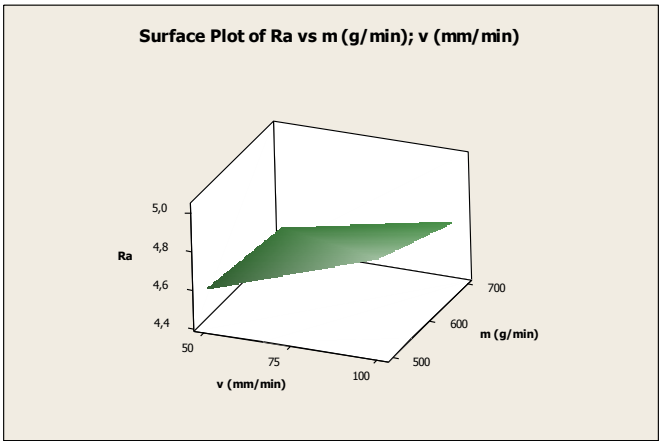


Fig. 6. Surface plot of surface roughness versus abrasive flow rate and traverse rate

Confirmation test is the final step in Taguchi method and is used to verify the optimal combination of the factor settings. For that purpose, a confirmation test should be carried out implying the optimal levels of the factors. Therefore, a confirmation test was performed using optimal condition $A_1B_2C_1D_2$ for surface roughness.

The predicted S/N ratio using the optimal levels of the design factors ($\hat{\eta}_{opt}$) can be calculated as:

$$\hat{\eta}_{opt} = \overline{\eta} + \sum_{i=1}^{p} \left(\overline{\eta}_{i,opt} - \overline{\eta} \right), \quad \overline{\eta} = \frac{1}{n_t} \sum_{i=1}^{n_t} \eta_i \ , \tag{4}$$

where $\overline{\eta}_{i,opt}$ is the mean S/N ratio for i-th factor at the optimal level, $\overline{\eta}$ is the total mean S/N ratio, k is the number of factors that significantly affect the quality characteristic, n_t is the total number of trials, and η_i is the S/N ratio in i-th trial in the orthogonal array (OA).

$$\hat{\eta}_{opt} = -13.40 + (-13.39 + 13.40) + (-13.28 + 13.40) + (-13.18 + 13.40) + (-13.33 + 13.40) = -12.98\, dB \quad , \tag{5}$$

In order to statistically judge the closeness of predicted to observed data, the confidence interval was determined. A confidence interval (CI) can be calculated using the equation [5]:

$$CI = \pm\sqrt{F_{\alpha(1,f_e)} V_e \left(\frac{1}{n} + \frac{1}{n_{ver}}\right)} \quad , \tag{6}$$

where $F_{\alpha(1,f_e)}$ is the F value from the F-table at a required confidence level of 1-α=0.95 at degree of freedom DF=1, and degree of freedom of error f_e=1, $F_{0.05(1,1)} = 161.45$, V_e=0,002302 is the error variance, n_{ver}=1 is the validation test trial number, and $n = \frac{N}{1+\nu} = 1.6$ is the effective number of replications where N=8 is the total number of experiments and ν =1x4=4 is the total degree of freedom (DF) of all parameters.

$$CI = \pm\sqrt{161.45 \cdot 0.002302 \cdot \left(\frac{1}{1.6} + \frac{1}{1}\right)} = \pm 0.78 \quad , \tag{7}$$

The 95% confidence interval of the predicted optimal S/N ratio is:

$$(\hat{\eta}_{opt} - CI) < \hat{\eta}_{opt} < (\hat{\eta}_{opt} + CI), \tag{8}$$

$$-13.76 < \hat{\eta}_{opt}(dB) < -12.20\,, \tag{9}$$

Real value of the surface roughness can calculate based on equation (1) as:

$$R_a = 10^{-\frac{\hat{\eta}_{opt}}{20}}\,, \tag{10}$$

$$R_a = 10^{-\frac{-12.98}{20}} = 4.46\ \mu m\,, \tag{11}$$

Predicted and the test observed value of surface roughness at the optimum levels of the factors are shown in Table 6.

Table 6. Predicted values and test results

	Optimal factor settings	
	Prediction	Test
Level	$A_1B_2C_1D_2$	$A_1B_2C_1D_2$
Surface roughness Ra (μm)	4.46	4.56
S/N ratio (dB)	-12.98	-13.18

Since the prediction S/N ratio is within confidence interval (CI), the combination of factor levels for optimization of surface roughness can be validated.

4. CONCLUSION

Factors of abrasive water jet machining, water pressure, abrasive flow rate, traverse rate and standoff distance, have effect on the surface roughness with contribution of 69.51%. Traverse rate is significant factor with strong effect on the surface roughness and effects on surface roughness with contribution of 49.91%. Water pressure effects on surface roughness with contribution of 0.10%, abrasive flow rate effects with contribution of 14.70%, and standoff distance effects with contribution of 5.55%. Interactions effect on surface roughness with contribution of 29.44%. Interaction water pressure-traverse rate effects on surface roughness with contribution of 25.94%, and interaction water pressure-standoff distance effects with contribution of 3.50%. If the water pressure and traverse rate increase the surface roughness increases. If the abrasive flow rate and standoff distance increase surface roughness decreases. Optimal levels of factors based on surface roughness in abrasive water jet machining using Taguchi method are given by $A_1B_2C_1D_2$, i.e. the optimal combination of the factor levels could be achieved by using a water pressure of 130 MPa, abrasive flow rate of 700 g/min, traverse rate of 50 mm/min, and standoff distance of 3mm. Regression model gives a good correlation between the surface roughness and the factors with coefficient of determination of R^2=99.8%.

ACKNOWLEDGMENT

The paper is a result of the technological project TR35034 which is supported by the Ministry of Education, Science and Technological Development of the Republic of Serbia.

REFERENCES

1. BABU, M., CHETY, K., A study on the use of single mesh size abrasives in abrasive water jet machining, Int. J. Adv. Manuf. Technol. (2006) 29, 532-540
2. AZMIR, M., AHSAN, A., RAHMAH, A., Investigation on abrasive water jet machining of kevlar reinforced phenolic composite using Taguchi approach, ICME 2007, Dhaka, Bangladesh, AM-13
3. KECHAGIAS, J., PETROPOULOS, G., VAXEVANIDIS, N., Application of Taguchi design for quality characterization of abrasive water jet machining of TRIP sheet steels, Int. J. Adv. Manuf. Technol. 09 December 2011
4. AYDIN, G., KARAKURT, I., AYDINER K., An investigation on surface roughness of granite mechined by abrasive water jet, Bull. Mater. Sci. Vol.34, No. 4, 2011, 985-992
5. TAGUCHI, G., CHOWDHURY, S., WU, Y., Taguchi's Quality Engineering Handbook, Wiley, 2005
6. RADOVANOVIC, M., Abrasive Water Jet Machining, Proceedings of 7th International Scientific Conference "Smolyan-2005", Smolyan, Bulgaria, 2005, pp 229-234
7. HERGHELEGIU, E., RADOVANOVIC, M., BRABIE, G., TAMPU, N., Influence of abrasive material quantity on surface quality generated by abrasive water jet operation, International Journal of Modern Manufacturing Technologies, 2011, Vol. 3, No. 2, pp 43-48
8. HERGHELEGIU, E., Contributions to the optimization of the water jet working parameters, dissertation, University ″Vasile Alecsandri″ of Bacau, Industrial Engineering, Bacau, Romania, 2011
9. JANKOVIC, P., RADOVANOVIC, M., BARALIC, J., Cut quality in abrasive water jet cutting, Proceedings of 34th International Conference on Production Engineering, Niš, Serbia, 2011, pp 435-438
10. RADOVANOVIC, M., JANKOVIC, P., MADIC, M., Predictive models of traverse rate in abrasive water jet cutting based on RA and GA, Academic Journal of Manufacturing Engineering, 2012, Vol. 19, Issue 1, pp 107-112
11. RADOVANOVIC, M., DASIC, P., STEFANEK, M., Some Possibilities for Determining Abrasive Water Jet Cutting Parameters, 13. International Scientific Conference CO-MAT-TECH 2005, Trnava, Slovakia, 2005, pp 969-976

CORRESPONDENCE

Prof. Dr Miroslav RADOVANOVIC
University of Nis, Faculty of Mechanical Engineering, A. Medvedeva 14, 18000 Nis, Serbia
e-mail: mirado@masfak.ni.ac.rs

Tribological Journal BULTRIB, **Vol. IV, 2014**
Papers from the International Conference **BULTRIB '13**
October 24-26, 2013, Sofia
Society of Bulgarian Tribologists
Technical University of Sofia

PHOTOCATALYTIC DEGRADATION OF METHYL ORANGE USING MECHANOCHEMICALLY PREPARED Fe_2O_3-ZnO MIXED OXIDES DOPED WITH SILVER

Nina G. KOSTOVA, Alexander ELIYAS, Martin FABIAN, Erika DUTKOVA, Peter BALAZ

Abstract: *The mixed oxide photocatalysts were synthesized by mechanochemical method. The effect of Ag dopant also was studied. The resultant photocatalysts were characterized by X-ray diffraction (XRD) and diffuse reflectance spectroscopy (DRS). The photocatalytic activity of mixed oxides was also evaluated by degradation of methyl orange (MO) as a model compound. The experimental results showed that the prepared Ag-Fe_2O_3/ZnO photocatalyst exhibited higher photocatalytic activity for the decomposition of MO than Fe_2O_3-ZnO mixed oxide.*

Key Words: *mechanochemical synthesis, mixed oxides, dopant, photocatalysis*

ФОТОКАТАЛИТИЧНО РАЗГАЖДАНЕ НА МЕТИЛ ОРАНЖ ВЪРХУ МЕХАНОХИМИЧНО СИНТЕЗИРАНИ Fe_2O_3-ZnO СМЕСЕНИ ОКСИДИ ДОТИРАНИ СЪС СРЕБРО

Нина Г. КОСТОВА, Александър ЕЛИЯС, Мартин ФАБИАН, Ерика Дуткова,Петер БАЛАЖ

Резюме: *Смесено-оксидни полупроводници бяха получени чрез механохимичен синтез. Беше изследвно и влиянието на добавката от сребро. Получените фотокатализатори са изследвани с рентгенов фазов анализ (XRD) и дифузно отражателна спектроскопия (DRS). Фотокаталитичната активност на смесените оксиди също беше определена в реакцията на разлагане на багрило метилоранж (МО) избрано като моделно съединение. Експерименталните резултати показаха, че полученият Ag-Fe_2O_3/ZnO фотокатализатор показа по-висока фотокаталитична активност в разлагнето на МО в сравнение с Fe_2O_3/ZnO смесен оксид.*

Ключови думи: *механохимичен синтез, смесени оксиди,, добавка, фотокатализ*

1. УВОД

Опазването на околната среда е едно от основните предизвикателства в съвременния свят. Замърсяването на въздуха и водата е глобален проблем [1]. През последните петдесетина години широко се прилага фотокатализа за превенция на щетите от от замърсяване с органични вещества на водите и въздуха [2]. За тази цел се употребяват полупроводници, като например титанов диоксид или цинков оксид (ZnO) [3-4]. Цинковият оксид е достъпен, евтин и не токсичен фотокатализатор с широка забранена зона, което частично възпрепятства неговото още по-широко приложение. Усилията на изследователите за подобряване на фотокаталитичната активност на прахообразния ZnO продължават. За тази цел се прилагат различни подходи като употребата на добавки от метали като Au, V, Fe или Pt, неметали като N, S, C P [5-6]. Друг възможен подход е смесване на два полупроводника, при което се осигурява подобряване на ефективността на получения смесенооксиден фотокатализатор [7]. Прилагат се различни химични и физични методи за получаване на фотокатализатори с подобрени свойства като зол-гел, хидротермален синтез, механохимичен синтез [8-9]. Използването на планетарна топкова мелница за механохимичен синтез на смесенооксиден фотокатализатор е подходящ метод за получаване на наноразмерни прахове [10-11]. Известно е, че влиянието на преходния метал върху фотокаталитичната активност зависи от много фактори, такива като вид на добавката, метод на внасяне й както и от

количеството на внасяната добавка. В настоящото изследване среброто беше избрано за модифициране на смесените оксидни фотокатализатори. Среброто притежава полезни свойства като химична стабилност, електро и топлопроводност, антибектериостатични свойства и нелинейно оптично поведение.

Целта на настоящото изследване е подобряване на фотокаталитичната активност на смесенооксиден фотокатализатор Fe_2O_3-ZnO посредством внасяне на Ag в процеса на смилане в топкова мелница.

2. ЕКСПЕРИМЕНТАЛНА ЧАСТ

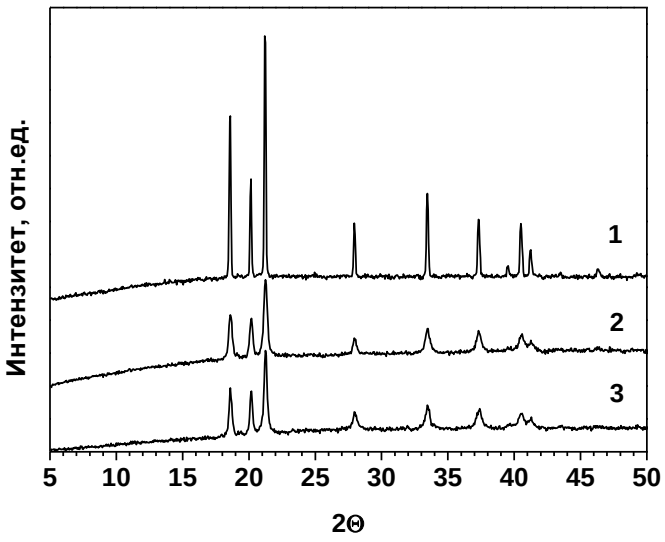
Планетарна топкова мелница (Fritch- Germany) беше използвана за получаване на образците. Съдът и използваните топки са изработени от волфрамов карбид. Обемът на съда беше 250 мл, а диаметъра на топките беше 10 мм. Във всички експериманти беше проведено влажно смилане с дестилирана вода като овлажняваща среда. Използваното при експериментите съотношение прах:топки беше 1:20. Смилането беше проведено при скорост на ротация 200 rpm, време на смилане 1 час. След смилането суспензията беше прехвърлена в стъклена чаша, последвано от сушене при 103^oC в продължение на 4 часа. Съдържанието на желязо в смесенооксидните образци беше 2 тегл.%. За внасянето на 0.5 тегл. % сребро беше използвано колоидно сребро с концентрация 0.1 г/л.

100 мг от прахобразния фотокатализатор се добавя към 100 мл разтвор на метил оранж (МО) с концентрация 10 мг/л. След това суспензията се поставя в реактора и се разбърква непрекъснато с магнитна бъркалка със скорост 500 об/мин. Прахообразтине фотокатализатори адсорбират метилоранж на тъмно. Адсорбционно-десорбционно равновесие беше достигано за 30 минути. С помощта на спринцовка се вземат 3.5 мл от суспензията. Твърдите частици се филтруват и разтвора от МО се прехвърля в кювета за спектрофотометрично определяне съдържанието на МО при λ=463 нм. След първото измерване при достигнато адсорбицонно-десорбционно равновесие се включва ултравиолетовата лампа и се измерва концентрацията на МО на равни времеви интервала.

Рентгеновите дифратограми на образците бяха записани използвайки дифрактометър ТУР М62 с Co K α лъчение. Дифузно отражателните спектри бяха получени на спектрофотометър Thermo Evolution 300 UV-vis използвайки спектралон като еталон.

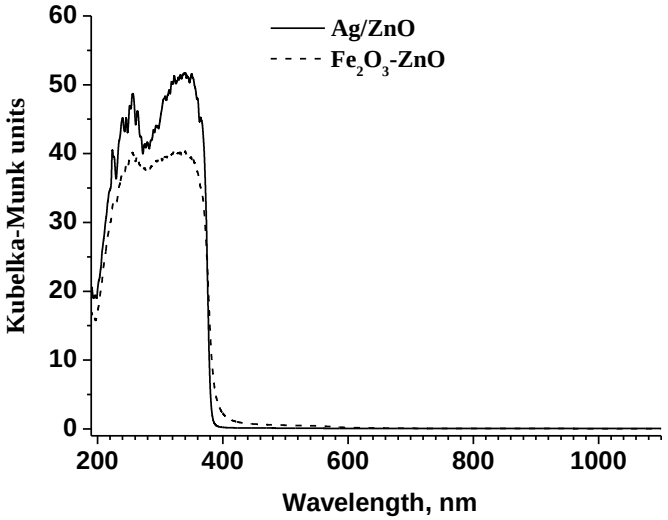
3. ЕКСПЕРИМЕНТАЛНИ РЕЗУЛТАТИ

Рентгенофазов анализ беше използван за изследване структурата и фазовия състав на механохимично синтезираните смесенооксидни фотокатализатори.



Фиг. 1. Рентгенови дифрактограми на 1 - ZnO; 2 - Fe_2O_3-ZnO и 3 - Ag/Fe_2O_3-ZnO фотокатализатори

На фигура 1 са представени рентгенограмите на образците изходен ZnO, смесения оксид Fe_2O_3-ZnO и на дотирания Ag/Fe_2O_3-ZnO. Дифрактограмите на образите показват характеристични линии на хексагонална фаза от ZnO (JCPDS 36-1451). Не беше регистрирано присъствие на нова фаза в рентгенограмите на механохимично синтезираните образци. В рентгенограмите на образците получените чрез смилане в топкова мелница е регистрирано уширение на дифракционните линии (Фиг.1 - 2,3) в сравнение с рентгенограмата на изходния ZnO (Фиг. 1-1). Това уширение свидетелства за съществено понижаване на размера на частиците в механохимично синтезираните образци. Добавянето на сребро не причинява отместване в позиците на пиковете на ZnO (Фиг. 1 - 3). Това може да се дължи на малкото количество на добавката и свидетелства за финното диспергиране на сребото.



Фиг. 2 Дифузно-отражателни спектри на 1- Ag/ZnO и 2- Fe_2O_3-ZnO фотокатализатори

Дифузноотражателните спектри на образците са представени на фигура 2. Образците показват интензивна абсорбция в ултравиолетовата област. Абсорбционните ивици в областта 200-400 нм отговарят на d-d електронни преходи между Zn^{2+} и O^{2-} лиганди. По-високият интензитет на ивиците в спектъра на смесеноокисдния Fe_2O_3-ZnO катализатор се дължи на наслагване с ивица дължаща се на d-d електронни преходи между Fe^{3+} и O^{2-} лиганди. Добавянето на желязо отмества края на абсорбционната ивица към видимата област.

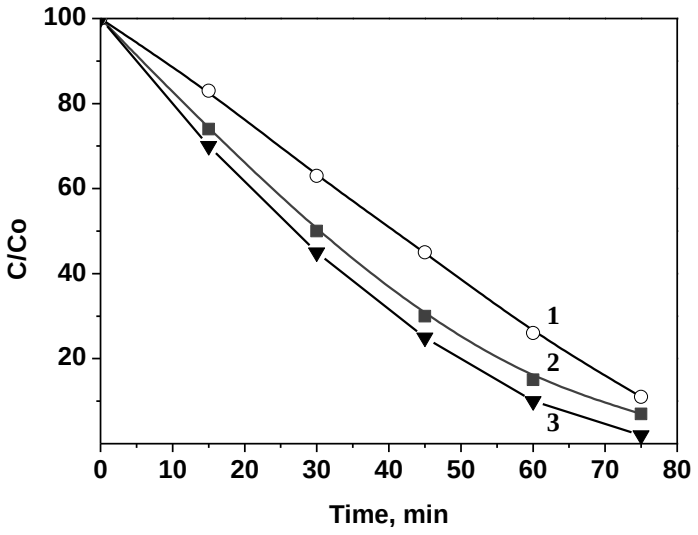


Fig. 3. Фотокаталитична активност на 1 - ZnO; 2 - Fe_2O_3-ZnO; 3 - Ag/Fe_2O_3-ZnO

Фотокаталитичната активност на образците беше определена чрез фотокаталитичното разлагане на метилоранж (МО) – замърсител в промишлените отпадни води. МО не може да бъде разграден в отсъствие на катализатор при облъчване със светлина.

На фигура 3 са представени кривите на фотокаталитично разграждане на МО при облъчване с ултравиолетова светлина в присъствие на механохимично синтезираните образци. $\mathbf{C_o}$ е началната концентрация на МО след достигане на адсорбционно-десорбционно равновесие. **C** е концентрацията на МО след облъчване с ултравиолетова лампа при различни времена на теста. Смесенооксидният фотокатализатор Fe_2O_3-ZnO показа по-добра фотокаталитична активност в разграждането на МО в сравнение с чист ZnO. Внасянето на сребро допълнително повишава фотокаталитичната активност (Фиг. 3 – 3). Цинковият оксид като полупроводник с широка забранена зона за да създаде двойка дупка-електрон изисква светлина с дължина на вълната под 388 нм. Включването на добавка от сребро подобрява фотоефективността на електроннитя процес. Весеното сребро потиска реакцията на рекомбиниране. Електрони ще бъдат преместени от материала с ниска работна функция (ZnO) към материал с висока работна сила (Ag), което води до пренос на електрони от цинковия оксид към среброто. В допълнение внесеното сребро повишава количеството на фотогенерираните носители на заряд в сравнение с изходния смесен оксид. Като резултат в процеса на фоторазлагане участват повече фотогенерирани електрони и дупки, довеждайки до по-висока фотокаталитична ефективност.

4. ЗАКЛЮЧЕНИЕ

Смесени оксиди с висока фотокаталитична активност за разлагане на метилоранж бяха получени чрез механохимичен синтез. За понижаване размера на частиците на фоктокатализаторите, както и за внасяне на допант в тях беше приложено смилане в топкова мелница. Фотокаталитичните експерименти показаха, че Ag/Fe_2O_3-ZnO катализатор има най-висока активност във фоторазграждане на метилоранж, което се дължи на по-ефективното разделяне на фотогенерираните двойки дупка-електрон.

БЛАГОДАРНОСТИ

Авторите изказват благодарности за финансовата подкрепа на Фонд Научни изследвания към Министерството на образованието и науката по договори ДНТС/СЛОВАКИЯ 01/3 и ДФНИ Е 01/7/2012.

ЛИТЕРАТУРА

1. Kamat, P. V., Meeting the clean energy demand: Nanostructure architectures for solar energy conversion, J. Phys. Chem. C 2007, **111**, 2834-2860
2. Fujishima, A., Honda, K., Electrochemical photolysis of water at a semiconductor electrode, Nature, **238,** 1972, 37-38.
3. Hoffmann, M.R., Martin, S.T., Choi, W., Bahnemann, D.W., Environmental application of semiconductor photocatalysis, Chem. Rev., **95**, 1995, 69-96.
4. Bloh, J.Z., Dillert, R., Bahnemann D.W., Transition metal-modified zinc oxides for UV and visible light photocatalysis, Environmental Science and Pollution Research **19**, 2012, 3688-3695.
5. Melinte, G., Baia, M., Georgescu, D., Baila, L., Iancu, V., Diamandescu, L., Popescu, T., Cotet, L.C., Barbu-Tudoran, L., Danciu, V., Simon, S., The influence of the Au nanoparticles dimension on the photocatalytic performances of TiO_2-Au porous composites, Acta Physica Polonica, **121**, 2012, 208-210.
6. Liu, Y., Chen, X., Li, J., Burda, C., Photocatalytic degradation of azo des by nitrogen-doped TiO_2 nanocatalyst, Chemosphere, **61**, 2005, 11-18.
7. Kibombo, H.S., Zhao D., Gonshorowski, Budhi, A.S., Koppang, M.D., Co-solvent induced gelation and the hydrothermal enhancement of the crystallinity of titania-silica mixed oxides for the photocatalytic remediation of organic pollutants, Journal of Physical Chemistry: C **115,** 2011, 6126-6135
8. Kuburovic, N.D., Golubovic, A., Todorovic, Z., Gasic, S., Solevic, T., Photocatalytic degradation of wastewater polluted by methyl-tertiary-butyl-ether using titanium- dioxide and doped titanium-dioxide, Proceedings of the 4th IASME/WSEAS Int. Conference on WATER RESOURCES, HYDRAULICS & HYDROLOGY (WHH'09), February 24-26, 2009, Cambridge, UK, p. 19-24, ISBN:978-960-474-057-4.

9. Motoc, A.M., Piticesc, R.R., Carcel, R.A., Duta, A., Raita, O., Hydrothermal synthezed TiO_2 based nanopowders for photocatalytic applications, Environmental Engineering and Management Journal, **10** (9) 2011, 1299-1303.
10. Eliyas, A., Fabian, M., Kostova, N.G., Stoyanova-Eliyas, E., Balaz, P. Testing of the photocatalytic activity of mechanochemically synthesized $ZnAl_2O_4$ nanoparticles in gas-phase reactor, NANOSCIENCE & NANOTECHNOLOGY, Nanostructured Materials Application and Innovation Transfer, Eds. E. Balabanova and E. Mileva, **13**, 2013 129-132, ISSN: 1313-8995.
11. Kostova, N.G., Kandeva, M., M. Fabian, Eliyas, A., Balaz P., Mechanochemical synthesis of nanosized mixed oxides, 13th International Conference on Tribology, SERBIATRIB'13 Kragujevac, Serbia, 15-17 May 2013, Eds. Miroslav Babicand Slobodan Mitrovic, 2013, 55-57, ISBN: 978-86-86663-98-6.

КОРЕСПОНДЕНЦИЯ

Nina KOSTOVA
Institute of Catalysis
Bulgarian Academy of Sciences
1113 Sofia
Bulgaria
e-mail: nkostova@ic.bas.bg

Alexander Eliyas
Institute of Catalysis
Bulgarian Academy of Sciences
1113 Sofia
Bulgaria

Martin FABIAN
Institute of Geotechnics
Slovak Academy of Sciences
043 53 Kosice
Slovakia
fabianm@saske.sk

Erika DUTKOVA
Institute of Geotechnics
Slovak Academy of Sciences
043 53 Kosice
Slovakia

PeterBALAZ
Institute of Geotechnics
Slovak Academy of Sciences
043 53 Kosice
Slovakia

Tribological Journal BULTRIB, **Vol. IV, 2014**
Papers from the International Conference **BULTRIB '13**
October 24-26, 2013, Sofia
Society of Bulgarian Tribologists
Technical University of Sofia

EXPERIMENTAL RESEARCH OF THE EFFECTS OF SLIPPER BEARING GEOMETRY AND WORKING CONDITIONS ON THE SYSTEM RIGIDITY IN AXIAL PISTON PUMPS

C. SİNANOĞLU[1*], E. YILMAZ[2], E.S. TOPAL[3], F. CANBULUT[4]

[1,2] Department of Industrial Design Engineering, Erciyes University, Kayseri 38039
[3,4] Department of Mechanical Engineering, Erciyes University, Kayseri 38039

Abstract: *In this study, the effects of loading pressure, orifice and various slipper bearing geometry on the rigidity in axial piston pumps were researched. In axial piston pumps the slope of the oil film on the hydrostatic bearings is very important. This slope is called rigidity and it is the ability to withstand changing loads in relation with the changing thickness of the oil film on the bearing. In experimental studies it is shown that the rigidity changes with varying revolutions, orifice diameter, and changes in pressure. However it is understood that the geometry of slipper bearings has a bigger effect*

Key Words: *Rigidty, orifices, axial piston pumps, hydrostatic bearings*

1. INTRODUCTION

Bearing rigidity in axial piston pumps is one important factor in selecting parameters of the bearing working under variable loads. Circular pocket hydrostatic axial bearings (slipper bearings) in hydraulic axial piston pump are under the influence of a wide variety of forces. Therefore, the sliding surface of hydrostatic bearing must have the necessary axial rigidity. The constitution of the slope of load film thickness curve is quite important for hydrostatic bearing applications. The value of this slope called rigidity is capability of the bearing to withstand the variation in the load depending on the variation of film thickness. Therefore, the bearing must be designed in such a way as to obtain maximum rigidity in minimum oil film thickness and maximum load.

Canbulut, Sinanoğlu and Yıldırım presented the effects of orifice diameter and the size of pocket in slippers with circular pocket, which affect the performance of swash plate axial piston pump and motor are examined using neural network. In their paper, theoretical and experimental results that orifice diameter and radius ratio significantly affect on bearing rigidity [1]. The same researcher was experimental investigation of the performance of slippers, in various working conditions, which affect the efficiency of pump with axial pistons. As slippers have a considerable impact on the performance of the system, the effects of surface roughness in the slippers with varying hydrostatic bearing area on lubrication have been studied. It was shown that the experimental and simulation results, neural network was exactly followed the desired results. This kind of neural network predictors could be applied on bearing systems in real time applications [2]. Another approach for different lubricant and lubrication condition can be given in (Durak, 2003). An experimental investigation has been presented for the performance of porous bearing under different lubricating conditions. The experimental results obtained in his study indicated that the correct selection of lubricant and suitable running conditions. [3]

Koç and Hooke have examined the design of hydrostatically balanced bearings as used in the slippers of high pressure axial pumps, and outlined a design procedure whereby the slipper behaviour, minimum film thickness and loss of high pressure fluid could be estimated. It was shown that for successful operation the slippers need to have small amounts of non-flamess on the running surfaces. In addition, good agreement between the measured and calculated film thickness was demonstrated [4]. The same researchers experimentally investigated the performance of hydrostatic slipper bearings in axial piston pumps and motors [5]. The effect of clamping ratio, offset loading and orifice size on the behaviour of overclamped and underclamped slippers was outlined. It was shown that the slippers run satisfactorily with no orifice and have their greatest resistance to tilting couples and to minimum film thickness. The underclamped slippers and slippers with larger orifice diameter run with relatively larger

clearance and tilt than those of overclamped slippers with no orifice. Cavitation tends to affect the slippers, especially at the rear of the slipper. Ineffective flood lubrication might be the cause of the cavitation and oil jet pressure must have maintained to prevent oil starvation. In high pressure hydraulic equipment the bearings and seals are usually designed to operate hydrostatically in partial. In some, such as the end plates or bushes of gear pumps and the valve plates of axial piston pumps, this is achieved by adjusting the pressurised areas so that the hydrostatic loads are nearly in balance, leaving a small residual clamping load to be carried by hydrodynamic pressures [6].

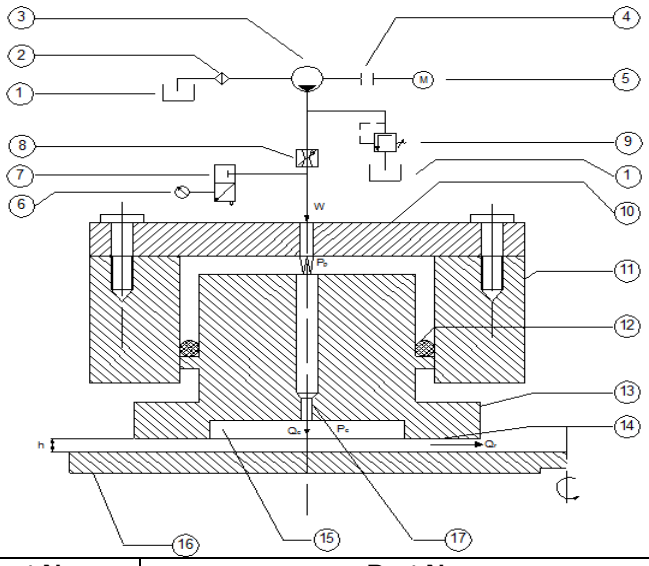
Wang and Yamaguchi presented the characteristics of disk-type hydrostatic thrust bearings supporting concentric loads, simulating the major bearing/seal parts of water hydraulic pumps and motors [7]. They evaluated the characteristics by studying the relationships among the load carrying capacity, pocket pressure, film thickness, and leakage flow rate.

Wang and Yamaguchi also theoretically investigated the load carrying capacity, power loses and stiffness of disk-type hydrostatic thrust bearings including the case of eccentric load for elastic and rigid materials respectively [8]. In their paper, a numerical analysis method was employed based on a two-dimensional elastohydrostatic problem with elastic deformation model.

In the scope of this project the slipper bearings and orifices made of brass has been examined on a hydrostatic axial pump test equipment. The effects of the size of orifice, pocket size, and the surface structure of the slipper bearings which have a great role in the efficiency of axial piston pumps and which work with the hydrodynamic and hydrostatic principles have been investigated in relation to its effects on bearing rigidity.

2. SYSTEM THEORY

Fig. 1 shows typical hydrostatic bearing and plate system used in this study. As can be seen in the figure, the slipper moves on slipper plate with a certain film thickness (h). The fluid coming from piston side is transferred to the pocket (bottom of the slipper) by orifice to equilibrate the slipper. While the system is running, the clearance (h) between the slipper and the slipper plate must be neither small enough to cause metal-metal contact nor too big to cause fluid leakage. Therefore, this critical area has to be precisely designed in consideration of the dynamic working conditions.



Part No	Part Name
1	oil tank
2	filter
3	pump
4	coupling
5	motor
6	manometer
7	pressure control valve
8	flow control valve
9	pressure relief valve
10	cylinder cover
11	cylinder block

12	o-ring
13	slipper
14	hydrodynamic bearing area
15	hydrostatic pocket
16	slipper plate
17	orifice

Fig. 1 Hydrostatic bearing and plate system [1]

The vertical load W (Fig. 1) acting on circular pocket hydrostatic bearing and formed by loading pressure P_p is kept in equilibrium by the fluid pressure between the load bearing face and the opposite element.

The vertical load [10] is

$$W = \frac{\pi P_c \left(R_d^2 - R_i^2\right)}{2\ln\left(R_d / R_i\right)} \tag{1}$$

where, P_c is pocket pressure, R_d and R_i are outer and inner radii of bearing respectively.

The flow-rate $\left(Q_c\right)$ transferred from loading area of the bearing to bearing pocket and the radial direction flow-rate $\left(Q_r\right)$ neglecting the speed of the hydrodynamic bearing are

$$Q_c = \frac{\pi d_c^4}{128\eta l_c}\left(P_p - P_c\right) \tag{2}$$

and

$$Q_r = \frac{P_c \pi h^3}{6\eta \ln\left(R_d / R_i\right)} \tag{3}$$

respectively, where d_c and l_c are the diameter and length of orifice, η is the dynamic viscosity of oil.

If P_c is drived from Eq.(3) and substituted into Eq.(1), we obtain

$$W = \frac{3Q_r \eta\left(R_d^2 - R_i^2\right)}{h^3} \tag{4}$$

If the fluid permanency is considered $\left(Q_c = Q_r\right)$ and Eq. (2)is placed to Eq.(4), the load expression becomes independent of viscosity

$$W = 3\pi \frac{k_c}{h^3} P_p \left(1 - \frac{1}{\overline{P}}\right) R_d^2 \left(1 - \frac{1}{\overline{R}^2}\right) \tag{5}$$

where, $\overline{P} = P_p / P_c$, $k_c = d_c^4 / 128.l_c$ and $\overline{R} = R_d / R_i$.

Generally, the rigidity of hydrostatic bearing system is denoted by

$$k = -\frac{dW}{dh} \tag{6}$$

The negative sign (-), is written to signify the positivity of rigidity equilibrium not in mathematical sense. Rigidity (k) can be driven in the following form from the Eq. (5) regarding to derivative of h film thickness

$$k = 3\frac{W}{h} \tag{7}$$

If necessary for the sake of the simplicity in working with dimensionless values, the bearing rigidity in dimensionless form can be expressed as follows

$$\bar{k} = 3\frac{\overline{W}}{\bar{h}} \tag{8}$$

where in $\bar{h} = h/R_d$, $\overline{W} = W/P_p R_d^2$, $\bar{k} = k/P_p R_d$.

3. EXPERIMENTAL PROCEDURE

3.1. Testing Equipment

The testing equipment consists of three main units. (fig 3.1). These are the control unit, test unit and the power unit. Both Axial piston pumps and slipper bearings on the pumps according to hydrostatic and hydrodynamic bearings principles. The main test unit is developed to be able to test the slippery bearings according to these principles. The main components that construct the main test unit are 3 slipper bearings and hydrolic loading cylinders. The slipper bearings form hydrostatic circular pocket bearing systems. A unit supported by these bearings is a servo motor driven slipper plate.

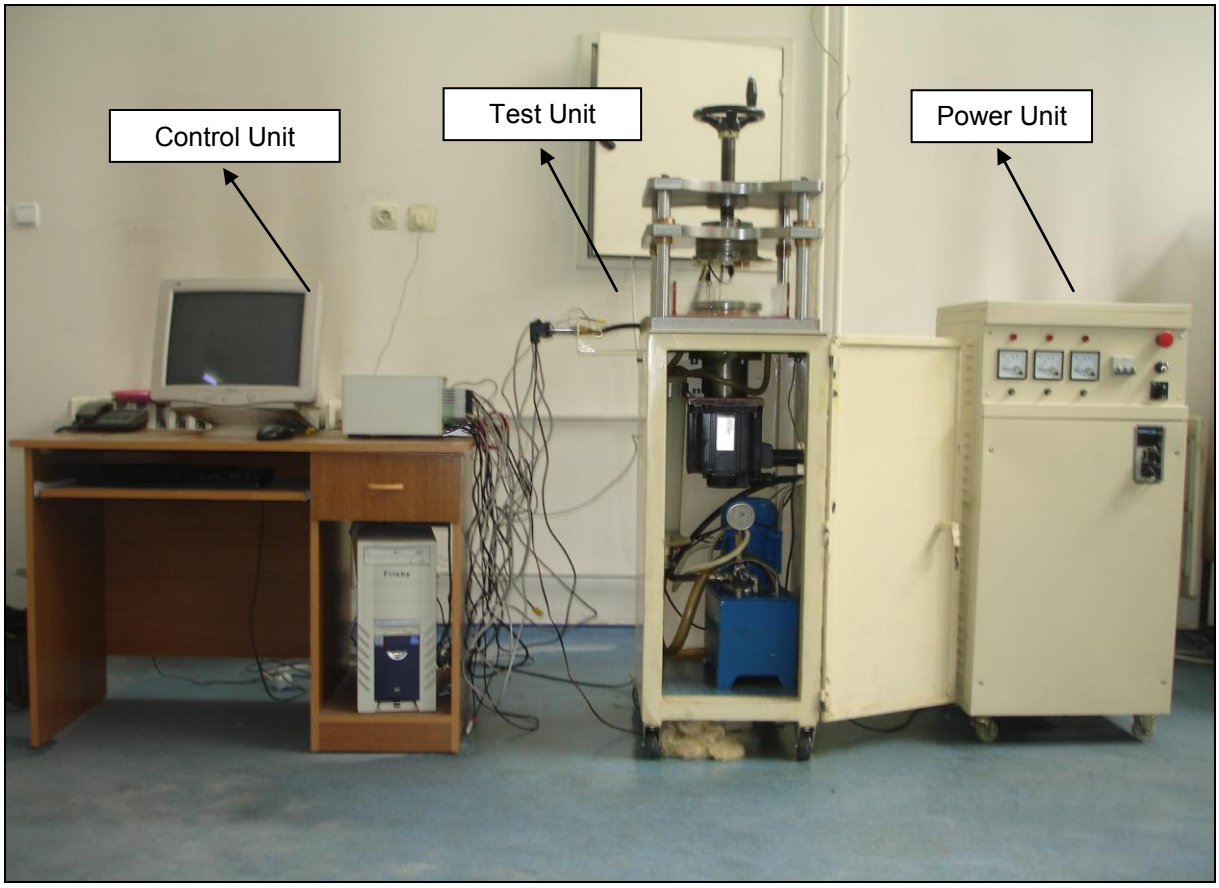


Fig 3.1. Test equipment

3.2. Experimental Study

In circular pocket bearings the lubricant is transferred to the liquid bearing pocket via orifice. This lubricant (fig 3.2) lubricates the slipper bearing and the turntable creating oil pressure between the two components and a lifting force.

The parameters measured on experimental study;

Pressure Measurements:

- Loading pressure
- Set pressures measured from three various locations in the set region of the slipper bearing with 120^0 angular
- Recess pressure measured from the single point in the location of slipper bearing recess

Flow Measurements:

- Output flow rate of the bearing (radial flow)

Temperature Measurements:

- Environment temperature
- Slipper bearing temperature
- Oil temperature measured from slipper bearing set region
- Oil temperature measured from slipper bearing recess region
- Oil temperature in the oil tank

The data obtained from this experiement are transfered to a computer through a data logger system. Mathematical calculations are done using measurements after the system has reached its regime (approx. 2-5 mins.). Shell Tellus 68-01 mineral oil is used as the lubricant liquid.

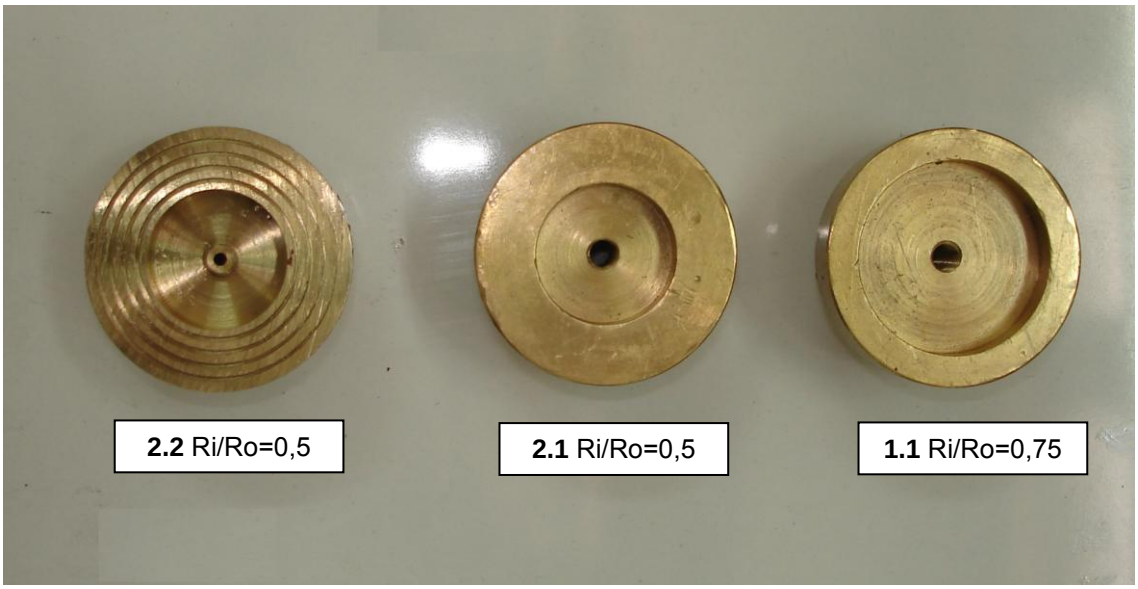


Fig 3.2 Slipper bearings used in the experiments

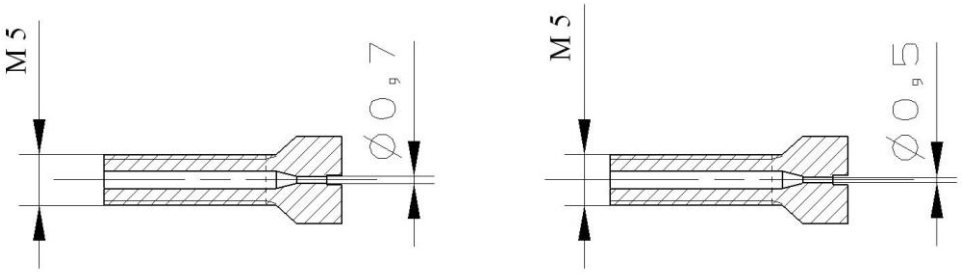


Fig. 3.3 Orifices used in the experiments (dc=0.7 - dc=0.5)

4. EXPREMENTAL RESULT

Experimental studies show that rigidity values differ according to the slipper bearing type and orifice diameter. It is observed that the hydrostatic bearing system has a higher rigidity value with higher pressures than lower pressures. It is also observed that the rigidity value declines with higher orifice diameters. At the same time the type of the slipper bearing used in the test affects rigidity. The changes of slipper bearing geometry has bigger effects on rigidity.

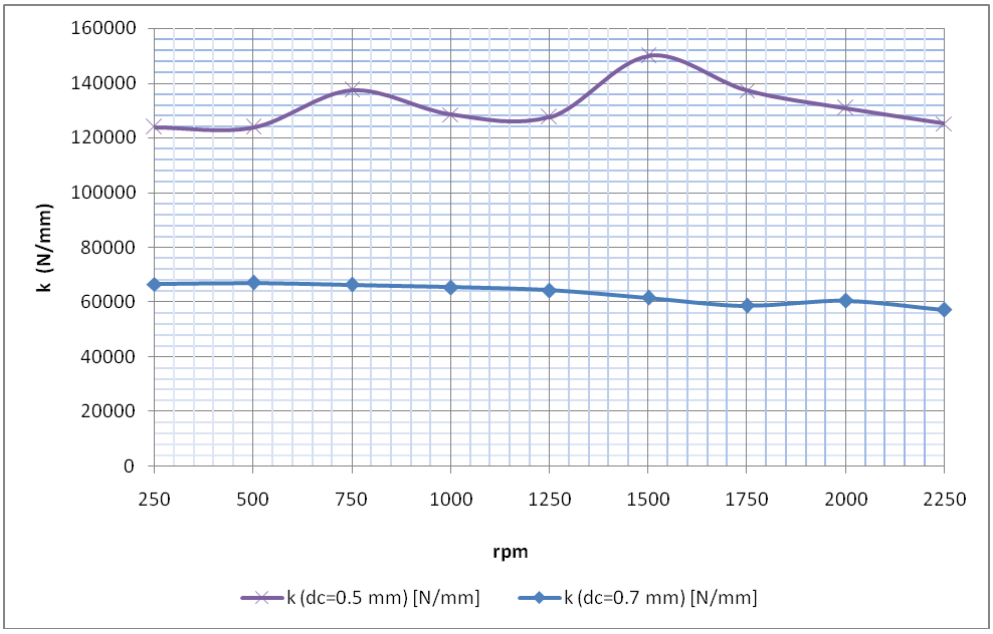


Fig. 4.1 Rigidity variations in the different orifices (20 Bar pressure, slipper bearing no. 1.1)

Fig 4.1 shows the differences of slipper bearing 1.1 (fig. 3.2) under 20 bars of pressure with different orifice diameters. The values show that the revolution speed has little effect on rigidity. The figure explains that changes in the diameter of the orifice have a greater impact. As the orifice diameter increases rigidity declines.

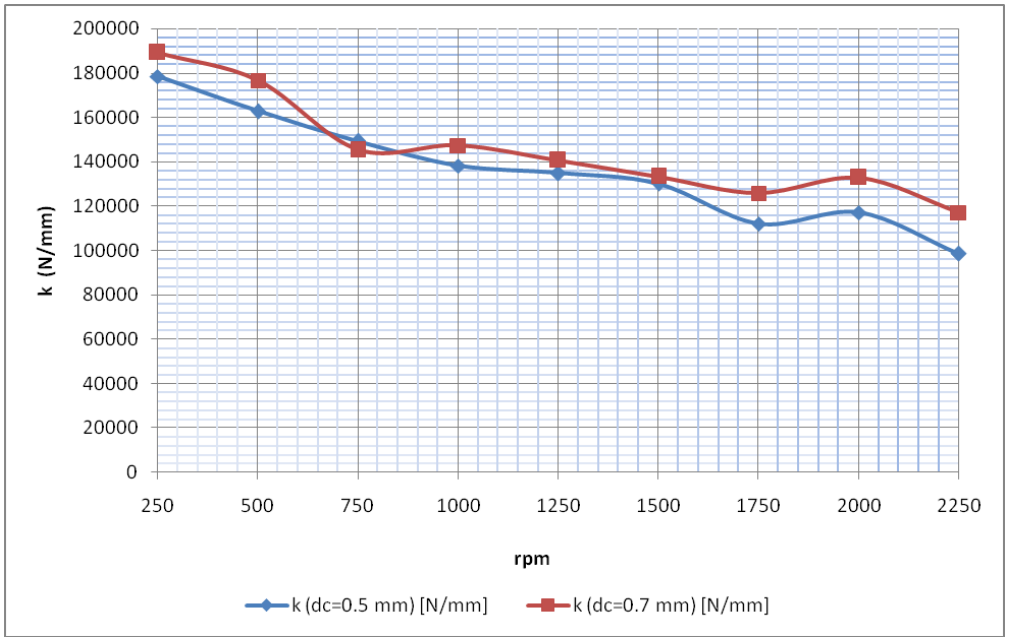


Fig. 4.2 Rigidity variations in the different orifices (20 Bar pressure, slipper bearing no. 2.1)

Fig 4.2 shows the differences of slipper bearing 1.1 (fig. 3.2) under 20 Bars of pressure with different orifice diameters. In this study the rigidity value falls as the orifice diameter and the revolution speed increase.

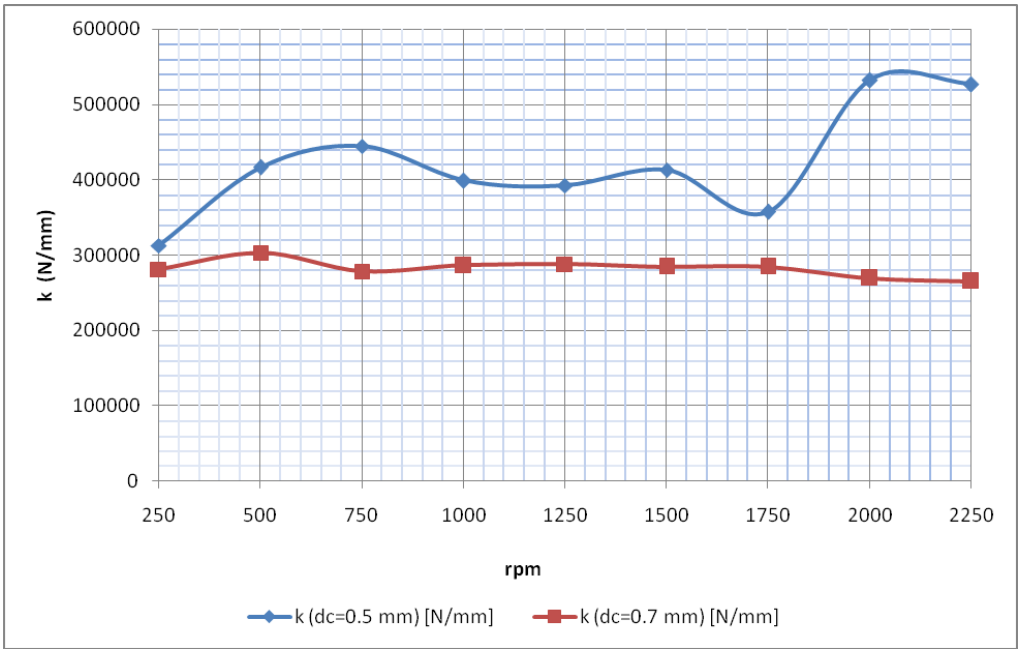


Fig. 4.3 Rigidity variations in the different orifices (20 Bar pressure, slipper bearing no. 2.2)

Fig 4.3 shows the differences of slipper bearing 1.1 (fig. 3.2) under 20 Bars of pressure with different orifice diameters. In this graphic also an increase in the diameter of the orifice creates a fall in the value of rigidity. The slipper bearing numbered 2.2 has the highest rigidity value.

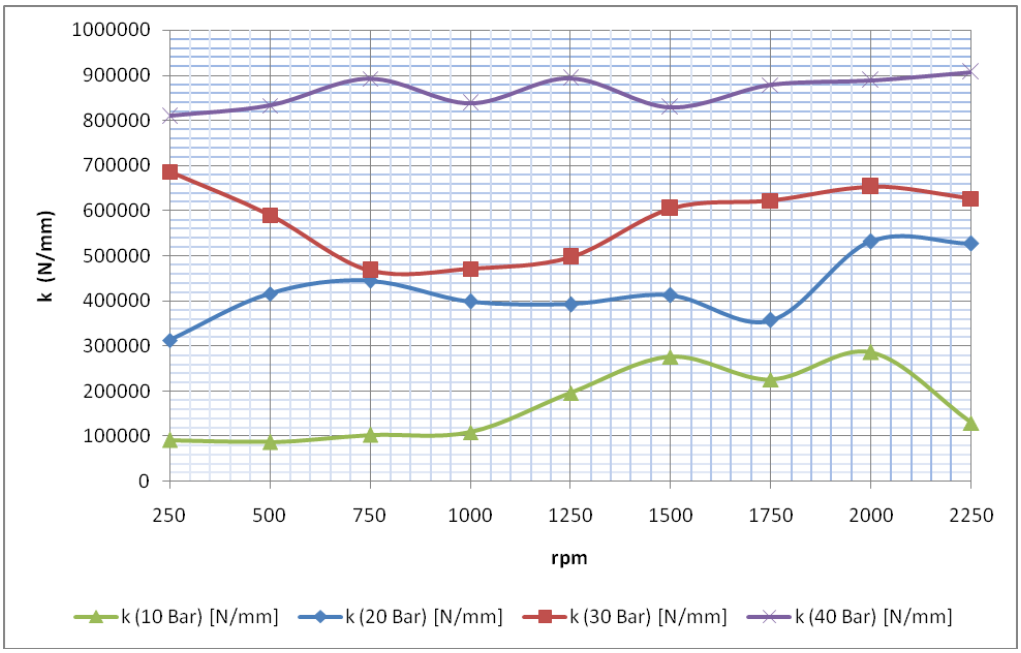


Fig. 4.4 Rigidity variations with dc=0.5 orifice, slipper bearing no. 2.2

Figure 4.4 shows the changes in slipper bearing number 2.2 under different loading pressures with dc=0.5 orifice. It is observed that as loading pressures increase rigidity also increases.

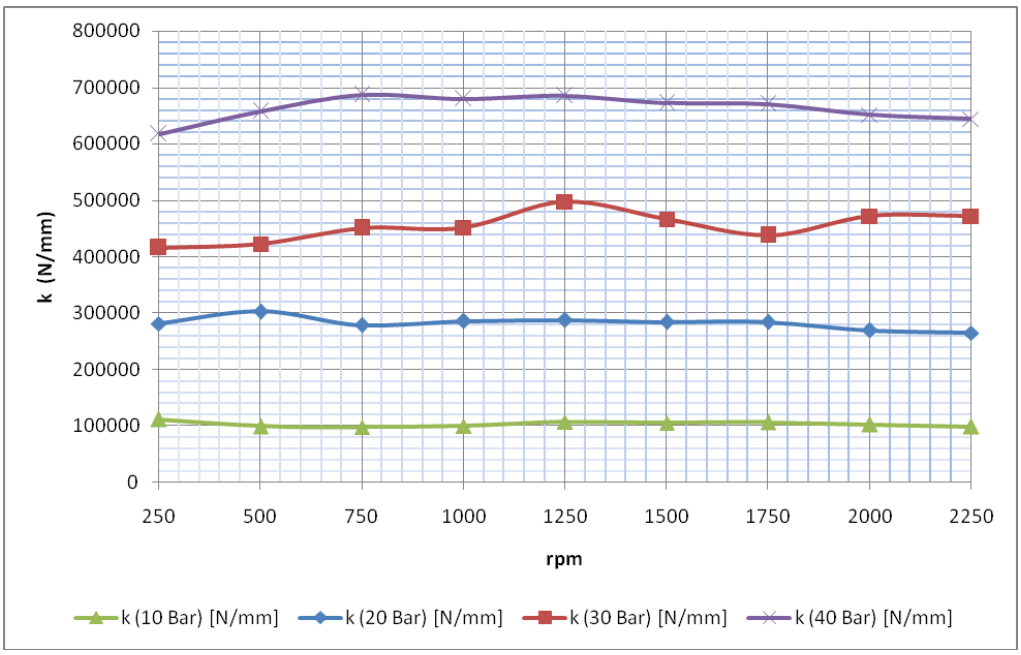


Fig. 4.5 Rigidity variations with dc=0.7 orifice, slipper bearing no. 2.2

Figure 4.5 shows the changes in slipper bearing number 2.2 under different loading pressures with dc=0.5 orifice. As loading pressure increases the rigidity value also increases. As seen on the last two graphics an increase in the diameter of the orifice creates a decline in the rigidity value

5. CONCLUSIONS

As a result of the studies conducted, the diameter of the orifice, slipper bearing geometry and loading pressure have a great effect on the rigidity value. Rigidity value declines with an increase in the diameter of the orifice. With the slipper bearings used in the test (fig 1. part no 16), an increase in the contact surface between the slipper plate and the slipper bearings (Ri/Ro) creates an increase in the rigidity value. However the slipper bearings 2.1 , 2.2 with the same (Ri/Ro) value

It is observed that even though the contact surface is smaller the rigidity value shows an increase. This is the result of sets cut in the slipper surfaces. The changes in the geometry of the slipper bearings also have serious effects on rigidity values. Also as shown in figures 4.3 and 4.4 an increase loading pressures also increases the rigidity value.

According to the figures obtained, with the smaller orifice diameter (dc=0.5) the rigidity value is higher compared to greater orifice diameter (dc=0.7). However considering varying revolution speeds the rigidity values show less change with greater orifice (dc=0.7) than with smaller orifice (dc=0.5).

As a result the study shows that the slipper bearing surface textures and orifice diameters have great effect on changes of rigidity values.

ACKNOWLEDGMENTS

This study is supported by Erciyes University Scientific Research Project Coordination Unit (Project Number: FBA - 9 - 1146)

REFERENCES

1. Canbulut, F., Sinanoğlu, C. and Yıldırım, Ş., 2004, “Analysis of effects of sizes of orifice and pockets on the rigidity of hydrostatic bearing using neural network predictor system”, KSME International Journal, Vol, 18, No. 3, pp. 432-442, (in press).
2. Canbulut, F., Sinanoğlu, C. and Yıldırım, Ş., 2004, “Neural Network Analysis of Leakage Oil Quantity In The Design of Partially Hydrostatic Slipper Bearings,” *Industrial Lubrication and Tribology*, (in press).
3. Durak, E., 2003, “Experimental Investigation of Porous Bearings Under Different Lubricant and Lubricating Conditions”, KSME International Journal, Vol, 17, No. 9, pp. 1276-1286.

4. Koç, E. and Hooke, C.J., 1997, “Considerations in the Design of Partially Hydrostatic Slipper Bearings,” Tribology International, Vol, 30, pp. 815-823.
5. Koç, E and Hooke, C.J., 1996, “Investigation into the Effects of Orifice Size, Offset and Overclamp Ratio on the Lubrication of Slipper Bearings,” Tribology International, Vol, 29, No. 4, pp. 299□305.
6. Koç, E., 1989, “Analytical and Experimental Investigation into the Sealing and Lubrication Mechanism of the Gear ends in Pumps,” Wear, Vol, 135, pp. 79-94
7. Wang, X. an Yamaguchi, A., 2002_a, “Characteristics of Hydrostatic Bearing/Seal Parts for Water Hydraulic Pumps and Motors. Part 1: Experiment and Theory,” Tribology International, Vol, 35, pp. 425-433.
8. Wang, X. and Yamaguchi, A., 2002_b, “Characteristics of Hydrostatic Bearing/Seal Parts for Water Hydraulic Pumps and Motors. Part 2: On Eccentric Loading and Power Loses,” Tribology International, Vol, 35, pp. 435-442.
9. Canbulut, F., Koç, E. and Canbulut, F., 1992, “The Effects of Sizes of Capillary Tube and Pockets on the Rigidity of Hydrostatic Bearing,” *5 th. National Machine Design and Manufacturing Congress*, ODTU, Turkey.

CORRESPONDENCE

Cem SİNANOĞLU
Department of Industrial Design Engineering, Erciyes University, Kayseri 38039
csinan@erciyes.edu.tr

Tribological Journal BULTRIB, **Vol. IV, 2014**
Papers from the International Conference **BULTRIB '13**
October 24-26, 2013, Sofia
Society of Bulgarian Tribologists
Technical University of Sofia

ВЪЗМОЖНОСТИ ЗА ПОВИШАВАНЕ РЕСУРСА НА РАБОТА НА ШПРИЦВАЩИ ИНСТРУМЕНТИ

Георги Мишев, Велко Рупецов, Мирослав Симов

POSSIBILITIES FOR INCREASING THE RESOURCE OF INJECTION MOLDS

Georgi Mishev, Velko Rupetzov, Miroslav Simov

Abstract: *Increasing the resource of injection moulds is a basic task of polymer products manufacturers. The task involves organizational, design and production actions.*

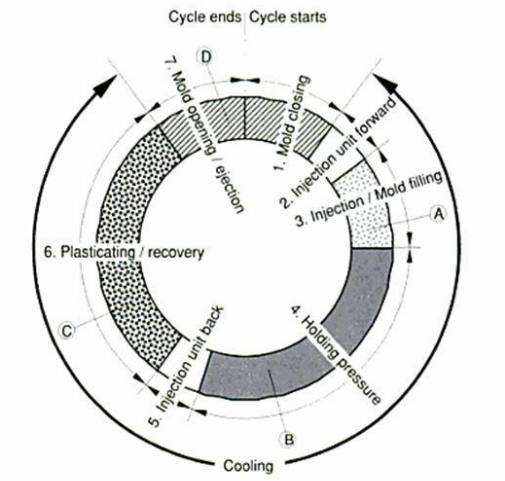
The paper deals with the requirements to instrumental materials for the production of injection moulds and the inputs affecting their choice. The most often applicable steels are shown. An analysis and classifying of the reasons for injection moulds failure is made based on the study of the operation of injection moulds in „Arexim Engineering“Ltd, the city of Smolian. Deposition of extra-hard VAD-coatings allows the improvement of wear-resistance and oxidation resistance of the working surfaces.

Key words: *injection mould materials, wear, wearresistance improvement.*

ВЪВЕДЕНИЕ

Нарастващото приложение на пластмасовите изделия в различни области на индустрията, особено в автомобилостроенето, ръчните електрически инструменти, космоса и др. се дължи на подобрените им физико-механични свойства, точност на размерите и формата, разнообразен и красив дизайн и др.

За производството на пластмасови изделия най-широко приложение е намерил процеса шприцоване, който се състои от три основни компонента: шприцмашина, материал (пластмаса на гранули) и инструмент (шприцформа-матрица). На фиг. 1 е показан цикъл за получаване на един детайл [4].



Фиг. 1. 1 - Затваряне на инструмента; 2 - движение на шприцващия агрегат напред; 3 - шприцване; 4 - допресоване; 5 - движение на шприцващия агрегат назад ; 6 - пластификация (дозиране); 7- отваряне на инструмента и изхвърляне на детайла.

За да се допълни цялата матрица с разтопения материал и да не се получат всмукнатини в детайла в цикълът, е предвидено допресоване. Шприцването е процес силно зависим от температурата на инструмента. От температурата в голяма степен зависят механичните и визуалните характеристики на произвеждания детайл.

I. ИЗБОР НА ИНСТРУМЕНТАЛНИ МАТЕРИАЛИ

При изделията от полимерни материали дизайнът на повърхнините играе важна роля. За да се отговори на високите изисквания по отношение на форма, функционалност, естетика, качество на продукта и дълъг живот на инструмента изборът на инструментален материал има важно значение.

Към инструменталните материали за изработване на шприцформи се предявяват много високи изисквания по-важни от които са:

- добра механична обработваемост;
- висока износоустойчивост;;
- стабилност на размерите;
- висока якост на натиск;
- висока корозионна устойчивост и др.

Върху изборът на материал за изработването на шприцформи влияят много фактори, като[1,5]:

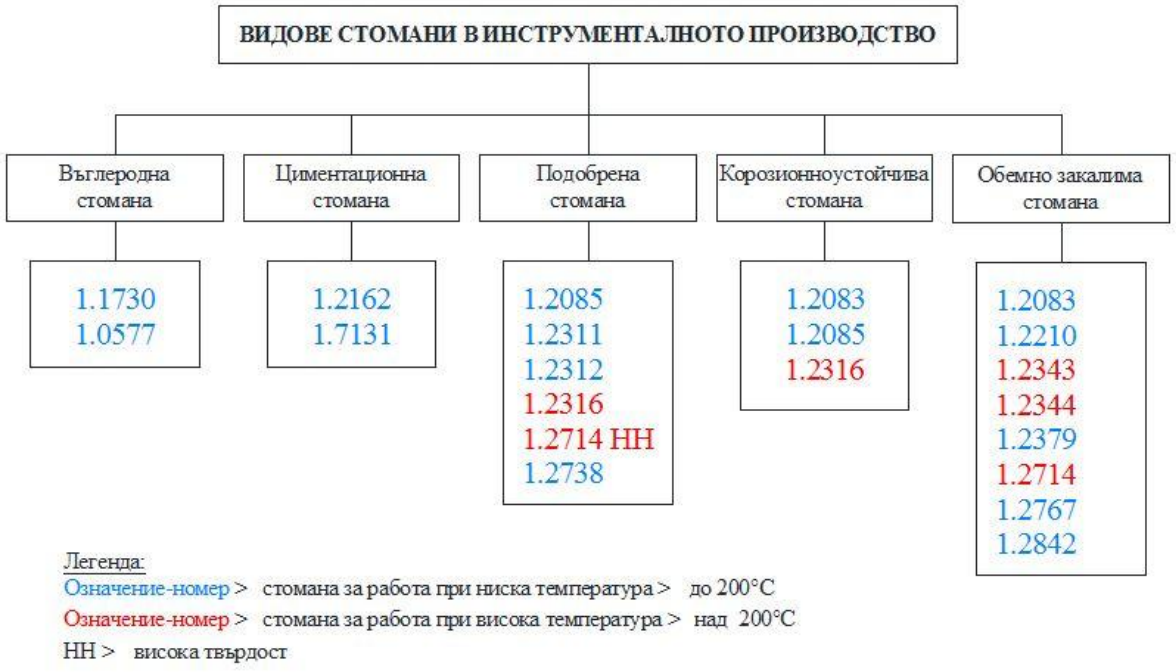
- функция, която ще изпълнява елемента от шприцформата;
- износване и живот на инструмента;
- брой на произвежданите детайли;
- метод на обработка на формоващите повърхнини;
- вид на полимера и др.

Работен ресурс (живот) на инструмента е термин, използван, за определяне на приемлив брой детайли, изработени от една шприцформа. Ресурсът на инструмента е пряко свързан с износването на работните повърхнини.

Преди изработване на инструменталната екипировка е необходимо да бъдат предварително известни основните фактори, влияещи върху износването и ресурса на инструмента: дълбочината на термообработка (при термообработени стомани), твърдостта на повърхността на инструмента и абразивните характеристики на материала (полимера).

Инструмент, закален до по-малко от 50 HRC, притежават не висока износоустойчивост. Ресурсът на инструмента се увеличава при увеличение на твърдостта до около 60 HRC.

Силите, участващи в процеса на шприцване под налягане са на натиск. Те са породени от притискането на двете половини на инструмента (сили на затваряне) и вътрешното налягане на стопилката.



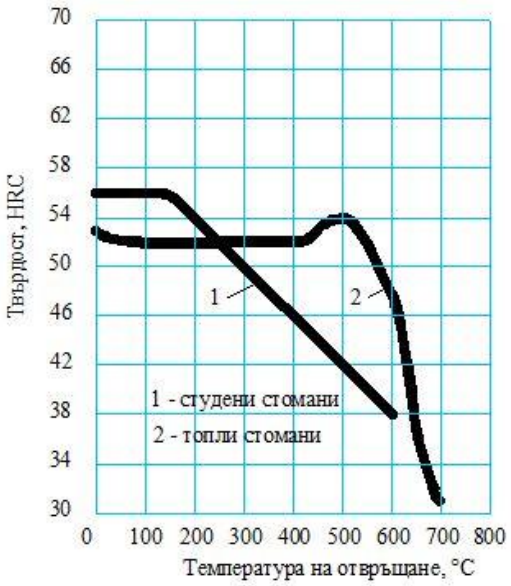
Фиг. 2. Видове стомани в инструменталното производство

Поради строго специфичните изисквания за всеки конкретен случай, или комбинация от изисквания и фактори – изборът на инструментални материали е индивидуално конструкторско решение, направено на база състав на материала и качествата му след предвидената термообработка. Най-често приложими видове стомани са посочени на фиг.2 [6,7]]

Инструменталните стомани за изработване на шприц форми се делят на две основни групи:

- стомани за работа на студено (студени) – при инструменти които се загряват в процеса на работа но тяхната температура не надвишава 200° С.
- стомани за работа при високи температури (топлоустойчиви) - нагряват се при тяхната постоянна работа над 200° С. При работните температури не трябва да стават фазови превръщания в стоманата, т.е. структурата трябва да е стабилна и устойчива на отвръщане.

Важна характеристика на инструменталните стомани също е изменението на твърдостта в зависимост от температурата на отвръщане – фиг. 3.



Фиг. 3. Поведение на твърдостта на инструментални стомани след отвръщане

Студените инструментални стомани имат висока начална твърдост, но още при температури на отвръщане над 200° С тя бързо пада. Началната твърдост на топлоустойчивите инструментални стомани е значително по-ниска, но тя остава постоянна до температури около 600° С (термична стабилност). Причина за това поведение са вътрешни дифузионни процеси при високи температури, които водят до образуване на твърди карбиди и това води до повишаване на твърдостта до нов максимум, наречен вторичен максимум.

II. АНАЛИЗ НА ПРИЧИНИТЕ ЗА ДЕФЕКТИРАНЕ НА ШПРИЦФОРМИТЕ

Шприц формите работят при много тежки режими - големи натоварвания; високи температури; големи износвания. Най-често срещаните натоварвания на шприц формите са:

- механично;
- корозионно;
- абразивно/ ерозийно;
- термично.

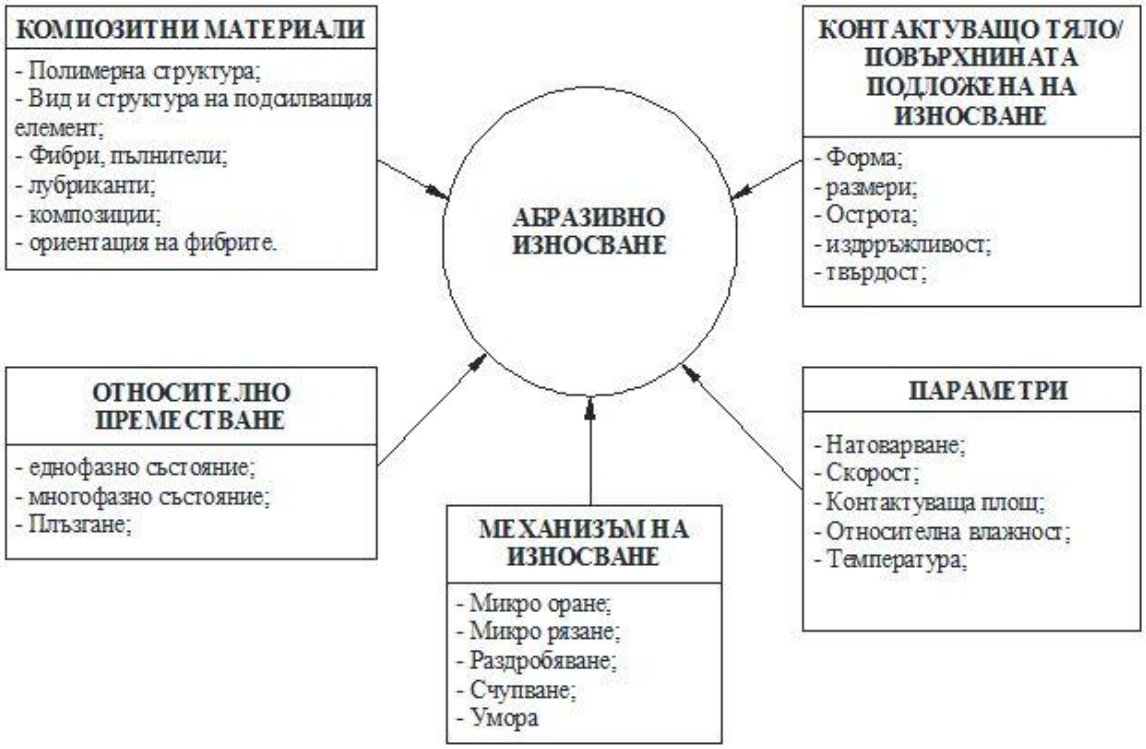
Те често си взаимодействат едно на друго, като по този начин са кумулативни (действат с натрупване).

Най -разпространената причина за корозионно разрушение на инструмента са процесите свързани с термично повреждане от стопилката като [1]:

- термична нееднородност в топло каналната система;
- прекомерно дългото време за задържане в шприцващия възел или в топло каналната система;

- влагата в гранулата; Немалка част от пластмасите лесно поглъщат влагата и трябва да бъдат щателно подсушени преди преработката.[2] Ако влагата се остави в материала, при определени условия тя може да реагира с други елементи, в резултат на което да корозират формещите повърхнини на шприцформата.
- химически агент образуващ пяна (например получаване на силно пореста структура);
- вещества забавящи горенето;

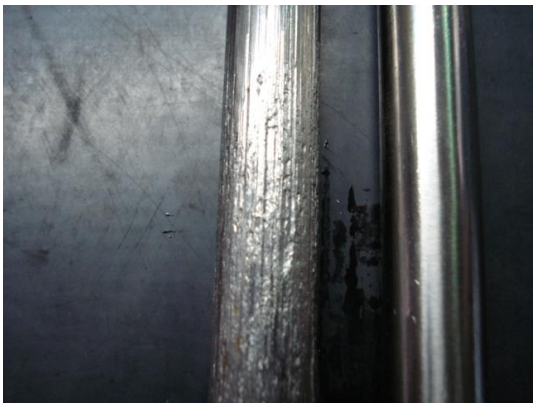
Разрушение на металните повърхнини от двата вида износване (абразивно и ерозийно) са породени основно от пълнители, подсилващи материали и др. твърди частици. Такова износване е загуба на материал от повърхността, причинено главно от триене при плъзгане. На фиг. 4 са показани факторите, водещи до абразивно износване.



Фиг. 4. Фактори водещи до абразивно износване.

Анализът на получените дефекти на шприц формите е направен на базата на изследване работата на тези инструменти в "Аресим Инженеринг – ЕООД" – Смолян.

На фиг.5 е показано механично износване (задиране) на изхвъргач вследствие на триене при плъзгане, съпроводено с висока температура и недостатъчно висока твърдост.



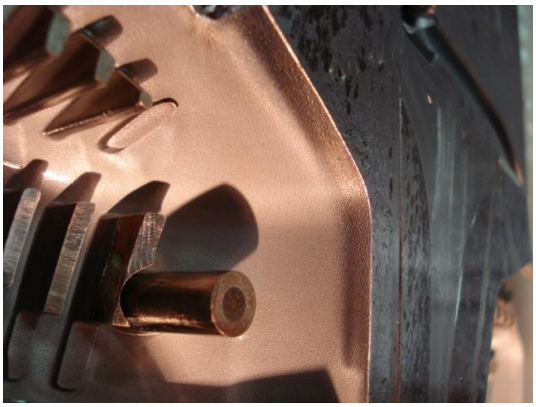
Фиг. 5



Фиг. 6

На фиг.6 е показано корозионно износване вследствие на въздействието на химически агресивни съставки в материала и влиянието на „Дизел ефекта“ при затварянето на газ под високо налягане.

На фиг.7 е показано абразивно износване на формещата повърхнина поради абразивното действие на стъклените влакна в материала.



Фиг.7



Фиг.8

На фиг.8 е показано откъртването на част от формата вследствие умора на материала, породена от циклично натоварване на огъване и опън, придружено с резки температурни промени.

На фиг.9 е показано наслояване (полепване) на остатъчни продукти от шприцването върху формата, които се откъсват по време на движението на възлите на инструмента и създават предпоставка за задирането им.



Фиг.9

III. МЕТОДИ ЗА ПОВИШАВАНЕ НА ИЗНОСОУСТОЙЧИВОСТТА НА ШПРИЦФОРМИТЕ

За намаляване на някои от получените дефекти на шприц формите би могло да се предприемат следните мероприятия:

- подобряване на газоотвеждането от инструмента;
- подобряване на сушенето на материала;
- оптимизиране на конструкцията и технологията за изработване на инструмента и правилен подбор на инструменталните материали.

Тези мероприятия са организационни, конструктивни и производствени, които самата фирма може да приложи.

За да се повиши ресурсът (животът) на шприц формите, което ще доведе до съществен икономически ефект, е необходимо да се предприемат следните мероприятия:

- повишаване твърдостта на работните повърхнини на инструмента;
- повишаване износоустойчивостта на работните повърхнини на инструмента;

За изпълнение на тези две мероприятия най-ефективни са методите за нанасяне на твърдосплавни покрития.

В последно време най-широко приложение са намерили методите за физическо (PVD) и химическо отлагане на (CVD) газове.

Изборът на един от двата метода зависи от материала за изработване на шприц формата, т.е от температурата на отгряване. Разновидност на PVD методът се явява електро дъговата технология за нанасяне на слоеве във вакуум (VAD), която позволява нанасяне на различни по състав и структура покрития [3]. С помощта на този метод могат да се получат покрития с твърдост по-висока от 40 GPa., известни като ”свръхтвърди”, както и висока износоустойчивост и устойчивост на окисление.

В последните години се разработиха технологии и съоръжения за нанасяне на нанокомпозитни свръх твърди покрития, чиито дебелина на слоя е до 1-2μm.

ЗАКЛЮЧЕНИЕ

Върху икономическите параметри на една фирма в голяма степен влияе работният ресурс на инструменталната екипировка. Това важи особено за фирма ”Арексим Инженеринг - ЕООД”- Смолян, в която над 90% от инструментите са шприц форми. Като се има в предвид, че тези инструменти са много сложни и скъпи повишаването на техният живот с 10 - 20% ще доведе до икономическа полза на фирмата. Повишаването на работния ресурс на шприц формите може да се постигне чрез използване на съвременните технологии за нанасяне на твърдосплавни покрития.

ЛИТЕРАТУРА

1. Peter Unger. Gastrow injection molds – 130 Proven Designs 4th. Edition. Hanser Publishers, Munich, 2006.
2. http://www.stle.org/resources/lubelearn/wear/
3. Пашински Ч., Получаване на свръхтвърди покрития, включително нанокомпозитни, чрез електродъгова технология и тяхното изследване, дисертация, София, 2013.
4. Tim A. Osswald,Lih-Sheng Turng,Paul J. Gramann. Injection Molding Handbook. Hanser Verlag, 2008 - 764 стр.
5. Herbert Rees. Mold Engeneering.Hanser Publishers, Munich,2002.
6. www.bohler-international.com
7. www.meusburger.com

КОНТАКТИ:

Георги Мишев, проф. д-р. инж.
Катедра „Машиностроителна техника и технологии“
Технически университет София, Филиал Пловдив
Ул. „Ц. Дюстабанов“ 25
4000 Пловдив , България
e-mail: gmishev@tu-plovdiv.bg

Велко Рупецов, гл.ас. инж.
ПУ„Паисий Хилендарски“ Пловдив- Технически колеж Смолян
Ул. „Д. Петров“ 28
4700 Смолян , България
e-mail: velko_r@abv.bg

Мирослав Симов, инж.конструктор
FESTO Производство ЕООД
Ул. „Димитър Македонски “ №4
4700 Смолян , България
e-mail: miroslav_simov@festo.com

Tribological Journal BULTRIB, **Vol. IV, 2014**
Papers from the International Conference **BULTRIB '13**
October 24-26, 2013, Sofia
Society of Bulgarian Tribologists
Technical University of Sofia

CHARLES COULOMB AND HIS CONTRIBUTION TO TRIBOLOGY

Katarina D. Živkovic, Mathematical High School, Belgrade, Serbia
Viara Požidajeva, Univesity of Mining & Geology, Sofia, Bulgaria

Abstract: *Serbian nobel prize winner Andrić said: "In the battle between old and new, scientific knowledge of the old is as necessary as correct understanding of the new". Knowing about the genesis of tribology, will make acquiring new knowledge easier. This paper goves a short overview of the beginnings regarding the acquisition of knowledge about friction and its evolution from empirics to science. This evolution certainly defined the work of Charles-Augustin de Coulomb. This paper also shows Coulomb's contribution to tribology.*

Keywords*: tribology, Coulomb friction, dry friction*

1.INTRODUCTION

The international term "tribology" is derived from the Greek word „τρίβοσ", which means friction, so that tribology basically means friction science. Such a definition of tribology as a science is very narrow and does not include all its domains of interest. Today, tribology is defined as a science which deals with: friction, wear and tear, lubrication and the interactionof contact surfaces, during their mutual movement [1], [2], [3].

Under friction we understand the resistence of a pair of surfaces of two bodies during their relative movement, caused by sliding, rolling or combined slide-rolling movement. Friction act against the relative movement of the body. Friction appearing on contact surfaces of two bodies is called external friction and is different to internal friction, which is caused by relative movement of elements within the volumes of solid, liquid or gaseous bodies [4].

2. SCIENCE FRICTION OF THE OLDEST TIMES TO THE COULOMB

At the beginning of his history, man has encountered the problem of transfer, or material handling. The first transport means, probably around 6000 BC were sledges. Ancient Egyptians put a board underneath the sledges to reduce friction and therefore the pulling force, which would be treated with water or oil (*Figure:1*).

The first person to make observations related to friction probably was the ancient philosopher **Aristotle** (384 - 322 BC). He analyzed the sliding of a body over a surface and found out that for the movement of the body to be uniform, the body should be continually acted upon in the same way.

After Aristotle and till the endof the 15th century, friction was not scientifically treated, because Leonardo da Vinci was the first person to systematically dealing with this matter.

Some of the basic settings of tribology are related to **Leonardo da Vinci** (1452-1519). In his unpublished manuscripts, named "Madrid codex", Leonardo da Vinci writes 1508: "...friction force depends on the material of the interacting surfaces, and also on the level of their machining and it does not depend on the contact surface; it is proportional to the load mass and it can be reduced by

implementing "rollers" or lubrication material between the frictioning surfaces"[6]..Leonardo was the first person to implement the termfriction coefficient.

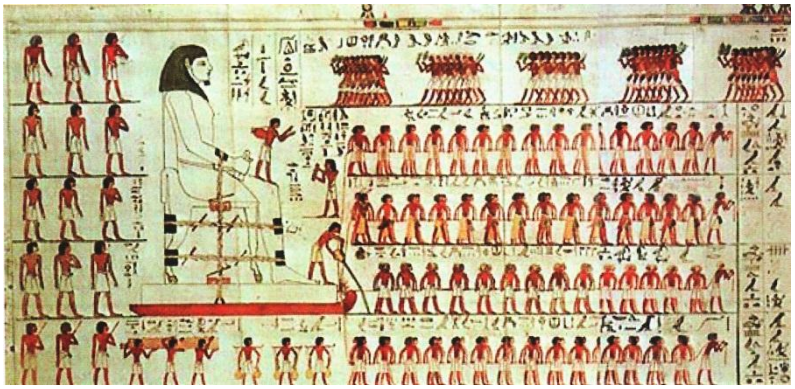


Figure 1: A drawing from an Egyptian tomb (El Bersheh approx. 1800 BC)

Almost two-hundred years after Leonardo da Vinci, **Guillaume Amontons** (1663-1705), 1699 . in his report pointed put two laws about slide friction, and they apply today. They are as follows:

1. zhe friction force is proportional to the normal force with which the body-puts .
2. The intensity of the friction force depends on the size of the contact surface of the body .

Amonton established an empirical law of linear dependency of the friction force on the load (*Figure:2*), which has the form:

$$F_T = \mu \cdot F_N$$

where:

F_T – friction force,

F_N – load perpendicular to the friction surface,

μ - coefficient of friction.

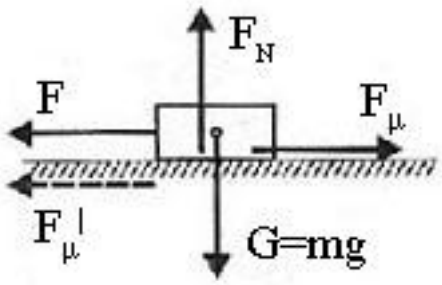


Figure 2: Forces acting on the body on a horizontal surface

From this elation we can derive the independence of the friction force from the nominal contact surface.

Another scientist, **Leonhard Paul Euler** (1707-1783) (*Figure:3*), the founder of machine dynamics, in his work, "On machines, in general", for the first time extracted the force of resistance that the machine overcomes during movement and divided it into friction force and inertial force.

He assumed that the friction force is a consequence of gravity, which tends to minimize the potential energy of a body. In Euler's model, sliding starts when the inclination of the roughness, which is assumed to be of triangular shape, becomes horiyontal on an inclined plane. If a typical inclination angle of the surface is α, the friction coefficient is $\mu = \text{tg}\ \alpha$. (*Figure:4).* Eur designated this

coefficient with the Greek letter μ and was the first to notice the difference between static and kinetic friction [7].



Figure 3: Leonhard Paul Euler (1707-1783)

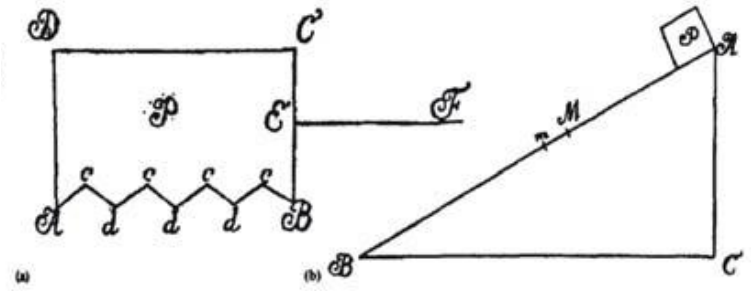


Figure 4: Triangular shaped roughness as the case of friction in Euler's model,

3. CHARLS AUGUSTIN COULOMB (1736-1806)

The great french scientist and army engineer Charles Coulomb (1736 – 1806) (*Figure:5*) is considered the founder of tribology.

The Coulomb family in Languedoc was known for generations of lawyers, and Henri Coulomb was the inspector of royal estates, when his son Charles-Augustin was born on June 14th 1736. In 1758, at age 22, Charles Coulomb goes to Paris, studies mathematics and was accepted to the Royal Engineering school in Meziers. He attended this school from 1760. to November 1761, when he became lieutenant.

Lieutenant Coulomb is sent to the port of Brest, where he maps the coastline. Accidentally, when a ship was to transport a group of engineers to the island of Martinique, one of the engineers fell sick, and Coulomb is ordered to replace him. In February 1762, lieutenant Coulomb arrives at Fort Royal, where he gets the task to build a new fortress (the old one was destroyed in 1759 by the English). For eight years Coulomb commanded the building of the fortress.

Coulomb returned to Paris in 1772 as an experienced and well accepted engineer; he was 36 years old. After his return to France, from 1772 to 1781, Coulomb lives in Bouchaine, Cherbourg, Besancon, Rochefort and Lille. At all this locations he has no complicated tasks, so that he had much time for research that was oriented towards the Academy of sciences in Paris. He found themes for research in his environment, at work, and in tenders from the Academy of sciences.

At that time, Coulomb already was an associate member of the Academy in Paris, thanks to his papers prepared while on Martinique, especially the one dealing with the application of infinitesimal calculus on the problems in statics. There he considers strength of material, bending and breaking of bars, the construction of arcs and other topics. Reviewers state that he has covered „the entire architectural statics". In July 1774, he becomes an external member of teh Academy of sciences in Paris. During the next seven years, he will be reading six papers before the Academy.

The Parisian Academy in 1773 makes a call for works on the topic „How to best design a magnetic needle". Two years later, this call is extended to another two years, because no paper has fulfilled the goal that was set, and the prize to be awarded is doubled. Coulomb, although he never dealt with magnetism, senses that the main problem lies in the behavior of the material, and he used his major experience: he focused on torque and friction. He finishes the paper on time and in 1776 he shares the prize with Van Svinden. This paper was the base for later measurement of electric and magnetic force.

In the following year, the Academy makes a call for papers about friction during sliding and during rolling, bending strength and about the application of the solutions to these problems on simple devices used in the Navy. Again the story is the same: from 1777-1779 there was no winner, the call was extended and the prize doubled. This time Coulomb wins the prize alone, in 1781. The paper contained a series of empirical formulae about friction,. The same year, Coulomb becomes an extraordinary member of the Parisian Academy, in the Mechanics section.

Coulomb did, one century after Amonton, introduce the third empirical friction law:

3. From the moment of slip, the friction force is independent from the relative sliding speed.

Therefore, these three laws are today known as da Vinci Amonton-Coulomb or Amonton-Coulomb's law on dry friction.

Coulomb studied the how friction occurs. Based on research, similar to Euler, he said that the microsized roughness at the contact location causes friction. Coulomb's findings on friction have dominated science for a centurz and a half, and many of his concepts are still accepted today, so that the term „Coulomb friction" still can be found in modern publications (*Figures:6 ans 7*). The instrument used for measurements in this field, the tribometer, as given its name by Coulomb [8].

Coulomb determined that the static friction force increases with the time that a body spends in staitonary condition.



*Figure 5***:** Charles Coulomb, (1736 – 1806)

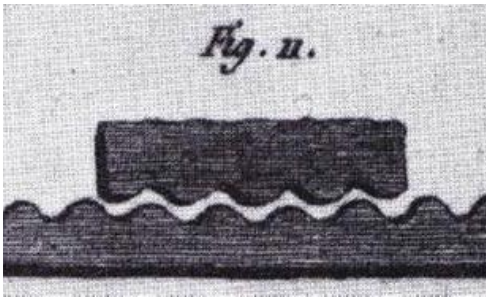


*Figure 6***:** Coulomb's sketch showing interaction between roughness elements as an origin of the friction force

In his work, "The theory of simple machines", Coulomb covered three basic aspects of friction: sliding resistence, rolling resistence and cutting resistence. Doing research on friction occurring during sliding of various metals, minerals and wood types, Coulomb generaliyed Amonton's law in the case when the friction force does not or very slightly depends on the load:

$$F_T = \mu \cdot F_N + A$$

where:

A – is a variable which takes into account the engaged surfaces and the proportionality of the contact surface.

Most materials have a static friction coefficient in dry contact with values between 0.3 ÷ 0.6. Values outside of this range are very rare (Teflon, for example, has a friction coefficient of 0.04). During the contact of rubber with other materials, the static friction coefficient can reach values from 1 to 2 [9].

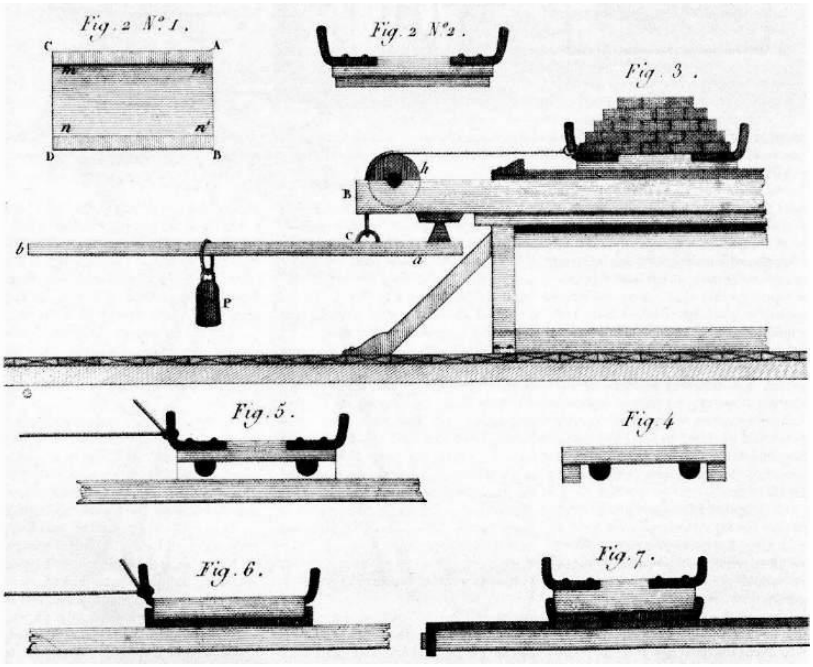


Figure 7: Coulomb's sketches for the determination of the friction force

For the rolling resistence, Coulomb gave the following formula:

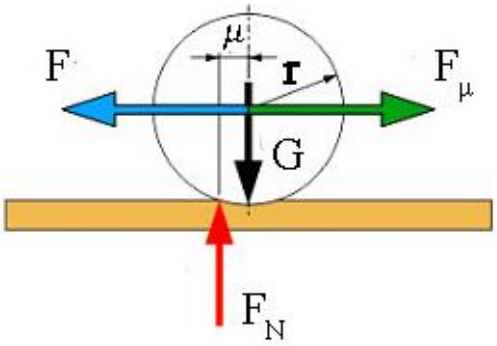


Figure 8: Forces that act on the body during rolling over a horizontal surface

$F_T = \mu_{KOT} \cdot F_N / r$

where:

F_N – force perpendicular to the load,

μ_{KOT} – rollinf friction coefficient,

r – cylinder radius.

Coulomb's contribution to tribologz lies in the fact that he was the first to find out that friction depends on a large number of factors, and that the relations between them were majorlz empirical. He noticed that the friction coefficient is influenced not only by load and sliding speed, but also by the type of material of engaged surfaces, their roughness level, position; fibres in the material, and even by humidity.

4. DEVELOPMENT OF SCIENCE FRICTION AFTER COULOMB

After Coulomb, there was a number of scientist that have contributed to the development of tribology.

Independently from Coulomb, **Samuel Vince** (1749-1821) in 1785 proposed the idea that the nature of static friction is related to cohesion and adhesion.

An alternative approach to friction was given by **John Theophilus Desaguliers**, who in 1734 caimed that molecular adhesion is the phenomenon most important in relation to friction. The intesitz of the corresponding force in this case is proportional to the contact surface, which contadicts Amonton's second friction law.

Some time later, **Jonh Leslie** (1776-1832), professor of physics in Edinburgh, considered the energy aspects of friction produced by solid bodies. Based on that analysis he concluded that they cannot be explained based on the idea that roughnesses of the „upper" body move over the roughnesses of the „lower" body, because in that case the potential energy lost when sliding down the roughness of the base would be regained in the climbing phase over the next roughness.

The fact that mechabnical energy does not vanish during friction, but is converted into heat, was forst discovered by **Benjamin Thomson, Count Rumford** (1753-1814). Rumford's discoveries meant a lot in explaining the phenomenon of friction, although the cause of heat produced through friction was still not clear enough [5].

The solution of this problem was made possible only in mid 19th century. In 1842 **J.R. von Mayer** (1814-1878), and in **James Joule** (1818-1889) in 1843 established the principle of equivalence of mechanical energy and heat, and **Hermann von Helmholtz** (1821-1894) introduced in 1847 the fundamental approach to energy and formulated it in the general form of the third law of energy maintenance.

This field of expertise further developed in the 20th century, because new experiment techniques and models were adopted, that enabled better analysis of the structure and microgeometry of real surfaces. Based on that, **Tomlinson** and **Deryagin** reconsidered the role of adhesion, and the macroscopic expression of friction in the way we register it as the consequence of molecular interaction and energy dissipation.

In 1950, **Frank Philip Bowden** (1927-1968) and **David Tabor** (1913 - 2005), using systematic experiments showed that the contacts between macroscopic bodies is established through a series of small peaks. Based on that, the term real cotact surface was introduced, and it is smaller of the natural geometrical contact surface.

5. REFERENCE

[1] Živković, D., Pozhidaeva, V. Molnar, R. Documentation Accompanying the Lubrication of Agricultural Machines and Requirements Relating to Quality Sistem Standards, Journal of theBalkan Tribological Association, Book 2, 2009. pp.270-280.

[2] Živković, D. Pozhidaeva, V. Sajfert, Z. Lubrication of Hay Press as Part of preventive maintenance**,** Journal of the Balkan Tribological Association, Book 3, 2010. pp. 453-460.

[3] Živković, D. Pozhidaeva,V. Veljić,M. Veljović,A. Information System and System of Quality Procedurs for Machine Lubrication, Journal of the Balkan Tribological Association, Book 4, 2011. pp. 652-664.

[4] Милтеновић, Војислав, Машински елементти, Машински факултет Универзитета у Нишу, Ниш, 2009.
[5] Mailer, Dejvid, Jan i Margaret, Kembrički rečnik-naučnici, Dereta, Beograd, 2003.
[6] Танасијевић Слободан, Основе трибологије машинских елемената, Научна књига, Београд, 1989.
[7] Letić Dušan, Sajfert Vjekoslav, Živković D. Katarina, Matemtičke konstate e, γ, $\sqrt{-1}$ – naučna monografija, Tehnički fakultet "Mihailo Pupin" Univrzitet u Novom Sadu, Zrenjanin, 2013.
[8] Mlađenović, M. Velikani fizike, Prirodno matematički fakultet, Univrzitet u Novom Sadu, Novi Sad, 2008.
[9] Snežana Radonjić, Jelena Baralić, Nedeljko Dučić, TIO-6, 6. Međunarodni Simpozijum, Tehnički fakultet Čačak, 2011.

Tribological Journal BULTRIB, **Vol. IV, 2014**
Papers from the International Conference **BULTRIB '13**
October 24-26, 2013, Sofia
Society of Bulgarian Tribologists
Technical University of Sofia

GENERALIZED ENERGY MODEL FOR SLIDING FRICTION COEFFICIENT AND EVOLUTION OF TRIBOSYSTEMS

Sergey Vasiliy FEDOROV

Abstract: *There is a belief in present-day tribology that the sliding friction coefficient has no physical significance and represents merely a convenient design parameter defined as the ratio of the force of friction F to the normal load N However, a theoretical (Triboergodynamics) analysis, a revised energetic interpretation of Amonton (Leonardo da Vinci) friction coefficient, and numerical calculations have shown the friction coefficient to be not only a basic but and most informative characteristic of the friction. May be it is an enigma of Leonardo da Vinci for modern engineers?*

Key Words: *energy balance, friction coefficient, evolution, nanostructure, wear standard*

1. INTRODUCTION

For discussion the basic conclusion about the essence of friction sliding coefficient of conceptual triboergodynamics theory [1-3] is proposed. The general evolution regularities of states and properties of tribosystem in the frame of triboergodynamics are analysed. Triboergodynamics is based on our modern knowledge of friction: 1. friction is a phenomenon of resistance to relative motion between two bodies, originating at their surfaces contact area; 2. friction is the process of transformation and dissipation of energy of external movement into other kinds of energy; 3. friction is the process of elasto-plastic deformation localized in thin surface layers of rubbing materials; and on analysis method to plastic deformation of ergodynamics of deformed solids [4].

2. TRIBOERGODYNAMICS METHOD

The friction is generally described by the energy balance equation and with thermodynamical point of view [1-3] is the process of two interrelated, oppositely directed and concurrent trends operating in a strained contact. According to the energy balance scheme (Figure 1) for plastic deformation and fracture [4] presented below, equations for friction work W_f, frictional force F and friction coefficient μ (without lubrication) has view

$$W_f = \Delta U_e + Q = \Delta U_{e1} + \Delta U_{e2} + \Delta U_{T1} + \Delta U_{T2} + \bar{Q}_1 + \bar{Q}_2, \quad (1)$$

$$\dot{W}_f = \dot{U}_e + \dot{Q} = \dot{U}_{e1} + \dot{U}_{e2} + \dot{U}_{T1} + \dot{U}_{T2} + \dot{\bar{Q}}_1 + \dot{\bar{Q}}_2, \quad (2)$$

$$F_l = \frac{\Delta U_e}{l} + \frac{Q}{l} = \frac{\Delta U_{e1} + \Delta U_{e2}}{l} + \frac{Q_1 + Q_2}{l}, \quad (3)$$

$$F_v = \frac{\dot{U}_{e1} + \dot{U}_{e2}}{v} + \frac{\dot{Q}_1 + \dot{Q}_2}{v} = F_{mechanical} + F_{molecular}, , \quad (4)$$

$$\mu_l = \frac{\Delta U_{e1} + \Delta U_{e2}}{Nl} + \frac{Q_1 + Q_2}{Nl} = \mu_{adapt} + \mu_{dis} = \mu_{adapt} + \mu_{T(dis)} + \mu_{\bar{Q}(dis)}, \quad (5)$$

$$\mu_v = \frac{\dot{U}_{e1} + \dot{U}_{e2}}{Nv} + \frac{\dot{Q}_1 + \dot{Q}_2}{Nv} = \mu_{deformation} + \mu_{adhesion}, \quad (6)$$

where $\Delta U_e = V_f \Delta u_e$; $Q = V_f q$; $\dot{U}_e = V_f \dot{u}_e$; $\dot{u}_e = \mathrm{d}u_e / \mathrm{d}t$; V_f - is the deformable (friction) volume; μ - friction coefficient; μ_{adapt} - adaptive friction coefficient; $\mu_{T(dis)}$ and $\mu_{\bar{Q}(dis)}$ - static and dynamical components of dissipative friction coefficient; ΔU_T - thermal component of internal energy; N - normal load; l - distance of friction. The latent energy density Δu_e is an integral parameter of tribostate and damageability (failure (Δu_e^*)).

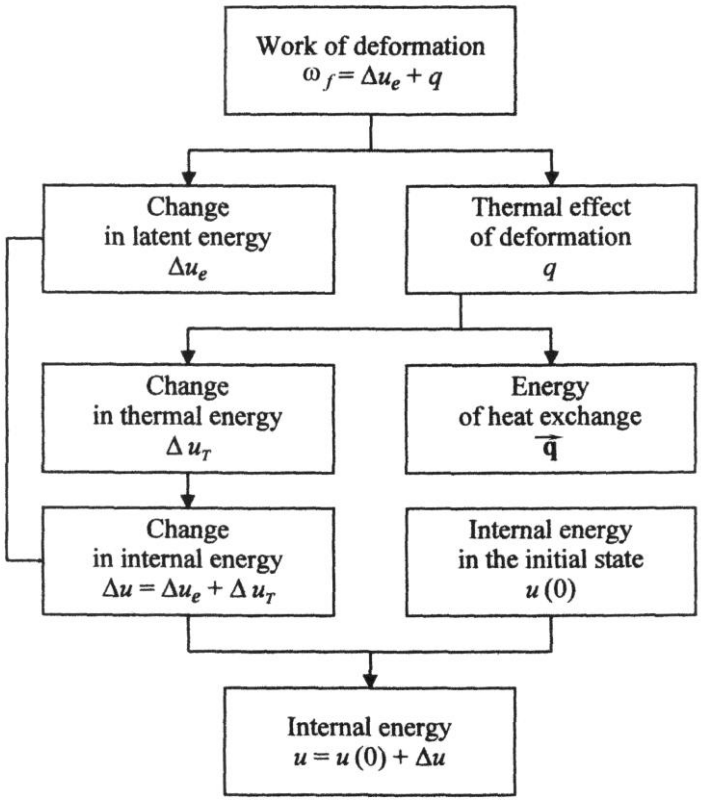


Fig. 1. Scheme of the energy balance for the plastic deformation of a solid body [4]

Thus, viewed thermodynamically, the work done by friction forces W_f (the friction power $\dot{W}_f$), the friction force F and the friction coefficient μ may be classified conventionally into two specific components with different kinetic behavior [3]. The first component is associated with microscopic mechanisms of adaptive type and relates to the change of latent (potential) energy ($\Delta u_{e1}, \Delta u_{e2}$) of various elementary defects and damages that are generated and accumulate in the deformable volumes of materials friction pair (Figure 2). This energy is a unique and integral characteristic of the submicro- and microstructural transformations that occur in plastically strained materials [4]. This energy is a measure of strain hardening and damageability of materials. The second component is associated with microscopic mechanisms of dissipative type and relates to dynamic recovery processes in which latent energy is released and heat effect of friction (q_1, q_2) take place. This energy originates in the motion and destruction of various elementary defects of opposite signs, the egress of these defects to the surface, the healing of reversible submicroscopic discontinuities, etc. The ratios of the components Δu_{e1} and Δu_{e2} as well as q_1, q_2 of the balance vary over a wide range, depending on the physical, chemical, and structural properties of the materials that comprise the friction couple and the friction process conditions.

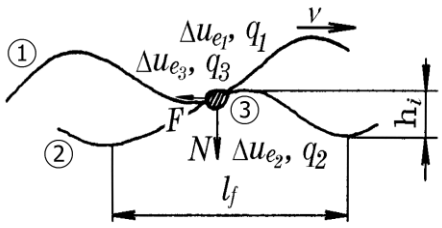


Fig. 2. Schematic view of elementary friction's contact [1-3]

Thus, the thermodynamic analysis of friction (plastic deformation and fracture) has led to generalized (two-term) relations for the force F and coefficient of friction μ, which agrees with current concepts of the nature of friction.

Relationships (1)-(6) which generalize the mechanism of energy dissipation at friction allow to classify the tribosystem states. According to ergodynamics of deformed solids (relationships $\Delta u = \Delta u_e + \Delta u_T$ and $q = \Delta u_T + \bar{q}$) and equations (1)- (6) , all exhibitions of friction and wear may be reduced conventionally at least to two basically different states: the first state defines all types of damage and wear, the second — the so-called "wearless" condition. The state of damage and wear is characterized by the components of energy balance (1)-(6), which are responsible for accumulation of internal energy in deformed volumes $\Delta u = \Delta u_{e1} + \Delta u_{e2} + \Delta u_{T1} + \Delta u_{T2}$, i.e. the process is irreversible. The "wearless" state is characterized by the components responsible for dynamic dissipation (reversibility) of strain energy into elastic and structural dissipated energy of friction contact $\bar{q} = \bar{q}_1 + \bar{q}_2$.

In its turn, the first state may be classified depending on the relation between potential Δu_e and kinetic Δu_T components of internal energy. It is subdivided conventionally into mechanical damage and wear (due to so-called structure activation) and thermal damage and wear (due to thermal activation). For instance, let the thermal component of internal energy Δu_T be equal to zero ($\Delta u_T = 0$) and the internal energy variation at damage and wear be defined only by variation of the potential component $\Delta u_e (\Delta u = \Delta u_e)$.

Then, the mechanical damage and wear with brittle fracture of surfaces take place. On the contrary, if we have $\Delta u_e = 0$ ($\Delta u = \Delta u_T$), then the thermal damage and wear with ductile fracture of surfaces take place. All the intermediate values of the components are associated with quasi-brittle or quasi-ductile fracture of solids.

In the most general case, the energy balance at dry friction (1) should be written as

$$W_f = \Delta U_{e1} + \Delta U_{e2} + \Delta U_{e3} + Q_1 + Q_2 + Q_3 \quad . \tag{7}$$

In the special case, where the friction is localized into volume of the "third body" equation (7) develops into

$$W_f = \Delta U_{e3} + \bar{Q}_3 . \tag{8}$$

According to thermodynamic theory of strength [4], the damageability parameter and the fracture criterion are defined in terms of the internal energy density u accumulated within the strained element of a solid body. A solid body is assumed to suffer fracture if the internal energy density has reached a critical value u^* in at least a single macrovolume that is responsible for fracture.

3. ENERGY INTERPRETATION OF AMONTON'S FRICTION COEFFICIENT

According to thermodynamic theory of strength [4], the structure parameter should be related to the portion of the accumulated plastic deformation that is responsible for strain hardening. This portion is uniquely and integrally defined by the density of the potential component of internal energy (that is, the latent energy density Δu_e) of various defects and damages that accumulate in a plastically strained material. With this in mind, if we neglect the heat effect Q of friction, one will infer from the thermodynamic analysis of friction of equations (1)-(6) that the Amonton (Leonardo da Vinci) friction coefficient is

$$\mu = \frac{\Delta U_e}{\mu^* N l} = \frac{F}{N}; \quad F = \frac{\Delta U_e}{l}; \quad Q \cong 0, \quad \mu^* = 1. \tag{9}$$

Consequently, the coefficient of friction has a very deep physical sense. On the one hand, it is the parameter which generally characterizes the resistance of relative displacement (movement) of surfaces, for it reflects the portion of energy, which «is done by friction away» as accumulated latent energy ΔU_e, by relation to parameter of external forces work $\mu^* N l$ (energy of external relative movement). On the other hand, it is the generalized characteristic of damage, for it is defined of the latent energy density Δu_e as integral characteristic of the structure defectiveness measure, because this energy is the generalized parameter of damage. Here too, coefficient of friction generally reflects the structural order (disorder) of deforming contact volume, since the parameter $\Delta U_e = \Delta u_e V_f$ is defined of the energy of defects and damages of different types, that are accumulated into contact volumes V_f solids.

Therefore, coefficient of friction is a true and generalized parameter of tribosystem state. From this conclusion we can say that the analysis of the evolution of the states of a tribosystem is primarily an analysis of the latent deformation energy accumulated within the contact friction volumes.

4. ENERGY REGULARITIES OF RUBBING SURFACES EVOLUTION

An analysis of modern experimental data using equations (1)-(9) has shown that the experimental friction curves of type $\mu = \mu(N, v)$ are the generalized friction curves that reflect the evolution (the change in the friction coefficient) of tribosystem.

We propose an energetic interpretation of the experimental friction curves $\mu = \mu(N, v)$ (Figure 3). According to our concept [1-3], the ascending portion of the friction coefficient curve μ is mainly controlled by processes associated with the accumulation of latent energy ΔU_e in various structural defects and damages. Here the increase in μ is due to the increasing density of latent (potential) energy Δu_e and the increasing adaptive friction volume V_f. The descending portion of the friction curve is mainly controlled by processes associated with the release and dissipation of energy $Q = \Delta U_T + \vec{Q}$. Here the decrease in μ is due to the decrease in latent energy density within the friction volume V_f or (which is virtually the same) to the decrease of the adaptive friction volume V_{adapt} ($u_e = u_e^*$) and to the increase of the dissipative volume V_{dis} ($\vec{q}^* = u_e^*$).

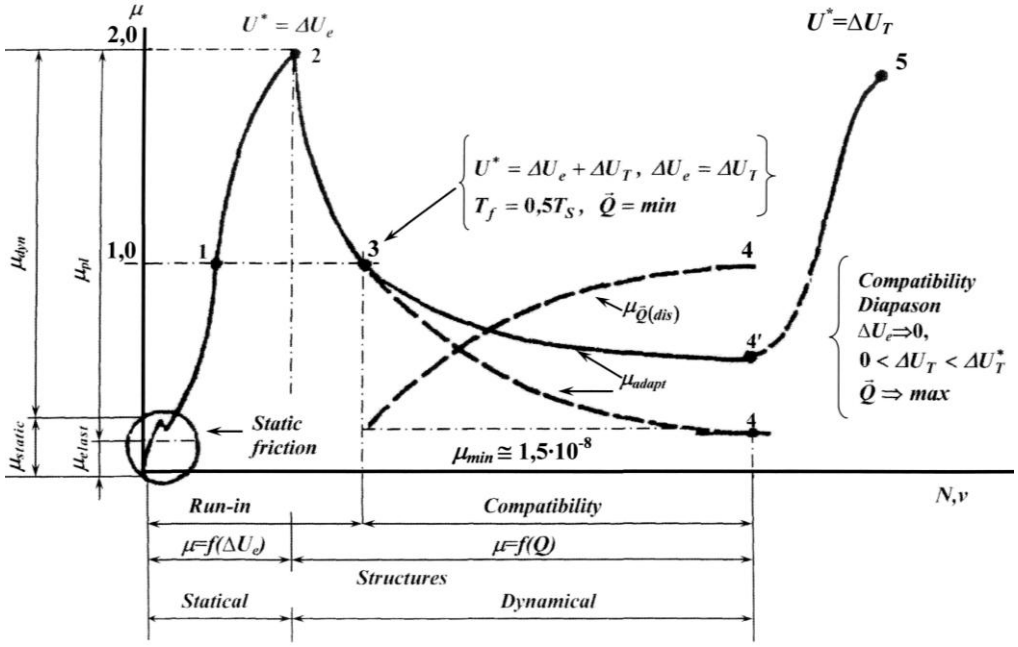


Fig. 3. Structural-energy diagram for evolution of rubbing surfaces [1-3]

Evolution of tribosystem, presented as a diagram view (Figure 3), has an adaptive-dissipative character (1)-(6) and reflects the competitive (dialectical) nature of friction. Evolution curve has the row of principal points (1-5) of transitional tribosystem states, which strictly obeys the balance principle of friction; there are morecharacteristic areas of tribosystem behavior between these points. These areas reflect the common properties of nonlinear dynamic of evolution.

One may specify conventionally the following stages and points in Figure 3: 0-1, the stage of static friction and strain hardening; 1, the limiting strain hardening point; 1-2, the excess energy uptake stage; 2, the galling point for external-to-internal friction transition (critical instability-adhesion); 2-3, the stage for temperature flash and dissipative structure formation;3, the compatibility point; 1-3, the adaptation and self–organization region; $3-4'$, the compatibility stage; and 4, the point of anomalously low friction; 5- thermal adhesion point.

Ideal evolution of tribosystem is symmetrical. The process is started and finished in elastic areas. Between these points there is the plastic maximum (superactivated state) of contact as selforganization and adaptation terms.

Generally, two stages may be envisioned in the evolution (adaptation) of a tribosystem. At the first stage (1-2) of adaptation the evolution of friction contact rushes to form some critical volume of friction V_f^* (point 2). It is elementary tribosystem that is the elementary and self-sufficient energy transformer.

This friction volume V_f^* is constant at the second stage of evolution, but here it is evolutionary developed owing to structural transformation; by this one may realize wide spectrum of compatibility friction structures (Figure 3). Second stage (2-4) is a stage of conversion of the critical friction volume V_f^* to an adaptive V_{adapt} and a dissipative V_{dis} volume. In the limit (point 4), this stage terminates in the complete conversion of the adaptive critical volume V_{adapt}^* to the dissipative volume V_{dis}^*. These two volumes reflect specific conversions of the energy of external mechanical motion with friction. The adaptive volume is associated with irreversible uptake of deformation energy. Within this volume, the latent deformation energy Δu_e accumulates and damage sites are generated. The dissipative volume is capable of transforming (dissipating $\bar{q}$) reversibly the energy of external motion. This volume accumulates no latent energy due to reversible elastical-ductile-plastic deformation. Culmination of tribosystem evolution is final and limited state (point 4). This is a state of anomalously-low friction and «wearlessness».

5. ABOUT MECHANICAL (NANO) QUANTUM OF DISSIPATIVE FRICTION STRUCTURES

As the result of more full evolution of elementary tribosystem (Figure 3, point 4) the unique nanostructure is formed and the basis of which is one mechanical (nano) quantum [5]. This mechanical quantum represents the minimum number of atoms that can be arranged in a structure capable of reversibly absorbing and dissipating (recovering) the energy of external mechanical motion. Mechanical quantum represents the least structural form of solid material body in conditions of plastic deformation too and under transition tribosystem across the limit activated state by development of selforganazing processes of tribosystem adaptation are formed. The universal size (volume) of mechanical quantum [3,5] is equal to:

$$V_Q = (e^3)^3 = (20{,}08553695...)^3 = 8103{,}083969... \text{ atom's oscillators.} \quad (10)$$

Mechanical quantum is dynamic oscillator of dissipative friction structure. Linear size of quantum is equal to diameter of spherical ideal crystal:

$$D_Q = 2 \cdot W \cdot \bar{d}_a \cdot (3/4 \cdot \pi)^{1/3} = 7{,}177 nm . \quad (11)$$

Here $\bar{d}_a$ - mean atomic diameter for metals; $W = e^3$ - parameter of state for mechanical quantum [3].

Mechanical quantum (Figure 4) can be examined as the elementary nanostructure of metal's solid body. Calculations have shown the number N_Q of such mechanical «quanta» (subtribosystems) within the elementary tribosystem's volume $V_f^* = V_{dis}^*$ to be $0{,}63 \cdot 10^8$, which is close to the safe number n_* of fatigue cycles.

In these terms (point 4) only one mechanical quantum [3] is the lost – standard wear. The tribosystem (friction contact) has the ideal damping properties – «wearlessness».

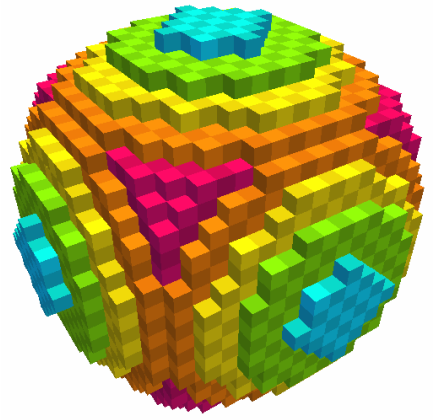


Fig. 4. Model of elementary nanostructure of friction (8103 atomic cubical cells) [5]

The quanta model of the surfaces damping with dissipative friction structures has been examined.

$$\mu_{diss\bar{Q}} = \frac{3R_{MQ}Tn_i}{Nl} = \frac{U_{1q}n_i}{U_{1q}n_*} = \frac{n_i}{n_*} = 1 - \mu_{adapt}, \tag{12}$$

$$\mu_{adapt} = 1 - \frac{n_i}{n_*} = \frac{n_{dest}}{n_*} \quad . \qquad n_i = n_* - n_{dest}; \tag{13}$$

Here $R_{MQ} = k \cdot 8103{,}083\ldots\left(\text{J}/K \cdot MQ\right)$ - universal constant of mechanical quantum (MQ); $3R_{MQ}T = U_{1q}$ - one mechanical quantum energy; n_i - the fatigue number (damping quanta (reversible component)); n_{dest} - the destruction quanta (irreversible process component) k - Boltzmann's constant.

According to the quanta damping model of surfaces under friction, when we have the state of more full evolution of elementary tribosystem, the all mechanical quanta to elastic and reversible transform the energy of external mechanical motion. Only one mechanical quantum (8103 atoms) is the minimum loss (the essence of «wearlessness»).

CONCLUSIONS

1. Energy balance analysis of the friction process has shown the friction coefficient is a basic and most informative characteristic of the friction process;
2. Energy analysis of the friction process allows us to examine the friction process as the evolution process;
3. From the energy balance equations of friction follows that the evolution of tribosystem has an adaptive-dissipative character.
4. The fuller evolution of tribosystem has symmetrical view - the friction process is started and finished within elastic area.
5. Experimental friction curves of $\mu = \mu(N, v)$ type may be examined as generalized friction experimental curves;
6. Under fuller evolution of friction contact (elementary tribosystem) the unique nanostructure is formed; the basis of this structure is the mechanical (nano) quantum and the contact (material mechanics point) consists of about $0{,}63 \cdot 10^8$ such quanta.
7. We can examine the mechanical quantum as the least structural form of solid material body and the standard of wear.
8. All parameters of compatibility (optimal) friction have to be in quanta levels - commensurable with the parameters of the one mechanical quantum.

REFERENCES

1. Fedorov, S.V., "General Model of Friction", Journal of Friction and Wear, 14, 3, 1993, 20-28.
2. Fedorov, S., "Method for the Energy Optimisation of Tribosystems", 9th International Tribology Colloquium, Januare 11-13, 1994, Esslingen.
3. Fedorov S.V., "The Foundations of Triboergodynamics and Physico-Chemical Prerequisits of Compatibility Theory", Kaliningrad State Technical University Press, Kaliningrad, 2003, 416.

4. Fedorov, V.V., “Ergodynamic concept of failure. 1. Basic statements of the ergodynamics of deformed bodies. Criteria of failure ductility”, Strength Of Materials (Translated from Russia), 23, 8, 1991, 883-889.
5. Fedorov, S. V., “The mechanical quantum of dissipative friction structures is the elementary tribonanostructure”, IV WTC2009, September 5-11, 2009, Kyoto.

CORRESPONDENCE

Sergey Vasiliy Fedorov

Department of Theory of Mechanisms and Machines and Machines Parts,
Faculty of Mechanics and Technology, Kaliningrad State Technical University,
236022, Kaliningrad, 1 Sovietsky prospect, Russia
fedorov@klgtu.ru

Tribological Journal BULTRIB, **Vol. IV, 2014**
Papers from the International Conference **BULTRIB '13**
October 24-26, 2013, Sofia
Society of Bulgarian Tribologists
Technical University of Sofia

PHASE CHANGES IN NANODIMENSIONAL COBALT FERRITE-TYPE MATERIAL ACTIVATED BY MECHANOCHEMICAL TREATMENT

Katerina ZAHARIEVA[1], Zara CHERKEZOVA-ZHELEVA[1], Boris KUNEV[1], Silvia DIMOVA[2], Martin TSVETKOV[3], Ivan MITOV[1], Maria MILANOVA[3]

[1]Institute of Catalysis, Bulgarian Academy of Sciences, "Acad. G. Bonchev" St., Block 11, 1113 Sofia, Bulgaria
[2]Institute of Polymers, Bulgarian Academy of Sciences, "Acad. G. Bonchev" St., bl. 103A, Bulgaria
[3]Faculty of Chemistry and Pharmacy, St. Kliment Ohridski University of Sofia, 1 J. Bourchier Blvd., 1164 Sofia, Bulgaria

Abstract: *The mechanochemical treatment* at *different activation times -1, 3, 5 and 7 hours was performed to initiate the phase changes in cobalt ferrite-type material obtained by co-precipitation. The results show that the higher milling times lead to presence of nanosized spinel ferrite with smaller particle size and cobalt iron phase. The intermediate oxihydroxide disappeared at milling time 5 hours. The co-precipitated cobalt ferrite-type photocatalyst tested for degradation of the Malachite green* oxalate *under UV light possess rate constant* $4x10^{-3}$ min^{-1} *and 78% sorption of the dye after the dark period.*

Key Words: *phase changes, mechanochemical activation, cobalt ferrite, photocatalyst*

1. INTRODUCTION

Milling is a important unit operation in the many fields such as chemistry, pharmacy, mineral processing of materials such as minerals, foods, medicine, chemicals and building materials [1,2]. The mechanical milling is a complex process which includes the optimization of a number of variables to obtain a desired phase or microstructure. The milling atmosphere, ball to powder ratio, milling speed, milling ball size, milling time, process control agent, starting powder size range, ductility of the initial powders should be considered to prepare the desired products. Presented parameters influence both the stages of milling and the quality of milled product [3]. The mechanochemical activation of crystalline solids conducted in high energy mills, can produce textural and structural changes which are of great significance for the development of new materials [4].

The present research is focused on the phase transformations in nanostructured cobalt ferrite-type material $Co_xFe_{3-x}O_4$, x=0.75 induced by mechanochemical treatment. For this purpose the co-precipitated nanosized cobalt ferrite was mechanochemically activated at different milling times. The phase composition and properties of obtained ferrite samples were investigated by X-ray diffraction analysis, Moessbauer and FTIR spectroscopy. The photocatalytic and sorption properties of co-precipitated nanodimensional cobalt ferrite-type material via photocatalytic decolorization of the Malachite green oxalate dye under UV irradiation are also discussed in our investigations.

2. EXPERIMENTAL

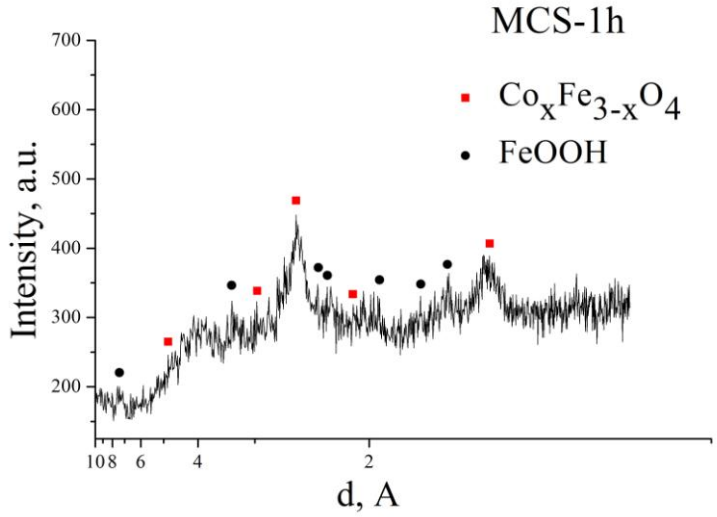
The initial nanodimensional cobalt ferrite-type sample ($Co_{0.75}Fe_{2.25}O_4$) with additional amount of intermediate phases - β-FeOOH and iron-cobalt hydrotalcite was prepared by co-precipitation procedure using 0.03 M aqueous solutions of $FeCl_2•4H_2O$, $FeCl_3•6H_2O$, $CoCl_2•6H_2O$ mixed in a ratio of 1:8:3 and precipitant 0.3 M NaOH in our previous investigations [5]. The synthesized cobalt ferrite-type material was mechanochemically treated at different milling times - 1, 3, 5 and 7 hours. Highenergy planetary ball mill type PM 100, Retsch, Germany was used for mechanochemical treatment. The milling activation process was carried out in argon atmosphere, milling container – 50 ml and rotation speed 500 rpm. The weight ratio between powder and balls is 1:30. The structure, phase composition and magnetic behaviour of obtained products were established by different techniques - X-ray diffraction analysis,

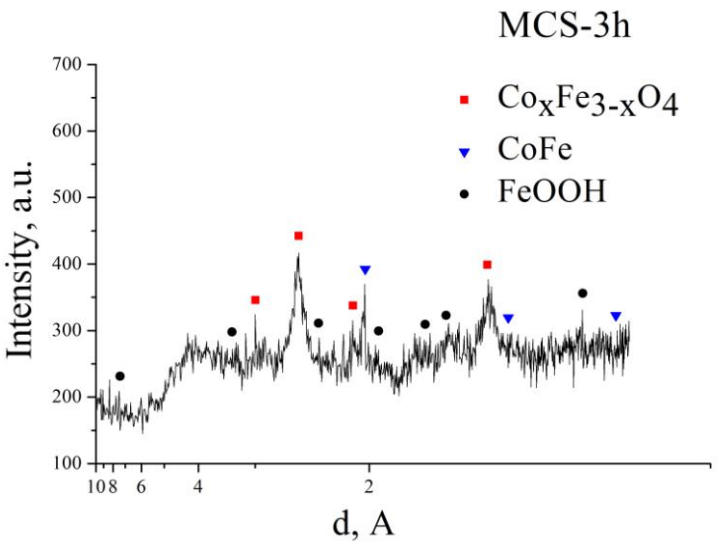
Moessbauer and FTIR spectroscopy. The X-ray diffraction measurements were made on TUR M62 apparatus with PC, HZG-4 goniometer at CoKα radiation. The Moessbauer spectra are registered with equipment Wissenschaftliche Elektronik GmbH, at a constant acceleration mode with ^{57}Co/Cr source and α-Fe as standard. FTIR studies in the region 400-4000 cm^{-1} were recorded on a Fourier infrared spectrometer Bruker-Vector 22 using KBr tablets.

The photocatalytic experiments were carried out with UV-illumination by lamp Sylvania 18 W BLB T8 and emission in the region 345-400 nm with maximum at 365 nm. The photocatalytic reaction was performed using aqueous solution of Malachite green oxalate dye (10^{-5} M) and 1 g/l co-precipitated nanosized cobalt ferrite-type catalyst. The dye concentration was determined spectrophotometrically using Specol 11 by the band at 622 nm.

3. RESULTS AND DISCUSSION

The X-ray diffraction analysis of starting co-precipitated cobalt ferrite-type sample discussed in our previous study [5] established the presence of non-stoichiometric ferrite phase $Co_xFe_{3-x}O_4$ (PDF-22-1086; 75-0449), additional phases as β-FeOOH (PDF-75-1594) and iron-cobalt hydrotalcite (PDF-14-0191) [5]. The recorded X-ray diffraction patterns of mechanochemically activated cobalt ferrite-type materials treated at different milling times – 1, 3, 5 and 7 hours are presented on Fig. 1. As can be seen the hydrotalcite phase is removed after one hour mechanochemical treatment. The oxihydroxide phase (β-FeOOH) (PDF-75-1594) observed at activation time 1 and 3 hours disappeared at 5 hours. The mechanochemical process after 3, 5 and 7 hours initiate the formation of non-stoichiometric spinel ferrite $Co_xFe_{3-x}O_4$ (PDF-22-1086; 75-0449) and cobalt iron (CoFe) (PDF-44-1433) phases.





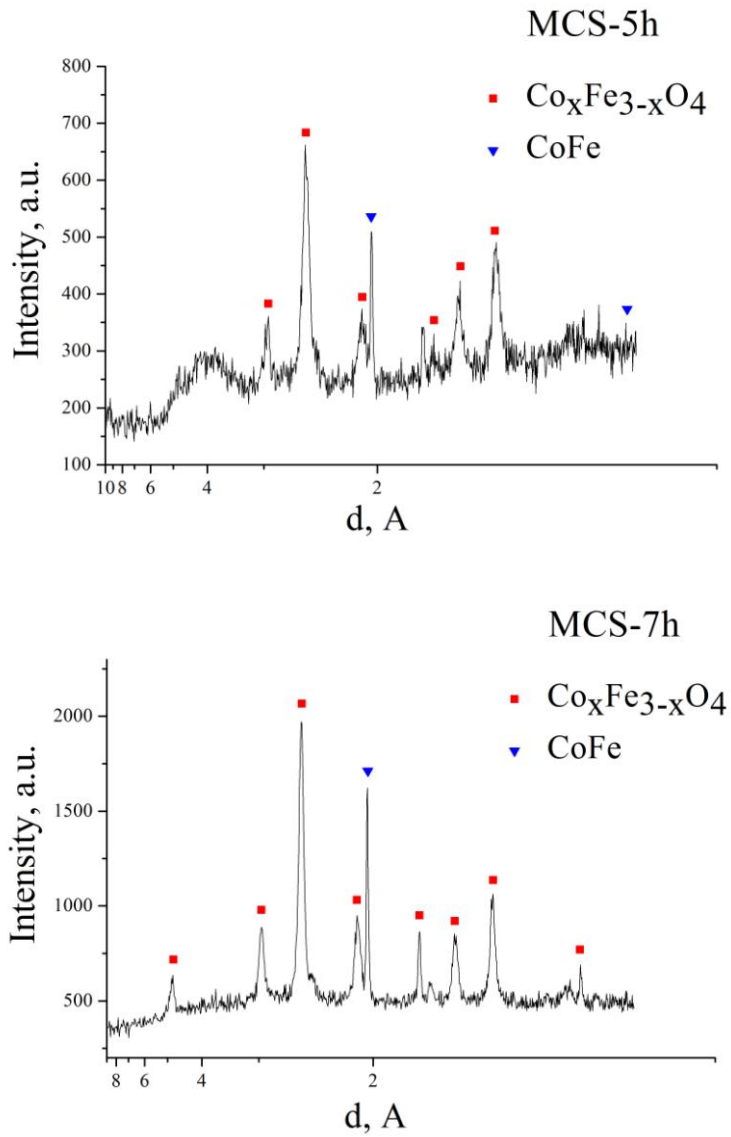


Fig. 1. XRD patterns of mechanochemically activated cobalt ferrite-type samples at different milling times – 1h (MCS-1h), 3h (MCS-3h), 5h (MCS-5h) and 7h (MCS-7h)

The average crystallite size, lattice microstrain parameter and unit cell parameter of investigated spinel ferrite phase was determined by Scherrer equation [6]. The obtained results are presented in Table 1. The calculated data correspond to the synthesized nanosized cobalt ferrite materials with mean crystallite size about 11.3 nm. The longer activation time reduced the particle size of spinel ferrites.

Table 1. Calculated values of mean crystallite size (D), lattice strain (ε) and unite cell parameter (a) of spinel ferrite phase

Sample	***D, nm***	***ε, a.u***	***a, A***
$Co_{0.75}Fe_{2.25}O_4$ MCS-1h	11,82	$4{,}2.10^{-3}$	6.037
$Co_{0.75}Fe_{2.25}O_4$ MCS-3h	11,78	$3{,}1.10^{-3}$	5.964
$Co_{0.75}Fe_{2.25}O_4$ MCS-5h	11,78	$1{,}7.10^{-3}$	5.898
$Co_{0.75}Fe_{2.25}O_4$ MCS-7h	9,91	$5{,}2.10^{-3}$	5.947

The Moessbauer spectra at room temperature of the obtained nanosized cobalt ferrite-type samples after mechanochemical treatment are displayed on Fig. 2. The presence of doublet lines only is registered in the Moessbauer spectra of co-precipitated (not shown) and mechanochemically treated cobalt ferrite-type material after one hour. The Moessbauer spectra of cobalt ferrite samples at 3 and 5 hours include a superposition of the sextet and doublet components. The Sn component belonging to the cobalt iron phase is observed in the spectra at mechanochemical activation for 5 and 7 hours The calculated Moessbauer parameters as isomer shift (IS), quadrupole splitting (QS), hyperfine effective magnetic field in the site of iron nuclei (H_{eff}), line widths (FWHM) and component relative weights (G) by fitting the spectra using CONFIT program are presented in Table 2. The calculated hyperfine parameters of doublet components could be assigned the presence of ferrite particles with superparamagnetic (SPM) behaviour. On the other hand the doublet components partially include also the existence of some iron ions in additional phase (oxihydroxide or hydrotalcite phase). The calculated hyperfine parameters of sextet components relate to tetrahedrally coordinated Fe^{3+} ions in a spinel phase – Sxt1 and octahedrally coordinated Fe^{3+} ions in a spinel phase – Sxt2 [5,6]. The Moessbauer results confirm the X-ray diffraction studies.

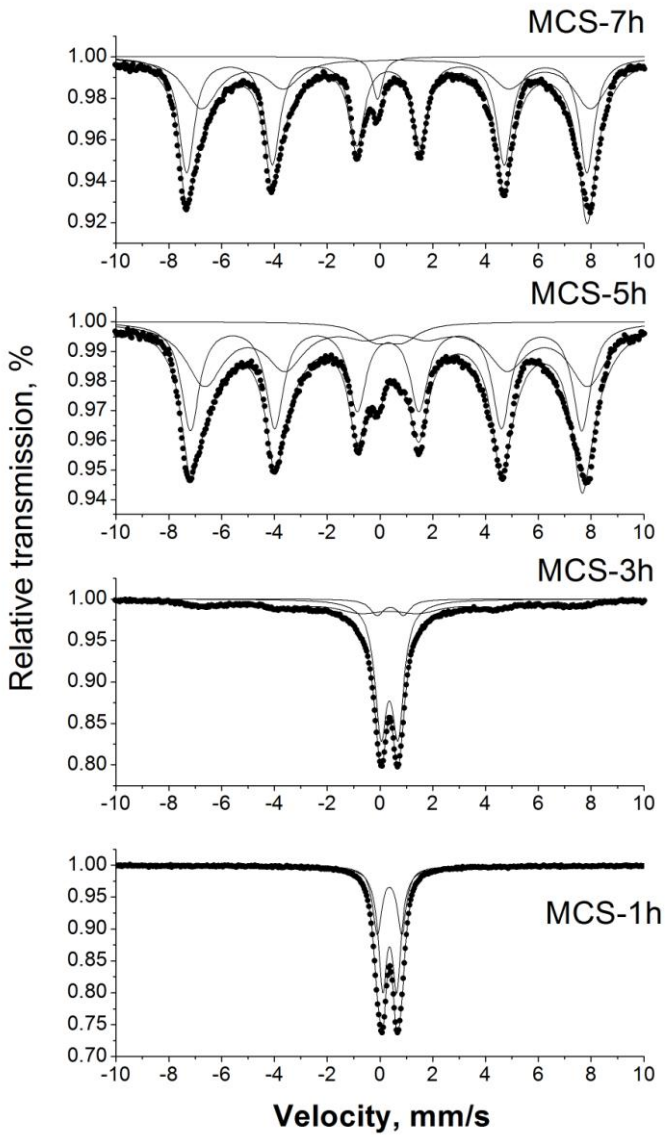


Fig. 2. Moessbauer spectra of mechanochemically activated cobalt ferrite-type samples at different milling times – 1h (MCS-1h), 3h (MCS-3h), 5h (MCS-5h) and 7h (MCS-7h) at RT

Table 2. Moessbauer parameters of samples

Sample	*Components*	*IS, mm/s*	*QS, mm/s*	*H_{eff}, T*	*FWHM, mm/s*	*G, %*
$Co_{0.75}Fe_{2.25}O_4$ MCS-1h	Dbl 1 Dbl 2	0.36 0.36	0.53 0.93	- -	0.40 0.41	62.4 37.6
$Co_{0.75}Fe_{2.25}O_4$ MCS-3h	Sxt 1 Dbl 1 Dbl 2	0.33 0.36 0.39	-0.05 0.65 1.01	42.9 - -	2.21 0.54 0.61	39.7 52.8 7.4
$Co_{0.75}Fe_{2.25}O_4$ MCS-5h	Sxt 1 Sxt 2 Dbl Sn	0.27 0.62 0.34 -0.08	-0.08 0 1.00 -	46.1 45.1 - -	0.81 1.72 1.48 0.45	51.3 42.2 5.1 1.4
$Co_{0.75}Fe_{2.25}O_4$ MCS-7h	Sxt 1 Sxt 2 Sn	0.29 0.61 -0.07	-0.06 0 -	47.1 45.8 -	0.70 1.54 0.45	61.5 35.7 2.8

The FTIR spectra in the range 400-4000 cm^{-1} of the mechanochemically activated cobalt ferrite-type samples by varying the milling times - 1,3,5 and 7 hours are illustrated on the Fig. 3. As can be seen from the Fig. 3, the obtained FTIR results are in agreement with XRD and Moessbauer investigations. The observed absorption bands around 590 cm^{-1} correspond to the stretching vibration of metal-oxygen (M-O) bond indicating the presence of cobalt ferrites. The located peaks at about 3400 cm^{-1} due to the stretching vibrations of hydroxyl groups [7].

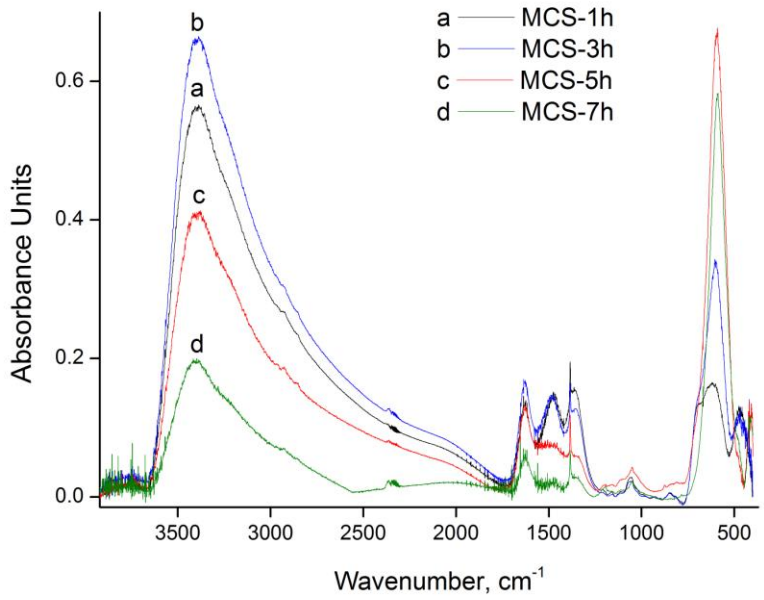


Fig. 3. FTIR spectra of mechanochemically activated cobalt ferrite-type samples at different milling times – 1h (MCS-1h), 3h (MCS-3h), 5h (MCS-5h) and 7h (MCS-7h)

The photocatalytic results about degradation of the Malachite green dye under UV irradiation using co-precipitated nanodimensional cobalt ferrite-type material as photocatalyst are presented in coordinates $-\ln(C/C_0)/t$, where C_0 is the concentration after the "dark" period, and C is the concentration after t min of irradiation (see Fig. 4). The apparent rate constant of ferrite catalyst $k=4 \times 10^{-3}$ min^{-1} is calculated assuming first- order kinetic. The nanostructured cobalt ferrite-type material shows a sorption ability 78% of the dye after the dark period.

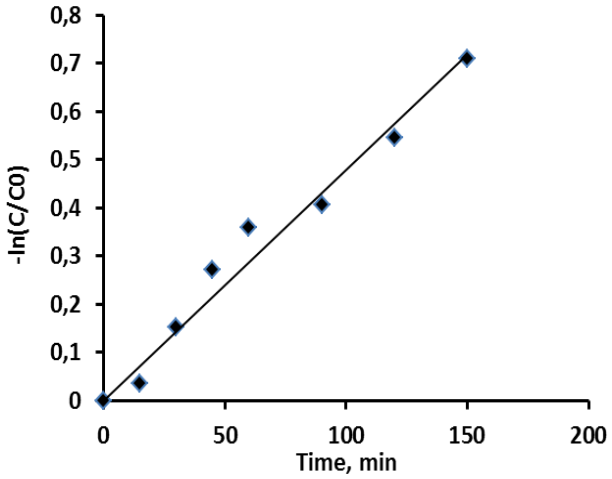


Fig. 4. Photocatalytic activity of co-precipitated cobalt ferrite-type material

4. CONCLUSION

The nanosized cobalt ferrite-type materials with high dispersity and mean crystallite size of spinel ferrite particles in the range 10 nm - 12 nm were obtained by mechanochemical activation. With increasing of milling time decreasing of particle size is established. The mechanochemical treatment leads to reduction and complete removal of additional oxihydroxide phase in mechanochemically activated cobalt ferrite-type materials. The formation of non-stoichiometric spinel ferrite and cobalt iron phases is observed during the milling process. The good sorption ability of 78% and photocatalytic activity $4x10^{-3}$ min^{-1}rate constant give a possibility to use the obtained nanodimensional cobalt ferrite-type material by co-precipitation as photocatalyst and absorbent for treatment of polluted waters.

ACKNOWLEDGMENTS

The present research studies are financially supported by Bulgarian Science Fund at the Ministry of Education, Youth and Science – Project DFNI-E01/7/2012.

REFERENCES

1. GOTOR, F.J., ACHIMOVICOVA, M., REAL, C., BALAZ, P., Influence of the milling parameters on the mechanical work intensity in planetary mills, Powder Technology, **233**, 2013, 1–7.
2. ZHANG, Q., SAITO, F., A review on mechanochemical syntheses of functional materials, Advanced Powder Technology, **23**, 2012, 523–531.
3. CANAKCI, A., ERDEMIR, F., VAROL, T., PATIR, A., Determining the effect of process parameters on particle size in mechanical milling using the Taguchi method: Measurement and analysis, Measurement, **46**, 2013, 3532–3540.
4. LUO, J., Synthesis of NiCuZn-ferrite powders by means of mechanochemical treatment, Materials Research Bulletin, **48**, 2013, 3527–3529.
5. CHERKEZOVA-ZHELEVA, Z., ZAHARIEVA, K., KUNEV, B., SHOPSKA, M., MITOV, I., Nanosize cobalt ferrites – preparation and physicochemical characterisation, Nanoscience and Nanotechnology, **13**, Eds. E. Balabanova, E. Mileva, 2013, 83-86.
6. SCHWERTMANN, U., CORNELL, R., Iron Oxides in the Laboratory, Weinheim, New York-Basel-Cambridge, 1991.
7. GHARAGOZLOU, M., Synthesis, characterization and influence of calcination temperature on magnetic properties of nanocrystalline spinel Co-ferrite prepared by polymeric precursor method, Journal of Alloys and Compounds, **486**, 2009, 660–665.

CORRESPONDENCE

Katerina ZAHARIEVA
Institute of Catalysis, Bulgarian Academy of Sciences, “Acad. G. Bonchev” St., Block 11, 1113 Sofia, Bulgaria
e-mail: zaharieva@ic.bas.bg

Tribological Journal BULTRIB, **Vol. IV, 2014**
Papers from the International Conference **BULTRIB '13**
October 24-26, 2013, Sofia
Society of Bulgarian Tribologists
Technical University of Sofia

MECHANOCHEMICAL SYNTHESIS AND PROPERTIES OF $LaMnO_3$

I.Yordanova, D. Paneva, Z. Cherkezova-Zheleva, B. Kunev and I. Mitov

Institute of Catalysis, Bulgarian Academy of Sciences, Acad. G. Bonchev Str., Bld. 11, Sofia 1113, Bulgaria

Abstract: *This study reports the synthesis of nanosize perovskite $LaMnO_3$ nanoparticles by a mechanochemical method using oxides of La and Mn as starting materials. Powders of Mn_3O_4 (prepared by precipitation of manganese nitrate) and commercial La_2O_3 were mixed in stoichiometric proportion and milled 6 h for obtaining this manganite. Their physico-chemical properties are studied by means of X-ray diffraction (XRD) and Fourier Transform Infrared (FT-IR).*

Key Words: *perovskite, mechanochemical activations, $LaMnO_3$*

1.INTRODUCTION

Nowadays metal oxides with transition elements are the object of a great research interest because they are associated with important advances in solid state physics and chemistry. Perovskite oxides display special attention due to their particular electrical, magnetic, catalytic and superconductive properties that can be taken in advantage to technological and basic materials science investigations [1-3]. Perovskite-type oxides, general formula ABO3 (where A and B are rare earth and transition metal cations, respectively) are very good oxidative catalysts and cheaper than noble metal supported catalysts. The redox properties of the transition cation, the availability of weakly bonded oxygen at the surface and the presence of lattice defects make perovskites such as LaMnO3 be suitable for the total oxidation of VOCs. One of the advantages of this type compounds is that partial substitution of A and B cations can lead to a modulation in the oxidation state of present metals, oxygen mobility and redox properties. Among the others, the compound LaMnO3 has been investigated thoroughly because it is of fundamental interest as a colossal magnetoresistive (CMR) material [2] and has been widely used in many applications including as electrode material for solid oxide fuel cells (SOFCs) [4],gas sensors, membranes for separation processes and catalysts etc. [5,6].Traditionally, perovskite is prepared by a conventional solid-state reaction [7] at high temperature. This leads to a material with large particle size, poor compositional homogeneity and which requires a high sintering temperature for bulk fabrication. To date, a variety of chemical methods have been developed to prepare perovskite nanoparticles at low cost and lower processing temperature, such as the citrate process [8], sol-gel process [9], Pechini method [10], to name just a few. However among these established synthesis methods, it is still critical to find simple and cost effective routes to synthesize nanocrystalline perovskite-type material by using cheap, nontoxic and environmentally benign precursors. An alternative method for mass production of these materials could be mechanochemical synthesis. This method is used in this work to obtain of nanosize lanthanum manganite. The goal of this work was to carry out the synthesis of this manganite (LaMnO3) without annealing treatment and evaluating its phisicochemical properties.

2. EXPERIMENTAL

1.1. Sample preparation

$LaMnO_3$ perovskite sample was prepared by two steps – precipitation of Mn_3O_4 and subsequent mechanochemical activation with La_2O_3. Aqueous solution of $Mn(NO_3)_2.6H_2O$ was precipitated with aqueous solution of NaOH (2 mol/l). NaOH added slowly with continuous stirring. The final pH of solution was 10. After that we washed the solution to neutral pH during filtering and at last the powder sample was dried 12 hours at 60ºC. Mixed powders of La_2O_3 (Alfa Aesar 99,9%(REO) and as-prepared Mn_3O_4 in stoichiometric ratio were milled. High-energy planetary ball mill type PM 100,

Retsch, Germany is used to promote mechanosynthesis. The process is carried out in for 6 hours and rotation speed 600 rpm. The weight ratio between balls and powder is 12:1.

1.2. Sample characterization

Powder X-ray diffraction (XRD) patterns were collected using a TUR-M62 apparatus (Germany) with Co-Kα radiation. Data interpretation was carried out using the JCPDS database. The PowderCell software [11] was applied to determine the lattice cell parameters and the average size of the crystallites and microstrains. Infrared spectra of the samples were recorded with a Nicolet 6700 FTIR spectrometer (Thermo Electron Corporation, USA) in the middle (400–4000 cm^{-1}) and far (250-600 cm^{-1}) regions. The materials were studied in transmission mode using (in KBr pellets).

3. RESULTS AND DISCUSSION

Figure 1 shows the XRD patterns of the synthesized manganese oxide precursor and sample prepared after 6 h milling.The low intensive diffraction peaks (Fig. 1a) correspond to the tetragonal Mn_3O_4 phase (JCPDS no 080-0382). The spectrum is change after mechanochemical treatment of this oxide with La_2O_3. Figure 1b shows the powder X-ray diffraction of $LaMnO_3$. All the observed reflections were indexed on the basis of a cubic cell with the refined cell parameter of a = 3.89 Å, which is close to the reported cell parameter of $LaMnO_3$ (JCPDS no. 75-0440). No presence of an impurity phase of initial oxides was observed in the mechanochemically prepared sample. Calculated values of mean crystallite size and microstrain are 14 nm and $2{,}1.10^{-3}$ respectively.

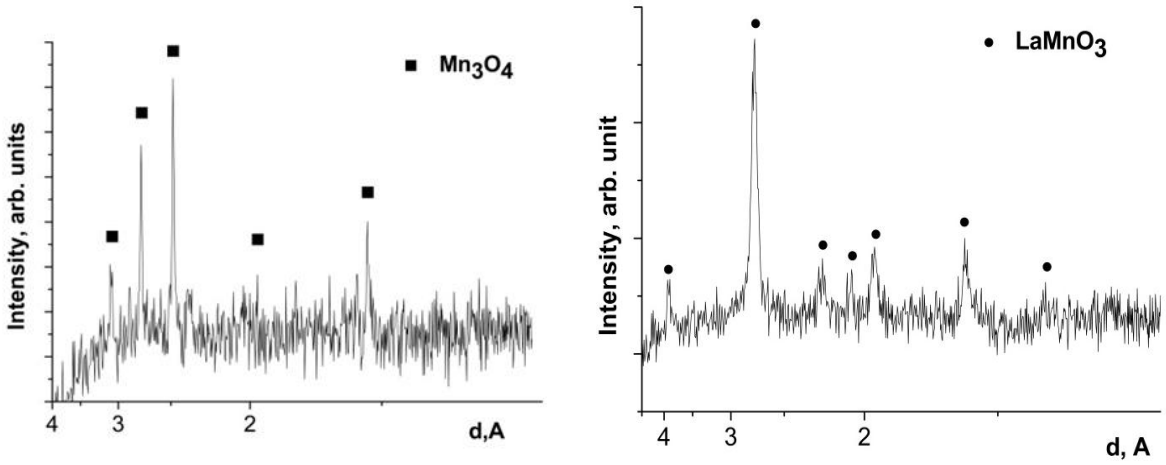


Fig. 1. X-ray diffraction spectra of manganese precursor (a) and $LaMnO_3$ perovskite sample (b).

The obtained after mechanochemical treatment product was investigated by infrared spectroscopy. Figure 2 shows the mid- and far- IR af this sample and far-IR of La_2O_3 precursor. Two intensive bands about 400 and 600 cm^{-1} are registered. In the literature [12] have three main absorptions in the regions 650-500 cm^{-1} (very intense), 450-250 cm^{-1} (with several maxima and components), and near 175 cm^{-1} (sharp). According to the interpretation of the spectra of different perovskite phases, the first absorption arises from the v3 vibrational mode of the perfect octahedral species MO_6 (F1u) that is active and belongs to the same F1, symmetry species also for the cubic perovskite structures. This mode is essentially an asymmetric M-O-M stretching. The loss of degeneracy upon lowering of the symmetry of the octahedron and the increase of the unit cell to more than one ABO_3 units cause this mode to split into several components. In the region 450-250 cm^{-1} the modes arising from the deformations of the MO_6 octahedra (v4, F1u) are expected; they have the same symmetries and activities also in the case of cubic perovskites. The spectra we have recorded agree with those reported in the literature. The band at 594 cm^{-1} corresponds to the stretching mode (vs), which involves the internal motion of a change in length of the Mn–O–Mn or Mn–O bond. The band at 405 cm^{-1} is due to the bending mode (vb), which is sensitive to Mn–O–Mn bond angle. The characteristic bans for La_2O_3 not registered in IR of lanthanum manganite sample.

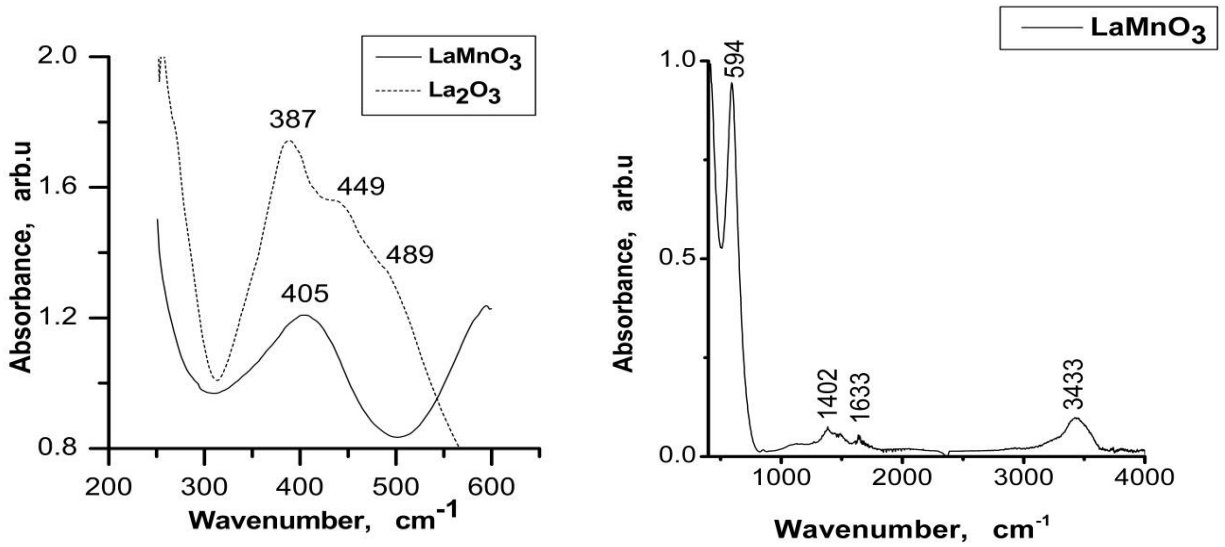


Fig. 2. FT-IR spectra of sample $LaMnO_3$ collected in FAR and MID regions

It was pointed out by Goldschmidt [13] that the ABO_3 type perovskite structure is stable only if the tolerance factor $t = (r_A+r_O)/ [2^{1/2}(r_B+r_O)]$ is nearly equal to unity, where r_A, r_B and ro are the radii of the cations A, B, and anion O respectively. A cubic structure is found if t=1. Deviation of t from unity indicates compressional or tensile stresses in various bonds. These structural stresses resulting from $t < 1$ in $LaMnO_3$ can be partially removed by cooperative rotation of $Mn0_6$ octahedra around different cubic axes giving rise to rhombohedral, orthorhombic, tetragonal, monoclinic and triclinic structures. Therefore lowering crystal symmetry (to orthorhombic and rhombohedral mainly) is the first mechanism of stabilizing perovskite structure. The second one is obtaining non-stoichiometric cubic perovskite. $LaMnO_3$ perovskites has been shown to tolerate a considerable portion of vacancies in the A site (La site) giving rise to compositions of the type $La_{1-\delta}MnO_3$ with the charge ompensated by Mn^{4+} ion formation [14].The Mn^{4+} content in lanthanum manganites can be varied by altering the firing temperature and atmosphere. The physicochemical characterization of mechanochemical synthesed material show cubic perovskite structure. We explain that with high and various temperatures in location of the contact between particles and walls and balls in triboreactor. This overheating have impulse character (alternation of the process arise tensions and relaxation). When the mechanical process and the formation of the stress field and its relaxation is greater than the time for the chemical reaction mechanochemical synthesis is performed. As result we obtain non-stoichiometric material with defects.

4. CONCLUSIONS

Specifically, the synthesis of $LaMnO_3$ by solid-state reaction using high-energy reactive ball milling from manganese oxide (as –prepared Mn_3O_4) mixed with lanthanum oxide in stoichiometric ratios without thermal treatment is reported. This is a useful route used to maximize defects while preserving the cubic perovskite structure determined by XRD and IR. The prepared material has high dispersion and high degree of microstrains which is of great importance of their catalytic behavior in reaction of oxidation of hydrocarbons.

ACKNOWLEDGEMENTS

The authors are grateful for the financial support of National Science Fund of Bulgaria under Project DFNI-E 01/7/2012.

REFERENCES

1. J. HEREMANS, J. Phys. D **26**, 1149 (1993).

2.C. N. R. RAO, B. RAVEAU In: C.N.R. Rao, B. Raveau, Editors, Colossal Magnetoresistance, Charge Ordering and Related Properties and Manganese Oxides, World Scientific, Singapore (1998).

3. K. DORR, J. Phys. D **39**, 2006, R125

4. O.YAMAMOTO, Y. TAKEDA, R. KANNO, M. NODA, Solid State Ionics **22**, 1987, 241.

5. M. ALIFANTI, J. KIRCHNEROVA, B. DELMON, J. Appl.Catal. A, Gen. **231**, 2003, 245.
6. R. SPINICCI, A. TOFANARI, A. Delmastro, D. Mazza, S.Ronchetti, J. Mater. Chem. Phys. **78,** 2002, 393.
7. L. SMART, E. MOORE. Solid State Chemistry: An introduction. 2 nd ed.Chapman & Hall, London, 1995.
8. H. M. Zhang, Y. Teraoka, N. Yamazoe, Chem. Lett.**665**,1987.
9. Ko, E. I. Sol-gel process, pp. 85-91. In G. Ertl, H. Knözinger and J. Weitkamp, eds. Preparation of Solid Catalysts. WILEY-VCH, Weinheim, 1999.
10. M.P. Pechini,. Method of preparing lead and alkaline earth titanates and niobates and coating method using the same to form a capacitor. U.S.Patent 3, 330, 697, 1967.
11. W. KRAUS, G. NOLZE, J. Appl. Cryst., **29**, 1996, 301.
12.M. Daturi, G. Busca, R.J. Willey Chem. Mater., **7**, 1995,2115-2126.
13. Jonker G H and Van Santen J H, Physica **16**, 1950, 337.
14. V. FERRIS, L. BROHAN, M. GANNE, M. TOURNOUX, Eur. J. Solid State Inorganic Chem. **32**, 1995,131.

Tribological Journal BULTRIB, **Vol. IV, 2014**
Papers from the International Conference **BULTRIB '13**
October 24-26, 2013, Sofia
Society of Bulgarian Tribologists
Technical University of Sofia

A SOLUTION FOR IMPROVING SEIZURE RESISTANCE IN METAL ON METAL TOTAL HIP PROSTHESES WITH SELF DIRECTED BALLS

Lucian CAPITANU[1*]
[1]Institute of Solid Mechanics of Romanian Academy, Bucharest, Romania
Address: 15 C-tin Mille str., district 1, Bucharest, 10141, Romania
E-mail: lucian.capitanu@yahoo.com
Virgil FLORESCU[2]
[2]Technical University of Civil Engineering Bucharest, Romania
Address: 124 Lacul Tei Boulevard, Bucharest 020396, Romania
E-mail: florescuvirgil@yahoo.com
Dumitru Catalin BURSUC[3]
[3]Carol I" National Defance Academy, Bucharest, Romania
E-mail: catalin258@yahoo.com

Abstract: *The Metal-On-Metal (MOM) Total Hip Prostheses (THP) with self directed balls has as its greatest advantage the replacement of the sliding movement between the femoral head and the acetabulum socket specific to regular hip prostheses with the rolling movement between the balls, the socket and the femoral head. The balls aren't fixed but rather are freely rolling between the femoral head and the acetabulum socket as a consequence of the movement of the femoral head and the frictional force, finding their own space to move in while imposing minimal resistance on rolling. The balls do not take up the entire space between the femoral head and the acetabulum socket. It is a well known fact that a rolling friction coefficient is always smaller than a sliding friction coefficient. The studied experimental models have allowed the measuring of values of this coefficient, of a maximum value of 0,05. Studies of lubrication with saline solution have indicated a lubrication schedule EHD, the minimum value for the thickness of the lubrication film (h_{min}), measured through the contact resistance methodology, being 0,06 μm. Notwithstanding, when continuously benchmarking the friction coefficient we detected seizure tendencies or even seizure. This paper presents the laboratory models of the ball-socket contact (taken as having an infinite radius, so on a flat surface), for different roughness values of the stainless steel surface SS315L (R_a = 0.015 μm; R_a = 0.045 μm; R_a = 0.075 μm; R_a = 0.075 μm and R_a = 0.190 μm), which allowed determination of friction coefficients of μ = 0.038; μ = 0.042; μ = 0.078 and μ = 0.080, respectively. In order to increase the wear resistance of the tested samples and the acetabulum sockets we have used thin covering layers of titanium nitride (TiN) and chromium nitride (CrN). The best performance derived out of tests using a CrN layer has been achieved on an sublayer of SS316 L, which under a surface roughness R_a = 0.015 μm determined a coefficient of friction of 0.035, without nearing seizure at any time under test conditions.*

Keywords: *MOM total hip prosthesis, self directed movement, wear, rolling friction coefficient, TiN and CrN surface coatings, EHD lubrication*

1. AIMS AND BACKGROUND

The Total Hip Prosthesis (THP) is one of the biggest successes of the 20th century in the field of orthopaedic biomechanical engineering. While less resources are consumed ensuring the primary and secondary mechanical stability of the THP, the loss of stability, a dynamic process, takes place throughout the life of the prosthesis. The loss of stability depends on the mechanical stress, the movements and the heat [1] on the supports of the artificial hip joint, the bone-cement and cement-stem interface strength for cemented stems [2], on the growth of bone inside of uncemented stems [3], the efficiency of the porous coatings of the femoral stems [4] and acetabulum sockets and on the resistance to wear of the femoral stems, acetabulum sockets and femoral heads of the THP [5]. So far, the most successful orthopaedic device is a progressive bio-tribo-system due to the on-demand nature of the components under the hostile environmental conditions specific to the human body. The

Co-Cr-Mo alloy and the Ti-6Al-4V alloy are the materials most used in manufacturing prosthetic femoral heads. Prosthetic femoral head damage remains a major problem with THPs in spite of all the technological advances such as coatings with mono or multi-thin films.

Titanium and its alloys are resistant to corrosion [6] and are therefore biocompatible with the manufacturing of orthopaedic implants, being light weight and having low elastic modulus. However, the use of these materials in joint implants is limited by their high friction coefficient and poor wear resistance. In order to improve their tribological properties, these materials have been subjected to surface modification treatments. Since TiN alloys are hard biocompatible materials [7, 8, 9] of excellent abrasion resistance, many advanced processing methods have been developed aiming at the production of a nitrided layer on the materials surface. In plasma nitriding [10], nitrogen atoms diffuse into the Ti matrix thus forming a top layer of TiN and Ti_2N compounds followed by a deeper diffusion layer. This layered structure produces a continuous hardness profile thus providing an adequate support of the protective layer [8]. The physical properties of the treated surface, however, depend strongly on the plasma technique and processing parameters. The excellent corrosion resistance of the Ti alloys results from the formation of a very stable protective oxide film strongly adhered to the metal surfaces. See also L. Capitanu et al [10] for a report of controlling the wear for a hip joint.

Notwithstanding these improvements, the conventional metal on polyethylene (MOP) THP is undergoing a progressive wear process [19-24]. Following the metallurgic industry advances in the fields of manufacturing and processing biocompatible alloys, the last 10-15 years have seen a reconsidering of the metal-on-metal (MOM) constructive method in order to better ensure EHD lubrication conditions of the femoral head – acetabulum socket device. There are several studies of this method. Leiming Gao et al [1] published a paper on the effect of the 3D physiological load and movement over the elasto-hydro-dynamic properties of the lubrication of the joints in a MOM THP. In this study they present a simulation of the EHD lubrication of a MOM THP taking into account both a static state as well as transitory movement during walking cycles in all three directions.

Leiming Gao, Peiran Yang, Ian Dyamond, John Fisher, Zhongmin Jin have released a paper on the effect of surface texturing on the analysis of the EHD lubrication for MOM THPs in which they have presented an advanced numerical model for calculating the EHD properties of a surface textured with cylindrical dimples. The dimpled structure has been numerically simulated to correspond to a static state as well as walking cycles.

Qingen Meng, Leiming Gao, Feng Liu, Peiran Yang, John Fisher si Zhonming Jin [13] have released a paper on the mechanics of contact and the EHD lubrication in a new THP implant with an asferical surface.

R. Pourzal, R. Theissmann, M. Morlock si A. Fischer [14] have analyzed micro-structural differences in various zones of the articulated surfaces of an MOM system with a reconditioned head demonstrating that wear-related particles at nano-scale are a limitation due to the theoretical damage to the human body. In order to investigate the release of wear-related particles in ultra-low wear conditions, one must first understand the micro-structural changes in the substrate. Previous studies on MOM THPs have shown the in situ formation of a nano-crystalline layer that, together with the mechanical mixing, allows the Co-Cr-Mo alloy to adapt to its current loading requirements and maintain a very low wear rate. However there is little information on wear resistance for hip surface replacements which are subject to different stress / deformation conditions.

Y. Yana, A. Neville et al [15] have published a paper on the effect of metallic nano-particles on bio-tribo-corosion of MOM THPs, centred around the particles in the third body and their effect on the tribology and the corrosion processes of the bearing surfaces. A hip movement simulator together with a electro-chemical cell have been used to study the bio-tribo-corrosion system. Pre-built cobalt particles have been used (28 nm diameter). The diameter of all the femoral heads used in this study has been 36 mm. The Open Circuit Potential (OCP) has been monitored with and without these nano-scaled Co particles.

C.X. Li, A. Hussain, A. Kamali [16] have presented considerations on conditions for non-bearing surfaces and their potential effect on tests for wear simulation, in which they show that the potential mass loss of the non-bearing surfaces (specimens) and its contribution to the total results of gravimetric readings are rarely mentioned in scientific papers. This study involved testing Co-Cr-Mo alloy discs for up to 1200 hours and the recovery of socket surfaces under different surface conditions. For the new generation of MOM hip joints the surfaces of the bearing are generally polished with a great degree of precision following the introduction of the international ISO 7202 standard for orthopaedic hip prostheses. Even so, the materials used, the shape and the finish of the bearing surface can show wide differences. These can be pre-worked, sanded, coated with Ti, hydroxyapatite (HA), with or without beads and so on. Even a layer comprised of the same material may be porous, non-porous, synterized, thermically pulverized or plasma pulverized at different temperatures and with different techniques. Under such kinematic and kinetic conditions as the ones described in the ISO

14242 standard, a variation of the state of the non-bearing surface is less probable to affect the wear process that takes place on the articulated surfaces during a simulation tests, given unchanged contact conditions.

S. Kataria, N. Kumar, S. Dash, A.K. Tyagi [17] have reported on the tribological behaviour and the deformation of the Ti layer under different sliding conditions, trying to explore the tribological properties of a Ti coating 1 micrometer thick on a D9 steel substrate. The friction tests have been undertaken using a tribometer with reciprocal linear movement, on steel spheres, alumina and silicon nitride.

W. Osterle, D. Klaffke, M. Griepentrog, U. Gross, I. Kranz si Ch. Knabe [18] have published a paper on the wear resistance of Ti-6Al-4V coatings for the bearing surfaces of the artificial hip joint in which they talk about the tribological tests (sphere/plane) undertaken in order to identify the right coating for bearing surfaces in hip joints whose acetabulum socket and femoral heads are made out of Ti-6Al-4V alloys. This alloy is highly appreciated for its low weight, good compatibility and the elastic properties similar to natural bones.

In parallel with reconsidering the potential for MOM prostheses there is ongoing research on new manufacturing and functional solutions.

The current paper discusses the Metal-On-Metal total hip prosthesis with self directed balls [19, 20]. It has the great advantage of replacing the relative sliding motion between the femoral head and the acetabulum socket, specific to a regular THP, with the rolling motion generated by the balls, the socket and the femoral head. The balls aren't fixed in a cage but freely roll continuously between the femoral head and the acetabulum socket, as a consequence of the motion of the femoral head and the generated friction, thereby finding the space where minimum resistance to rolling is met. The balls do not occupy the entire space found between the head and the socket and some free space is technologically allowing the movement of the balls. It's a known fact that a rolling friction coefficient is always smaller than a sliding friction coefficient. As such, so should the wear. Several studies have been published on the load transfer in rolling balls THPs [21]; the wear and tear of the femoral head of a THP [22, 23] and the stability of hip endoprosthetics [24].

2. MATERIAL AND METHODS

For lab experiments three MOM THPs with self directed balls have been manufactured, using commercially available femoral heads and stems, having:

1 – Socket, balls and the closing/adjustment nut made entirely out of stainless ASTM SS 316L stainless steel, having 150 HV 30 hardness (fig. 1, 2, 3 and 4);

2 – 316L stainless steel socket with a 3 μm Ti N coating, having 2000 HV 0.02 micro-hardness.

3 – 316L stainless steel socket with a Cr N coating, having 627 HV 5 micro-hardness.

Figure 1 comparatively shows the classic THP and the new self directed balls THP, the latter being dismantled, showing the stem, the femoral head, the socket including the balls and the closing-adjustment nut, its components.



(a) (b)

Fig. 1. Comparison of the classic THP (left) and a dismantled self directed balls THP (a), showing its components (b): the stem, the femoral head, the socket including the balls and the closing-adjustment nut.

For a clearer view Figure 2 shows an overhead view of the acetabulum socket and the SS316L rustproof steel balls. The layer of balls is not complete, there being a free space by design,

that allows the movement of the balls as a consequence of the motion of the femoral head and the friction between the balls, the head and the socket.

The transversal forces acting on the femoral head are shown in Figure 3.



Fig. 2. Overhead view of the acetabulum socket and the SS316L rustproof steel balls.

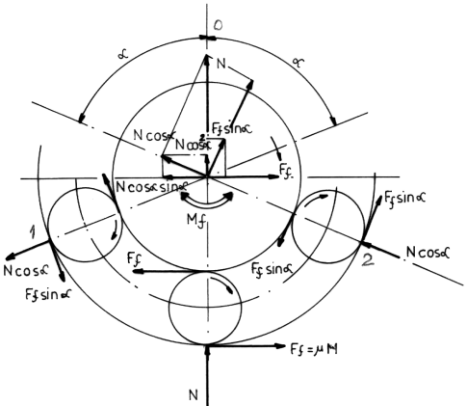


Fig. 3. Transversal forces acting on the femoral head of a THP with self directed balls [19].

One can easily observe that overall, most of the friction components will cancel each other (given an even number of balls). The initial consideration was that the absence of a ball from the total number allowed by the available space between the femoral head and the acetabulum socket would ensure the self directed motion of the balls. The lab experiments on a simplified testing bench (Figure 4) with a 2D oscillating motion of ± 30^0 on a vertical plane (non-anatomical position) have demonstrated that the space created is insufficient.

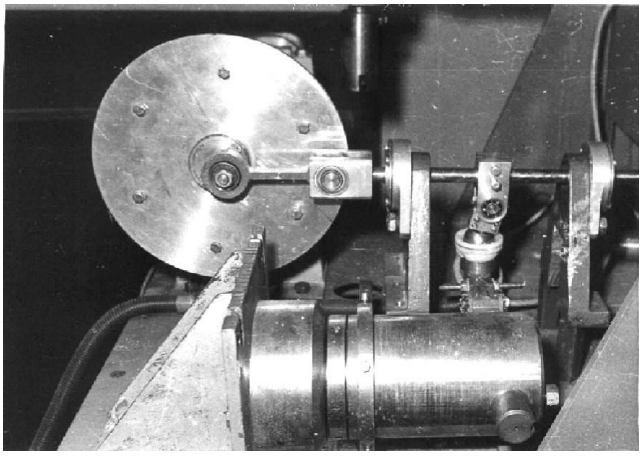
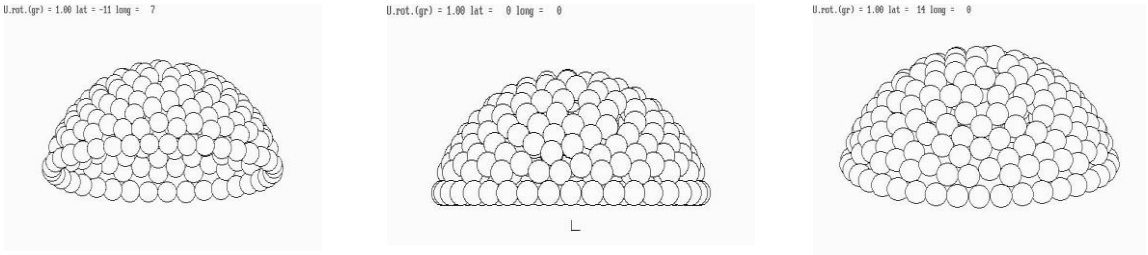


Fig. 4. Testing bench with a 2D oscillating motion of ± 30^0

A complex geometrical analysis of the distribution of the balls as well as Fortran software for calculating the number of balls per row have been produced [19], obtaining:

$$n_0 = 37 \; ; \; n_1 = 19 \; ; \; n_2 = 19 \; ; \; n_3 = 19 \; ; \; n_4 = 19 \; ; \; n_5 = 19 \; ;$$
$$n_6 = 19 \; ; \; n_7 = 19 \; ; \; n_8 = 14 \; ; \; n_9 = 9 \; ; \; n_{10} = 5 \; ; \; n_{11} = 1 \; .$$

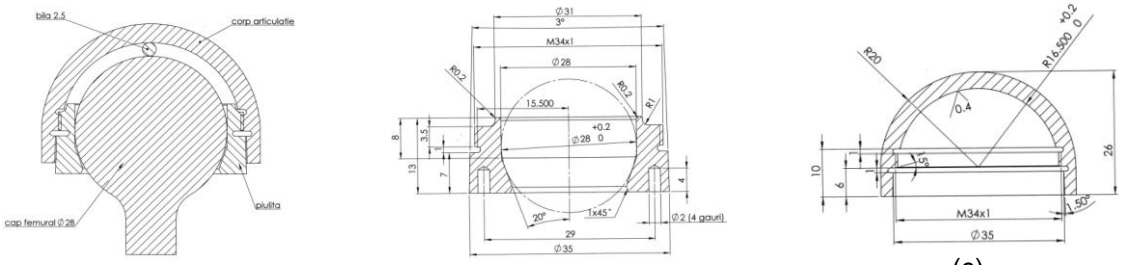
Figure 5 shows the way to arrange the balls from three different perspectives (15^0; 0^0 and -15^0).



(a) (b) (c)

Fig. 5. (a) Lateral view adjusted by β = 15^0; (b). Frontal view (β = 0^0); (c). Lateral view adjusted by β = - 15^0 [20].

The main design and the design of the articulated body and the closing-adjustment nut are shown in Figure 6 (a) and (b).



(a) (b) (c)

Fig. 6. CAD Designs of the self directed balls prosthesis (a), the closing-adjustment nut (b) and the SS316L acetabulum socket (c).

Measurements taken using the friction coefficient on the contact surface have revealed some seizure tendencies so two other SS316 L stainless steel prostheses models have been manufactured, using yitanium nitride (TiN – Figure 7) or chromium nitride (CrN – Figure 8) as the interior coating.

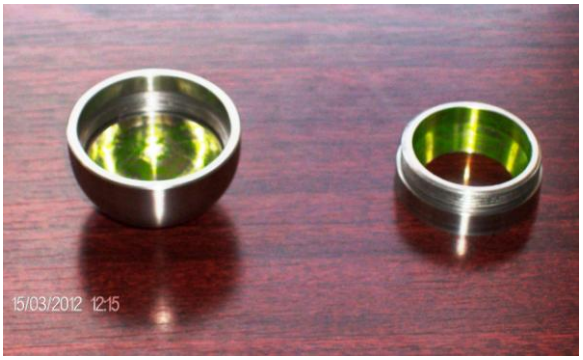


Fig. 7. SS316L acetabulum socket and closing-adjustment nut with interior TiN coating



Fig. 8. SS316 L acetabulum socket and self directed balls with interior CrN coating

The coatings have been created using the Pulse Laser Deposition method (PLD), with help from our colleagues at the National Laser and Plasma Physics Institute of Bucharest – Magurele and support from Professor Dr. Ioan Mihailescu.

The SS 316L stinless steel (SREN X2CrNiMo18-14-3) has the following chemical composition:

C	Si	Mn	P (max)	S	Cr	Mo	Ni
≤ 0.03	≤ 1.00	≤ 2.00	0.045	≤ 0.015	17.0-19.0	2.50-3.00	12.50-15.00

Experiments have been made using a ball – plane device, presented elsewhere [25], assuming an infinite radius for the acetabulum socket (flat surface). The tests have shown the presence of seizure tendencies even when the acetabulum socket is coated with thin layers of TiN or

CrN. The testing device can determine the seizure load, the thickness of the lubricating film and, through microscopy, photograph the wear marks and then calculate the volume of removed material.

For the sake of clarity Figure 9 shows an image of the friction torque components with single dot contact (spherical nut on a flat disc) used in testing.



Fig. 9. The friction torque used in experimental modelling.

Under static conditions the compression efforts due to the single dot contact, p_{max} si p_{med} (maximum and average contact pressure) are given by:

$$p^3_{max} = 1.5\, PE^2 / \pi r^2 (1 - \mu^2)^2 \quad (1)$$

$$p_{med} = \frac{P}{\pi a^2} \quad (2)$$

while the radius a, of the circular contact surface, is:

$$a^3 = 1.5\left(1 - \mu^2\right) P \frac{r}{E} \quad (3)$$

where P is the load; a the radius of the contact surface and r the radius of the sphere.

For steel made friction couple components the values of the above equations become:

$$p_{max} \approx 5800 \sqrt[3]{P} \quad (4)$$

$$p_{med} \approx 1700 \sqrt[3]{P} \quad (5)$$

$$a \approx 0.09 \sqrt[3]{P} \quad (6)$$

Particular care has been given to finishing the friction surfaces of the samples. The state of the surface, being defined by its topography, the micro-structure of the superficial layer and its oxidation state, has a major contribution to the wear process. Due to the complexity of creating the surface through an abrasion process, the safest way to ensure a consistently reproducible surface is by strictly adhering to all the stages of the finishing process. The following stages have been established: the turning of the shape, the finishing turning, thermal treatment, grinding, fine adjustment and finally the super finishing of the work surface. While all the stages, up to the fine adjustment, are using traditional manufacturing techniques, it is worth mentioning that the overall intensity of the process is purposefully maintained at a low level in order to protect the superficial structure of the material.

The super finishing stage uses the metallographic polishing techniques and includes: wet polishing using abrasive paper of 32 μm and 17 μm granulation, diamond paste polishing of 6 μm and

1 μm granulation and, finally, wet polishing using alumina suspension having a 2000 Á granulation. The surfaces are then cleaned with alcohol and distilled water and then dried. The storage of the finished samples is done in sealed containers on a silica gel layer.

Following the super finishing stage we have obtained four different roughness values for the SS316 L sample surfaces: R_a = 0.015 μm, R_a = 0.045, R_a = 0.075 μm si R_a = 0.190 μm.

The roughness of the surfaces has been determined using a profilometer with parameter translator and graphic recording. The instrument allows not only the recording of the surface profiles but also the determination of the R_a and r.m.s. values, defined as:

$$R_a = \frac{1}{l}\int_0^l |y| dx \tag{7}$$

$$r.m.s = \sqrt{\frac{1}{l}\int_0^l y^2 dx} \tag{8}$$

4. RESULT AND DISCUSSION

4.1. Evolution of the surface state in the wear process

Experimental determinations were made under these test conditions:

- Load: variable between P = 20 ÷ 300 N for determining of seizure limit. A load of 50 N was used for wear tests.
- Sliding speed: main speed for determining the wear rate was u = 174 cm/s. To determine the influence of speed on the wear, the device allows achieving the following speeds:

u = 60 cm/s; u = 18 cm/s and u = 3,2 cm/s.

- Lubricant: BSF (Body Simulated Fluid) having a density of 1183 kg/m^3 and a viscosity of 0.84 Pa·s (HyClone, SH30212.03).

Using the above mentioned parameters, the couple operates in elasto-hydro-dynamic regime.

Archard [8] proposed the following relationship for the minimum thickness of the lubricant film:

$$\frac{h_0}{r} \approx 0.84\left(\frac{\alpha u \mu_0}{r}\right)^{0.741}\left(\frac{Er^2}{P}\right)^{0.074} \tag{9}$$

where: h_0 - minimum thickness of lubricant film; r - radius of the sphere; α - pressure coefficient of viscosity; u - velocity sum; μ_0 - dynamic viscosity at atmospheric pressure; E - reduced elasticity modulus; P – load.



(a) (b)

Fig. 10. (a) Variation of lubricant thickness in the x = 0 plane and (b) the z = 0 plane, as a function of load, at speed u = 8 cm/s.
▪ 0.7 N; ▼ 1.1 N; ▫ 1.5 N; ◊ 3 N; ▪ 4.6 N; ▲ 7.8 N; ○ 10.8 N

Relationship (9) successfully reproduces the dependence of h_0 on the main quantities u, μ_0, r and P. The exact determination of the minimum lubricant film thickness depends on the knowledge of pressure coefficient α for the lubricant used and the accuracy of the numerical coefficients of relationship (9). In working conditions, using an estimated value α, a minimum lubricant film thickness of $h \approx$ 0.06 μm was obtained. The spatial form of lubricant film in the loaded area is shown in Fig. 10

(a) and (b), which represents the longitudinal and cross sections of lubricant film (in relation to the movement) on the symmetry axes.

Curves were obtained experimentally, under conditions close to those used by Dowson [9]. Significantly higher values for minimum thickness h_0 are noticed even at speed u = 23 cm/s. To observe the wear of fixed surface as a function of couple roughness in ideal conditions the following solution was used: roughness of the couple was focused on one of surfaces, in particular on the mobile one. The fixed surface will always have the minimum achievable roughness of about $R_a \approx$ 0.015 μm. The composed roughness of the couple, expressed as standard deviations, σ, is:

$$\sigma^2 = \sigma_1^2 + \sigma_2^2 \tag{10}$$

where σ_1, σ_2 represent the standard deviations of the two surfaces.

If one of the surfaces has a small roughness value, i.e., $\sigma_1 << \sigma_2$, then $\sigma \approx \sigma_1$. It is therefore possible to study the influence of roughness on the wear, just by changing the roughness of a single surface. Under these conditions and at a load P = 50 N, speed u = 1.74 m/s and volume temperature of the lubricant θ = 50 ^{0}C, it was determined the evolution of the surface wear function of the time, for the following roughness of the mobile surface: R_a = 0.015 μm; R_a = 0.045 μm; R_a = 0.075 μm and R_a = 0.19 μm. Figures 11 and 12 exemplify the cross profile and the optical micro-photography of the seizure marks of the sample surfaces with R_a = 0.015 μm and R_a = 0.19 μm, for a 30 second test.



Fig. 11. Central cross profile and the image of the wear marks. R_a = 0.015 μm, t = 30 sec. Sample 835.



Fig. 12. Central cross profile and the image of the wear marks. R_a = 0.19 μm, t = 30 sec. Sample 849.

The oscilloscope recordings of the contact resistance (the breakage of the lubricating film – BSF) have shown seizure tendencies while the wear volume of the flat sample has increased with its roughness as a consequence of the heavy wear of the tips present in the topography of the surface during the initial testing period. The recording is presented in Figure 13.

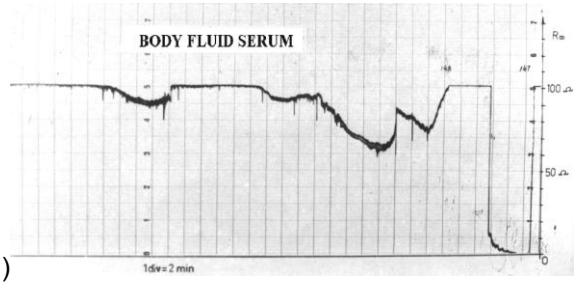


Fig. 13. Oscilloscope recordings of the contact resistance (the breakage of the lubricating film – BSF) for SS 316L. Sample 849.

Figure 14 shows the double logarithmic friction and wear evolution relationship as a function of the test duration and the roughness of the surface.

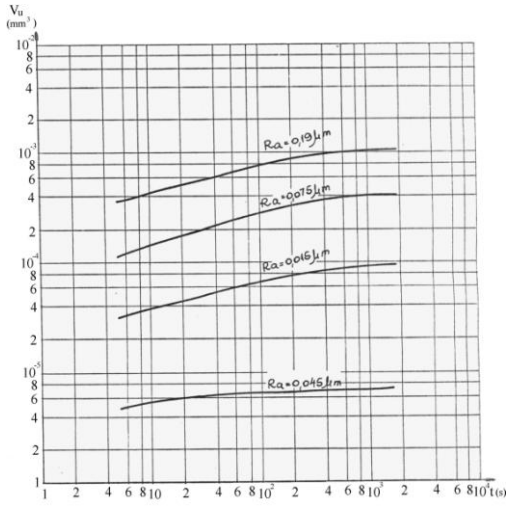


Figure 14. Friction and wear evolution as a function of time for different roughness values of the flat surface

Regarding usage tests it must be stated that at the same time as measuring surface wear the friction coefficient has also been measured. Surprisingly, the minimum friction coefficient doesn't coincide with minimum wear. Figure 15 shows the data points of a V_u / μ model for the four roughness values used.

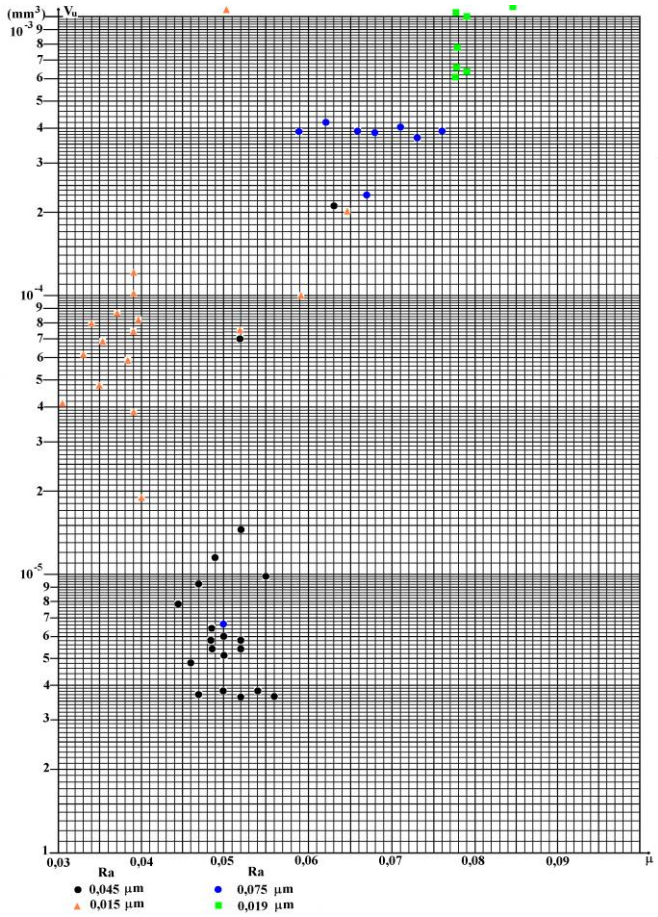


Fig. 15. The variation of used material as a function of the friction coefficient

Figure 15 indicates the existence of a minimum wear volume for roughness R_a = 0.045 µm. At the same time the friction coefficient reaches a minimum at roughness R_a = 0.015 µm.

The rapid decrease of the wear speed as a function of time is obvious, exception being the surface roughness value of R_a = 0.045 μm. 25% to 50% of the wear recorded in a 30 minute wear test is being produced during the first three seconds. Increasing the test time from 5 to 30 minutes only increases the wear by 10%. The wear evolution is explained by the conformation of the surfaces that results in changing of the lubricating conditions. It must be noted that the value of static wear is determined by the initial wear (during the first few seconds). This observation allows the usage of the wear value of t = 5 min. as representative for the usage conditions. Using this duration the spread of values is greatly decreased.

The different roughness values used have resulted not only in differences in the used volume of material but also in differences in the shape of the wear scar. For surfaces with R_a = 0.015 μm, R_a = 0.075 μm, (t =3 sec.) and R_a = 0.19 μm, (t =3 sec.), the wear is of an adhesive type (metallic aspect with emphasized fissures). For surfaces with R_a = 0.045 μm, the prevailing wear is of an oxidative type. Once wear speed is reduced, following the conformation of the surfaces, the R_a = 0.075 μm and R_a = 0.19 μm surfaces also enter an oxidative wear stage.

For R_a = 0.045 μm the wear is reduced to such an extent that during the entire test time the lubrication conditions remain largely unchanged.

The average values of volume of used material (calculated using the imprint method [11] that consists in considering the wear imprint as on a spherical surface, photographing it using optical microscopy, dividing it into ten equidistant spherical segments, calculating their volumes and summing them up using the approximate formulas (4), (5) and (6)) for the four roughness values are:

$$R_a = 0.015\ \mu m;\ \rightarrow V_u = 7.0 \times 10^{-5}\ mm^3;\ \rightarrow\ \mu = 0.038;$$
$$R_a = 0.045\ \mu m;\ \rightarrow V_u = 7.0 \times 10^{-6}\ mm^3;\ \rightarrow\ \mu = 0.042;$$
$$R_a = 0.075\ \mu m;\ \rightarrow V_u = 3.7 \times 10^{-5}\ mm^3;\ \rightarrow\ \mu = 0.068;$$
$$R_a = 0.190\ \mu m;\ \rightarrow V_u = 1.0 \times 10^{-3}\ mm^3;\ \rightarrow\ \mu = 0.080.$$

For R_a = 0.015 μm, R_a = 0.075 μm and R_a = 0.19 μm roughness, the values for the volume of used materials vary according to the degree of stress for the contact determined by the h_{min} / σ parameter of the lubricating pellicle.

For R_a = 0.045 μm roughness we have also observed an influence on the grind. After the first 5 minutes the entire contact surface is oxidized. The imprint obtained after another 5 minutes using the same liner has a particular shape, the oxidized area halving itself at the boundary of the load area. It follows that after grinding the lubrication conditions improve. For super finished surfaces there was no obvious grinding improvement.

Regarding the influence of the initial roughness on the wear and the friction coefficient it must be said that the surface wear is a value determined by the fraction of the surface that stays in contact and should therefore be a monotonous function of the h / σ film parameter. The minimum wear value must coincide with the minimum surface roughness value. Time-observed wear evolution leads to the conclusion that, under the tested conditions, the minimum wear value is obtained for a particular (and not the minimum) roughness value. To verify this result a great number of determinations have been performed for the four different roughness values: R_a = 0.015 μm; R_a = 0.045 μm; R_a = 0.075 μm and R_a = 0.19 μm. The existence of the optimal roughness value may be explained either through the effect on the lubricating film or through a modification of the mechanical properties of the surface. In the latter case, for the optimal roughness, the decrease of the h / σ ratio is cancelled by an increase in wear resistance. In order to limit the possibility of seizure we used thin coatings of TiN and CrN on the flat SS316 L surface (Figure 9), resulting in a micro-hardness value of 2000 HV 0.02 for the TiN coating and a 627 HV 5 value for the CrN coating. Figure 16 shows the PLD coating process that was used, as described in [9].

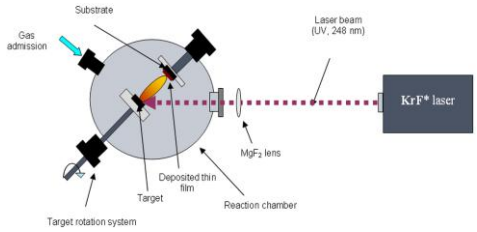


Fig. 16. The PLD process

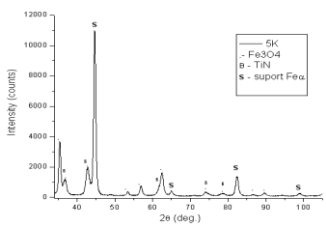


Fig. 17. X - Ray analysis of theTiN coating on the SS316 L surface

The structures of the coatings have been analysed using X-Ray diffraction. An example of this analysis is shown in Figure 17. Checking the adherence of the coating has been done using scratch tests and is presented in [10].

Figure 17 shows that for 43.5^0, austenite γ – Fe (111), for 50.6^0 γ – Fe (200), while for 74.7^0 γ – Fe (220). The presence of ferrite can also be observed for an angle of 44.6^0 α - Fe (110). The sample used for the TiN coating has been corrosion tested by submerging in a 3% NaCl solution at 25 ^{0}C. No corrosion was observed after three weeks. In conclusion these coatings have an excellent corrosion resistance as well as an increased hardness.

The TiN coated surfaces have been polished for the same roughness states as the uncoated surfaces. The wear profiles and the seizure marks have been recorded. Figures 18 and 19 show the central cross profiles and the micro-photographs of the SS316 L sample surfaces with TiN coatings of 2000 HV 0.02 micro-hardness and roughness values of R_a = 0.015 μm and R_a = 0.045 μm after 5 minutes of testing.



Fig. 18. Central cross profile and TiN wear mark photography R_a = 0.015 μm, t = 5 min. Sample 1057



Fig. 19. Central cross profile and TiN wear mark photography R_a = 0.045 μm, t = 5 min. Sample 1058

In the particular case of a TiN coated sample (1057), for R_a = 0.045, the variation of the contact resistance has been observed on the oscilloscope recording, such that after 48 minutes the breakage tendency of the lubricating pellicle was apparent and after 66 minute effective seizure took place for a load of 50 N at the relative speed v = 1.73 m/s and the contact temperature $\theta = 50^0$C.

During the adherence tests for the TiN coatings we have plotted diagrams of the applied force as a function of the scratching distance for highlighting critical events. These are presented elsewhere.

Even so, the modelling of the ball on disc device that showed seizures for SS 316 L also showed seizures for SS 316 L with a TiN coating (Figure 20).

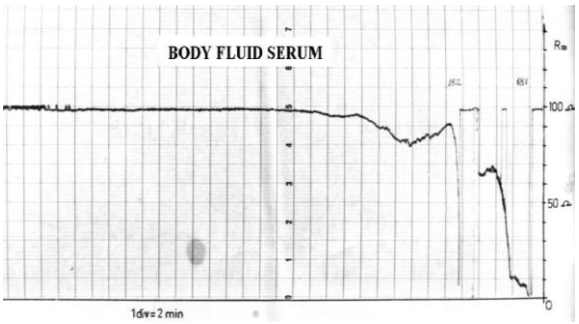


Fig. 20. Oscilloscope recording of contact resistance (breakage of the lubricating pellicle BSF) for TiN coating on SS 316L surface. Sample 1057.

The following shows the cross-cut profile and the micro-photography taken after the seizure of the SS 316 L samples coated with CrN through the PLD process, for a micro-hardness of 627 HV 5 (Figure 21). The metallic samples coated with CrN have been polished to the same surface roughness values as the uncoated or the TiN coated ones.



Fig. 21. Central cross-cut profile and CrN wear mark photography. R_a = 0.045 µm, t = 45 min, N = 50 N, v = 1.73 m/s, θ = 50^{0}C. Sample 706.

Figure 22 shows the oscilloscope recording of the contact resistance for the CrN coating. Here too we can observe seizure but after more than 1200 hours of continuous testing under the same lab conditions.

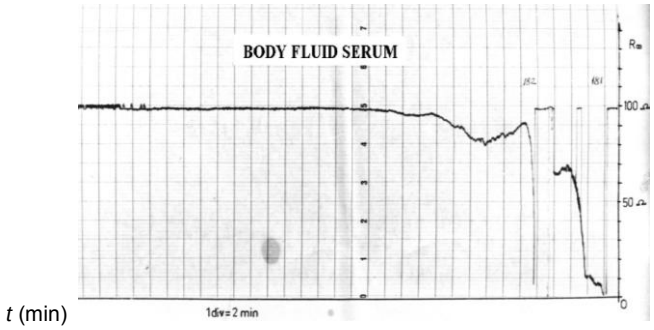


Fig. 22. Oscilloscope recording of the contact resistance for the CrN on SS 316L coating. Sample 706.

Comparing Figures 11-12 (uncoated SS 316 L), 18 -19 (TiN coated SS 316 L) and 21 (CrN coated SS 316 L) the superior performance of the CrN coating stands out, due to its increased hardness.

In fact, this observation is very well highlighted by comparing the inner surface photography of the SS 316 L acetabulum socket coated with CrN and TiN (Figure 23) after 1200 hours of continuous testing on the testing device presented in Figure 4.



(a) (b)

Fig. 23. Inner surface photography of the SS 316 L acetabulum socket coated with CrN (a) and TiN (b) after 1200 hours of continuous testing on the testing bench presented in Figure 4.

Experimental lab measurements for the global rolling friction coefficient in the three total hip prostheses with self directed balls have been made on the simplified test bench (Figure 4) with 2D

vertical plane ± 30^0 oscillating motion (non-anatomical position), for a load of 3200 N (4 BW) under BSF lubrication conditions. The global rolling friction coefficient values in a static state have been established as follows:

1 – ASTM SS 316 L prosthesis with a hardness value of 150 HV 30: μ = 0.048.

2 – ASTM SS 316 L prosthesis coated with a 3 μm layer of Titanium Nitride (TiN) with a hardness value of 2000 HV 0.02: μ = 0.042.

3 - ASTM SS 316 L prosthesis coated with a 2 μm layer of Chromium Nitride (CrN) with a hardness value of 627 HV 5: μ = 0.035.

It's worth mentioning that J.H. Dumbleton [26] has established sliding friction coefficient values of between 0.04 and 0.12 for classic prostheses using a UHMWPE socket on a stainless steel femoral head under saline lubrication conditions.

4. CONCLUSION

The MOM total hip prosthesis with self directed balls seems to offer good functioning parameters for a low rolling friction coefficient (< 0.05) under experimental conditions. It was found that for the SS 316 L socket coated with a 2 μm chromium nitride layer (CrN) with a hardness value of 627 HV 5, the friction coefficient value is μ = 0.035. This is an encouraging find. Moreover, it is close to those values established by the ball on plane modelling proving that the assumption of infinite radius for the interior surface is a realistic one.

From determinations of the evolution over time of the wear in ball on flat conditions, it resulted that, in the experimental conditions used, minimal wear occurs at a certain value of roughness and not at the minimal roughness.

Surprisingly, the minimum friction coefficient, does not coincide with minimal wear.

The existence of a minimum in the wear curve results for roughness R_a = 0.045 μm. At the same time the friction coefficient is minimal at roughness R_a = 0.045 μm. A mathematical relationship between the friction coefficient and wear cannot therefore be established.

Notwithstanding, this paper has limitations and extended research continues to be necessary for the precise determination of the complex lubrication mechanism in the total hip prostheses with self directed balls.

ACKNOWLEDGMENTS

The authors would like to thank their colleagues from the National Laser and Plasma Physics Institute, Prof. Dr. Ioan Mihailescu and Liviu Duta, PhD, for their support in producing the thin film coating. We'd also like to thank the Romanian Academy for the logistic support offered in the production of this paper.

REFERENCES

1. G.BERGMANN, G. DEURETZBRACHER, M. HELLER, F. GRAICHEN, A. ROHLMANN, J. STRAUSS, G.N. DUDA. Hip contact forces and gait patterns from routine activities J. Biomech. 34 (2001) 859-71.

2. M. PEREZ et al, Probabilistic analysis of the influence of the bonding degree of the stem–cement interface in the performance of cemented hip prostheses. J Biomech, 39 (2006) 1859-72**.**

3. M. R. ABDUL KADIR, U. HANSEN, R. KLABUNDE, D. LUCAS, A. AMIS. Finite element modelling of primary hip stem stability: The effect of interference fit. J. Biomech. 41 (2008) 587-594.

4. J. ORLIK, A. ZHUROV, J. MIDDLETON. On the secondary stability of coated cementless hip replacement: parameters that affected interface strength. Med. Eng. Phis 25 (2003) 825-31.

5. D. Najjar M. Bigerelle,, H. Migaud, A. Iost. Identification of scratch mechanisms on a retrieved metallic femoral head. Wear, 258 (2005) 240-50.

6.C.S. JAVORSKY, J.A.T BORGES da COSTA, I.L MULLER, T.R. STROHAECKER, G.E. ENGLERT. Corrosion Resistance of Plasma Nitrided Ti-6Al-4V Alloy in Hank's Solution. Anais do Congresso NACE-Brasil Corrosão'99, Vol.1, pp.433-440. (São Paulo, SP, NACE-Brasil, 1999).

7. B. COLL, et al. in Technical Bulletin from Multi-Arc Scientific Coatings/Innovatique S.A. 1998.

8. K. RIE et al. Surf. and Coat. Tech. **74-75** (1995) 973.

9. M. PELLMAN, in Technical Bulletin from Multi-Arc Scientific Coatings/Innovatique S.A. 1998.

10. B.S. YILBAS, et al. Corrosion. Science, **37** (1995).1627.

11. L. GAO., F. WANG, P. YANG, Z. JIN. Effect of 3D physiological loading and motion on elastohydrodynamic lubrication of metal-on-metal total hip replacements. Medical Engineering & Physics **31** (2009) 720-729
12. L. GAO L., F. WANG., P. YANG, Z. JIN. Effect of surface texturing on the elastohydrodynamic lubrication analysis of metal-on-metal hip implants. Tribology International **43** (2010) 1851-1860.
13. Q. MENG, L. GAO, L. FENG, P. YANG, J. FISHER, Z. JIN. Contact mechanics and elastohydrodynamic lubrication in a novel metal-on-metal hip implant with an aspherical bearing surface. Journal of Biomechanics **43** (2010) 849-857.
14. R. PPURZAL, R. THEISSMANN, M. MORLOCK, A. FISCHER. Micro-structural alterations within different areas of articulating surfaces of a metal-on-metal hip resurfacing system. Wear **267** (2009) 689-694.
15. Y. YANA, A. NEVILLE , D. DOWSON, S.WILLIAMS, J. FISCHER. The effect of nanoparticles on the behavior of the metal on metal total hip prosthesis biotribocorrosion. Wear **268** (2010) 683-688.
16. C.X. LI, A. HUSSAIN, A. KAMALI. Consideration of non-bearing surface condition and its potential effect on hip wear simulation test results. Wear **268** (2010) 762-789.
17. S. KATARIA, N. KUMAR, S. DASH, A.K. TYAGI. Tribological and deformation behaviour of titanium coating under different sliding contact conditions. Wear **269** (2010) 797-803.
18. W. OSTERLE, D. KLAFFKE, M. GRIEPENTROG, U. GROSS, I. KRANZ. CH. KNABE. Potential of wear resistant coatings on Ti–6Al–4V for artificial hip joint bearing surfaces. Wear **264** (2008) 505-517.
19. L. CAPITANU, V. FLORESCU, L.L. BADITA. New concepts in durability improvement of hip joints endoprostheses. American Journal of Materialas Science (Vol. 2, No. **6**, December 2012), DOI: 20.5923/j.materials.20120206.05.
20. L. CAPITANU, V. FLORESCU, L.L. BADITA. A new concepts in durability improvement of hip endoprostheses. Biomechanics 2012, 16-19 September, Bialystok, Poland, Book of Abstracts p. 47-50, ISBN 978-83-62582—26-6.
21. L. CAPITANU, V. FLORESCU, L.L. BADITA. Studies regarding Load Transfer Mechanism in MOM Total Hip Prostheses with Rolling Balls". Journal of Materialas Science and Engineering A. **4**, 2013. (ISSN 2161-6213, USA).
22. L. CAPITANU, L.L. BADITA, D.C. BURSUC. Damage of the femoral head of total hip prosthesis". Journal of the Balkan Tribological Association, **18**, No. 4, 642-653 (2012).
23. L.L. BADITA, D.C. BURSUC, L. CAPITANU. About the wear process of the Co-Cr-Mo femoral head of a total hip prosthesis". SISOM 2011, Bucuresti, 25-26 May 2011, p. 154-163, ISSN 1843-5459.
24. L. CAPITANU, L.L. BADITA, D. STANCULESCU, M. POPESCU. „Stability of hip endoprostheses". Chapter 5 pp. 87-157, in J. Paolo Davim (Editor) „Biomedical Tribology", NOVA Publishers, Inc. New York, USA, 2011, 189 p. ISBN 978-1-61470-056-2.
25. L. CAPITANU, V. FLORESCU, D.C. BURSUC. Preliminary study on the seizure trend of a MOM-THP with self – directed balls. Proceedings of Serbiatrib'13, Kragujevac, Serbia, 15 – 17 May, 2013, pp. 331-340, ISBN 978-86-86663-98-6.
26. J.H. DUMBLETON. The tribology of natural and artificial joints. Elsevier, New York, 1981.

CORRESPONDENCE

Lucian CAPITANU
Institute of Solid Mechanics of Romanian Academy, Bucharest, Romania
15 C-tin Mille str., 1 district, Bucharest, 10141, Romania
e-mail: luciancapitanu@yahoo.com

Tribological Journal BULTRIB, **Vol. IV, 2014**
Papers from the International Conference **BULTRIB '13**
October 24-26, 2013, Sofia
Society of Bulgarian Tribologists
Technical University of Sofia

MODELLING POSSIBILITIES OF VERY HIGH TEMPERATURES AND PRESSURES AT FRICTION CONTACT PLASTICS FILLED WITH GLASS FIBRES ON STEEL

Dorin RUS[1] **, Virgil FLORESCU**[1]
[1]Technical University of Civil Engineering Bucharest, Romania
Address: 124 Lacul Tei Boulevard, Bucharest 020396, Romania
E-mail: florescuvirgil@yahoo.com
Lucian CAPITANU[2]
[2]Institute of Solid Mechanics of Romanian Academy, Bucharest, Romania
Address: 15 C-tin Mille str., district 1, Bucharest, 10141, Romania
E-mail: lucian.capitanu@yahoo.com

Abstract*: Often for the laboratory studies, modeling of specific tribological processes raises special problems. One such problem is the modeling of some temperatures and extremely high contact pressures, allowing modeling of temperatures and pressures at which the injection or extrusion processing of thermoplastic materials takes place. Tribological problems occur mainly in thermoplastics materials reinforced with glass fibers. They produce an advanced wear to the cylinders and screws of processing machines, in short time. Obtaining temperatures around 210 °C and higher, as well as pressures around 100 MPa is very difficult in the laboratory. This paper reports a simple and convenient solution to get these conditions, using friction sliding couplings with linear contact, cylindrical sleeve plastic filled with glass fibers on plate steel samples, steely and super-finished. Steel C120, which is steel for matrix and Rp3 steel, a high speed steel for tools, were used. Obtaining the pressure was achieved by continuous request of the sleeve in rotational movement up to its elasticity limits, when the dry friction coefficient reaches or exceeds the value of 0.5. By dissipation of the power lost by friction in flat steel sample, are reached contact temperatures at the metal surface that reach and exceed 230 °C, being placed in the temperature values of the injection. Contact pressures (in load conditions and materials used) ranging from 16.3 - 36.4 MPa were obtained depending on the plastic material used and the glass fibers content.*

Key words: *plastics with glass fibres, dry friction, linear contact, contact temperature, contact pressure, experimental simulation*

1. AIMS AND BACKGROUND

Preventive maintenance guide cylinder/ screw to combat wear of the cylinder in extrusion and injection molding of XALOY Inc. company [1] mentions that in the wear of the injection machine are involved four main factors: alignment of the screw and the cylinder; conditions of the processing such as the pressure, temperature and geometry of the screw; processed material characteristics such as the lubricating ability of the molten resin and the presence and nature of any additives, fillers and contaminants, and last but not least, the metals used to produce the cylinder and the screw. In consideration of the four main factors mentioned, the three main wear types of the cylinder and screw are adhesive, abrasive and corrosive wear.

Adhesive wear is the result of metal on metal contact between the screw and the cylinder's wall. With the naked eye, a new screw and cylinder seem to have very smooth surfaces, bright. But an enlarged cross-sectional view shows that the real surface consists of a series of ridges and valleys. If the top of a ridge on the surface of the screw encounters the top of a ridge on the cylinder's wall, the collision energy is sufficient to cause momentary adherence, in the form of a thin weld. If the screw continues to rotate, the welding is sheared. After repeated collisions, particles begin to be removed from the surface that becomes a source of abrasive wear. For example, the severity of adhesive wear is related to incompatibility between the screw and the cylinder materials. Thus, a screw of Stellite 6,

which has been used for four months in the cylinder or in the X - 800, a composite of tungsten carbide particles in a nickel alloy matrix was found to be an inconsistent combination that is not recommended. Materials differ substantially in their trends of adherence to each other. The use of compatible materials is one of two key ways to combat adhesive wear. The other is to minimize the metal to metal contact between the screw and cylinder.

Good alignment will minimize metal to metal contact. Ideal is that the screw to be perfectly straight, the cylinder to be perfectly straight, and their alignment to be perfect. Significant investments were made to have resistant screws and cylinders, but even the perfectly straight screw, aligned in a straight cylinder, perfectly aligned, cannot prevent absolutely metal to metal contact. The reason is that in real mode, during the work, there are other forces involved. One of them is related to the misalignment due to the heat. Because they do not have the same size and shape, the screw and the cylinder are inherently a different warm of the mass. Also, they usually are made of different materials. This leads to different rates of thermal expansion, which produces misalignment.

Another source of metal on metal contact is screw's buckling, caused by the discharge of pressure at its front end. Effects of length (L) and diameter (D) of the screw is particularly important on buckling and on the contact with the cylinder's wall. For example, the length of the screw, with L/D ratios of 24:1 or 30:1, is especially prone to buckling effects. Also, the smaller diameter of the spindle of the most screws is a new factor in the buckling effect.

Physical laws, also produce a third potential source of contact between screw and cylinder deformation under its own weight. Being supported only at one end, a screw is of course a cantilever device. Deflection of the lever arm is proportional to its length at power 4. As a result, the length of screw is liable to deformation. Applying the formula for the deflection of lever arm, a screw extruder with an L/D of 24:1 will deform by 1.5 mm. Of course, it cannot deviate more, because it stops on the cylinder's wall. A 200 mm thick screw would deviate a little more, about 11.6 mm, if it would be free to do so. When the cylinder is filled with molten plastic under pressure, the melt separate the screw from the cylinder's wall and acts as lubricant.

However two precautionary measures should be noted [2]. One is that the cylinder is completely filled with molten plastic. If during processing it contains undissolved or partially melted particles, the intermittent contact between the screw and the cylinder's wall can take place.

Another relates to taking into consideration the fact that the plastic materials melts differ in lubrication properties of melting. Rheological curves of linear polymers, such as, for example, high or low density polyethylene, shows the continuity of the flow to a certain level of shearing stress. Then, there is a ridge on this curve. This discontinuity can cause disruption and of the melted film and can increase the adhesive wear.

The second of the three wear forms found in plastics processing machineries is the abrasion. In the cylinder of the machine two types of abrasion produce. One is abrasion with two bodies as a result of axial movement of the filler particles (for reinforcement) or glass fibers in the extruder. Because the cylinder and screw materials are highly resistant to wear, the effect of two bodies wear are not of great interest. If the abrasive particles become trapped in the space between the screw mounted on the cantilever and the cylinder's wall, the three bodies wear appears. As a result of the deflection force acting on the cantilever screw, the particles become quite efficient cutting tools, resulting generally in grooves and scratches in the direction of screw's motion.

The third type of wear encountered in plastics processing equipment is the corrosion wear. This type of wear is encountered in situations like processing of fluoropolymers, fire-resisting resins and composite resins containing volatile corrosion substances. Solution against corrosive wear is mainly a matter of selecting the materials for the cylinder and screw. Experience has shown that X - 309 alloy is the best material for resistance at corrosion wear.

H. Dominghaus [3] presented severe abrasion and corrosion wears of some screws and cylinders of 30, 45 and 60 mm in melting and kneading areas.

W. Knappe and W.D. Mahler [4] have reported the wear of different alloys coated with nitride in PA6.6 injection with 35% GF in a space of screw-cylinder interspace δ = 0.2 mm, an external pressure P_a = 1100 kp / cm, injection time T_s = 6 sec., injected volume V_s = 25 cm^3, plastics injected temperature of approximately 310 °C. The worst behavior had 18550 DIN nitrided steel in the bath. They have shown corrosion occurred at PA 6.6 + 35 % GF injection for 20 hours, at a temperature of 280 °C and a pressure of 100 MPa.

H. Ladwig and K.D. Sommer [5] analyzed the wear of some screws after 20000 functioning cycles, showing its dependence on the manner of execution of the screw.

W.W. McCandless et al [6] reported on a comprehensive analysis of the wear and corrosion behavior of cylinders and of screws for plastics processing machines. All these works relate to quantitative and qualitative observations made on processing machines.

P. Boey, W. Ho and S.J. Bull [7], from the University of Newcastle - UK, studied the effect of temperature on the abrasive wear of the deposited layers and of hybrid surfaces treatments of the

working bodies from injection processing machines produced at processing of polymers composites with glass fibers, adapting ASTM G65/1994 standard.

In an injection machine, the polymer pellets are pushed and move along the cylinder due to the action of a rotating screw, while they are heated and melted. As a result, the cylinder and the screw will be in contact with the composite solid polymer pellets, with the semi plasticized polymer and the molted one, the contact differing on the length of screw-cylinder assembly. As a result of the high mechanical stresses to which it is subjected and its mode of construction, the screw will have an inherent vibration in the cylinder, which leads to the metal/ metal contact and appearance of adhesive wear. The occurrence of corrosion wear is also possible due to the action of the polymeric material or other additives on metal surfaces, in particular at temperatures above 200 -250 °C registered against the cylinder nozzles and the mold in which this is injected. Boey et al. realized these tests in order to rank abrasion resistance of the materials, treatments and metallic coatings of the working bodies of the processing by injection machines, although the test conditions do not provide modeling of all wear forms. The experimental installation was achieved by adjusting the scheme with rubber (ASTM G65) rotary drum, but the drum has been replaced by one of the same steel used to manufacture the screw of processing by injection machine. Periphery of the steel drum was heated to the desired temperature by blowing hot air, ensuring a deviation of about ± 10 °C to the operating temperature. The drum is streaked and allows training of the plasticized material, which acts at the interface with study samples (heated by a thermal resistance thermometer).

The test sample is depressed by a light load, on the plastic material layer, by means of a pivoting system with lever and weights. In order to increase the efficiency of the heating process and to reduce the heat losses, by convection, nozzles were used for blowing hot air and its focus on the grooves of the drum. Test sample holder was heated independently of the drum, the temperature being controlled with an accuracy of ± 2 °C.

Compared to the ASTM G65/1994 test, the abrasive sand has been replaced by polymer granules, supplied from a bin into the space between the drum and the test sample. In static conditions, it is maintained at a short distance from the drum by means of a flat spring. The spring allows the transmission of the load on the granules passing through the contact area. The pressure and duration of contact may be changed by changing the load and the speed of the drum. Striations practiced on the drum surface are designed to enhance the driving ability of the granulated polymer and thus to reduce the possibility of metal/ metal contact appearance.

For the simulation and limitation of direct contact of the screw with the cylinder of processing by injection machine, was used a flat spring mounted at one end of the loading rocker-arm, the other end being embedded in a solid stop. Changing the spring stiffness leads to space adjustment between the test sample and the drum. Normally, this space is so determined as to be smaller than the size of the composite material grains.

When the rocker-arm is stressed, the test sample holder produces the bending of the flat spring, thus appearing a force opposite to the normal stress of the test sample. Bending is indeed very small compared to the thickness of granular material layer and therefore under static conditions it does not result in direct metallic contact between the drum and the test sample. When a polymer granule is taken by the grooved drum and placed in the contact area, the flat spring is not stressed and the test load is fully applied to the polymer particle.

By controlling the stiffness of flat spring and the position of the attachment point the metal/ metal contact can be prevented for any static load applied. Bending of the spring during testing is monitored by a transducer in order to determine the size of the metal/ metal contact. This occurs over a period of less than 5% of the total time of the test, which is compatible with observations made on processing by injection machines.

The maximum operating temperature of 250 °C and was carried out by heating with hot air system and by heating the test sample holder by means of two thermal resistances of 75 W. Directing the hot air blown through the nozzle of a compressor placed at an angle of 90° to the surface of the drum is carried out by means of a reflective mirror. This led to a strong increase in temperature of the drum while reducing the heat losses. Maximum temperature of the drum can reach 300 °C, while supporting plate of the test sample can reach 316 °C. But practically, the maximum temperature of the test should not exceed 250 °C, value at which the polymer starts to degrade.

The wear rate of the samples was measured by loss of mass and volume. The measurements of mass loss are generally highly accurate, but in the case of tests carried out at temperatures around 200 °C or more, they are not conclusive, because the polymer melt is trapped in the pores of the microstructure and in cracks and cannot be removed by ultrasonic cleaning. Therefore, for a better assessment of the wear rate it is also necessary to measure the volume of worn material.

All these methods [4, 7] are very difficult to reproduce in a tribology laboratory especially due to very high temperature at which the tests should be made. Therefore, a method has been designed

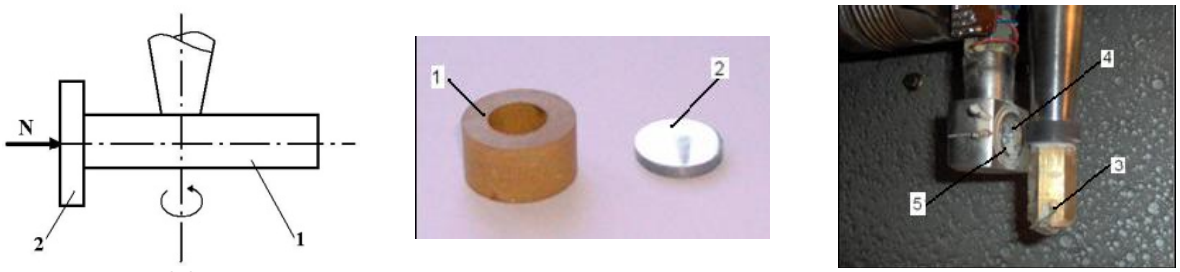
to provide the temperature of polymer/ metal contact by dissipation of the power lost by friction, which converts into an increase in temperature of contact surfaces.

2. MATERIAL AND METHODS

In order to study the metallic counter-part's wear in dry contact with glass fibres reinforced plastic materials Timken type friction couples (with linear contact), cylinder on plan are used, which allows to attain high contact pressures, hence high contact temperatures. In this matter it is possible to observe, whether and in which conditions the plastic material transfer to the metallic surface takes place as well as the influence of the glass fibres filling during this phenomenon, and its effect on the surface's wear. As it is not followed the polymer's wear, but only the polymer's friction influence, over the samples' metallic surfaces wear, is used the unidirectional sliding movement.

2.1. Experimental method

The tests are performed using experimental equipment containing a Timken type couple with linear friction contact, continuously controlling the normal and friction loads, and contact temperature. The unidirectional movement and the linear contact allow to attain very high contact pressures and temperatures. The friction couple is built out of a plastic cylinder Nylonplast AVE polyamide + 30% glass fibres, which rotates at different speeds against the polished surface of a steel plan disk. The cylinder has an outer diameter of 22.5 mm and 10 mm height. Was chosen as sample steel disks with 18.2 mm diameter and 3 mm thickness. The disks' surfaces were polished successively using sandpaper of different granulations (200, 400, 600 and 800) and, finally, were polished on the felt with diamond paste. Mirror polished surfaces, with roughness *R*a of 0.05 μm were obtained. This metal surface's quality allows to eliminate the influence of the metallic surface's state on the friction coefficient's evolution and visualization, to make measurements using optical microscopy and to accurately record the wear traces appeared on the metallic surfaces. Figure1 shows the friction couple (a) and its installation within the experimental equipment (b). Modul in care se misca bucsa impotriva mostrei plane este ilustrat in Fig. 1c.



(a) (b) (c)

Figure 1. Friction couple (a) and its installation in the experimental equipment (b), where 1 - cylindrical liner; 2 – steel disk sample; 3 – nut; 4 – hole; 5 - knife-edge, (c) the way how the liner moves against the disk

Figure 2 shows the scheme of the experimental equipment.

The friction couple is build out of a cylindrical liner (1) and a plane disk type sample (2). The liner is fixed with the help of a nut (3) on the driving shaft (4). The disk sample is placed in a special hole made within the elastic blade (5). The sample disk base is built in such a manner so that the base allows the sample to make small rotations around the edge of a knife fixed in the sample's bezel, perpendicularly on the driving arbor. In this way a uniform repartition of the load on the entire linear contact between the liner and steel sample is ensured, even if there are small building or assembling imperfections. An electric motor (7) puts the shaft (4) into a rotation movement using trapezoidal transmission belts (6). The normal and tangential (friction) efforts through resistive converter strain-gauges, assembled on the elastic blade (5). The use of a pair of converters strain-gauges connected within the circuits of two strain-gauges bridges, offers the possibility to make simultaneous measurements, while separately, gives the possibility to measure the normal and friction forces. The normal load to the elastic blade (5) is applied, through a calibrated spring system (8). The installation allows to register the friction force on an *X*-*Y* recorder. The tests' duration is controlled through an alarm clock and the contact temperature is measured with the help of a miniature thermocouple (9), connected to a millivoltmeter calibrated in mV. The installation offers the possibility to study the wear behaviour by using also several other radiometers techniques. For this purpose, the installation

includes a tank (10) assembled on a base (11) and a tube collecting the radioactive wear particles (12).

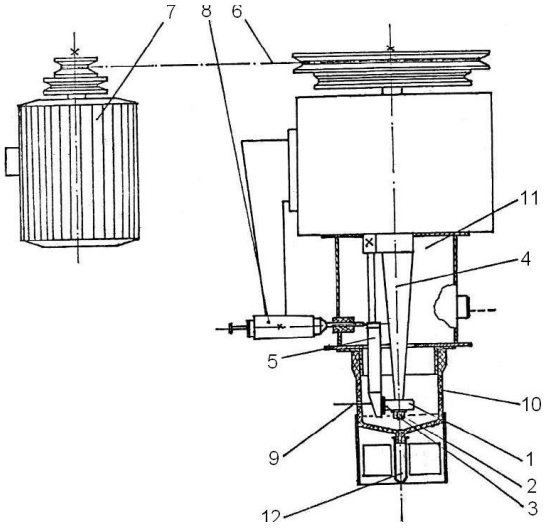


Figure 2. The scheme of experimental equipment with linear contact friction couple, Timken type.

The uni-directional testing was used because the purpose of investigations was the study of metallic surface wear. The tests are performed, based on Hooke's law, at normal loadings of 10; 20; 30; 40 and 50 N, loadings which are adequate to some contact pressures all calculated considering the elastic contact hypothesis, that is: 16.3; 23.5; 28.2; 32.6 and 36.4 MPa (for Nylonplast AVE polyamide with 30% glass fibres) respectively, sliding speeds are used, adequate to the diameter of the plastic composite sample, which are: 0.1856; 0.2785; 0.3713; 0.4641; 0.5570; 1.114 and 1.5357 m/s, and which resulted as a consequence of electric motor's speed and the belt pulleys' primitive diameters.

2.2. Analytical method

The Timken frictional couple (with linear contact) under loading reveals the appearance of some wearing trace on the plane surface of the metallic material. The wearing trace is produced by the penetration of the plane semi couple material by the cylindrical bush (Figure 3).

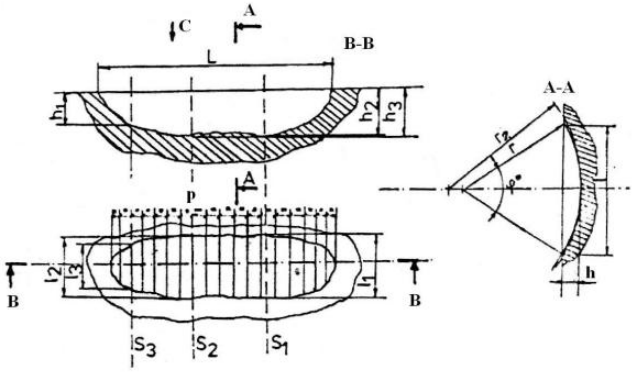


Figure 3. The imprint scheme (top) and elastic deformation of the cylindrical liner in the contact area (bottom) for Timken friction couples (a – theoretical, and b – practical)

Theoretically, considering the bush as rigid and accounting for the generally low non-uniformity of the imprint, this could be considered as being formed by a series of cylindrical sectors having the length *q*. Assuming that, the area of the lateral surface of the cylindrical sector is a circle segment, it results:

$$S_i = 0.5r^2\left(\pi\varphi_i^0/180° - \sin\varphi_i\right) \tag{8}$$

where: S_i - lateral surface of the cylindrical sector; φ_i - the angle; r - the circle radius

The radius r could not be identified with the cylindrical bush radius for the plastic/metal couples. And this fact is possible due to the elastic deformation of the bush under loading conditions, which has as effect the increment of the radius in the contact area. We illustrate this by the sketch plotted in Fig. 2.

Using r_1 for the undeformed bush radius and r_2 for the radius – in the contact area – of the deformed bush, we could notice from figure 1b that $r_2 > r_1$.

Increasing the bush radius in the contact area conducts to the decrease of the depth of the wearing trace from h_1 - (Fig. 4a), which would appear if the elastic deformation of the bush would be neglected, to the value h - (Fig. 4b), with the quantity h_2:

$$h_2 = h_1 - h \tag{9}$$

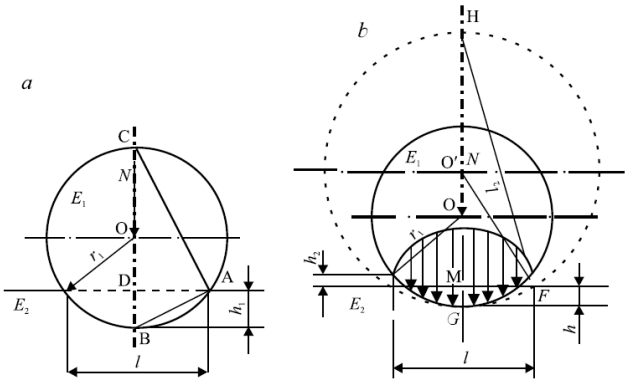


Figure 4. The elastic deformation of the cylindrical liner on the contact area (bottom) for Timken friction couples (a – theoretical, and b – practical)

Using l for the width of the wear imprint, from ΔABC, it results:

$$(2r_1 - h_1)h_1 = l^2/4$$

Because the value of the depth h_1 is very small, the term h_1^2 is neglectable and we could write:

$$h_1 = l^2/8r_1 \tag{10}$$

Similary, in ΔFGH, we have:

$$(2r_2 - h_2)h_2 = l^2/4$$

Using the same assumption, for the term h_2,we obtain:

$$h_2 = l^2/8r_2 \tag{11}$$

Introducing (10) and (11) in (9) it results:

$$h = l^2(1/r_1 - 1/r_2)/8 = l^2(r_2 - r_1)/8r_1r_2 = l^2/8r \tag{12}$$

where r is the equivalent curvature radius given by:

$$1/r = 1/r_1 - 1/r_2 = (r_2 - r_1)/r_1r_2 \tag{13}$$

From (12) it results:

$$(r_2 - r_1)/r_1r_2 = l^2/8h_2 \tag{14}$$

Considering that the frictional couple is loaded in the elastic domain with an elliptic distribution of stresses, the Hertz formula for computing the width of the wear imprint is:

$$l^2/4 = 8Nr\left(1-\nu^2\right)/\pi EL \tag{15}$$

where: v - Poisson ratio; L - the length of the wear imprint; E - equivalent Young modulus.

Using index 1 for quantities related to the cylindrical bush, and index 2 for those related to plane half-couple, the equivalent elasticity modulus is given by:

$$1/E = 0.5\left[\left(1-\nu_1^2\right)/E_1 + \left(1-\nu_2^2\right)/E_2\right] \tag{16}$$

Because the numerical values of ν_1 and ν_2 are between 0.3 and 0.32 the equivalent elasticity modulus could be approximated by:

$$E = 2E_1E_2/0.91\left(E_1+E_2\right) \tag{17}$$

From (15) we could express the width of the wear imprint:

$$l = 4\left[2Nr\left(1-\nu^2\right)/\pi EL\right]^{1/2} \tag{18}$$

Introducing in (18) the equivalent elasticity modulus and the equivalent radius expressions, the numerical value of Poisson ratio, one could obtain:

$$h_2 = 0.527N\left(E_1+E_2\right)/LE_1E_2 \tag{19}$$

Considering the relations (10) and (19), we have for the depth of the wear imprint the expression:

$$h = \left(l^2/8r_1\right) - 0.527N\left(E_1+E_2\right)/LE_1E_2 \tag{20}$$

Assuming that the wear imprint is the sum of some cylindrical sectors, expanding in series the relation (8), neglecting the high-order terms and reducing the similar terms we could obtain, for the area of the lateral surface of a sector, the expression:

$$S_i = r^2\phi^3/12 \tag{21}$$

Replacing in the relation above the angle ϕ with the ratio l/r and accounting for (13) and (14), we obtain:

$$S_i = l^3\left(r_2-r_1\right)/12r_1r_2 = 2lh_2/3 \tag{22}$$

Replacing the value of h_2 obtained from (20) in (22) we could obtain the expression for the area of lateral transversal surface of a cylindrical sector:

$$S_i = 0.35l\left(E_1+E_2\right)Nl/E_1E_2L \tag{23}$$

The wear volume of metallic material will be:

$$V_u = \sum_{i=1}^{n}\left(S_iq_i\right) = 0.351\left(E_1+E_2\right)Nl_m/E_1E_2 \tag{24}$$

where l_m is the mean width of the wear imprint.

Practically, it is needed to measure the width of wear imprints in three points established before, computing then the mean value of this width. With this value we could obtain the volume of worn metallic material V_u and the mean of the depth of removed layer h_{mu}.

The studies concerning the metallic sample wear are generally based on the elastic contact hypothesis. For these plane half-couple the values for the equivalent elasticity module are: A. Nylonplast AVE polyamide + 30% glass fibres; E_{2A} = 40.25 MPa. B. Noryl polyamide + 20% glass fibres; E_{2B} = 31.76 MPa. C. Lexan polycarbonate + 20% glass fibres; E_{2C} = 42.08 MPa.

Assuming that the plastic liner does not crush, the condition $p\max < \square 0.5H$ is imposed, where H stands for theBrinell hardness. The required condition allows to establish the following values of the maximum loadings (contact pressure) of the couple:

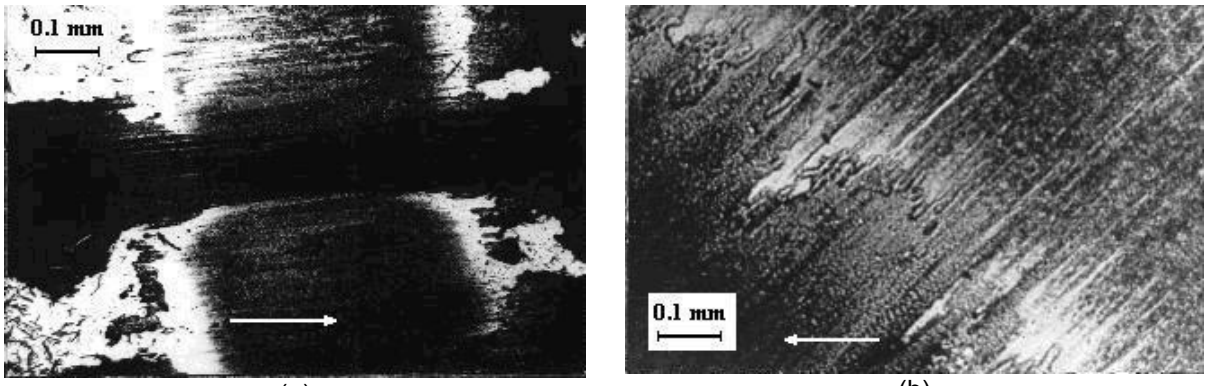
p_{A1} = 16.3 MPa; p_{A2} = 23.5 MPa; p_{A3} = 28.2 MPa; p_{A4} = 32.6 MPa; p_{A5} = 36.4 MPa; p_{B1} = 12.3 MPa; p_{B2} = 17.4 MPa; p_{B3} = 21.4 MPa; p_{B4} = 24.6 MPa; p_{B5} = 27.6 MPa; p_{C1} = 16.9 MPa; p_{C2} = 23.9 MPa: p_{C3} = 29.3 MPa; p_{C4} = 33.8 MPa; p_{C5} = 37.8 MPa.

The experimental tests are performed considering broader domains to vary the relative speed and normal loadings, or contact pressures. Couples with liner made from thermoplastic material with linear contact on a steel surface (C120, Rp3, a.s.o.) are used.

Tests have aimed in addition to the wear of metallic surface and coefficient of dry friction and contact temperature following friction at different loads (contact pressures) and sliding speeds.

4. RESULT AND DISCUSSION

The wear tests were detailed presented elsewhere [9]. While measuring the wear traces widths with the help of optical microscopy, microphotographs are also taken, in order to identify the plastic material's transfer and the metallic surfaces' wear mechanisms. These microphotographs prove that the wear mechanisms vary from one couple to another, due to surfaces' nature: metallic and composite plastic material, especially their hardness (59 HRC for C120 hardened steel and 62 HRC for Rp3 hardened steel), the glass fibres content, 30% and 20%, the composite plastic materials' elasto-plastic characteristics while in contact with metallic surfaces. Considering the same loading conditions, the two couples to which is made reference have a different behaviour. On C120 steel sample (Fig. 5), at a normal load of 20 N and a contact temperature of 150°C, there are plastic material transfer bridges, crossing on the wear traces (Fig. 5a), as well as the glass-fibres torn from the polymer matrix.



(a) (b)

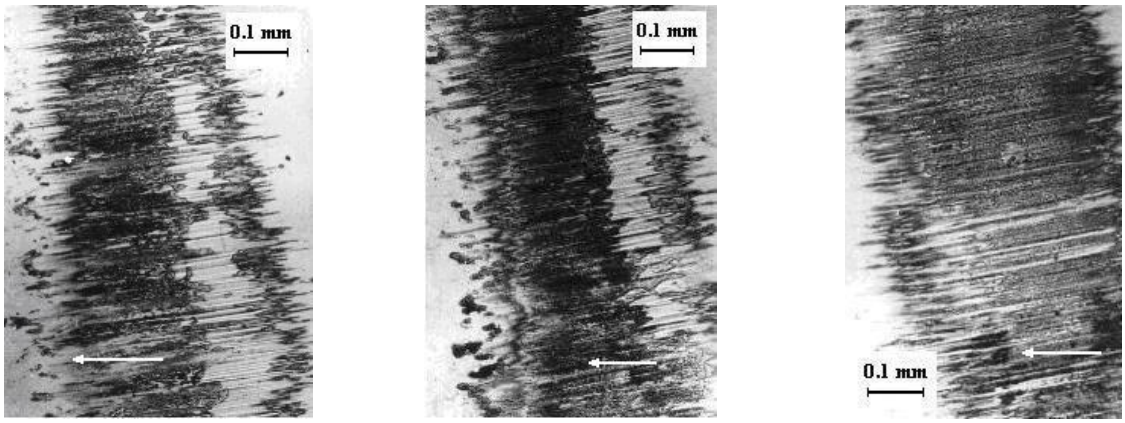
Figure 5. Wear, glass fibres and plastic material transfer on C120 steel surface, following the friction with Nylonplast AVE polyamide reinforced with 30% fine glass fibres (a), in experimental conditions (sliding direction is indicated by the arrow): v = 27,85 cm/s; N =20 N; T = 150 ^{0}C; t = 60 min and (b) in experimental conditions v = 27.85 cm/s; N = 30 N; T = 175 ^{0}C; t = 60 min.

Considering the same mechanical stress conditions (load and relative speed), the microscopic inspection of the Rp3 steel samples, while in friction contact, with the same composite plastic material, reveals a less pronounced plastic material transfer through adherence onto the metallic surface, visible on the left side in Figs 6 (a) and 6 (b). If the test duration is double (120 min), practically there is no plastic material transfer as one can see in Fig 6 (c).

If the test duration is double (120 min), practically there is no plastic material transfer as one can see in Fig 6 (c).

It is considered that due to high registered contact temperature (237 ^{0}C) the transfer takes place for sure, but the transferred material is subsequently removed through friction from the contact

area, under the form of wear particles following the glass fibres abrasive action. After this stage, the abrasive wear due to glass fibres becomes predominant.



(a) v = 27.85 cm/s; N = 40 N; t = 60 min; T = 217 ^{0}C.

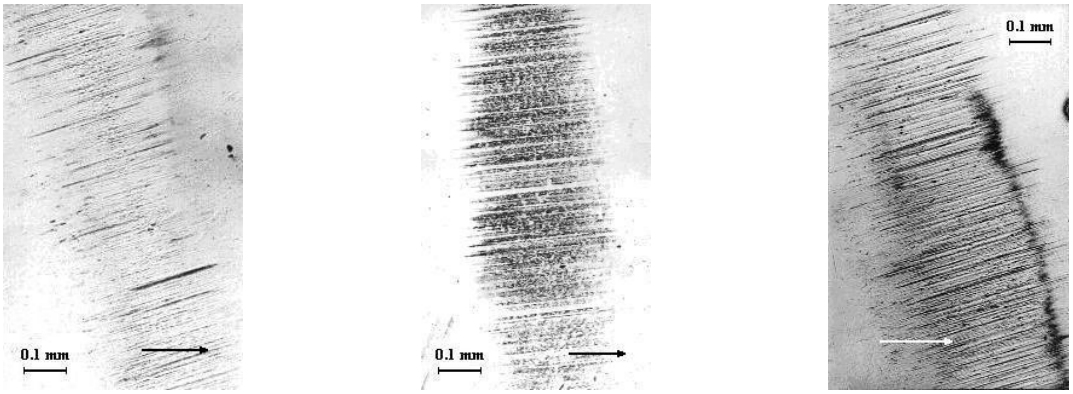
(b) v = 27.85 cm/s; N = 30 N; t = 120 min; T = 175 ^{0}C.

(c) v = 27.85 cm/s; N = 40 N; t = 120 min; T = 237 ^{0}C.

Figure 6. Wear and plastic material transfer on C120 steel surface, following the friction with Nylonplast AVE polyamide reinforced with 30% short glass fibres (sliding direction is indicated by the arrow)

It is possible that the less pronounced plastic material transfer emphasized on the Rp3 steel surfaces to be due to this steel's chemical composition and structure.

We detect the same findings in the case of Noryl polyamide + 20% glass fibres in friction on the same steels, but to a lesser scale. In the case of Lexan 3412 polycarbonate reinforced with 20% glass fibres friction onto the same metallic surfaces and considering the same stress conditions, generally speaking there is no plastic material transfer – Figs. 7 (a) and 7 (b) The transfer appears only if the load reaches 40 N, which corresponds to a contact pressure of 33.8 MPa, and when the contact temperature reaches 251 ^{0}C - Fig. 7 (c). We do consider that probably the polycarbonate has a lesser transfer capacity than the polyamide.



(a) v = 27.85 cm/s; N = 20 N; t = 60 min; T = 164 ^{0}C.

(b) v = 27.85 cm/s; N = 30 N; t = 120 min; T = 185 ^{0}C.

(c) v = 27.85 cm/s; N = 40 N; t = 120 min; T = 251 ^{0}C.

Figure 7. Wear and plastic material transfer on Rp3 steel surface, following the friction (sliding direction is indicated by the arrow) with Lexan 3412 polycarbonate reinforced with 20% short glass fibres

In the case of polyamide reinforced with 30% glass fibers plastic transfer on steel surfaces is manifested up to around a temperature of 240 °C, when it comes to the vitrification state of the plastic bushing surface (glass transition temperature).

Table 1 summarizes the experimental results concerning the friction coefficient, mean wear rate (linear and volumetric) and contact temperature. Results show the growth of these quantities at increase of glass fibers content, normal load and sliding speed.

Table 1. The range of mean wear's rate, friction coefficient's and contact temperature's rate for tested friction couples

Friction couple	Mean friction coefficient	Volumetric wear rate (10^{-6} cm^3/h)	Linear wear rate (10^{-4} mm/h)	Contact temperature (^{0}C)
v = (18.56 – 46.41) cm/s; N = (10 – 50) N				
Polyamide + 30% glass fibres/C120	0.51	0.139 – 1.621	0.965 – 8,549	155 – 240
Polyamide + 30% glass fibres/Rp3	0.47	0.214 – 1.169	2.382 – 6.004	150 - 225
Polycarbonate + 20% glass fibres / C120	0.43	0.244 – 1.309	3.592 – 6.366	140 – 230
v = (46.41 – 111.4) cm/s; N = (10 – 50) N				
Polyamide + 20% glass fibres/C120	0. 40	0.440 – 2.578	3.269 – 6.794	145 – 230
Polyamide + 20% glass fibres/Rp3	0.36	0.473 – 2.549	3.792 – 6.627	130 – 220

Although cannot be made a mathematical correlation between friction coefficient and contact temperature, it is obvious that the contact temperature increases while increasing the friction. Contact temperature increase causes transfer of plastics, whether in the form of transfer bridges, or plastic material depositions and glass fibers on the edge output of the wear scar.

4. CONCLUSION

In order to study the metallic counter-part's wear in dry contact with glass fibres reinforced plastic materials Timken type friction couples (with linear contact), cylinder on plan are used, which allows to attain high contact pressures, hence high contact temperatures.

In this matter it is possible to observe, whether and in which conditions the plastic material transfer to the metallic surface takes place as well as the influence of the glass fibres filling during this phenomenon, and its effect on the surface's wear. As it is not followed the polymer's wear, but only the polymer's friction influence, over the samples' metallic surfaces wear, is used the unidirectional sliding movement.

In the case of sliding friction thimble with linear contact, plastic material on steel, contact temperature increase can achieve in certain stress conditions (contact pressure and sliding speed) elasto-plastic transition temperature of the polymer and even of the vitrification state of its surface.

Presented paper has some limitations. Thus, the contact temperature was measured using a miniature thermocouple inserted into a hole of 1 mm practiced in the middle of the back surface of the flat metallic sample up to 0.5 mm behind the surface friction. Although small, this distance with the friction surface makes that the measured contact temperatures to be relatively lower than the real ones. Another limitation consists in the fact that the elastic contact hypothesis in which contact pressures were hardly calculated can be accepted in the case of the elasto-plastic transition temperature of the plastic material reinforced with glass fibers.

However, by modeling the linear dry sliding contact, the bush of plastic material reinforced with short glass fibers on flat steel surfaces, were obtained the contact pressures and temperatures similar to those found in processes of processing by injection or extrusion of plastic materials reinforced with short glass fibers.

ACKNOWLEDGMENTS

The authors would like to thank their colleagues from the Institute of Solid Mechanics and University of Civil Engineering for your logistic support.

REFERENCES

1. xxxxx. Combatting barrel and screw wear in extrusion and injection molding. Barrel / screw preventive maintenance guide. Quality and Innovation, 2000. XALOY INC.
2. ANDERSON R. Monitor screw & barrel wear to avoid quality, production woes. Flite Technology Inc.
3. DOMINGHAUS H. Verschleiβprobleme bei der Verarbeitunggefullter Kunststoff Rundschau 18, 8, 1971, pp. 383-389.

4. KNAPPE W., MAHLER W. Modellversuche zum Verschleiß in Kunststoffverarbeitungsmaschinen. Kunststoff Rundschau 19, 2/3, 1972, pp. 45-51.
5. LADWIG H., SOMMER K.D. Verscuche zur Erhöhung der Verschleißfestigkeit von Zylindern und Schnecken bei der Verarbeitung von glassfaserverstärkten Polyamiden auf Spritzgießmaschinen. Plastverarbeiter. 21 (1970), pp. 259-260.
6. McCANDLESS W.W. et al. Verschleißfeste und korrosionbeständige Zylinder und Schnecken für Kunststoffmaschinen. Industrie – Anzeiger. 91 (1969), Nr. 25, pp. 25-29.
7. BOEY P., HO W., BULL S.J. The effect of temperature on the abrasive wear of coatings and hybrid surface treatments for injection-moulding machines, Wear 258 (2005), pp.149-156.
8. CAPITANU L., IAROVICI A., ONISORU J. *On polyamide and polycarbonate materials behaviour under dry friction*,The Annals of University “Dunarea de jos” Galati, fascicle **VIII**, Tribology, 2003, ISSN 1221-4590.
9. CAPITANU L., FLORESCU V. Tribological aspects of wear of polished steel surfaces in dry friction contact on polymer composites with glass fibres. American Jounal of Materials Science 2013, 3(1): 8 - 18. DOI 10.5923/j.materials.20130301.02.

Tribological Journal BULTRIB, **Vol. IV, 2014**
Papers from the International Conference **BULTRIB '13**
October 24-26, 2013, Sofia
Society of Bulgarian Tribologists
Technical University of Sofia

QUALITATIVE CORRELATION BETWEEN FRICTION COEFFICIENT AND METAL SURFACE WEAR IN THE CASE OF LINEAR FRICTION DRY CONTACT WITH REINFORCED POLYMERS WITH GLASS FIBRE

Dorin RUS[1] **, Virgil FLORESCU**[1]
[2]Technical University of Civil Engineering Bucharest, Romania
Address: 124 Lacul Tei Boulevard, Bucharest 020396, Romania
E-mail: rusdorin@gmail.com; florescuvirgil@yahoo.com

Lucian CAPITANU[2*]
[1]Institute of Solid Mechanics of Romanian Academy, Bucharest, Romania
Address: 15 C-tin Mille str., district 1, Bucharest, 10141, Romania
E-mail: lucian.capitanu@yahoo.com

Liliana-Laura BADITA[3]
[3]National Institute for Research and Development in Mechatronics and Measurement Technique, Bucharest, Romania
Address: 6-8 Sos Pantelimon, Bucharest, 021631, Romania
*E-mail: badita_l@yahoo.com

Abstract*:* In this paper we tried to present a qualitative correlation, based on extensive experimental determinations between the value and the evolution of the friction coefficient in the case of linear dry contact, thermoplastic material reinforced with short glass fibres (SGF) and various steel surfaces. The aim was to highlight the evolution of the wear process depending on the evolution of the friction coefficient. As a result, it was possible to graphically illustrate the evolution of the friction coefficient and the change of the wear process, emphasizing the abrasive, adhesive and corrosive wear. It was aimed and it was highlighted the evolution of the plastic material transfer function of the contact temperature, namely of the power lost by friction (product between the contact pressure and sliding speed, *pv*). It has been demonstrated that in the case of a 30% SGF content it can reach and even exceed contact temperatures very close to the flow limit of the plastic material. We tried, believing successfully, the graphic illustration of the evolution of the steel surface wear and of the contact temperature, depending on the friction coefficient. It was analysed in detail the influence of the normal load and sliding speed, but also of the metallic surface roughness on the friction coefficient.

Key words: friction coefficient evolution, wear of steel surface, contact temperature, plastic material transfer, hardness of steel surface influence

1. AIMS AND BACKGROUND

Composite thermoplastic materials are biphasic materials consisting of a mass of polymer and the reinforcement embedded in it. The polymer provides the compressive strength of the material, while the reinforcement improves the tensile strength. Homogeneity of the material and its cohesion has an important role in obtaining some good mechanical characteristics. Thus, the disposal of the reinforcement considerable influences the tensile strength feature. Also the elasticity of the polymer can improve the compression resistance or bending resistance of the reinforcement material. The role of the basic polymer is first of all mechanical and is to provide the bond with the reinforcement fibres. It is the one that transmits the efforts between the reinforcement fibres. Therefore, it is necessary to ensure a minimum adhesion between these two phases. The adhesion cannot be achieved by mechanical means, is necessary to achieve a chemical bond for the polymer coating with the basic polymer. The treatments performed for this purpose are specific to each thermoplastic material.

Basic polymer acts as a bridge between the reinforcement glass fibres. If the binder is slightly deformable, the fibres cannot move, so only a small number of them support loading. The polymer must allow a balanced distribution of efforts between the reinforcement fibres, but in the same time must limit their movement to prevent an excessive deformation of the product. Also, the basic polymer ensures the tightness against humidity, because most of the reinforcement fibres have a high affinity for water, resulting in the loss of some of the properties. The glass nature has importance on the time constancy of mechanical, electrical and chemical properties of reinforced thermoplastic material. In order to obtain stable products alkali-free glass is used, because all of the fibres with a high content of Na or K have characteristics that decrease rapidly in time, as a result of their superficial hydrolysis by the action of humidity. In order to improve the mechanical properties, in particular elastic modulus, glasses containing metal oxides are used in certain proportions.

The glass fibres used to reinforce the thermoplastic materials, when they are free of defects, have a minimum tensile strength of 25 MPa, and with their usual surface defects achieve maximum 15 MPa, although the glass itself has a resistance of 0.5 – 0.6 MPa. Elastic modulus achieves 750 – 790 MPa. Fibres have elongations of 2 – 3 %, total elastic elongation. No permanent deformations occur before breaking and no hysteresis at normal temperature.

Also, the presence of the glass fibres leads to reduction of the factor time in the creeping process. Dimensional changes due to water absorption remain a problem of hygroscopy, polymers inherent. By incorporating glass fibres in the thermoplastic materials their mechanical properties are preserved, in a wide temperature range.

Thermoplastic materials with glass fibres structurally present a mechanical association of glass and polymer fibres. Thermoplastic compounds are characterized by high plasticity under certain conditions of temperature and by their returning to the initial stage by cooling. In the plastic stage they can be processed into finished products.

Ever since the year 1964 Bowdon and Tabor [1] experimentally found that the values of the friction coefficients of the "clean" metals couplings on plastic materials and in the presence of some moderate loads are similar to those of the plastic material/ plastic material friction couplings. They considered that the shear force is due to friction of the micro-junctions formed on the contact surface of the two semicouplings.

In the specialty literature there are works which give values of the friction coefficient of plastic material/ metal, plastic material/ plastic material, reinforced or unreinforced couplings, operating both under dry friction and in the presence of lubricants. Jacobi [2] presents for polyamide reinforced with glass fibres, values of the friction coefficient ranging between 0.04 and 0.5. Bilik [3] determined for the friction coefficient of the polyamides/ steel, values up to 2.0. All the mentioned works emphasize the fact that the value of friction coefficient is not constant, it depends on the relative sliding speed, contact pressure, surface roughness, temperature, etc.

Clerico [4] studying the friction behaviour of the polyamide/ metal coupling found that the friction coefficient values are higher for short periods of operation, than for long term operation of the coupling. He indicates friction coefficient values from 0.1 up to 0.65 for the first three hours of coupling's operation, values that decrease up to 0.42 in the next 67 operation hours. He explains this by the viscoelastic properties of the polymer.

Hrusciov şi Babicev [5, 6] shows the growth of microcutting component of the friction force for plastic material reinforced with fibreglass/ steel couplings, with increasing the polymer content.

Bely [7], Bartenev and Laventiev [8] studied the influence of the polymer's nature and of the glass fibres orientation in its mass, on the friction coefficient. They found that the friction coefficient values increase when glass fibres have not the same orientation in the basic polymer.

Watanabe et al [9] show the increase of the friction coefficient with the increase of the normal load. They explain the influence of temperature on the friction coefficient value's decrease by the intensification of plastic material transfer to the steel.

Lancaster [10] taking care of the friction behaviour of the polymers reinforced with different natures fibres, established the dependence of the friction coefficient of the ratio $\eta v d^3/N$ for lubricated couplings beak (of diameter d) / disc type. He found the decrease of the friction coefficient with the reduction of the metallic surfaces roughness and with the increase of the mentioned report value. The friction coefficient decreases from 0.19 to 0.04 when the ratio $\eta v d^3/N$ increases from 10^{-14} to 10^{-11} m^2, for a roughness of 0.15 μm of the steel surface. For roughness of 0.46 μm, the friction coefficient is constant when the mentioned report increases from 10^{-14} to 10^{-11} m^2.

Studying the friction behaviour of the thermoplastic materials, Barlow [11] provides for friction coefficient of these on steel, values of $0.1 \div 0.28$, in the presence of a lubricant. He notes the increase in the value of friction coefficient with the increase of the relative sliding speed between the surfaces of friction torque.

West [12] examining the friction behaviour of the polyethylene/ steel coupling shows the reduction of the friction coefficient from 1.24 to 0.78, when the normal load increases from 10 to 5000 N. He demonstrates that for normal loads of 250 (1500 N, the friction force is proportional to the factor ($N^{0,88}$), and the friction coefficient is proportional to ($N^{-0,22}$).

Bartenev, Lavrentiev et al [13] establish in the case of plastic materials friction on metallic surfaces, the increase of friction force with increasing the logarithm of sliding speed. This dependence is expressed by Vinogradov, for friction on metals of crystalline polymers. In the case of adhesion processes preponderance, he finds also an increase of the friction force with the normal load.

From the above, it can be concluded that the friction process of thermoplastic materials is extremely complex, a variety of parameters influencing the value of the force and of the friction coefficient. These parameters, physical and mechanical, influence the friction process in the presence of a lubricant in the contact region, and in the absence thereof. Although relatively numerous, the published works do not allow a complete characterization of the process, due to the heterogeneity of the materials tested and the experimental conditions used as well as of the contact types variety and of the research installations used.

If realized researches and published works on the friction behaviour of the thermoplastic material reinforced with glass fibres/ metal coupling are quite numerous, not the same can be said about those published in the wear domain. The data presented in the specialty literature concerning the wear of this coupling, refer to certain limited domains of use of the reinforced thermoplastic materials. Most papers treat qualitative aspects of the wear phenomenon, just few presenting and its qualitative side. Thus, Bowden and Tabor [14] have highlighted the importance of the distribution of stresses on the contact surface, showing that in the case of a Hertzian contact with a pressures elliptical distribution, the central area of the contact surface will be more seriously damaged than the marginal areas due to higher values of surface tensile stresses (μp) and reach to exceed a certain critical value $(\mu p)_c$.

Jost [15] highlights that for the polyamide/ metal coupling adhesion wear predominates both in the dry friction conditions and in the presence of the lubricant.

Lancaster and Evans [16] studying the wear behaviour of reinforced polymers under hydrodynamic lubrication, observed the decrease in wear rate with increasing the value of the factor $\eta v d^3 / N$ for beak type couplings with diameter *(d)*, made of plastic material, in friction on metal discs. The decrease is more pronounced, as the metal surface roughness is more reduced. He set for polyamide (PA) + MoS_2/ steel coupling ($R_a = 0.15\ \mu m$), the wear rate of 5×10^{-6} mm^3/Nm and for the (PA) + graphite/ steel coupling ($R_a = 0.15\ \mu m$), the wear rate of 5×10^{-7} mm^3/Nm, while for the (PA) + glass/ steel coupling ($R_a = 0.15\ \mu m$) the wear rate reaches 4×10^{-4} mm^3/Nm, and 3×10^{-6} mm^3/Nm for (PA) / steel coupling ($R_a = 0.15\ \mu m$).

Shen and Dumbleton [17], comparatively studying the wear behaviour of high density polyethylene and polyoxymethylene (Delrin 150 commercial type), processed by injection, establish for the wear coefficient values from 7.8 to 28.6×10^{-10} cm^2/N. They propose to calculate the linear wear of high density polyethylene (UHMWPE), a relation of the type:

$$h = kpx$$

where: h – linear wear; k - wear factor; p - nominal pressure; x - sliding distance.

Based on the above relation they have established for the wear factor of high-density polyethylene, values ranging from 1.3 - 3 x 10^{-11} cm^2/daN.

L. Capitanu, A. Iarovici and J. Onisoru [18] reported about the behaviour of polyamide and polycarbonate reinforced with glass fibres in friction on steel surfaces, and L. Capitanu and V. Florescu [19] presented some tribological aspects of the steel surfaces wear in dry friction on polymer composites with glass fibres.

2. MATERIAL AND METHODS

Friction and wear processes were analysed for a relatively wide range of tribological parameter values that affect it (load, relative speed, temperature). Range of values used for the parameters mentioned include both values commonly encountered in industrial applications, as well as some extreme values, less common, but that are of interest from the point of view of the friction and wear mechanism. Thus, although the values of the stresses and the speeds some parts made of thermoplastic materials usually work are between 0.2 – 1 MPa and respectively 1 – 500 cm/s, attempts were made at speeds and loads greater than or less than the ranges mentioned.

The two elements of friction couplings (cylindrical sleeve and flat sample) were made of plastic material and metal, respectively. The metallic elements of the examined couplings were made

of steels of different qualities and with different surface states. Of tested steels only a few qualities widely used in industrial practice have been selected for presentation.

For friction and wear tests polyamides and polycarbonates were selected from the wide range of thermoplastic materials processed in industry, in view of their increased reinforcing possibilities with glass fibres and high density polyethylene because of its use as a replacement of metals in some practical applications.

Experimental tests have been conducted using polyamides and polyesters reinforced with 20% and 30% of glass fibres. For comparison, friction-wear tests were performed and with unreinforced polyamides and polycarbonates.

For the experimental tests have been used thermoplastic matherials whose characteristics are shown in Table 1.

A certain variation of such characteristics according to the various commercial types is observed, variation which occurs in rather limited ranges. From, Table 1, it is noted the improvement of physico-mechanical properties of materials reinforced with glass fibres, compared to the unreinforced ones.

Nylonplast AVE Polyamide [20] has incorporated 30% glass fibres having a diameter of 12 μm, resulting in an accentuated decrease of products deformation. Thus, at 50ºC and a compression of 140 daN/cm^2, deformation decreases from 1.4% in the case of unreinforced polyamide to 0,2% for the reinforced one.

Noryl Polyamide [21], reinforced with 20% glass fibres is characterized by a very low water absorption and high value of elastic modulus.

Lexan Polycarbonate [22], reinforced with 20% glass fibres, has a high mechanical strength, a very good dimensional stability, and high resistance to shock.

Makrolon polycarbonate [23], unreinforced, has high resistance to shock, outstanding dimensional stability, low water absorption and low deformability.

Technyl Polyamide [24], although unreinforced with glass fibre, presents due to its high capacity of crystallization, a high consistency of mechanical properties, low deformability, good resistance to bending, strength and shock, a good friction resistance.

Friction and wear behaviour of the materials above, considered significant for the polyamides and polycarbonates tribological manifestation, has been studied and will be presented in detail in this paper.

In Figure 1 is shown a series of photomicrographs intended to restore some details on the structure of thermoplastic materials tested.

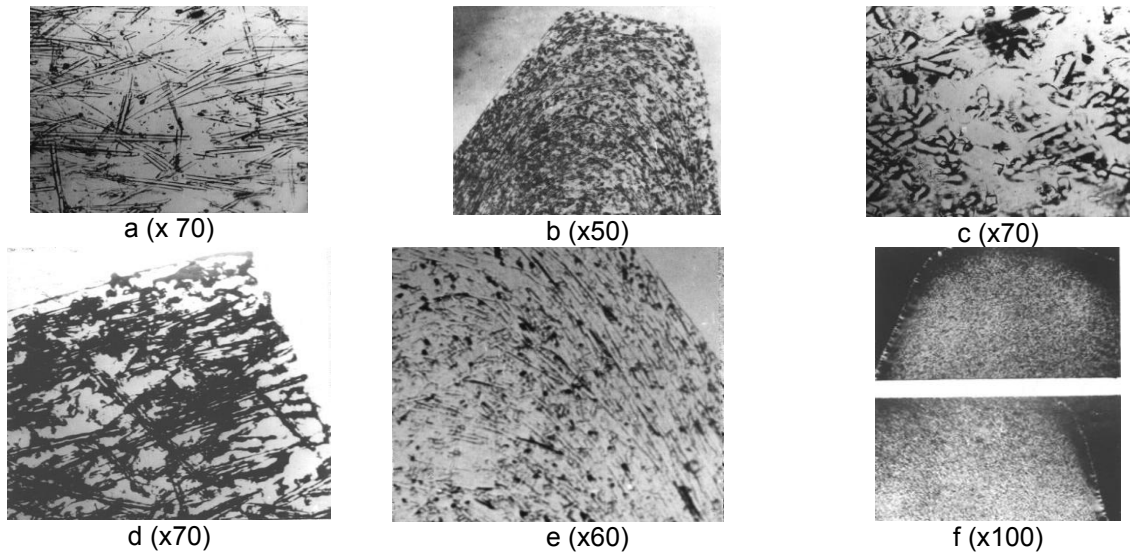


Figure 1. Microphotographs of the structures of thermoplastic materials reinforced with glass fibres, submitted to friction and wear tests. a. Nylonplast AVE Polyamide + 30% glass fibres; b. an image of the cross section from a dent of a gear wheel manufactured through injection from Nylonplast AVE Polyamide + 30% glass fibres; c. the image of a cross section for a sample made of Noryl Polyamide + 20% glass fibres; d. image of the microstructure of Lexan Polycarbonate reinforced with 20% glass fibres of approximately 8 μm diameter; e. a cross section of the dent of a gear wheel manufactured from Lexan polycarbonate reinforced with glass; f. The image seen in polarized light of the microstructure of non-reinforced Technyl polyamide.

In Figure 1.a is shown the microstructure of Nylonplast AVE Polyamide reinforced with 30% glass fibres with a diameter of approximately 12 μm [20].

Figure 1.b presents a cross-section from a dent of a gear wheel manufactured through injection from Nylonplast AVE Polyamide + 30% glass fibres [20].

In Figure 1.c is shown the image of a cross section for a sample made of Noryl Polyamide + 20% glass fibres [21].

Figure 1.d renders the image of the microstructure of Lexan Polycarbonate reinforced with 20% glass fibres of approximately 8 μm diameter [22].

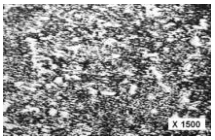
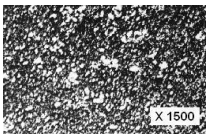
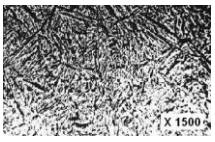
Figura1. e shows a cross section of the dent of a gear wheel manufactured from Lexan polycarbonate reinforced with glass [23].

Figure 1.f shows the image seen in polarized light of the microstructure of non-reinforced Technyl polyamide.

Metallic contrapieces of tribological tested couplings were made of the following steels: C 120 steel hardened 59 HRC; Rp3 steel, hardened 62 HRC and 33 MoC 11 steel hardened 51 HRC.

The mechanical characteristics, chemical compositions and some microstructure considerations of these steels are given in Table 1.

Table 1. Physical-mechanical and metallographic characteristics of the metals submitted to friction -wear tests.

<table>
<tr><th>Steel</th><th>Metallographic Characteristics</th><th colspan="10">Chemical composition (%) and mechanical characteristics</th></tr>
<tr><td rowspan="3">Rp3</td><td rowspan="3">
Carbides uniformly segregated, on matertesite field. Small residual austenite (attack nital 2%).</td><td>C</td><td>Si</td><td>Mn max</td><td>S max</td><td>P max</td><td>Cr</td><td>Mo max.</td><td>V</td><td>Ni max.</td><td>W</td></tr>
<tr><td>0.7
0.8</td><td>0.2
0.4</td><td>0.45</td><td>0.02</td><td>0.025</td><td>3.5
4.4</td><td>0.6</td><td>1.0
1.4</td><td>0.4</td><td>17.5
19.5</td></tr>
<tr><td colspan="10">Hardened in oil, 1250 ^{0}C – 1350 ^{0}C; Hardness 62 HRC</td></tr>
<tr><td rowspan="3">C120</td><td rowspan="3">
Precipitate of globular carbides uniformly distributed in a martesite mass slightly tempered (attack nital 2%).</td><td>C</td><td>Si</td><td>Mn</td><td>S max</td><td>P max</td><td>Cr</td><td>Mo</td><td>V</td><td>Ni max.</td><td>W</td></tr>
<tr><td>1.8
2.2</td><td>0.15
0.35</td><td>0.15
0.45</td><td>0.02
5</td><td>0.03</td><td>11
13</td><td>-</td><td>-</td><td>0.35</td><td>-</td></tr>
<tr><td colspan="10">Hardened in oil, 930 ^{0}C – 960 ^{0}C; Hardness 59 HRC</td></tr>
<tr><td rowspan="3">33MoC11</td><td rowspan="3">
Acerose martesite, slightly tempered (attack nital 2%)</td><td>C</td><td>Si</td><td>Mn</td><td>S max</td><td>P max</td><td>Cr</td><td>Mo</td><td>V</td><td>Ni max.</td><td>W</td></tr>
<tr><td>1.8
2.2</td><td>0.15
0.35</td><td>0.15
0.45</td><td>0.025</td><td>0.03</td><td>11
13</td><td>-</td><td>-</td><td>0.35</td><td>-</td></tr>
<tr><td colspan="10">$\sigma_{0.2}$ = 7 MPa; σ_r =9 MPa
Hardened in oil; Hardness 51 HRC</td></tr>
</table>

The surfaces of metal samples were processed by grinding, wet polishing with aluminium oxide and polishing with diamond paste for different grain sizes. This technology has allowed to obtain surfaces with R_a = 0.025 μm, R_a = 0.045 μm, R_a = 0.075 μm and R_a = 0.125 μm. For the experiments were used samples with roughness higher or lower than the one mentioned above, for a more complete characterization of the friction and wear process.

Due to the wide range of loads and speeds considered, and the need to achieve the greatest possible variety of working conditions (contact pressures, sliding speeds and temperatures) for a more complete characterization of the tribological behaviour of composite material/ steel coupling was used an experimental installation with Timken type friction torque (with linear contact). This can achieve very high contact pressures (between 16 and 36 MPa).

Testing installation has been presented in detail elsewhere [19].

3. RESULTS AND DISCUSSION

Tests carried out have had the purpose of determining the influence of the main factors affecting the friction in the case of thermoplastic material reinforced with glass fibres/ metal couplings. It is well known the law established by Coulomb (1780) that the friction force F_f is direct proportional to the normal force N:

$$F_f = \mu N \tag{1}$$

Multiple studies conducted later have shown that μ, the friction coefficient, is not only dependent on the normal force.

Relations for variations of the friction force, depending on the load applied can be considered, of the form:

$$F_f = aN + bN^n \tag{2}$$

or more simply:

$$F_f = a + bN \tag{3}$$

or:

$$F_f = a + bN^n \tag{4}$$

Last relationships lead to the conclusion that when the normal force is equal to 0, the friction force has other value than 0 ($F_f = a$). Although this could be explained by the presence of a remanent force of adhesion of the two surfaces, even after the removal of the normal load, however, we consider more accurate the use of a relationship of the form:

$$F_f = kN^n \tag{5}$$

where n is subunitary.

Friction coefficient, according to Coulomb's Law, has the expression (of rel.1), $\mu = F_f / N$. We can express the friction coefficient for the plastic materials and in the following form:

$$\mu = \tau_f / p_c \tag{6}$$

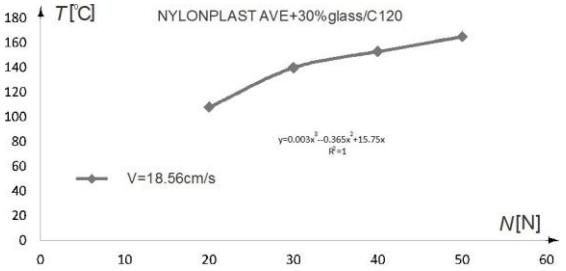
where τ_f represents the shear strength of the softer material, and p_c represents the flow pressure of the same material. Because $p_c = HB/3$, results:

$$\mu = 3\tau_f / HB \tag{7}$$

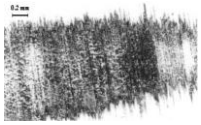
Equation (7) is in agreement with the experimental preliminary results.

Increasing the friction coefficient increases the wear rate, but no one managed to establish a mathematical relation between the two quantities, although this is widely recognized. In the following we shall give some suggestive graphical representations that make a qualitative correlation between the two quantities, and tying them to the contact temperature.

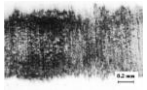
The influence of load on the friction coefficient of the Nylonplast AVE PA + 30% glass fibres/ C120 steel coupling is shown in Figure 2 for Timken type coupling (with linear contact), at the sliding speed of 18.56 cm/ s. It can be seen the increase of the friction coefficient of with the increase of normal load applied to the coupling. The variation of friction coefficient is nonlinear, in accordance with equation (5).



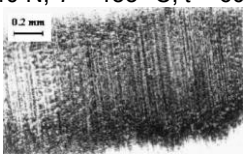
N = 20 N; *T* = 108 ^{0}C; *t* = 60 min



N = 30 N; *T* = 140 ^{0}C; *t* = 60 min



N = 40 N; *T* = 153 ^{0}C; *t* = 60 min.



N = 50 N; *T* = 165 ^{0}C; *t* = 60 min.

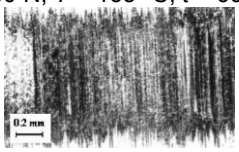
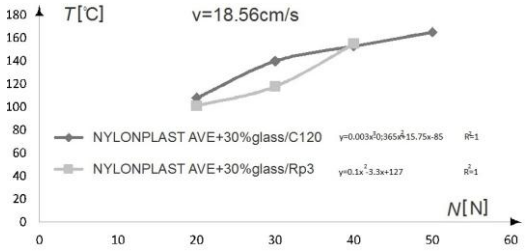


Figure 2. Variation of friction coefficient and contact temperature function of the normal load at the sliding speed of 18.56 cm/ s for Nylonplast AVE PA + 30% SGF/ C120 steel

At this sliding speed the dry friction coefficient on C120 steel has values between 0.27 and 0.37, the contact temperature ranging between 108 and 165ºC. In the case of friction on Rp3 steel, dry friction coefficient values (Figure 3) are between 0.25 and 0.38, the contact temperature ranging between 78 and 155ºC.



v = 18.56 cm/s; *N* = 10 N; *T* = 78 ^{0}C; *t* = 60 min.



N = 20 N;*T* = 101 ^{U}C; *t* = 60 min.



N = 30 N;*T* = 118 ^{U}C; *t* = 60 min.



N = 40 N;*T* = 155 ^{U}C;*t* = 60 min.



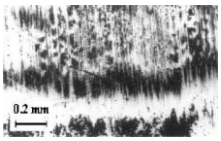
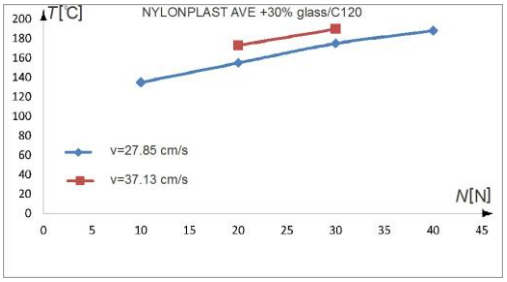




Figure 3. Variation of the friction coefficient and contact temperature function of the normal load at sliding speed of 18.56 cm/s for PA Nylonplast AVE + 30% SGF/ Rp 3 steel coupling

Figure 4 shows the variation of the friction coefficient and contact temperature function of the normal load for PA Nylonplast AVE + 30% glass fibres/ C120 steel coupling, at sliding speeds of 27.85 and 37.13 cm/s.



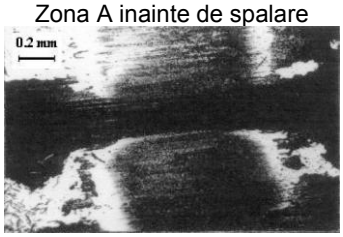
v = 27.85 cm/s

N = 10 N; T = 135 ^{0}C; t = 60 min.

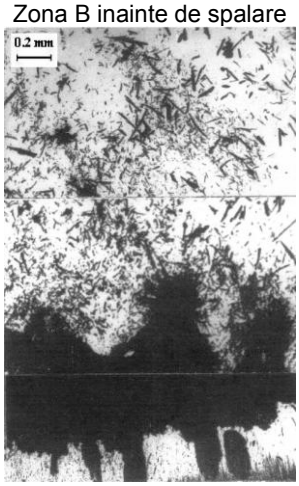
N = 20 N; T = 150 ^{0}C; t = 60 min.



Zona A inainte de spalare



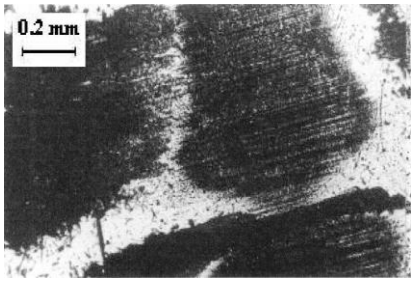
Zona B inainte de spalare





N = 30 N; T = 175 ^{0}C, 60 min.

N = 40 N; T = 188 ^{0}C, 60 min.



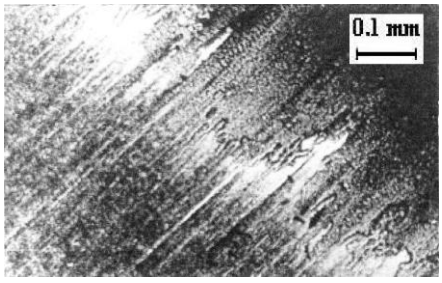


Figure 4. Variation of the friction coefficient and contact temperature function of the normal load for PA Nylonplast AVE + 30% SGF/ C120 steel coupling, at sliding speed of 27.85 cm/s.

At this sliding speed the dry friction coefficient has values between 0.32 and 0.35, the contact temperature ranging between 108 and 165ºC. In the case of friction on Rp3 steel, dry friction coefficient values (Figure 3) are between 0.27 and 0.38, the contact temperature ranging between 135 and 188ºC, function of the applied normal load.

Comparing the images of the three figures the mixed character, adhesive and abrasive of the metallic surface wear is easily seen (Figures 2 and 3) at low load (20 N), followed by strong transfer of plastic materials at loads of 30 – 40 N, with transfer bridging at 30 N and even plastic flow at 40 N, when the temperature of metallic surface reaches 188ºC (figure 4). At the beginning of the wear process, the glass fibres are got away from the polymer matrix, broken and expelled on the output of the wear defects.

The characteristic of wear of metallic surface is changing noticeable at the speed of 37.13 cm/s, becoming predominantly abrasive, the adherent material being removed and deposited on the output of the wear traces. It begins to appear the corrosion wear manifested by pinches localized in the centre of the wear traces. Figure 5 shows the wear traces after 60 min of testing at this speed. The friction coefficient varies between 0.33 and 0.37, and the contact temperature varies between 135ºC and 190ºC.

N = 10 N; *T* = 135 ^{0}C. *N* = 20 N; *T* = 173 ^{0}C. *N* = 30 N; *T* = 190 ^{0}C.

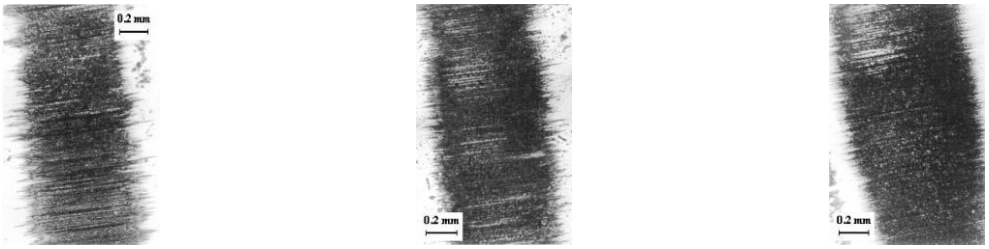


Figure 5. Changing of the preponderant character of the wear and contact temperature function of the normal load for PA Nylonplast AVE + 30% SGF / C120 coupling, at speeds of 37.13 cm/s.

Evolution of contact temperature and of C120 steel surface wear appearance at the speed of 55.70 cm/s, for the same friction torque, is shown in Figure 6, when the friction coefficient varies between 0.37 and 0.40 and contact temperature is between 150 and 267ºC. The wear character becomes visible adhesive when the applied load increases at the value of 40 N (contact temperature 238ºC).



N = 10 N; *T* = 150 ^{0}C; *t* = 60 min. *N* = 20 N; *T* = 191 ^{0}C; *t* = 60 min.

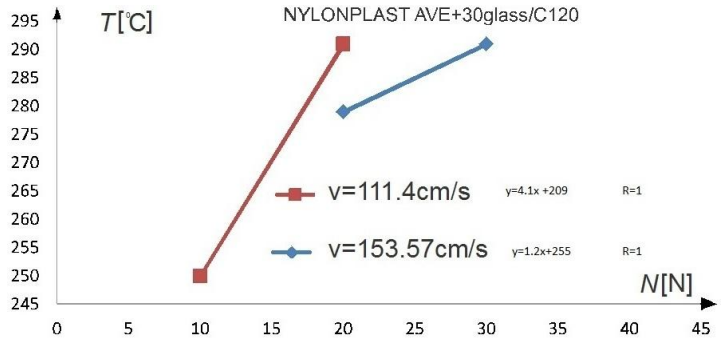


N = 30 N; *T* = 267 ^{0}C; *t* = 60 min. *N* = 40 N; *T* = 238 ^{0}C; *t* = 60 min.



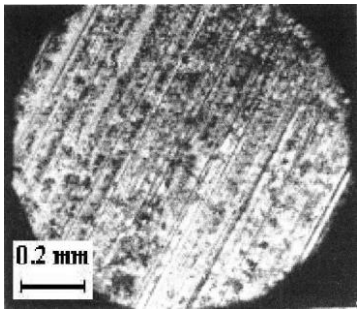
Figure 6. Evolution of contact temperature and of C120 steel surface wear appearance at the speed of 55.70 cm/s, for PA Nylonplast AVE + 30% SGF / C120

At the highest sliding speeds used for testing, 111.4 and 153.57 cm/s, in the case of C120 steel friction coefficients between 0.37 and 0.48 are reached, the measured contact temperatures ranging between 279 and 295ºC. This makes the wear to manifest mainly by adhesion and corrosion (Figure 7).

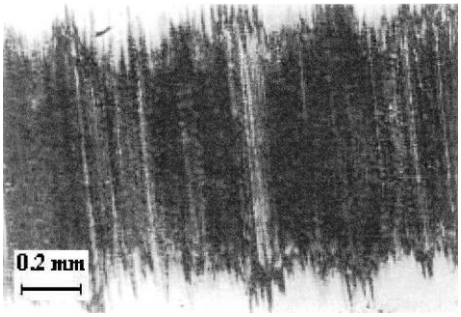


v = 111.4 cm/s

N = 20 N; T = 279 ^{0}C; t = 60 min.

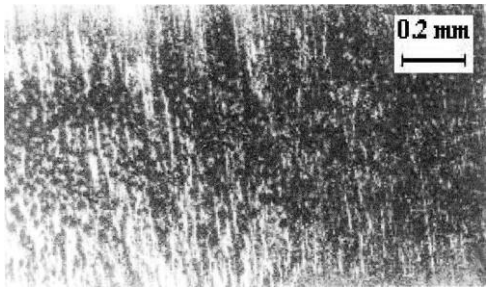


N = 40 N; T = 291 ^{0}C; t = 60 min.



v = 153.57 cm/s

N = 30 N; T = 267 ^{0}C; t = 60 min.



N = 40 N; T = 238 ^{0}C; t = 60 min.

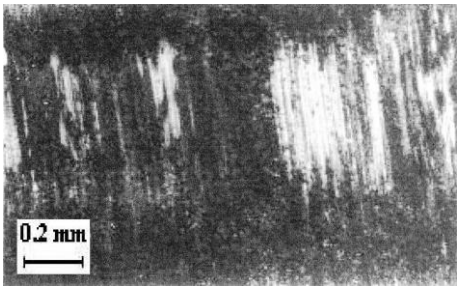
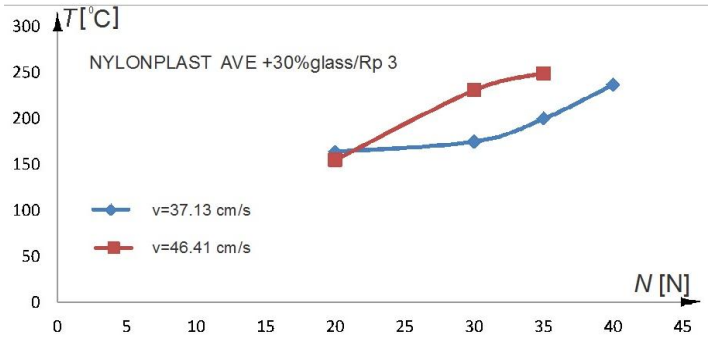


Figure 7. Evolution of contact temperature and of steel surface wear appearance at the speeds of 111.4 cm/s and 153.57 cm/s, for PA Nylonplast AVE + 30% SGF / C120

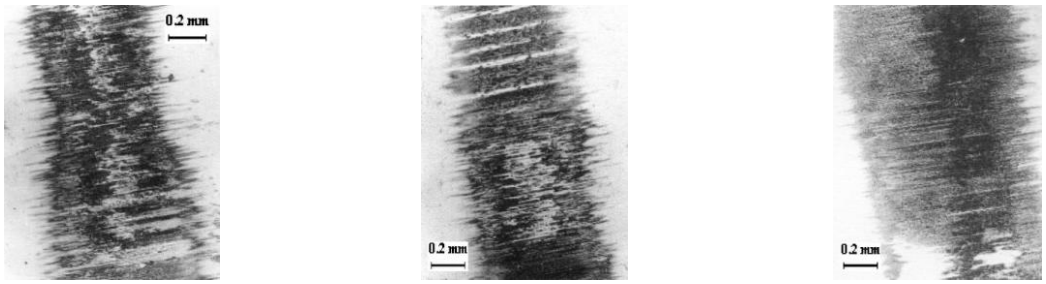
At higher loads (50 N), the tests are inconclusive because the surface of polymeric sample moves into vitrification (transition at the glassy state) due to very high temperature, covering it with a glass layer.

In the case of friction of polymer with 30% glass fibres on Rp3 steel surfaces that are harder (62 HRC) up against C120 steel surfaces, can make the same findings on wear evolution function of the normal load and sliding speed as in the case of C120 steel. Thus, under the same test conditions, the wear increases with increasing the normal load of the sliding speed, friction coefficients are somewhat lower, ranging in 0.27 - 0.42 domain, but the contact temperatures are between 164 and 249ºC, in used test conditions. For example, Figure 8 shows the contact temperature variation function of the normal load, at the speeds of 37.13 and 46.41 cm/s, for the friction of polyamide Nylonplast AVE + 30% SGF on Rp3 steel surfaces.



***v* = 37.13 cm/s**

N = 20 N; *T* = 164 ^{0}C; *t* = 60 min. *N* = 30 N; *T* = 175 ^{0}C; *t* = 60 min. *N* = 40 N; *T* = 237 ^{0}C; *t* = 60 min.



***v* = 46.41 cm/s**

N = 20 N; *T* = 155 ^{0}C; *t* = 60 min. *N* = 30 N; *T* = 231 ^{0}C; *t* = 60 min. *N* = 40 N; *T* = 249 ^{0}C; *t* = 60 min.

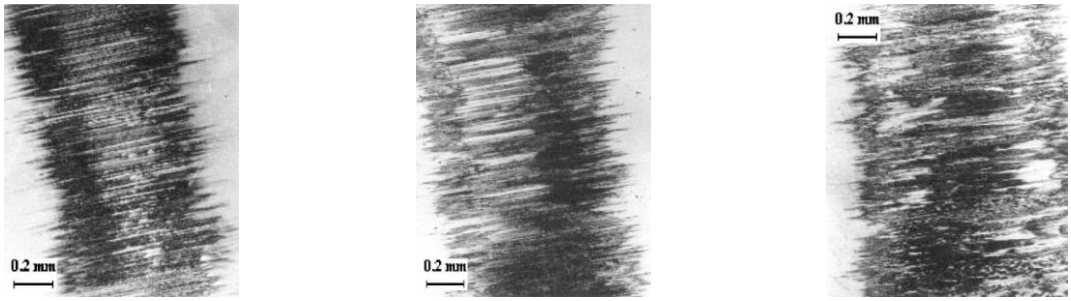
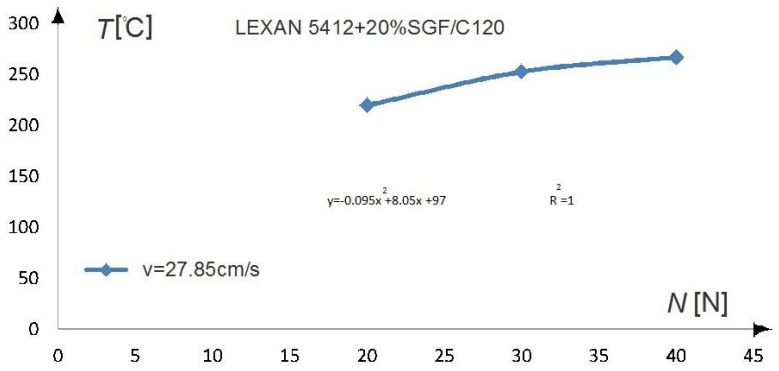
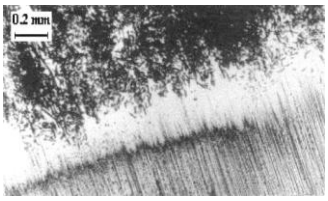


Figure 8. Evolution of contact temperature and of steel surface wear appearance at the speeds of 37.13 cm/s and 46.41 cm/s, for PA Nylonplast AVE + 30% SGF / Rp3

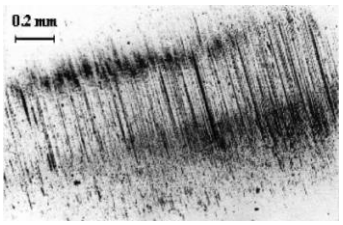
In the case of friction of polyamide Noryl + 20% SGF and polycarbonate Lexan 5412 + 20% SGF friction coefficient value varies between 0.35 and 0.50, and contact temperatures vary between 220 and 251ºC, function of the test conditions. On the input side of the wear stamp a massive transfer of polymer removed by abrasion and torn reinforcing fibres manifests, and on the output side of the wear trace a massive transfer of plasticized polymer from the composite material matrix occurs. For example, Figure 9 shows the diagram of contact temperature variation and images of the phenomena described above.



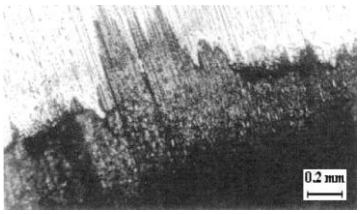
***v* = 27.85 cm/s, *t* = 60 min.**



Fibre de sticla smulse, depuse pe marginea de intrare a amprentei de uzura



Amprenta de uzura



Material plastic transferat pe marginea de iesire a amprentei

Figure 9. Evolution of contact temperature and of steel surface wear appearance at the speed of 27.85 cm/s, for PC Lexan 3412 + 20% SGF / C120

4. CONCLUSION

From the above, we can draw several conclusions:

- the wear process of metallic surfaces in dry friction contact against plastic materials reinforced with short glass fibres evolves over time, depending on loading, moving from the initial abrasive wear caused by glass fibres, at adhesion wear characterized especially by the transfer of plastic material on the metallic surface, but also by corrosion;
- the friction coefficient has values in a wide range comprised between 0.2 and 0.5;
- contact temperatures increase function of the applied load and the sliding speed, reaching values of 295ºC, resulting in plasticizing of plastic material and exceeding the transition temperature at the glass and even the flow one;
- the friction coefficient values of the reinforced plastic materials, on the surfaces of the C120 steel samples are higher than those obtained on the surfaces of Rp3 steel samples. The explanation for this phenomenon lies in the difference in hardness of samples surfaces made of the two steels. This behaviour confirms equations (6) and (7). Equation (7) is consistent with the results shown in Figures 2 and 8;
- friction coefficient values on C120 steels, of the thermoplastic materials reinforced with glass fibres, pass through a minimum located in the normal loads domain of 20-30 N. In the case of the same materials friction on the Rp3 steel surfaces, the increase of the friction coefficient with normal load is quasilinear. The explanation for this phenomenon is that, under the action of the tension states, the C120 steel undergoes superficial hardening manifested by the increase of its hardness in the friction area. Hardening occurs at contact pressures between 1.75 and 2.0 MPa, corresponding for the linear contact couplings used for a load of 20 N. At higher loads, respective greater efforts, the harden layer is destroyed and entails the increase of the friction coefficient as result of hardness decreasing;
- although it can not establish a mathematical relation between the friction coefficient, contact temperature and metallic surface wear, we believe that the manner of graphical presentation of the wear state of the metallic surafce and the contact temperature (friction coefficient) is significant for the plastic material/ steel contact.

However, this research has some limitations.

Thus, at high contact temperatures, is unlikely that the elastic contact assumption in which the modelling was made, to be valid.

Also, the contact temperatures were measured at 1 mm below the metallic contact surface, so obviously the real temperature was higher.

Evaluation of the friction coefficient was done over time as an average of the friction coefficient during the test and not as a friction coefficient at a certain time.

ACKNOWLEDGMENTS

The authors would like to thank their colleagues from the Institute of Solid Mechanics and University of Civil Engineering for your logistic support.

REFERENCES

1. BOWDEN F.P., TABOR D. - Friction and Lubrication, Metheuen & Co. Ltd. London, 1967.
2. JACOBI H.R. - Neue Erkenntnisse uber Gleitenschaften von Polyamiden, Kunststoffe, 47, 5, 1957, pp. 234-239.
3. BILIK M. - Parî trenia metal-plastmassa v maşinah i mechanizmah, Izd. Maşinostroienie, Moskva, 1965.
4. CLERICO M. A - Study of the Friction Wear of Nylon against Metal, Wear, 13,3, 1969, pp. 183-197.
5. HRUŞCIOV M.M. - Resistance of Metals to Wear by Abrasion, as related to Hardness, Proc. Conf. Lubr. And Wear, Inst. Mech. Eng., London 1957.
6. HRUŞCIOV M.M, BABICEV M.A. - Resistance to Abrasive Wear of structurally Inhomogeneous Materials. Friction and wear in Machinery, part 2, ASME, New York, 1958, pp.5-23.
7. BELY V.A., SVIRIDENOK A.I. et.al. - Friction and Wear in Polymer based Materials, Pergamon Press, 1982.
8. BARTENEV G.M., LAVRENTIEV V.V.- Trenie i Iznos polimerov, Izd. Himia, Leningrad, 1972.
9. WATANABE M., KORUSAWA M., MATSUBARA K.- The Frictional Properties of Nylon, Wear 32,3, 1968, pp. 185-191.
10. LANCASTER J.K.-Lubrication of Carbon Fibre reinforced Polymers, Wear, 28, 3, 1972, pp. 315-352.
11. BARLOW D.A. - Some Observations of the Friction Properties of Vinyl, Wear, 20, 2, (1972), pp.151-157.
12. WEST G.H., SENIOR J.M. - Frictional Properties of Polyethylene, Wear, 19, 1, 1973, pp.37-52.
13. BARTENEV G.M., LAVRENTIEV V.V., KONSTANTINOVA N.A .- The actual Area and friction Properties of Elastomers under Frictional Contact with Solid Surfaces, Wear 18, 6, 1971, pp.439-448.
14. BOWDEN F.P., TABOR D. - The Friction and Lubrication of Solids, part I-II, Clarendon Press, Oxford, 1964.
15. JOST H. - Zum Verschleissverhalten von Polyamid, Plaste und Kautschuk, 17, 4, 1970, pp.266-270.
16. LANCASTER J.K., EVANS D.C.-Wear of Polymers in Treatise on Mat. Sci. And Technology, Academic Press, 1979, 13, 86.
17. SHEN C., DUMBLETON J.H. - The Friction and Wear Behavior of Polyoximethylene in Convection with Joint Rplacement, Wera, 38, 2, 1978, pp. 291-303.
18. CAPITANU L., IAROVICI A., ONISORU J. - On polyamide and polycarbonate materials behaviour under dry friction, The Annals of University “Dunarea de jos” Galati, fascicle VIII, Tribology, 2003, ISSN 1221-4590.
19. CAPITANU L., FLORESCU V. - Tribological aspects of wear of polished steel surfaces in dry friction contact on polymer composites with glass fibres. American Jounal of Materials Science 2013, 3(1): 8 -18. DOI 10.5923/j.materials.20130301.02.
20. Nylonplast AVE Polyamide, Informazione Technica, Rhodiatace Sp.A, Milano, Aug. 1984.
21. Le Noryl, un material technique pour l’industrie automobile, Plastique Modernes et Elastomers, 27, 3, 1975.
22. Lexan, Polycarbonate Resin, General Electric, Product Data, February. 1969.
23. Makrolon. - Description des types, Bayer A.G., 1985.
24. Technyl, Rhone Paulenc, 5, 1983.

CORRESPONDENCE

Lucian CAPITANU
Institute of Solid Mechanics of Romanian Academy, Bucharest, Romania
15 C-tin Mille str., 1 district, Bucharest, 10141, Romania
e-mail: lucian.capitanu@yahoo.com

Tribological Journal BULTRIB Vol. 4, 2013
Papers from the Conference **BULTRIB '13,** October 24-26, 2013
Technical University of Sofia
Compiled by: Dr. Mara Kandeva, The Society of Bulgarian Tribologists

EFFECT OF THE THICKNESS OF THE FRICTIONAL LINING ON THE THERMOELASTIC BEHAVIOUR IN THE DRY CLUTCHES

Oday I. Abdullah, Josef Schlattmann, Mumtaz Jamil Akhtar

Abstract: *when the clutch starts to engage, frictional heat will be generated due to the difference in the velocities between the driving and driven shafts. A finite element method has been used to investigate the effect of thickness of frictional facing on thermoelastic behavior of the clutch disc. The coupled thermal and elastic analysis has been carried out for the single-disc clutch system (flywheel, clutch disc and pressure plate). The results present the contact pressure distribution, heat flux and temperature field distribution. Analysis has been completed using two-dimensional axisymmetric model. Thickness of the frictional facing of a clutch disc is a significant parameter that affects the thermoelastic behavior of the clutch system. The results show that the values of the temperature and contact pressure will increase dramatically when the thickness of the frictional facining decreases.*

Key Words: *Transient thermal analysis, frictional heat, dry clutch, FEM, thermoelastic behavior.*

1. INTRODUCTION

Experience shows that the most premature clutch failures can be attributed to an excessive surface temperature generated during the slipping period. To prevent the clutch failure before an expected life cycle, it is necessary to know the maximum surface temperature and contact pressure and how these parameters vary with the known conditions of loading, physical properties, dimensions of the clutch disc and degree of air cooling.

Belhocine and Bouchetara [1] studied the thermal behavior of the ventilated brake discs of vehicles using ANSYS software. The modeling of temperature distribution in the disc brake is used to identify all the factors and important parameters that involve during the braking operation such as the type of braking, geometric design and material of the disc. The numerical simulation for coupled transient thermal field and stress field is carried out by sequentially thermal-structural coupled method based on ANSYS to evaluate the stress fields and deformations which are established in the disc with the pressure on the pads.

Shahzamanian et al. [2] investigated the thermoelastic contact problem of functionally graded (FG) rotating brake disk with heat source due to contact friction using finite element method. In this work the material properties of disk are assumed to be represented by power-law distributions in the radial direction. The inner and outer surfaces considered are metal and ceramic, respectively. Pure material is considered for the brake pad. Coulomb contact friction is assumed as the heat source. The results show that the maximum value of radial displacement in mounted FG brake disk is not at outer surface. It is found that all the area between pad and brake disk is in full contact status when the ratio of pad thickness to brake disk thickness is 0.66.

Abdullah and Schlattmann [3, 4, 5, 6, 7, 8 & 9] investigated the temperature field and energy dissipated from dry friction clutch during a single and repeated engagement assuming uniform pressure and uniform wear conditions. They also studied the effect of pressure between contact surfaces on the temperature field and the internal energy of clutch disc varying with time using two approaches; heat partition ratio approach to compute the heat generated for each part individually whereas the second applies the total heat generated for the whole model using a contact model. Furthermore, they studied the effect of engagement time and sliding velocity function, thermal load and dimensionless disc radius (inner disc radius/outer disc radius) on the thermal behavior of the friction clutch in the beginning of engagement.

This work presents a modeling analysis of transient thermoelastic behavior of single-disc clutch system. A finite element method is used to investigate the transient thermoelastic analysis. The present work is based on the fully coupled thermal and elastic fields. This paper shows the effect of thickness of frictional facings on the temperature field and contact pressure distribution in a clutch system. The wear effects are neglected in this analysis as sliding occurs for very short time.

2. FINITE ELMENT ANALYSIS

The finite element simulation of the clutch system involves the construction of two different models. One is used to solve the elastic problem to yield the displacement field and the contact pressure distribution whereas the other model is used to solve the transient thermal problem to account for the change in temperature field. The two models are however coupled to each other since the contact pressure from the first model is needed to define the frictional heat flux for the second model. Furthermore, temperature field from the thermal model is required for the computation of contact pressure from elastic model for the next load step.

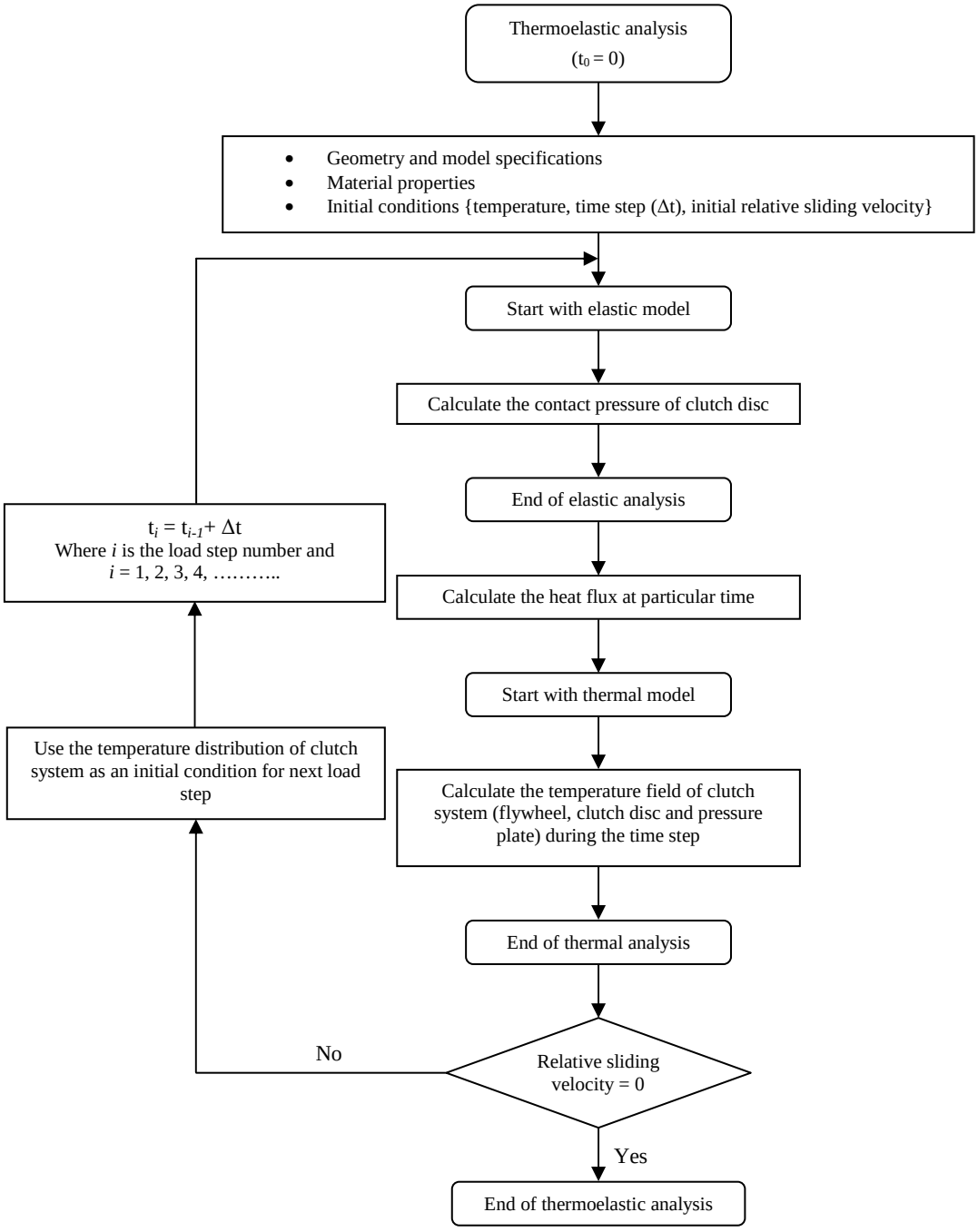


Fig. 1. Schematic diagram of FE simulation

To account for the coupling and variation of sliding speed with the time, clutch engagement time is divided into small time steps. At each time step, the instantaneous nodal temperatures are used in elastic contact model to determine the contact pressure distribution. The pressure distribution is assumed to remain constant during the subsequent time. Fig. 1 shows the schematic diagram for the finite element simulation of a coupled-field problem of clutches.

The first step in this analysis is the modeling. Due to the symmetry in the geometry (frictional lining without grooves) and boundary conditions of the friction clutch (taking into consideration the effect of pressure and thermal load due to the slipping), two-dimensional axisymmetric FEM can be used to represent the contact between the clutch elements during the slipping period as shown in figure 2. The axisymmetric finite element models (elastic and thermal) of friction clutch system with boundary conditions are shown in figures 3 & 4. In Figure 4, h is the flow of heat to the environment due to convection and $Q_{gen.f}$, $Q_{gen.c}$ and $Q_{gen.p}$ are the amounts of heat flux that enter to the flywheel, clutch disc and pressure plate respectively. Four values of thickness for the frictional facing were selected to achieve this analysis (1, 2, 3 and 4 mm). In all computations for the friction clutch model, material has been assumed a homogeneous and isotropic material and all parameters and material properties are listed in Table 1. Analysis is conducted by assuming there are no cracks in the contact surfaces.

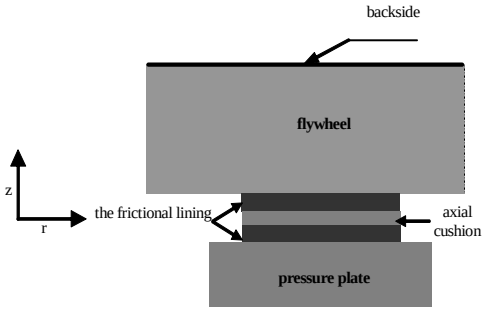


Fig. 2. The Contact model for clutch system

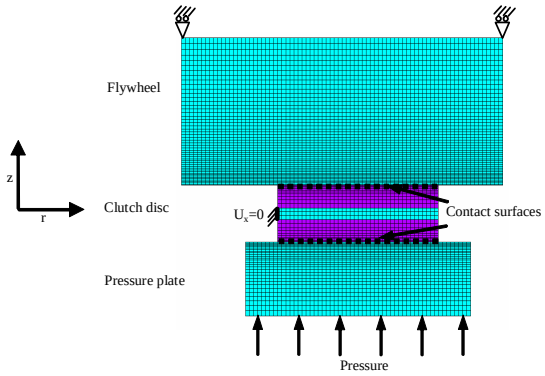


Fig. 3. FE model with boundary conditions (elastic model)

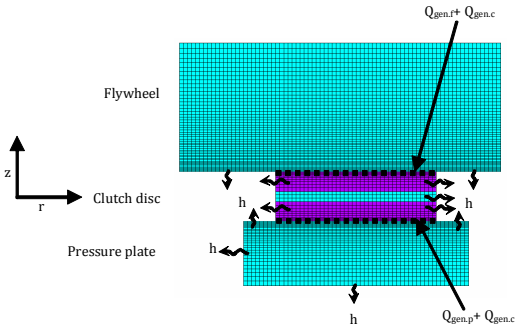


Fig. 4. FE models with the boundary conditions. (Thermal model)

3. RESULTS AND DISCUSSIONS

The contact pressure distribution, temperature field and heat flux of the single-disc clutch system have been determined at a single engagement. In this work, effect of thickness of frictional facing on the thermoelastic behavior has been investigated.

Figures 5-12 show the contact pressure distribution for both sides of the clutch disc (flywheel and pressure plate sides) for different values of thickness of frictional facing (t) at selected time intervals. The behavior of contact pressure for both sides of the clutch disc is almost similar. The values of contact pressure increase when the thickness of frictional lining decreases. The maximum values of contact pressure occur at thickness equal to 1 mm for both sides of the clutch disc. During the slipping period the values of contact pressure increase with time and the maximum values occur

near the inner radius of the clutch disc. The maximum values of contact pressure when t = 1mm are found to be 3.55 MPa and 3.53 MPa corresponding to the flywheel and pressure plate sides respectively.

Figures 13-20 demonstrate the heat flux distribution with disc radius for both sides of the clutch disc (flywheel and pressure plate sides) for different values of t at selected time steps. For both sides of the clutch disc, the trend of heat flux is approximately similar. It can be seen that when the thickness of frictional facing decreases, the values of the heat flux will considerably increase. The maximum values of the heat flux at t = 1mm are found to be 7.99 MW/m^2 and 8.00 MW/m^2 for flywheel and pressure plate sides respectively.

Figures 21-24 illustrate the temperature field along the radius of the clutch disc for different values of thickness t at selected time intervals. The maximum value of temperature occurs when the thickness of frictional facing is 1mm. It can be noted, that the peak values of temperature occur near the mean radius of the clutch disc for both sides of the clutch. The maximum values of temperature at t = 1mm during the slipping period are found to be 494.8 K and 494.6 K corresponding to the flywheel and pressure plate sides respectively.

Figure 25 shows the history of maximum temperature for different thicknesses of frictional facing. The maximum value of temperature is found to be 494.88 K with t = 1mm.

The temperature distributions of clutch system (flywheel, clutch disc and pressure plate) for different thicknesses of frictional facings at time 0.24s during a single engagement is shown in figures 26-29.

Table 1. The properties of materials and operations

Parameters	Values
Inner radius of friction material & axial cushion, r_i [m]	0.06298
Outer radius of friction material & axial cushion, r_o [m]	0.08721
Thickness of the axial cushion [m], $t_{axi.}$	0.0015
Inner radius of pressure plate [m], r_{ip}	0.05814
Outer radius of pressure plate [m], r_{op}	0.09205
Thickness of the pressure plate [m], t_p	0.00969
Inner radius of flywheel [m], r_{if}	0.04845
Outer radius of flywheel [m], r_{of}	0.0969
Thickness of the flywheel [m], t_f	0.01938
pressure, p [MPa]	1
Coefficient of friction, μ	0.20
Number of friction surfaces, n	2
Young's modulus for friction material, E_l [GPa]	0.30
Young's modulus for pressure plate, flywheel & axial cushion, (E_p, E_f, and E_{axi}), [Gpa]	125
Poisson's ratio for friction material,	0.25
Poisson's ratio for pressure plate, flywheel & axial cushion	0.25
Density for friction material, (kg/m^3), ρ_l	2000
Density for pressure plate, flywheel & axial cushion, (kg/m^3), (ρ_p, ρ_f, and ρ_{axi})	7800
Specific heat for friction material, [J/kg K]	120
Specific heat for pressure plate, flywheel & axial cushion, [J/kg K]	532
Conductivity for friction material, [W/mK]	1
Conductivity for pressure plate, flywheel & axial cushion [W/mK]	54
Thermal expansion for friction material and steel [K^{-1}]	$12e^{-6}$
Slipping time, t_s [s]	0.40

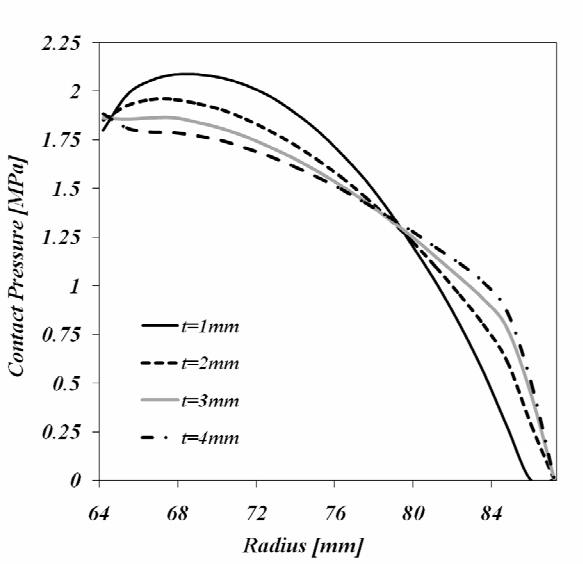


Fig. 5. Contact pressure distribution at flywheel side with varying thickness of friction surfaces at time =0.12s

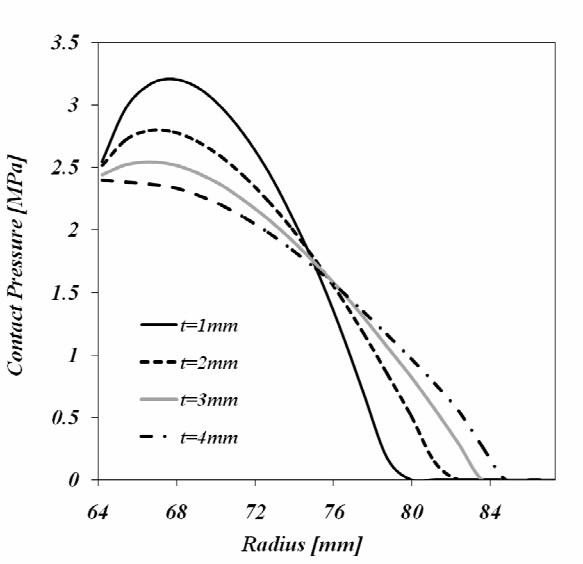


Fig. 6. Contact pressure distribution at flywheel side with varying thickness of friction surfaces at time =0.24s

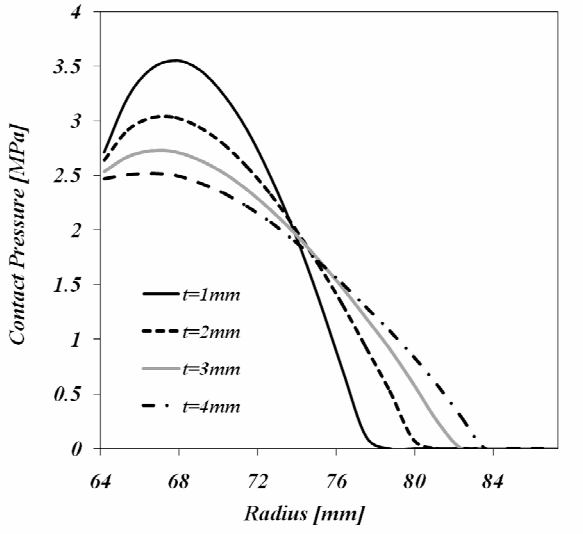


Fig. 7. Contact pressure distribution at flywheel side with varying thickness of friction surfaces at time =0.36s

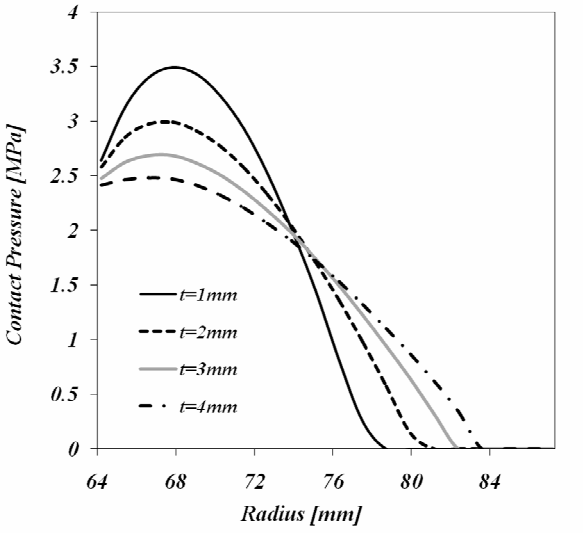


Fig. 8. Contact pressure distribution at flywheel side with varying thickness of friction surfaces at time =0.40s

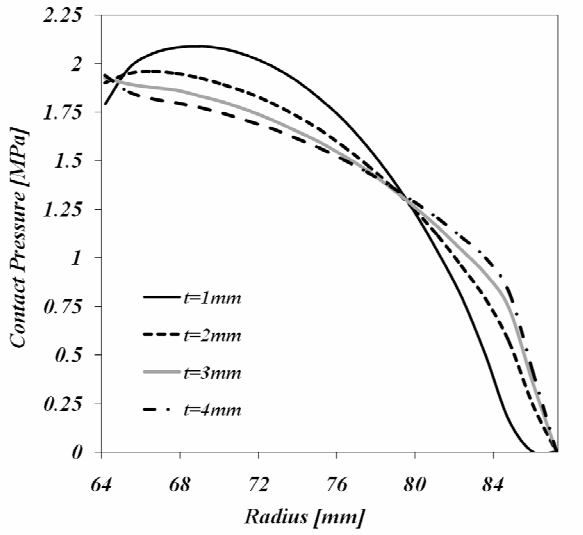


Fig. 9. Contact pressure distribution at pressure plate side with varying thickness of friction surfaces at time =0.12s

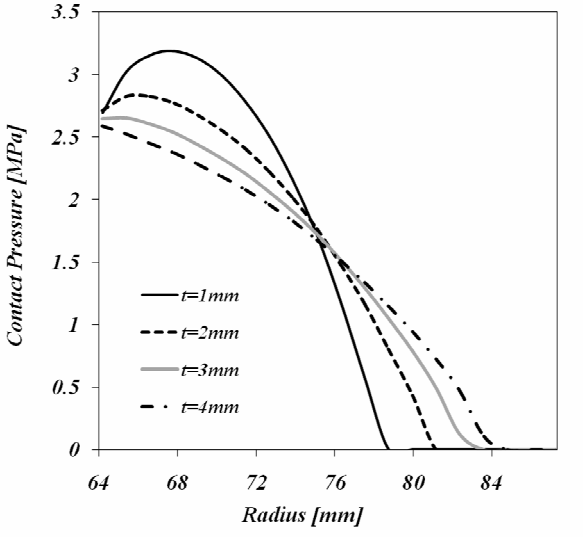


Fig. 10. Contact pressure distribution at pressure plate side with varying thickness of friction surfaces at time =0.24s

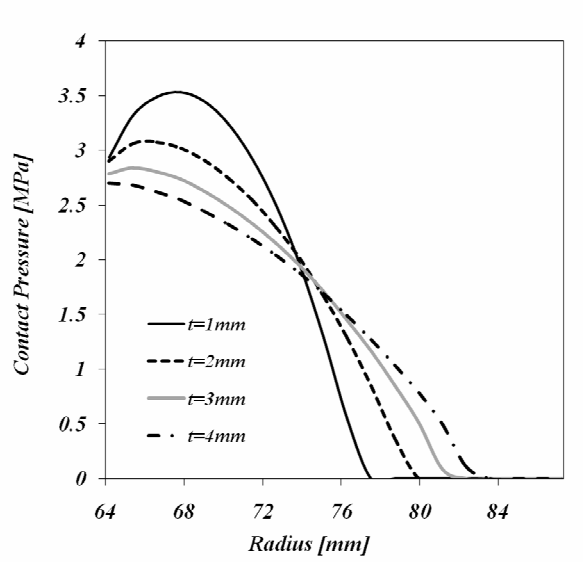


Fig. 11. Contact pressure distribution at pressure plate side with varying thickness of friction surfaces at time =0.36s

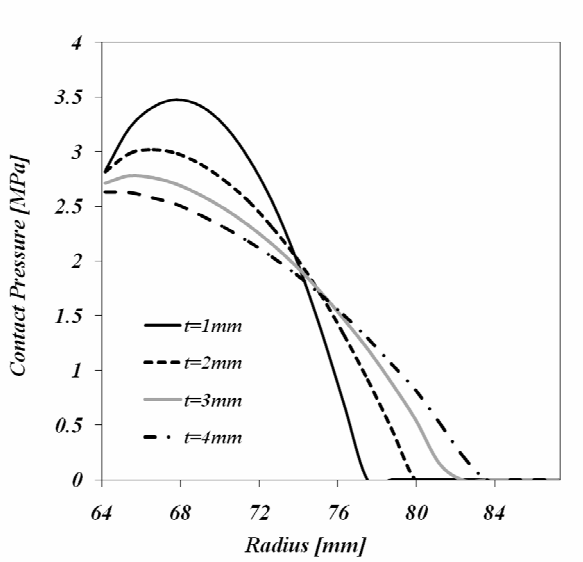


Fig. 12. Contact pressure distribution at pressure plate side with varying thickness of friction surfaces at time =0.40s

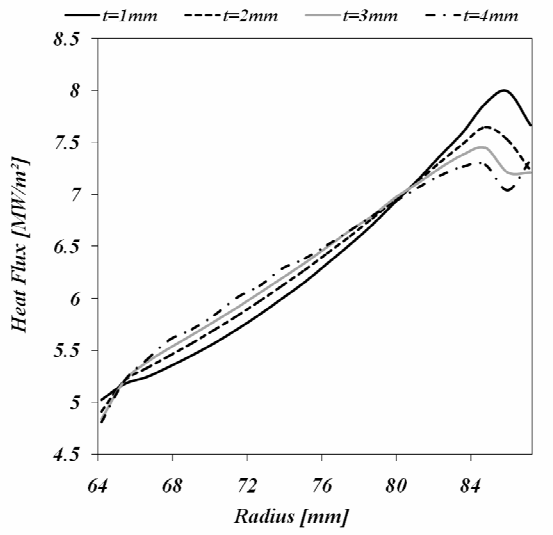


Fig. 13. Heat flux distribution at flywheel side with varying thickness of friction surfaces at time =0.04s

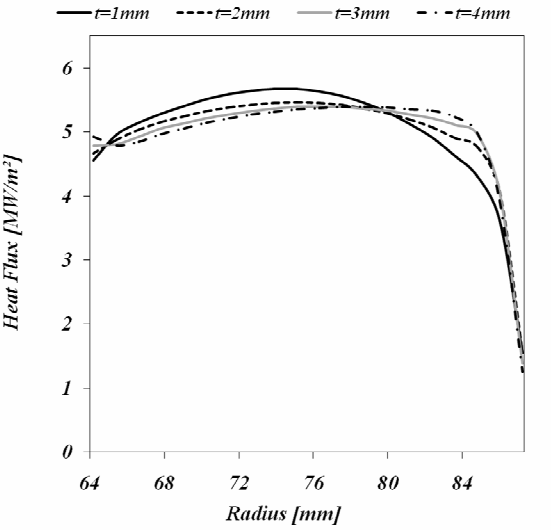


Fig. 14. Heat flux distribution at flywheel side with varying thickness of friction surfaces at time =0.12s

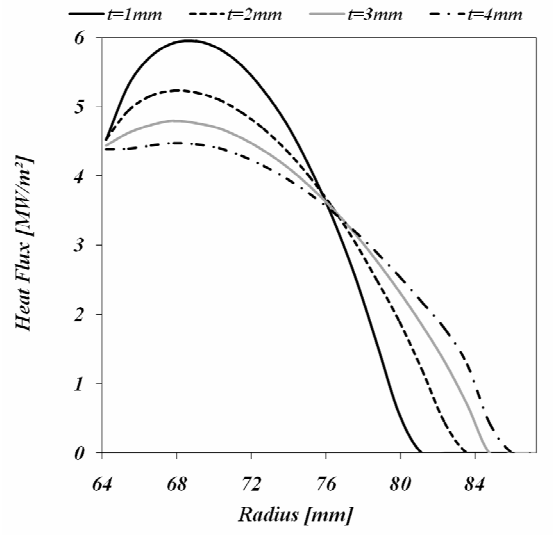


Fig. 15. Heat flux distribution at flywheel side with varying thickness of friction surfaces at time =0.24s

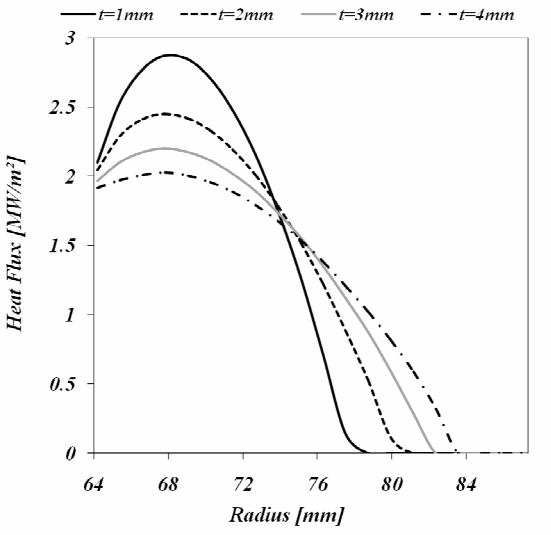


Fig. 16. Heat flux distribution at flywheel side with varying thickness of friction surfaces at time =0.36s

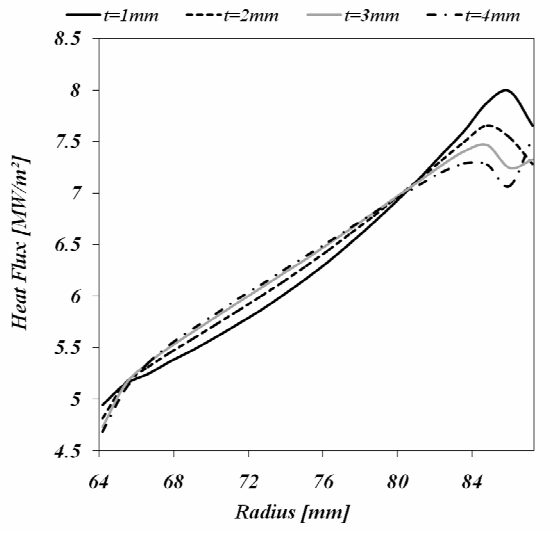


Fig. 17. Heat flux distribution at pressure plate side with varying thickness of friction surfaces at time =0.04s

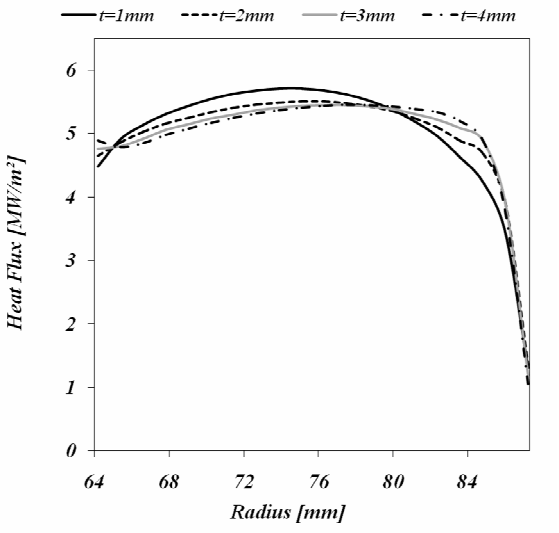


Fig. 18. Heat flux distribution at pressure plate side with varying thickness of friction surfaces at time =0.12s

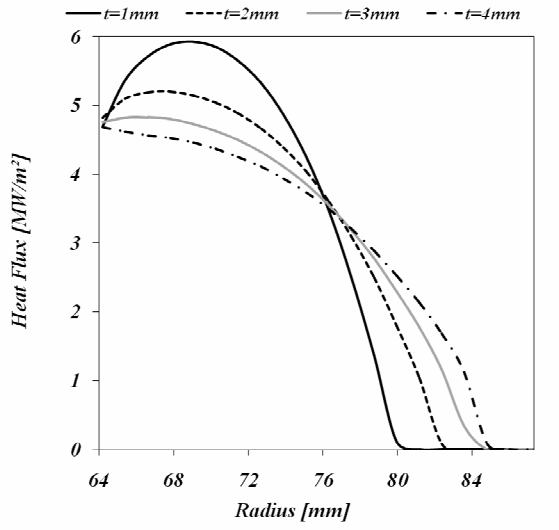


Fig. 19. Heat flux distribution at pressure plate side with varying thickness of friction surfaces at time =0.24s

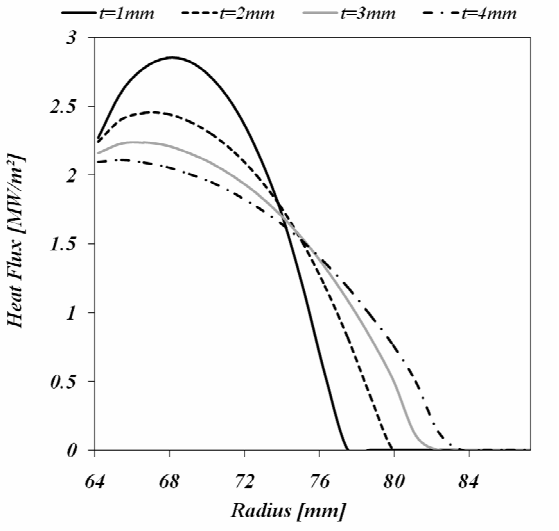


Fig. 20. Heat flux distribution at pressure plate side with varying thickness of friction surfaces at time =0.36s

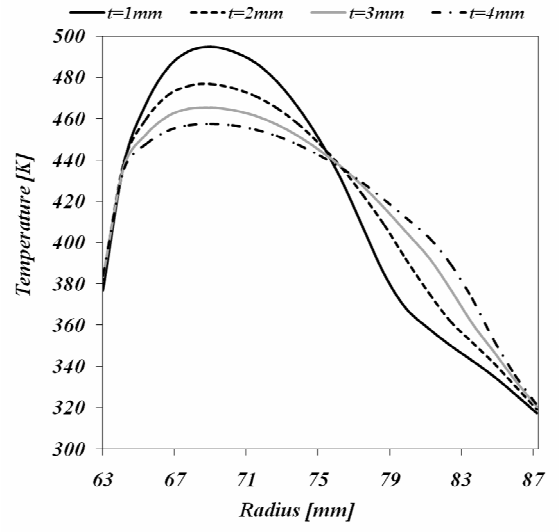


Fig. 21. Temperature distribution along the radius at flywheel side at time =0.24s

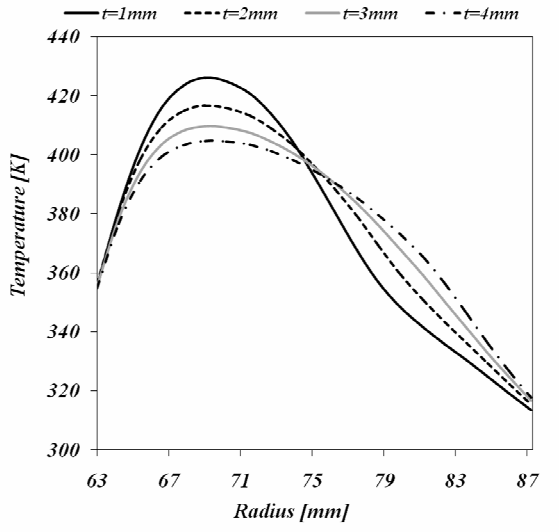


Fig. 22. Temperature distribution along the radius at flywheel side at time=0.40s

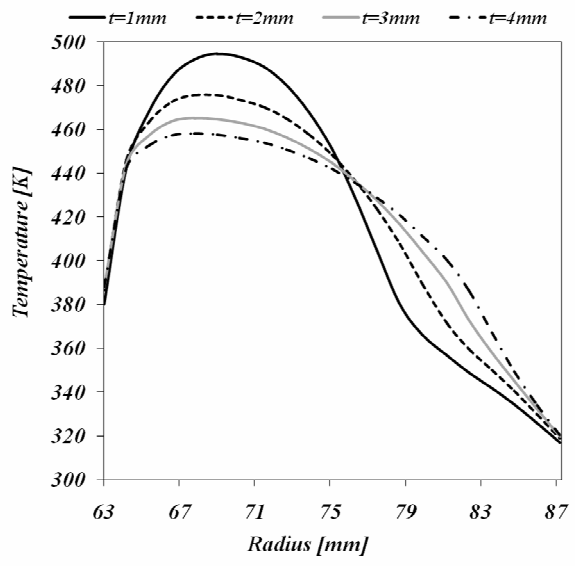


Fig. 23. Temperature distribution along the radius at pressure plate side at time=0.24s

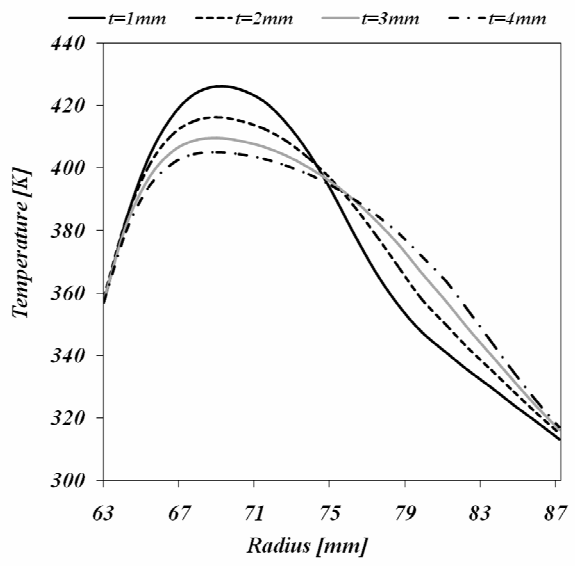


Fig. 24. Temperature distribution along the radius at pressure plate side at time =0.40s

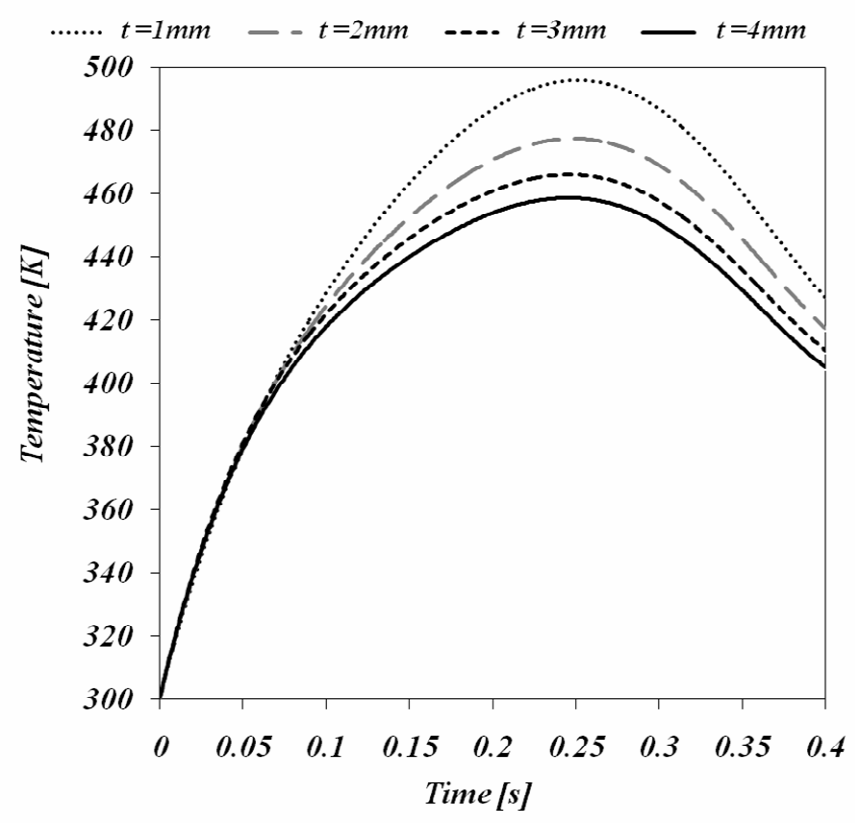


Fig. 25. Maximum temperature history curves with varying thickness of friction surfaces

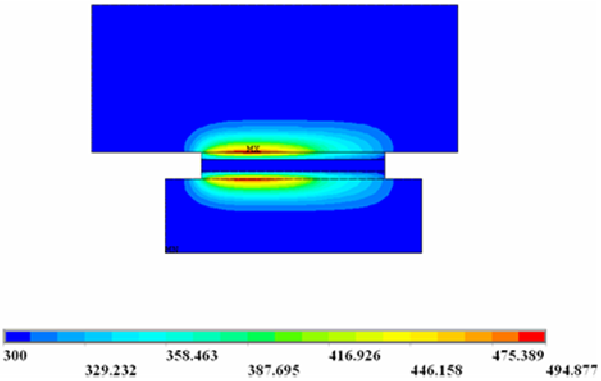


Fig. 26 . Temperature field distribution with t = 1mm at time = 0.24s (T_{max}= 494.8K)

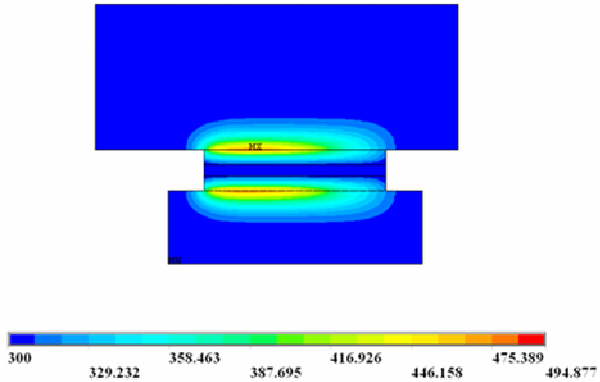


Fig. 27 . Temperature field distribution with t = 2mm at time = 0.24s (T_{max}= 476.8K)

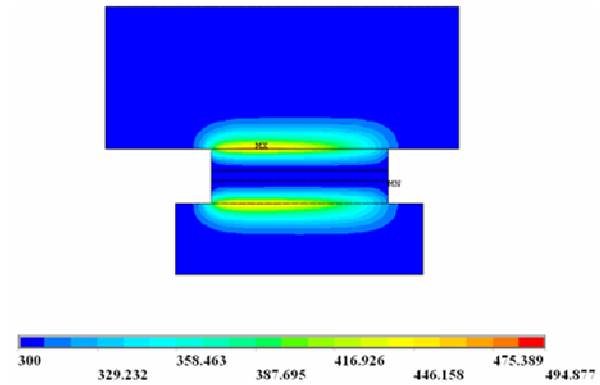


Figure 28. Temperature field distribution with t = 3mm at time =0.24s (T_{max}= 465.4K)

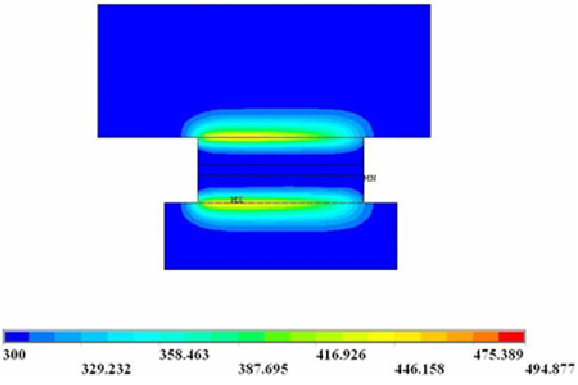


Figure 29. Temperature field distribution with t = 4mm at time =0.24s (T_{max}= 458.1K)

4. CONCLUSIONS

In this work, transient thermoelastic analysis of a single-disc clutch system (flywheel, clutch disc and pressure plate) during a single engagement has been performed. Two dimensional axisymmetric models (elastic+thermal) were used to simulate the single-disc clutch system. This work highlights the effect of thickness of frictional facing on pressure distribution and temperature field of a clutch system during the slipping period. It can be seen from results that the thickness of frictional facing is an essential parameter in the design of clutches. To obtain a successful design of a clutch it is very important to find the optimal dimension for the thickness of frictional facing. When the thickness of frictional facing was decreased from 4mm to 1mm, an increase of 41.1% and 8% was found in maximum contact pressure and maximum temperature respectively. The values of contact pressure and temperature increase dramatically when the thickness of the frictional facing decreases. If a clutch disc with thickness of frictional facing less than the optimal thickness would be used, failure of the clutch before a normal expected life is very certain.

REFERENCES

1. BELHOCINE, ALI, AND MOSTEFA BOUCHETARA. "THERMOMECHANICAL MODELLING OF DRY CONTACTS IN AUTOMOTIVE DISC BRAKE." INTERNATIONAL JOURNAL OF THERMAL SCIENCES60 (2012): 161-170.
2. SHAHZAMANIAN, M. M., ET AL. "FINITE ELEMENT ANALYSIS OF THERMOELASTIC CONTACT PROBLEM IN FUNCTIONALLY GRADED AXISYMMETRIC BRAKE DISKS." COMPOSITE STRUCTURES 92.7 (2010): 1591-1602.
3. ODAY I. ABDULLAH AND JOSEF SCHLATTMANN, "THE EFFECT OF DISC RADIUS ON HEAT FLUX AND TEMPERATURE DISTRIBUTION IN FRICTION CLUTCHES," JOURNAL OF ADVANCED MATERIALS RESEARCH, VOL. 505, PP. 154-164, 2012.
4. ODAY I. ABDULLAH AND JOSEF SCHLATTMANN, "FINITE ELEMENT ANALYSIS OF DRY FRICTION CLUTCH WITH RADIAL AND CIRCUMFERENTIAL GROOVES," IN PROCEEDING OF WORLD ACADEMY OF SCIENCE, ENGINEERING AND TECHNOLOGY CONFERENCE, PARIS, 2012, PP. 1279-1291.
5. ODAY I. ABDULLAH AND JOSEF SCHLATTMANN, "EFFECT OF BAND CONTACT ON THE TEMPERATURE DISTRIBUTION FOR DRY FRICTION CLUTCH," IN PROCEEDING OF WORLD ACADEMY OF SCIENCE, ENGINEERING AND TECHNOLOGY CONFERENCE, BERLIN, 2012, PP. 167-177.
6. ODAY I. ABDULLAH AND JOSEF SCHLATTMANN, "THE CORRECTION FACTOR FOR RATE OF ENERGY GENERATED IN THE FRICTION CLUTCHES UNDER UNIFORM PRESSURE CONDITION," JOURNAL OF ADVANCES IN THEORETICAL AND APPLIED MECHANICS, VOL. 5, NO. 6, PP. 277 – 290, 2012.
7. ODAY I. ABDULLAH AND JOSEF SCHLATTMANN, "FINITE ELEMENT ANALYSIS OF TEMPERATURE FIELD IN AUTOMOTIVE DRY FRICTION CLUTCH," JOURNAL OF TRIBOLOGY IN INDUSTRY, VOL. 34, NO. 4, PP. 206-216, 2012.
8. ODAY I. ABDULLAH, JOSEF SCHLATTMANN AND ABDULLAH M. AL-SHABIBI, "TRANSIENT THERMOELASTIC ANALYSIS OF MULTI-DISC CLUTCHES," IN PROCEEDINGS OF 9TH ARNOLD TROSS COLLOQUIUM, HAMBURG, JUNE 2013.
9. ODAY I. ABDULLAH AND JOSEF SCHLATTMANN, "STRESSES AND DEFORMATIONS ANALYSIS OF A DRY FRICTION CLUTCH SYSTEM" JOURNAL OF TRIBOLOGY IN INDUSTRY, VOL. 35, NO. 2, PP. 155-162, 2013.

CORRESPONDENCE

Abdullah Oday
Hamburg University of Technology
Address
Technical University Hamburg-Harburg, Institute G-2/Amp
Denickestrasse 17 (Building L), Room 2047
21073 Hamburg
e-mail: oday.abdullah@tu-harburg.de

Tribological Journal BULTRIB, **Vol. IV, 2014**
Papers from the International Conference **BULTRIB '13**
October 24-26, 2013, Sofia
Society of Bulgarian Tribologists
Technical University of Sofia

INCREASE THE WEAR RESISTANCE OF INJECTION MOLDS USING PVD COATINGS

Geogy MISHEV Stefan DISHLIEV Velko RUPETSOV

Abstract: *Injection molds to produce plastic products are subject to heavy abrasion wear. Increase their wear resistance significantly reduces the production cost. In the current work are presented results of the researches to increase the wear resistance of injection molds made of steel 1.2343. PVD nanocomposite coating ncAlTiN/αSi_3N_4 was examined. Study the wear rate is done using the volumetric method, which was made corresponding computer program. The survey results are embedded in "Arexim-Ingeneering" - Smolyan / BG.*

Key Words: *Injection molds; Nanocomposite coatings; PVD; Wear rate*

ПОВИШАВАНЕ НА ИЗНОСОУСТОЙЧИВОСТТА НА ШПРИЦФОРМИ С ПОМОЩТА НА PVD - ПОКРИТИЯ

Георги МИШЕВ Стефан ДИШЛИЕВ Велко РУПЕЦОВ

Резюме*: Шприцформите за производство на пласмасови изделия са подложени на интензивно абразивно износване. Повишаването на тяхната износоустойчивост води до значително намаляване на себестойността на произвежданата продукция. В настоящата работа са представени резултати от изследванията за повишаване на износоустойчивостта на шприцформи, изработени от стомана 1.2343. Изследвано е нанокомпозитното покритие ncAlTiN/αSi_3N_4 отложено по PVD метода,. Изследването на износването се извърши с помощта на обемния метод, за който бе направена съответна компютърна програма. Резултатите от изследването са внедрени в „Arexim-Ingeneering" – Смолян/БГ.*

Ключови думи*: Шприцформи; Нанокомпозитноти покрития; PVD-метод; Интензивност на износване*

1. ВЪВЕДЕНИЕ

Износоустойчивостта на инструментите в машиностроителното производство е основен фактор за производителността и себестойността на произвежданата продукция. Износването на инструментите води до загуба на точността на производствените изделия. [2, 4].

Повишаването на износоустойчивостта на инструментите е един от основните проблеми в практиката за увеличаване на живота им, следователно и голям източник за икономия. Този проблем има голямо значение при разработване на инструменти, където се наблюдава постоянна тенденция за увеличаване на скоростта, температурата, механичните напрежения при работа на инструмента, като същевременно се запазва неговата функционалност и дълготрайност.

За повишаване на износоустойчивостта на инструментите основно се използват методите за нанасяне на твърди покрития. Като универсално покритие широко приложение намира титановия нитрид (TiN) в областта на режещите инструменти, формообразуващите инструменти, инструментите за пластична обработка за повишаване на тяхната товароносимост, износоустойчивост и трайност [1, 5]. В настоящия момент акцентът пада върху използването на свръхтвърди градиентни нанокомпозитни покрития от типа nc-$(Al_{1-x}Ti_x)N$/α-Si_3N_4, които имат набор от свойства, гарантиращи подходящото им използване за подобряване качеството на обработващи инструменти [6]. Тези покрития са особено подходящи за

инструменти, работещи при тежки натоварвания и достигане на висока температура. Отлагането им върху разнородни инструментални и други видове материали води не само до модификация на материала на повърхностния слой, но и до образуването на принципно нов вид композиционен материал. При правилно избран технологичен процес на получаване, тези покрития имат редица предимства.

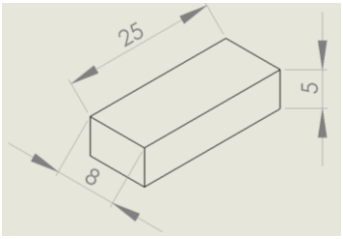
2. ЦЕЛ НА РАБОТАТА

Настоящата работа има за цел да изследва интензивността на износване на покритието ncAlTiN/αSi_3N_4, нанесено по метода PVD върху подложка от стомана 1.2343, използвана за изработване на шприцформи. За постигането на тази цел е необходимо да се решат следните задачи:

1. Изготвяне на опитни образци от стомана 1.2343 и покриването им с нанокомпозитното покритие ncAlTiN/αSi_3N_4 по метода PVD;
2. Избор на методика за експериментално изследване на износоустойчивостта на опитните образци със съответното покритие;
3. Провеждане на експериментални изследвания;
4. Анализ на резултатите и изводи.

3. ИЗГОТВЯНЕ НА ОПИТНИ ОБРАЗЦИ

За провеждане на експерименталните изследвания бяха изработени опитни образци от стомана 1.2343 (X38CrSiMo5), под формата на правоъгълен паралелепипед, с размери показани на фиг.1, използвана за изработване на шприцформи.



Фиг. 1. Форма и размери на опитните образци

Образците бяха подготвени както следва:

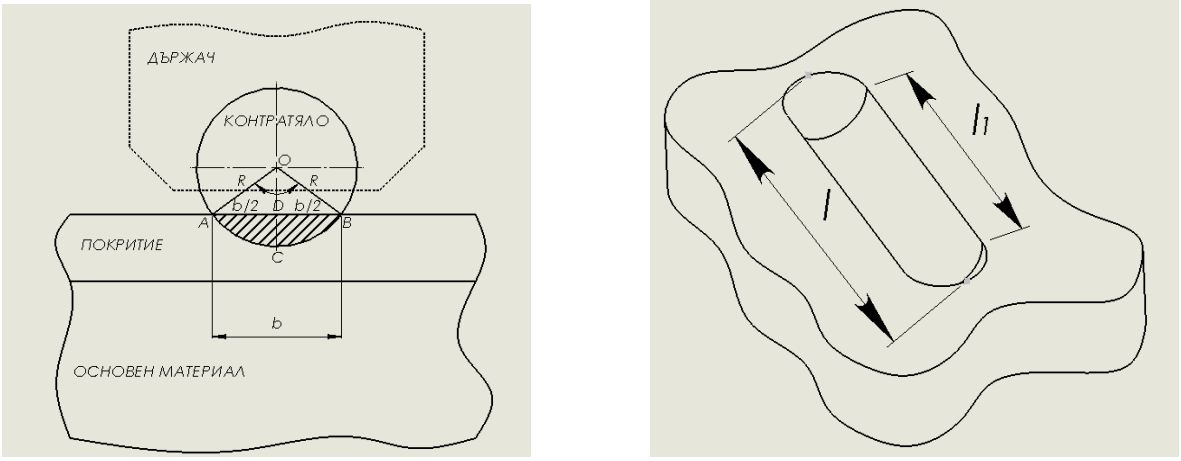
- незакалени шлифовани (означени като 2343 A) с твърдост 145 HB и грапавост на повърхнините *Ra = 0,8 μm*;
- закалени шлифовани (означени като 2343 B) с твърдост 52 HRC и грапавост на повърхнините *Ra = 0,8 μm*;
- закалени полирани (означени като 2343 C) с твърдост 52 HRC и грапавост на повърхнините *Ra = 0,2 μm*.

След изготвянето им същите бяха покрити с нанокомпозитно покритие ncAlTiN/αSi_3N_4 по метода PVD.

4. МЕТОДИКА ЗА ЕКСПЕРИМЕНТАЛНО ИЗСЛЕДВАНЕ НА ИЗНОСОУСТОЙЧИВОСТТА ПО ОБЕМНИЯ МЕТОД НА ТЪНКИ, ТВЪРДИ ПОКРИТИЯ

Методиката се състои в следното: Минералокерамично контратяло, оформено с радиус *R=2,45mm*, се движи праволинейно възвратно-постъпателно върху повърхността на изпитван образец, образувайки следа с профил на напречното сечение – сегмент (фиг.2) [3].

Следата може да бъде разделена на три части. Праволинейна част, която представлява отрез от цилиндър и два края, които съединени заедно представляват отрез от елепсоид. Използвайки параметрите радиус *R*, широчината на следата *b* (хордата, отсичаща сегмента) и централния ъгъл AOB се намира лицето на напречното сечение на следата *S*. На базата на определената стойност за лицето на напречното сечение на следата и нейната дължина се определя нейният обем, респективно обема на количеството снет материал от повърхността на образеца. Обемът на следата *V* може да се представи като сбор от обемите на праволинейната част (отрез от цилиндър) V_1 и двата края V_2 (отрез от елепсоид).



Фиг. 2. Принципна схема за определяне на износоустойчивостта чрез определяне на обема снет метал

Интензивността на износване I_w се определя със зависимостта:

$$I_w = \frac{V}{N.L},\ mm^3/N.m \qquad (1)$$

където: V - обема на количеството снет материал (следата), mm^3;
N - нормалното натоварване, N;
L - изминат път или пробег на образеца спрямо контратялото, m.

Обемът на следата се определя като:

$$V = V_1 + V_2,\ mm^3 \qquad (2)$$

Обемът на праволинейната част на следата (отрез от цилиндър) се определя със зависимостта:

$$V_1 = S.l_1,\ mm^3 \qquad (3)$$

където: l_1 - дължина на праволинейната част на следата, mm;
S - лицето на напречното сечение на следата, mm^2.

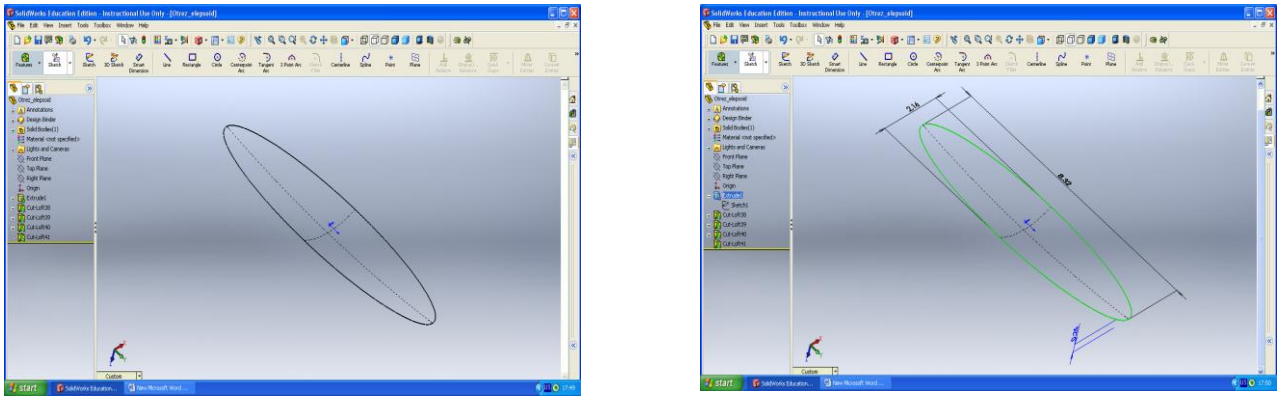
	A	B	C	D	E	F
1						
2	R=	2,45				
3	B=	0,225				
4						
5	ALPHA=	0,091869038	5,2638634	SIN(ALPHA)=	0,0917399	
6		[radian]	[degree]			
7						
8	S=	0,000387716				
9						
10	L=	11,00				
11	V=	0,004265				
12						

Фиг. 3. Изображение на диалоговия прозорец на програмата за пресмятане на обема на следата

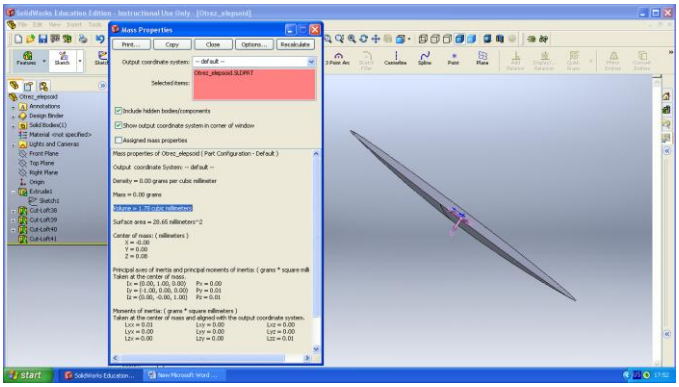
За по-удобно, бързо и точно изчисляване на параметъра V_1, бе генерирана програма в *EXCEL* (фиг.3). При задаване на различни стойности за параметрите широчина и дължина на праволинейната част на следата и на базата на константния радиус на контратялото, програмата пресмята централния ъгъл α, лицето на напречното сечение на следата и стойността на обема.

За определяне на обема V_2 бе генериран модел на двата края на следата (отрез от елепсоид) с продукта ***Solid****Works* (фиг.4). Моделът бе построен използвайки параметрите

широчина на следата *b*, дължината на края на следата $\frac{l-l_1}{2}$ и дълбочината на следата *h* от фиг.2.



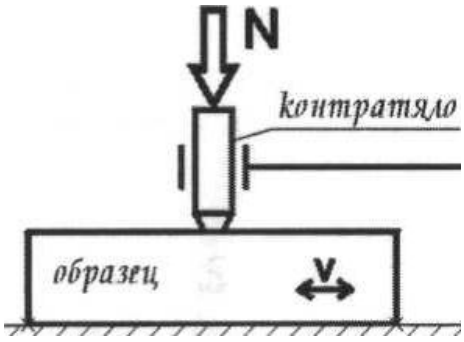
Фиг. 4. Модел на двата края на следата (отрез от елепсоид), генериран с продукта SolidWorks



Фиг. 5. Изображение на диалоговия прозорец, който дава информация за обема на построения модел (отрез от елепсоид)

5. ЕКСПЕРИМЕНТАЛНИ ИЗСЛЕДВАНИЯ И РЕЗУЛТАТИ

Експерименталните изследвания на износоустойчивостта бяха осъществени върху експериментален стенд, чийто принципна схема е показана на фиг.6. Реализира се триеща двойка между изпитвания образец и контратялото. Образецът извършва праволинейно възвратно-постъпателно движение със скорост *V*, а контратялото е позиционирано неподвижно натоварвайки образеца с определена натоварваща сила *N*. Скоростта на праволинейното възвратно-постъпателно движение и големината на натоварваща сила могат да се избират в зависимост от желания режим на работа на трибодвойката.



Фиг. 6. Експериментален стенд, принципна схема

Изследванията се проведоха в две серии за всеки един от покритите образци (2343 А; 2343 В; 2343 С) и еталонните (непокрити) образеци (ЕТАЛОН А; ЕТАЛОН В; ЕТАЛОН С) в зависимост от времето на работа на триещата двойка. Режимите на работа на стенда са показани в табл.1. Реализира се ускорено износване при сухо триене на опитните образци без задиране при стайна температура. Количествените стойности на параметрите, получени след експерименталните изпитвания и интензивността на износване на покритите образци и еталонните (непокрити) образци са дадени в табл.2.

Графичните зависимости на обемите на следите от износване при изпитване на покритите образци и еталонните (непокрити) образци при съответните режими са дадени на фиг.7, фиг.8, фиг.9, фиг.10.

Графичните зависимости на интензивността на износване на покритите образци и еталонните (непокрити) образци при съответните времена на изпитване са дадени на фиг.11, фиг.12, фиг.13, фиг.14.

6. АНАЛИЗ И ИЗВОДИ

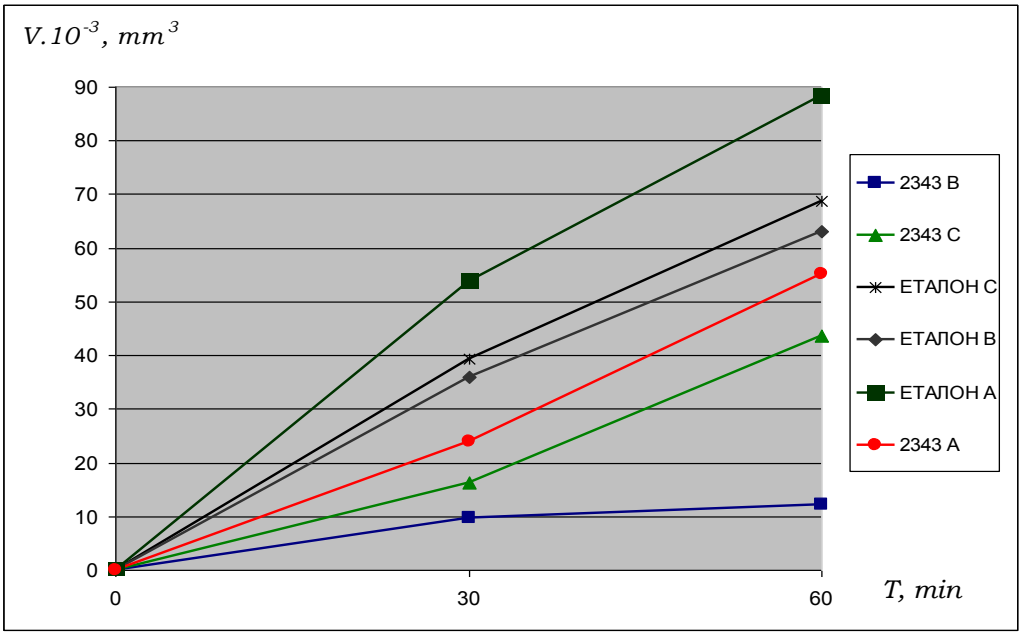
От получените резултати е видно, че полирането на триещите повърхнини не играе съществена роля върху износването. Полирането на работните повърхнини на инструмента би трябвало да се прилага когато на изделието трябва да се придаде супергладка повърхнина. Нанокомпозитното покритие от типа ncAlTiN/αSi_3N_4, нанесено върху инструменти изработени от стомана 1.2343 повишава износоустойчивостта от 1,5 до 2 пъти.

Таблица 1. Режими на работа на стенда

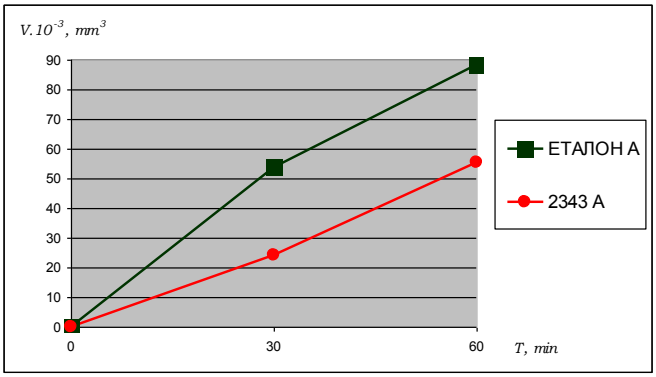
Образец с покритие	**Време на работа** ***T, min***	**Скорост** ***V, mm/s***	**Дължина на работния ход (следата)** ***l, mm***	**Натоварване** ***F, N***	**Изминат път (пробег)** ***L, m***	**Контратяло**
2343 A с ncAlTiN/ αSi_3N_4	30	6,78	11	0,65	12,21	Минералокерамична пластина
	60	6,78	11	0,65	24,42	
2343 B с ncAlTiN/ αSi_3N_4	30	6,78	11	0,65	12,21	Минералокерамична пластина
	60	6,78	11	0,65	24,42	
2343 C с ncAlTiN/ αSi_3N_4	30	6,78	11	0,65	12,21	Минералокерамична пластина
	60	6,78	11	0,65	24,42	
2343 A ЕТАЛОН	30	6,78	11	0,65	12,21	Минералокерамична пластина
	60	6,78	11	0,65	24,42	
2343 B ЕТАЛОН	30	6,78	11	0,65	12,21	Минералокерамична пластина
	60	6,78	11	0,65	24,42	
2343 C ЕТАЛОН	30	6,78	11	0,65	12,21	Минералокерамична пластина
	60	6,78	11	0,65	24,42	

Таблица 2. Експериментални резултати

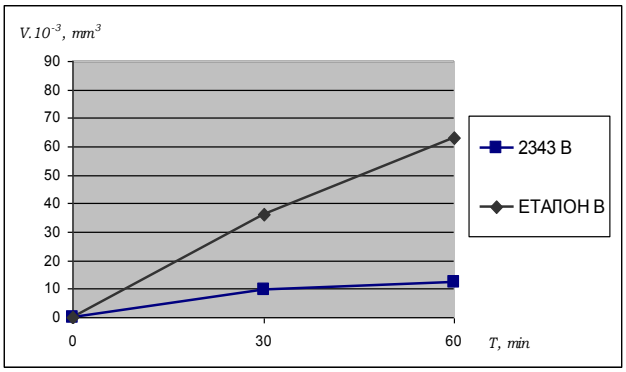
Образец с покритие	*T, min*	*R, mm*	*b, mm*	*S, mm²*	*V, mm³*	I_W, mm³/N.m
2343 A с ncAlTiN αSi₃N₄	30	2,45	0,400	$2,181.10^{-3}$	$23,996.10^{-3}$	$3,023.10^{-3}$
	60	2,45	0,528	$5,025.10^{-3}$	$55,272.10^{-3}$	$3,482.10^{-3}$
2343 B с ncAlTiN αSi₃N₄	30	2,45	0,296	$8,831.\ 10^{-4}$	$9,715.\ 10^{-3}$	$1,224.10^{-3}$
	60	2,45	0,320	$1,116.10^{-3}$	$12,277.10^{-3}$	$0,773.10^{-3}$
2343 C с ncAlTiN αSi₃N₄	30	2,45	0,352	$1,485.10^{-3}$	$16,345.10^{-3}$	$2,059.10^{-3}$
	60	2,45	0,488	$3,965.10^{-3}$	$43,615.10^{-3}$	$2.747.10^{-3}$
2343 A ЕТАЛОН	30	2,45	0,523	$4,883.10^{-3}$	$53,713.10^{-3}$	$6,768.10^{-3}$
	60	2,45	0,617	$8,028.10^{-3}$	$88,312.10^{-3}$	$5,563.10^{-3}$
2343 B ЕТАЛОН	30	2,45	0,458	$3,276.10^{-3}$	$36,043.10^{-3}$	$4,541.10^{-3}$
	60	2,45	0,552	$5,743.10^{-3}$	$63,178.10^{-3}$	$3,980.10^{-3}$
2343 C ЕТАЛОН	30	2,45	0,472	$3,587.10^{-3}$	$39,457.10^{-3}$	$4,971.10^{-3}$
	60	2,45	0,568	$6,258.10^{-3}$	$68,848.10^{-3}$	$4,337.10^{-3}$



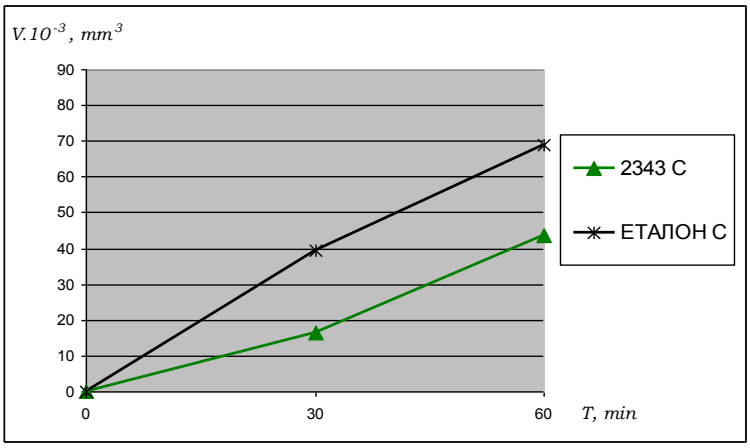
Фиг. 7. Графични зависимости на обемите на следите от износване за покритите образци и еталонните (непокрити) образци



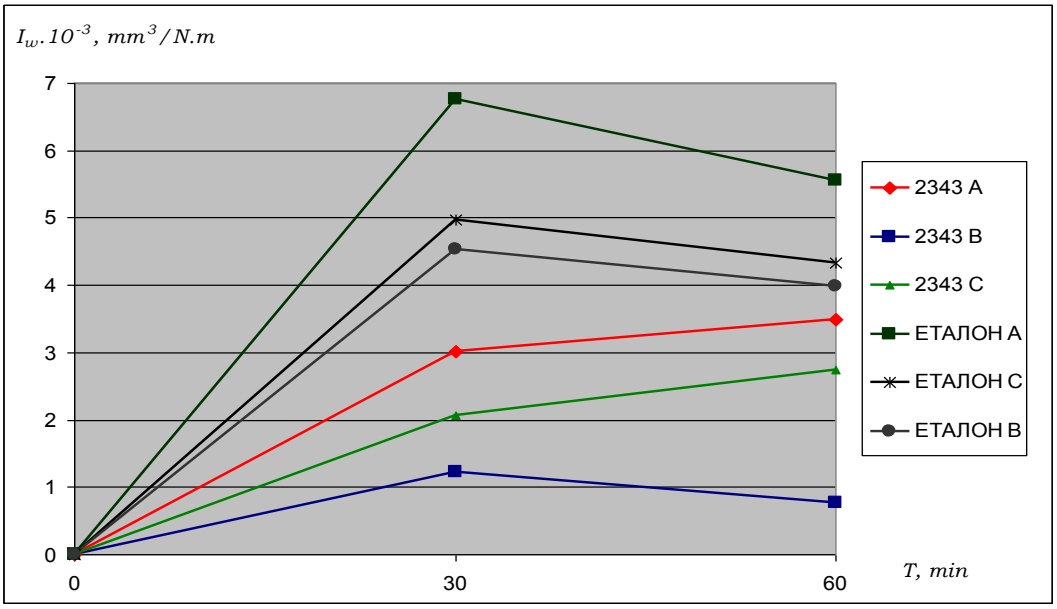
Фиг. 8. Графична зависимост на обемите на следите от износване за покрити и еталонни (непокрити) образци от незакалена шлифована стомана 1.2343



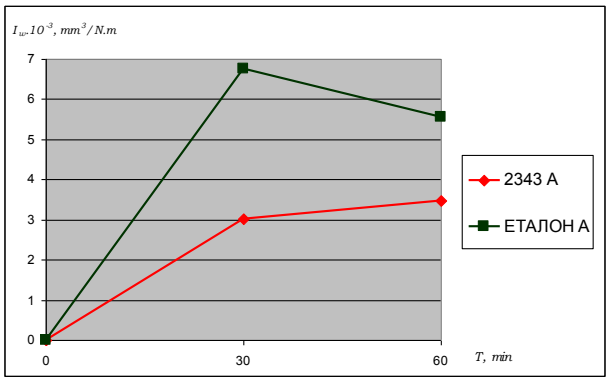
Фиг. 9. Графична зависимост на обемите на следите от износване за покрити и еталонни (непокрити) образци от закалена шлифована стомана 1.2343



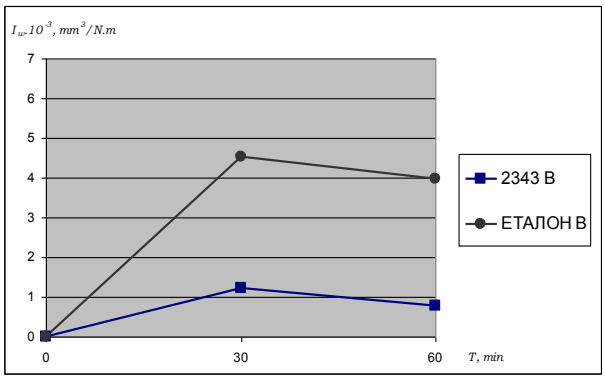
Фиг. 10. Графична зависимост на обемите на следите от износване за покрити и еталонни (непокрити) образци от закалена полирана стомана 1.2343



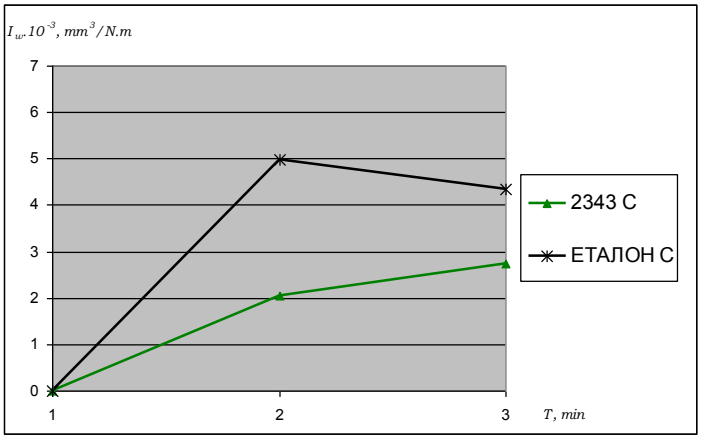
Фиг. 11. Графични зависимости на интензивността на износване за покритите образци и еталонните (непокрити) образци



Фиг. 12. Графична зависимост на интензивността на износване за покрити и еталонни (непокрити) образци от незакалена шлифована стомана 1.2343



Фиг. 13. Графична зависимост на интензивността на износване за покрити и еталонни (непокрити) образци от закалена шлифована стомана 1.2343



Фиг. 14. Графична зависимост на интензивността на износване за покрити и еталонни (непокрити) образци от закалена полирана стомана

ЛИТЕРАТУРА

1. Йорданов М. Чобанов П. Стефанов Г.; Адхезия и коефициент на триене на термично обработени покрития от TiN, отложени върху щампова стомана 5ХНМ; Механика на машините, т.60, 2005, с.8285.
2. Полцер, Майснер, Основи на триенето и износването. “Машиностроение”, 1984.
3. С. Дишлиев; Методика за експериментално изследване износоустойчивостта на тънки твърди износоустойчиви покрития. Двадесет и втора международна научно - техническа конференция “Автоматизация на дискретното производство” Созопол - Юни 2013 ISSN-1310-3946
4. Крагельский И.В., Алисина В. Триене, изнашивание и смазка, том 1,2; Москва, “Машиностроение”, 1978.
5. Michalczewski R., Piekoszewski W., Szczerek M., Tuszynski W.; Thin hard coatings for application in machine components; Proceedings of international conference “THE” Coating in Manufacturing Engineering, 5-7 October, Chalkidiki, Greece, 2005, ISBN 960-243-6174.
6. Pashinski Ch., Kakanakov R., Kolaklieva L.; Superhard nc-$(Al_{1-x}Ti_x)N$/a-Si_3N_4 gradient nanocomposite coatings for machining tools; Journal of the Technical University – Sofia, Plovdiv branch, Bulgaria; “Fundamental Sciences and Applications” Vol. 19, 2013; International Conference Engineering, Technologies and System TECHSYS 2013; Bulgaria; ISSN 1310 – 8271.

КОРЕСПОНДЕНЦИЯ

Георги МИШЕВ
Технически университет София - филиал Пловдив
Пловдив 4000, ул. "Цанко Дюстабанов" №25
e-mail: gmishevpl@yahoo.com

Стефан ДИШЛИЕВ
Университет по хранителни технологии – Пловдив
Пловдив 4000, бул. “Марица” №26
e-mail: stefan_dishliev@abv.bg

Велко РУПЕЦОВ
Технически колеж Смолян, ПУ – “Паисий Хилендарски”
Смолян 4700, ул. “Дичо Петров” №28
e-mail: velko_rupetsov@tk-smolian.eu

Tribological Journal BULTRIB, **Vol. IV, 2014**
Papers from the International Conference **BULTRIB '13**
October 24-26, 2013, Sofia
Society of Bulgarian Tribologists
Technical University of Sofia

THE BEHAVIOUR OF ROLLING GARNET PORPHYROBLASTS IN TRIBOZONES

Evgenia KOZHOUKHAROVA

Abstract: *The deformed helicite microstructure "snowball' which is characterized by spiral-shaped inclusion trails in a garnet porphyroblast, is thought to be formed during syntectonic growth and rolling of the porphyroblast. This idea does not agree to observed features of destruction of the garnet as well as the theoretical and experimental data of behaviour of a crystal under stress. Most of the facts observed are in favor of syntectonic deformation of pretectonically crystallized porphyroblast.*
Key Words*: snowball structure, syntectonic growth, deformation.*

ПОВЕДЕНИЕ НА РОТИРАЩИ ГРАНАТОВИ ПОРФИРОБЛАСТИ В ТРИБОЗОНИТЕ

Евгения КОЖУХАРОВА

Резюме: *Деформационната хелицитова микроструктура "снежна топка", която се характеризира със спирално разположена редица от включения в гранатов порфиробласт, се приема, че е образувана при синтектонско нарастване на ротиращ се гранат. Тази идея обаче, противоречи на установените следи от разрушаване на граната, както и на теоретичните и експериментални данни за поведението на кристалите при стрес. Повечето от наблюдаваните факти са в подкрепа на синтектонска деформация на предтектонски кристализирал порфиробласт.*
Ключови думи*: структура "снежна топка", синтектонски растеж, деформация*

1. ВЪВЕДЕНИЕ

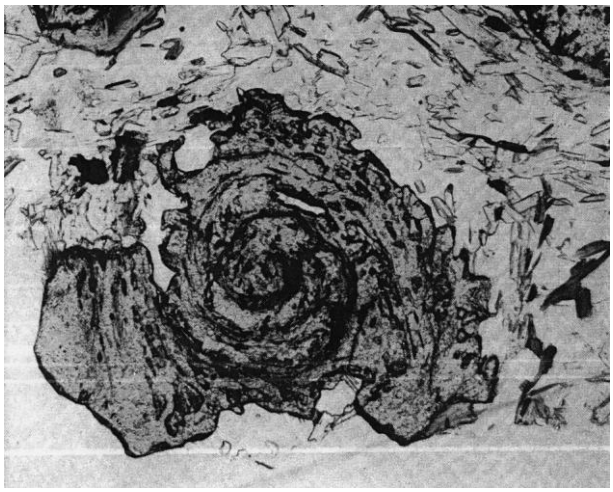
Деформацията на различните минерали в зоните на триене при метаморфните скали не са изучени достатъчно в аспекта на трибологията. Деформационните структури често се интерпретират в традиционните постановки на метаморфната петрология, основани на микроскопски наблюдения, без да се отчитат редица експериментални и теоретични данни за структурните изменения на минералите в условия на механична активизация.

Характерна деформация на ротиращ се метаморфен минерал в трибозона е т.н. „снежна топка", наблюдавана при гранатови порфиробласти в слюдени и карбонат-слюдени шисти. Микроструктурата „снежна топка", вариант на хелицитовата, се характеризира със спирално подреждане на низ от включения в гранатов порфиробласт (фиг. 1). Счита се, че тя индикира ротация на кристала в зони на междуслойни плъзгания, синхронно на неговия растеж. Подобен извод обаче, противоречи на съвременните данни за поведението на кристалната решетка, която в условия на стрес и триене се деформира и разрушава, а не изгражда.

Същността на въпроса, който поставяме е: възможен ли е растеж на гранатовия порфиробласт в условия на междуслойни тектонски движения, едновременно с неговата ротация и деформация.

2. ФОРМИРАНЕ НА ДЕФОРМАЦИОННАТА СТРУКТУРА „СНЕЖНА ТОПКА”

Спираловидната структура „снежна топка” е била обект на множество изследвания след първото фигуриране (фиг. 1) и публикация на Флет [5]. Доказано е, че кристалът израствайки в слюден шист, запечатва фолиацията, маркирана често чрез редица от включения като графит, рутил и др. Движестите се слоеве увличат в ротация по-устойчиви на триене минерали, какъвто е гранатът, които при въртенето изместват посоката на фолиацията спрямо първоначалното й положение. Вярва се, от повечето изследователи, че характерната спирала се получава, при нарастване на порфиробласта, като всеки новообразуван слой фиксира чрез включенията съществуващата в скалата фолиация, при въртенето последната се измества, следва образуване на нов слой по периферията на кристала, нова ротация и завъртане на включенията-маркери и така нататък (фиг. 2а). Често спираловидната структура е подчертана от вътрешни слоеве от кварц.

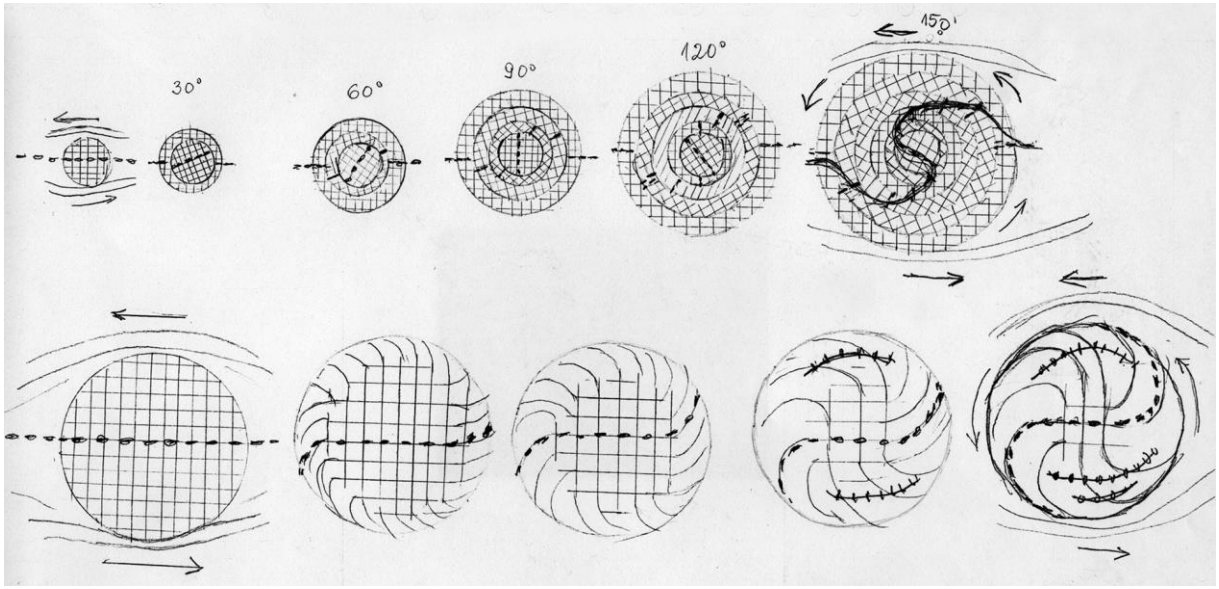


Фиг.1. Типична микроструктура „снежна топка” в гранатов порфиробласт [9]

Спрай [9] подържа идеята за синтектонски растеж на порфиробластите, но отбелязва, че това е трудно да се докаже. [Вернон [11] посочва като индикатори за синдеформационен растеж интензивните огъвания на ивицата от включения и поява на микробудини в периферията на кристала. Посочените индикатори за растеж всъщност показват по-интензивна деформация в периферията на ротиращия се кристал, а не нарастване. Други автори [3] оспорват аргументите, изтъквайки, че отделна ротация на порфиробластите спрямо кренулацията на матрикса не винаги съществува. Доказателство за нарастване някои автори [7] виждат в зоналността на кристала, считайки, че тя същевременно указва за изменение на кристализационните условия - температура и налягане по време на растежа на кристала. Независимо от дискусиите за механизма на формиране на спиралната структура, традиционната интерпретация за синтектонския растеж на порфиробласти в метаморфните скали още е актуална [12, 4].

Известно е [6,10], че при силен стрес, предизвикан от междуслойно триене и ротация на по-устойчиви минерали, какъвто е гранатът, настъпва деформация в кристалната решетка. Появяват се точкови, линейни и планарни дефекти, последните преминаващи в дислокации. Планарни дислокации в гранати по (211) са заснети на ТЕМ [8]. Те благоприятстват вътрешните хлъзгания на отделни домени. Всички илюстрирани фигури от различни автори [2, 7, 9, 11] показват главно вътрешна пластичност на кристала при ротацията, същевременно с разрушаването му, но не и нарастване. Известно е [1] наличието на четири винтови оси в кристалната решетка на граната, по които са подредени SiO_2 тетраедри. Възможно е винтовите оси да оказват влияние върху пластичността на граната и формиране на спираловидни дислокации на

транслиране на деформационните домени, каквито подобни транслации при натиск се наблюдават при. кварца.



Фиг. 2. Схема на два възможни варианта за формиране на микроструктурата „снежна топка”:
а) ротация и синтектонски растеж;
б) ротация и деформация на предтектонски порфиробласт.

На фиг.2 схематично са представени два предполагаеми механизма на образуване на спираловидната структура в ротиращия се между два триещи се слоеве порфиробласт. Ако кристалът нараства едновременно с въртенето си, най-външната зона би трябвало винаги да фиксира чрез маркиращите включения фолиацията на метаморфната скала.и освен това да е най-здрава (фиг.2а). На фиг.1 обаче се вижда обратното - включенията са ориентирани перпендикулярно на фолиацията, а зоната е силно разбита. Ако се приеме обаче, че порфиробластът е образуван предтектонски, то по време на движенията и ротацията, триенето и ротацията му, деформацията започва от най-външната зона, в началото пластично и постепенно увлича и усуква по-вътрешните (фиг. 2б). Вероятно спираловидната деформация се улеснява от появата на дислокационни зони в кристалната решетка на граната и наличието на винтови оси в нея. По дислокационните зони деформацията е деструктивна и подчертана от разрушените, посттектонски прекристализирали продукти, като кварц и др. Тъй като порфиробластът се върти в нехомогенна твърда среда, която оказва съпротивление и силно триене по повърхността му, деструктивните изменения са най-силни във външната зона, която често е разкъсана.

3. ЗАКЛЮЧЕНИЕ

Спираловидната структура „снежна топка” е деформационна, наложена върху предтектонски образуван порфиробласт, който при тектонско междуслойно триене се ротира и деформира пластично и деструктивно. Вследствие специфичната кристална структура на граната, при деформацията се образуват вътрешни дислокационни зони на плъзгане и деструкция. Растеж на кристала по време на тектонски движения, противоречи на принципите на деформация на минералите при стрес и следователно не е възможен.

ЛИТЕРАТУРА

1. Костов, И. Минералогия. – Техника, София; 734 с. **1993**.

2. Bard, J.P. Microtextures des roches magmatiques et metamorphiques.– Masson, Paris; 192 p. **1980**

3. Bell, T. H., S. E. Johnson Porphyroblast inclusion trails the key to orogenesis. – *Journal of Metamorphic Geology, 7;* 279- 310. **1989**

4. Fettes, D., J. Desmons. Metamorphic rocks. A. Classification and Glossary of Terms. – Cambridge University Press; 244 p. **2008.**

5. Flett,J. H.. Geology of Ben Wyvis, Carn Chuinneag. – Met. Geol. Surv. Scotland. **1912.**

6. Heinike, G.. Tribochemistry. – Academie Verlag, Berlin; 495 p. **1984.**

7. Robyr, M., W. D. Carlson, C. Passchier, P. Vonlanthen. Microstructural, chemical and textural records during growth of snowball garnet. – J. metamorphic Geol.. doi:10.1111/j.1525-1314.2009.00824.x **2009.**

8. Smith, B. K. The Influence of Defect Crystallography on Some Properties of Orthosilicates.– In: *Thompson, A. B., Rubie, D. C. (Ed.) Metamorphic Reactions, Kinetics, Textures and Deformation*. New York, Springer, **1985;** 251-268.

9. Spry, A. Metamorphic textures. – Pergamon Press Ltd.; 350 p. **1969.**

10. Tkacova, K. Mechanical Activation of Minerals. – Esevier, Bratislava; 155 p. **1989.**

11. Vernon, R. H. 2004. A practical guide to Rock Microstructure – Cambridge University Press; 594 p. **2004.**

КОРЕСПОНДЕНЦИЯ

Доц. д-р Евгения КОЖУХАРОВА
Геологически институт БАН
E-mail:< Ekozhoukharova@abv.bg>

Tribological Journal BULTRIB, **Vol. IV, 2014**
Papers from the International Conference **BULTRIB '13**
October 24-26, 2013, Sofia
Society of Bulgarian Tribologists
Technical University of Sofia

ИЗСЛЕДВАНЕ НА СЪСТАВА И СТРУКТУРАТА НА ЕЛЕКТРОИСКРОВО НАНЕСЕНИ ПОКРИТИЯ СЛЕД НАГРЯВАНЕ

Тодор Пеняшки - ИПАЗР - София, ул. "Шосе Банкя №3

STUDY OF THE INFLUENCE OF TEMPERATURE ON THE STRUCTURE OF THE DEPOSITED ELECTROSPARK COATINGS

Todor Penyashki - IPAZR - Sofia, Road Bankia, № 3
Research Institute for Land Reclamation and machinery - Agricultural Academy

Abstract: *The present work is to study the phase composition and micro hardness of electrical discharge caused coatings with pseudo amorphous structure, after heating at 200, 400 and 600 ° C. The coatings are caused by carbide composites based of WC on high-speed steel R6M5. Established the nature of variation of the phase composition, and micro hardness of coatings, depending on the material of the electrode stratification, parameters of modes stratification, and temperature of heating. Results makes it possible for different operating conditions of the layered products to select modes and materials for lamination to ensure the maximum possible wear resistance of coatings .*

Key Words: *electrospark alloying, impulse energy, coating, electrode for lamination*

Актуално направление в областта на електроискровото напластяване /***ЕН/*** е получаването на покрития с все по-висока твърдост и износоустойчивост. Това се постига чрез създаване на нови материали за напластяващи електроди [1] и чрез развитие и усъвършенстване на оборудването за напластяване. Поради високите температури и високата скорост на охлаждане при ***ЕН*** се формират крайно неравновесни по състав и структура покрития с наличие на остатъчни напрежения, кристални дефекти, микропори и др. [1,2,3]. При използването на машините „ЕЛФА" е установено [4] , че с увеличение на енергията на единичния импулс /***Ее/*** нарастват преноса на електроден материал върху напластяваното изделие , респективно дебелината и грапавостта на получените покрития, нараства и степента на дисперсност – структурата издребнява и при енергия на единичния импулс ***Ее*** = 10^{-2}J се получава бял слой с ултрадисперсна хетерогенна структура и строеж близък до аморфния. При Ее>10^{-2}J започва зараждане на аморфни участъци в покритието. С по-нататъшно увеличение на ***Ее*** расте и степента на аморфизиране и при енергии ***Ее*** > 0,05J слоя е почти изцяло аморфен. На рентгенограмите в тези случаи присъства една единствена характеристична линия в областта на мартензитната и аустенитна фази. За установяване доколко е устойчиво полученото състояние и може ли то да бъде полезно за практиката възниква необходимост от изучаване на състава, структурата и свойствата на покритията след нагряването им, което е и обект на настоящата работа.

ПОСТАНОВКА НА ЕКСПЕРИМЕНТИТЕ

Проведено е изследване на фазовия състав, структурата и микротвърдостта на „псевдоаморфните" покрития след нагряване при различни температури с последващо охлаждане. След всяко нагряване бе определян фазовия състав и беше измервана микротвърдостта на покритията.

Условия за ЕН

Покритията са нанасяни на машина „Елфа 541" с допълнителни източници на енергия върху шлифовани пластини с размери 12x12x3mm от бързорежеща стомана Р6М5,

термообработена до твърдост HRC 63-65. Използувани са твърдосплавни напластяващи електроди със следните условни означения:

-ВК и Р25 – на основа съответно WC и WC и (Ti,Ta,Nb)C със спойваща маса от кобалт –Co;

- ТНМ и ТН – на основа съответно TiC и TiN със спойваща маса от Ni, Mo и Cr.

За напластяването са подбрани режими с най-ниската, средна и най-високата енергия на единичния импулс за машините «Елфа», а също и режими с по-висока енергия, получена от допълнителен източник. Стойностите на електрическите параметри на режима за ***ЕН*** – тока I, капацитета C, коефициента на запълване τ и продължителността на импулсите Ti, както и диапазона на изменение на параметрите на нанесените с тях покрития – грапавост Ra, дебелина δ, и микротвърдост Hv са показани в ***Таблица1***.

Методика на измерванията

След нанасянето на покритията, пластините са загрявани във вакуумна пещ до температури t = 200, 400 и 600^0 C с 15 min задържане, след което се охлаждаха бавно в пещта.

След всяко нагряване е изследван фазовия състав чрез рентгенов дифрактометър „Дрон2" в Co-Kα лъчение.

Микротвърдостта на белия слой , на границата слой-основа и на ~ 5 и10μm дълбочина в основата е измервана на напречен металографски шлиф чрез микротвърдомер „Laitz". Броят на паралелните измервания на микротвърдостта е 5.

Таблица1. Стойности на параметрите на режима за ЕН и на получените покрития

Table 1· Values of the parameters of the regime of ESA, and the resulting coatings

№	Електрод Electrode	I, A current of pulses	C, μF capacity	Ti, μs Pulse duration	τ a duty cycle	Ra, μm / layer roughness	δ, μm Layer thickness	Hv, Mpa.10^3 Layer Micro hardness
1.	Р25	14,4	0,2	3	0,1	1,14	4,83	11,36
2.	Р25	14,4	0,5	8	0,1			12,44
3.	Р25	16	0,2	12	0,1	1,18	5,0	14,79
4.	Р25	16	0,7	20	0,1	1,39	5,4	14,53
5.	Р25	14,4	1	12	0,1	1,36	6,5	15,45
6.	Р25	50	-	10	0,04	1.42	7,63	16,76
7.	Р25	60	1	20	0,1	2,44	16,66	17,84
1	ВК	14,4	0,2	3	0,1	1,20	5,1	13,79
5.	ВК	14,4	1	12	0,1	1,37	6,6	14,32
6.	ВК	50	-	10	0,04	1,76	8,68	15,39
7.	ВК	60	1	20	0,1	2,46	21,6	16,15
1.	ТН	14,4	0,2	8	0,1	0,63	3,9	11,37
4.	ТН	14,4	1	12	0,1	1,12	5,1	13,06
5.	ТН	50	-	10	0,02	1.28	5. 54	13,81
1.	ТНМ	14,4	0,2	3	0,1	0,82	3,79	11,80
5.	ТНМ	14,4	1	12	0,1	1,19	4,83	12,89
6.	ТНМ	50	-	10	0,02	1,35	5,46	13,29

АНАЛИЗ НА ПОЛУЧЕНИТЕ РЕЗУЛТАТИ

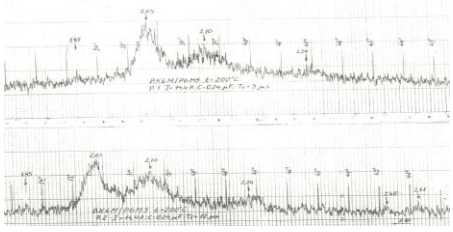
В *Таблица1* са дадени режимите за ***ЕН*** , както и стойностите на параметрите на получените с тях покрития с напластяващи електроди ***ВК*** и ***Р25***. Аналогични са и резултатите, получени с останалите два електрода, с тази разлика, че при напластяване с тях грапавостта и дебелината на получените покрития са по-ниски.

От проведените изследвания на фазовия състав при стайна температура се установява, че при ***ЕН*** с електрод ***ВК*** повърхностният слой се състои от фазите на основата – мартензит – Feα, аустенит- Feγ, и сложни желязо-волфрамови карбиди от типа Fe_3W_3C и $Fe_2(W,Mo)_4C$, чието количество е по-високо от това в основата.

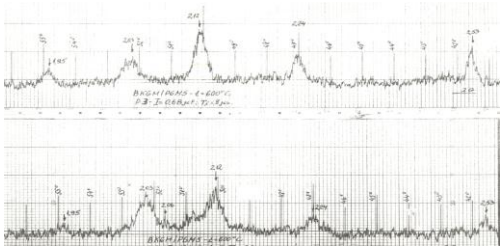
Структурните максимуми на характеристичните линии на мартензита и аустенита са разширени и отместени спрямо тези на основата - ***Фиг.1***, което е показател за наличие на твърди разтвори на W и Co в желязото, кристални дефекти и за издребнявяне на структурата [3]. Анализирайки дифрактограмите, може да се заключи, че фазовият състав на покритието се отличава от този на основата главно по обогатяването и с Fe_3W_3C и $Fe_2(W,Mo)_4C$, а структурата – с по-високата степен на неравновесност и на дисперсност. С увеличение на енергията на единичния импулс ***Ее*** /в посока от Режим1 към режим 7 - ***Таблица1***/ височината /интензитетът/ на структурните максимуми намалява, а характеристичните линии се разширяват, което затруднява разграничаването на отделните фази. Нараства степента на смесване на фазите, а структурата издребнява и става все по- дисперсна, приближавайки се към аморфната такава. В рентгенограмите се наблюдава уширение на дифракционните максимуми и намаляване на интензитета на линиите в зоната на максимумите на Fe_α и Fe_γ - $2\theta = 48 \div 54^o$. За степента на дисперсност и аморфизиране може да се съди по уширението и сливането на характеристичните линии на отделните фази. Колкото по-голямо е наблюдаваното уширение и колкото по-малък е интензитета /височината/ на линиите, толкова по-висока е степента на аморфизиране на слоя. Слоят представлява смес от видоизменените материали на ***НЕ*** и основата – в случая стомана Р6М5. С увеличение на ***Ее*** нарастват количеството пренесен аноден материал и микротвърдостта на слоя [2,3]. При режима с максималната за машините „ЕЛФА" енергия - №5 – ***Таблица1***, се наблюдава намаляване на интензитета и разширение на характеристичните линии на фазите, което може да се приеме като показател за повишаване на дисперсността на частиците и появата на псевдоаморфно състояние на слоя. При увеличение на ***Ее*** над 0,025J – до 0,5 J микротвърдостта и дебелината на покритията съществено се увеличават / по-високата енергия води до получаване на покрития с над два пъти по-голяма дебелина от получената с конвенционалния източник на машините „ЕЛФА"/. Разширяват се и структурните максимуми, като при най-високите енергии се получават описаните в [4] състояния с един широк максимум в зоната на мартензита и аустенита, което е показател за наличието на аморфно състояние на покритието. Характерните разлики в рентгенограмите и строежа на покритията са ултрадисперсност, липса на отделни фази, получаване на смеси от двата материала, по-високи стойности на Ra, δ, Hv . При ***ЕН*** с електрод ***Р25*** –***Фиг.2*** освен изброените по-горе фази в покритията е регистрирано наличие и на сложен титано-волфрамов карбид от типа /Ti,W/C_{1-x}. Това показва, че в процеса на преноса WC и TiC претърпяват частична дисоциация.

При **ЕН** с електроди ***ТН*** **и** ***ТНМ*** в състава на покритията присъстват и карбиди от типа TiC_{1-x} и $Ti(C,N)_{1-x}$. Количеството на желязо-волфрамовите карбиди е по-малко отколкото в получените с ***ВК*** и ***Р25*** покрития и е съизмеримо с това на основата. Разширението на структурните максимуми на $Fe\gamma$ и $Fe\alpha$ и отместването им е по-слабо изразено отколкото при тези, получени при напластяване с електроди ***ВК*** и ***Р25***, т.е. твърдите разтвори са с по-ниска концентрация и степента на дисперсност също е по-ниска. С увеличение на енергията за напластяване по интензитета и ширината на структурните линии се установява, че расте количеството на карбидите, на аустенита и степента на легирането му, а количеството на мартензита намалява. Разширяват се и структурните максимуми, но отделните фази са разграничени, т.е. при най-високите енергии не се получава широкия максимум в зоната на мартензита и аустенита, който е показател за наличието на аморфно състояние на покритието.

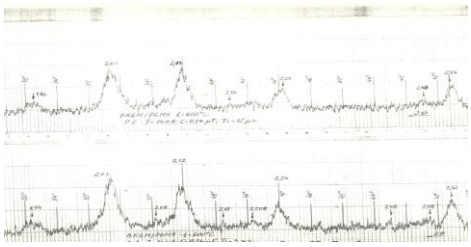
След отгряването във фазовия състав и структурата на покритията се наблюдават следните изменения:



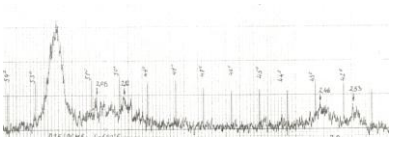
I14,4A,C0,2μF,Ti3μs,t200^{0}C
I14,4A,C1 μF,Ti12μs,t200^{0}C



I14,4A,C0,7μF,Ti8μs,t600^{0}C
I150A,Ti20μs,t600^{0}C



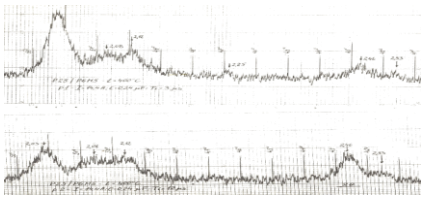
I14,4A,C1μF,Ti12μs,t600^{0}C
I14,4A,C0,2μF,Ti3μs,t600^{0}C



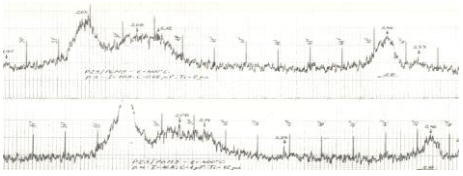
I14,4A,C0,2μF,Ti3μs,t20^{0}C

Фиг. 1. Рентгенограми на ЕН покрития от НЕ ВК върху ст.Р6М5
Fig. 1. Radiographs of ESA coatings of electrode BK on the st.R6M5

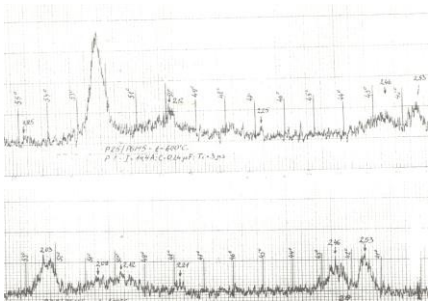
При температура t =200^{0}C при покритията нанесени при режимите с ниска енергия -№1 и 2 – ***Таблица1*** и ***НЕ ВК*** започва разделяне и стесняване на линиите на карбидите и основата - характеристичните линии на фазите започват да се стесняват, а интензитета на структурните максимуми на карбидите и на фазите от основата, намиращи се в зоната на „халото" започва да нараства. При температури t = 400^{0}C линиите на карбидите се засилват, а на мартензитната и аустенитна фази намаляват по интензитет и се стесняват. При 600^0 линиите се стесняват още



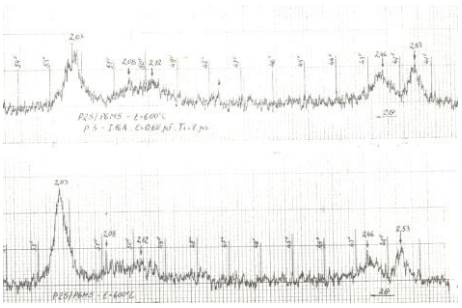
I14,4A,C0,2μF,Ti3μs,t400^{0}C
I14,4A,C0,2μF,Ti12μs,t400^{0}C



I14,4A,C0,7μF,Ti8 μs,t400^{0}C
I14,4A,C1μF,Ti12 μs,t400^{0}C



I14,4A,C0,2 μF,Ti3 μs,t 600^{0}C
I50A, Ti50 μs,t 600^{0}C



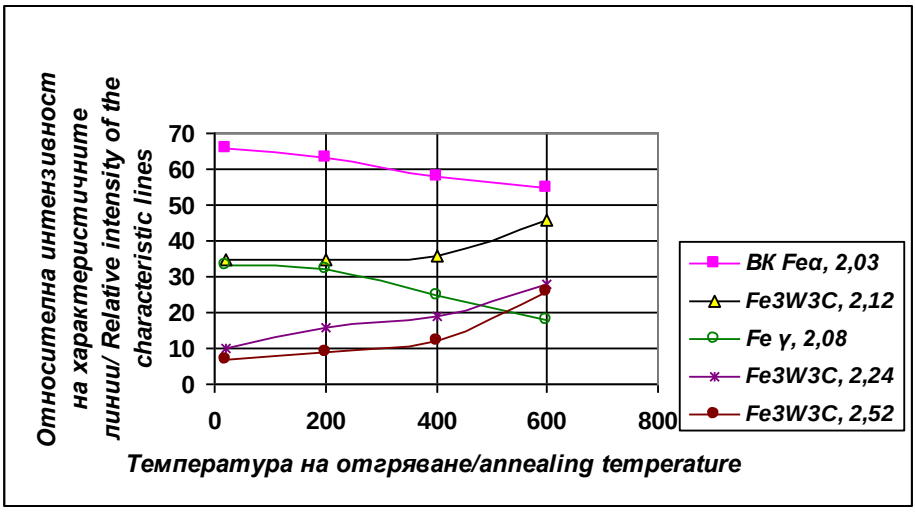
I16A,C0,7 μF,Ti8 μs,t 600^{0}C
I14,4A,C0,2 μF,Ti12 μs,t 600^{0}C

Фиг. 2. Рентгенограми на ЕН покрития от НЕ Р25 върху ст.Р6М5
Fig. 2. Radiographs of ESA coatings on electrode P25 on the st.R6M5

повече, интензитетът им нараства и се доближават до тези на основата в изходно състояние – преди напластяването. Интензитетът на максимумите на карбидите нараства и става значително по-висок от този в изходното състояние. Появяват се следи от $Fe_2(W,Mo)_4C$ и (Cr,Fe,Mo), а широчината на характеристичните линии на Fe_γ става още по-малка.

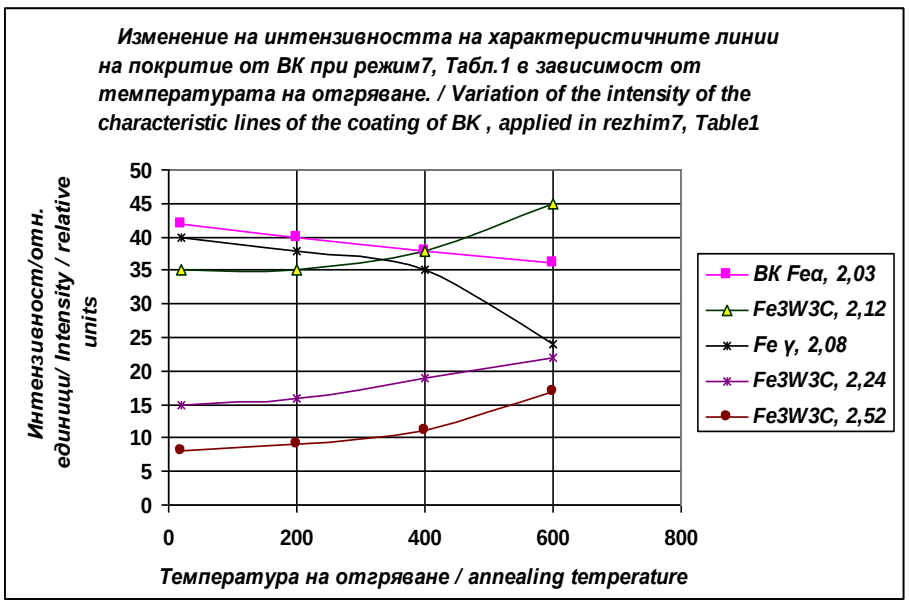
При покритията, нанесени с високоенергийните режими -№ 4,5 и 6 – ***Таблица1***, скоростта на описаните процеси е по-ниска, т.е. колкото по-висока е енергията на единичния импулс, толкова по-дълго време и при по-висока температура се запазват първоначалното ултрадисперсно и аморфно състояние и се съхранява твърдия разтвор на волфрама в желязото. Разделянето, засилването на интензитета и стесняването на линиите и процесът на кристализирането е по-бавен и започва при 400^0, а при t=600^{0}C не е изцяло завършен - характеристичните линии са все още по-широки, интензитетът на карбидите – по-нисък от този

при останалите режими. Така например интензитетът и широчината на карбидните фази при режим 6 при t =600^{0}C са близки до тези на покритието, нанесено с режим 3 след отгряване при 200^{0}C, или на режим 4 след отгряване при 400 ^{0}C . Това показва, че при използване на ***Ее*** по-висока от 0,02J псевдоаморфното състояние се запазва при нагряване до 600^{0}C. Характерът на изменение на интензивността I_I на характеристичните линии при ***ЕН*** с ***НЕ ВК*** е показан на ***Фиг.3***. С увеличението на температурата намалява ширината на максимумите, т.е. започва разпадане на твърдите разтвори и намаляване на степента на неравновесност и дисперсност, като горното е по-силно изразено при покритията, нанесени с електроди ***ТН*** и ***ТНМ*** и при по- ниски енергии. При покритията, нанесени при режимите с по-висока енергия, скоростта на описаните процеси е по-ниска. Така например при режим 4 разпадането на твърдите разтвори и на неравновесното състояние все още не е изцяло завършено, интензитетът на дифракционните максимуми на карбидите е по- нисък от този при режимите с по-ниската енергия, ширината им – по-голяма, а количеството на карбидите при t =400^{0}C е близко до това при режим 1 и t =20^{0}C. – ***Фиг. 2*** и ***Фиг.3в,г.*** При режимите с най-висока енергия -5 и 6 разпадането едва започва.



а) Изменение на интензитета на характеристичните линии на покритие нанесено с електрод ВК при режим1, Таблица1 в зависимост от температурата на отгряване

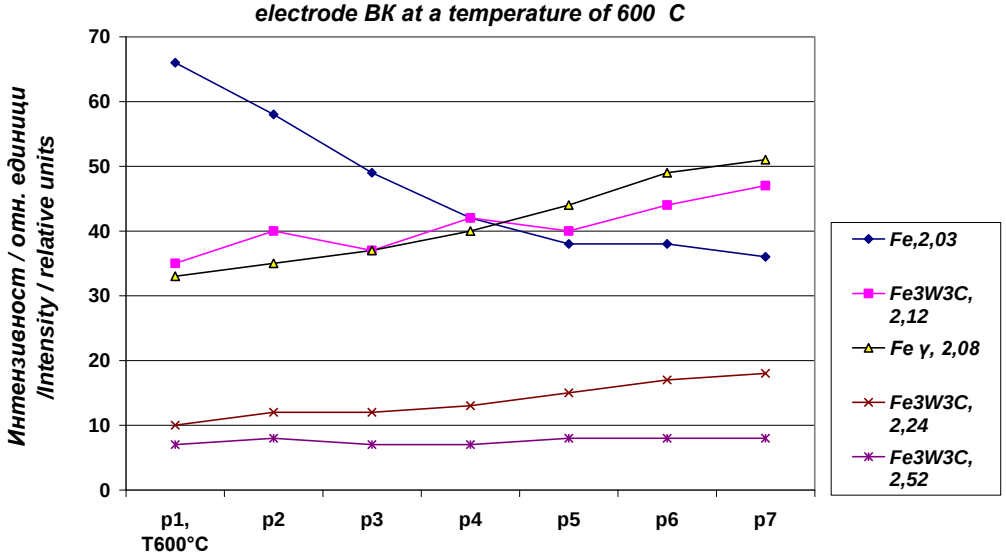
a) Change of the intensity of the characteristic lines of a coating applied to an electrode in WC mode1, Table 1 in dependence on the temperature of the annealing



б) Изменение на интензитета на характеристичните линии на покритие нанесено с електрод ВК при режим7, Таблица1 в зависимост от температурата на отгряване

b) Change of the intensity of the characteristic lines of a coating applied to an electrode in WC mode1, Table 1 in dependence on the temperature of the annealing

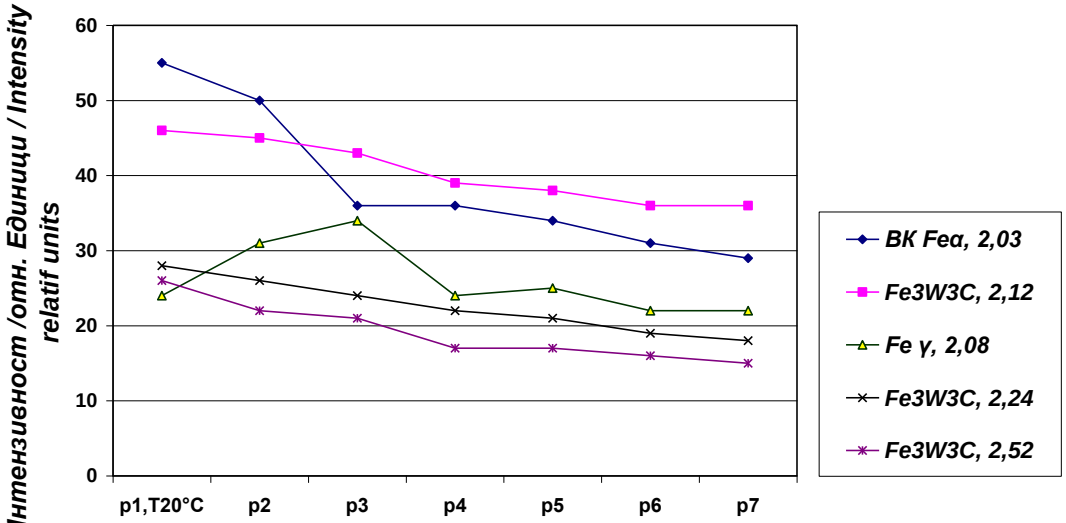
Интензивност на характеристичните линии на покритие от електрод ВК при температура 600 С / Intensity of the characteristic lines of the coated of electrode ВК at a temperature of 600 C



Номер на режима за електроискрово напластяване, Табл.1 / Number of mode for elektrospark stratification, Table 1

в)Интензивност на характеристичните линии на покрития нанесени с електрод ВК при температура на отгряване600^{0}C

c) Intensity of the characteristics lines of coatings caused by electrode ВК -temperature 600^{0}C



Режим за ЕН, Табл.1 / Mode of ESA, Table 1

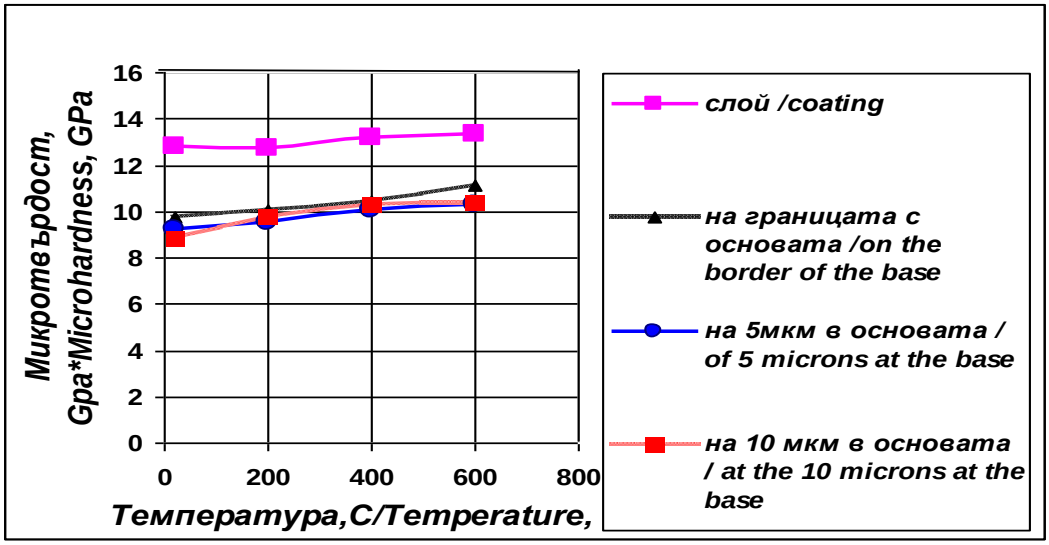
г)Интензивност на характеристичните линии на покрития нанесени с електрод ВК - температура 20^{0}C

d) Intensity of the characteristics lines of coatings caused by electrode WC -temperature 20^{0}C

Фиг.3(а,б,в,г) Изменение на интензивността на характеристичните линии в зависимост от температурата на отгряване , Напластяващ електрод – ВК
Figure 3 (a, b, c, d) Changes in the intensity of the characteristic lines depending on the annealing temperature, stratification electrode - WC

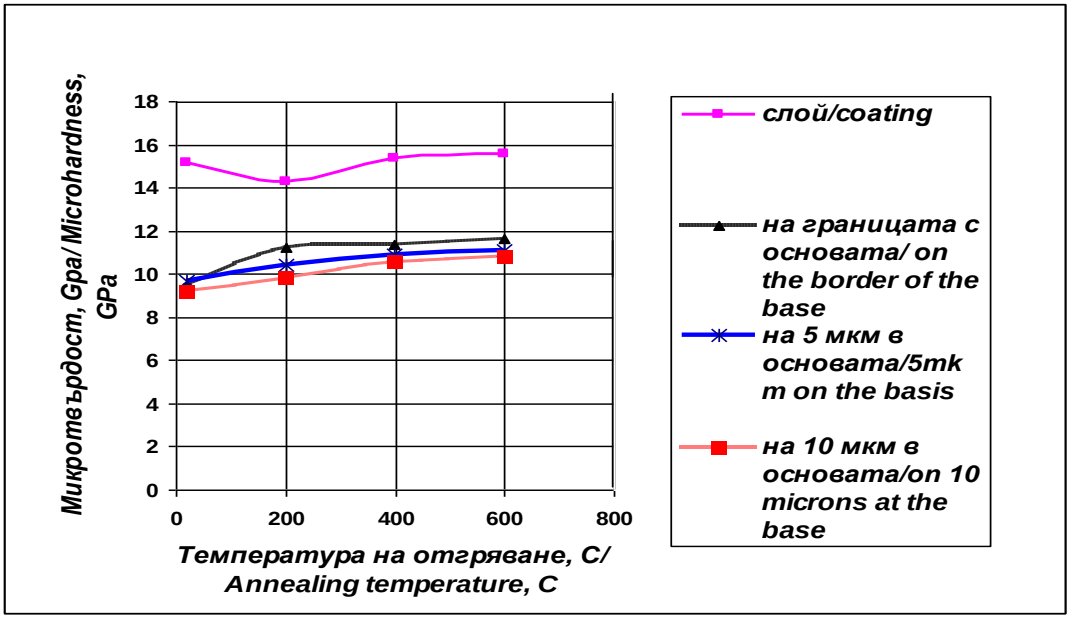
Фиг4. Изменение на микротвърдостта на покрития от електрод ВК в зависимост от температурата на отгряване

Fig4. Amendment of microhardness of the coating of the electrode according to the VC in the temperature of the annealing



а) Изменение на микротвърдостта на покрития от електрод ВК нанесени при режим1, Таблица1 в зависимост от температурата на отгряване

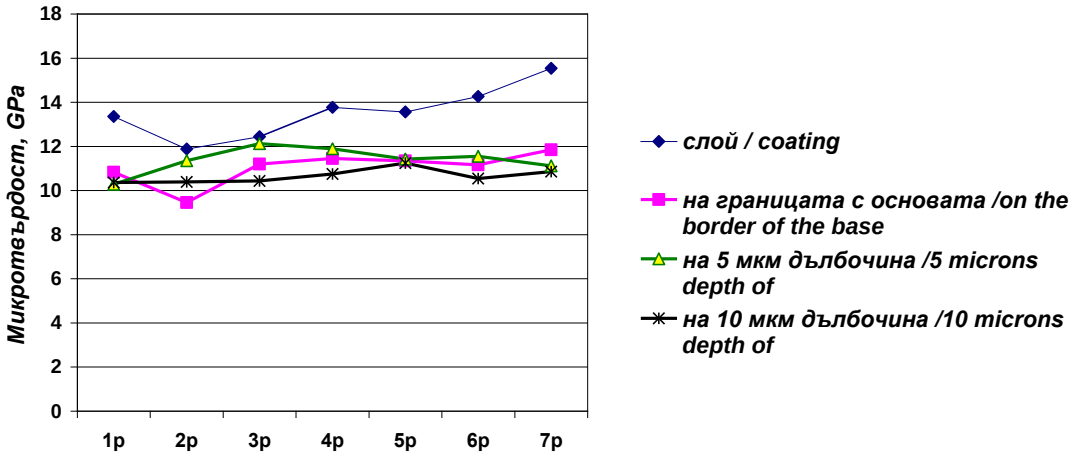
a) Amendment of micro hardness of coatings electrode WC done in mode1, Table 1, depending on the annealing temperature



б) Изменение на микротвърдостта на покрития от електрод ВК нанесени при режим7, Таблица 1 в зависимост от температурата на отгряване

b) Amendment of micro hardness of coatings electrode WC done in mode7, Table 1, depending on the annealing temperature

Микротвърдост на покрития от НЕ ВК след отгряване при 600 /
Microhardness of the coating by laminating of electrode ВК after annealing at 600 C.



Номер на режима за напластяване - Табл.1 /Number of mode overlay coating process - Table 1

в) микротвърдост на покрития от електрод ВК при температура на отгряване600^{0}C
c)Micro hardness of coatings applied WC electrode at annealing temperature of 600^{0}C

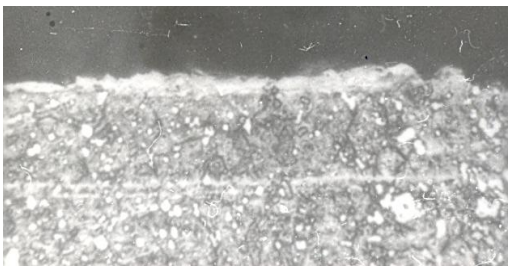
По-високата степен на насищане на твърдите разтвори на покритията от ***ВК*** и ***Р25*** , както и полученото аморфно състояние, предполагат и по-добра адхезия с основата и по-високи якостни и експлоатационни характеристики, което ги прави пригодни за условия на експлоатация, придружени от ударни натоварвания. Полученото аморфно състояние е устойчиво до 600^{0}C , което го прави подходящо не само за триещи се изделия, но и за металообработващи инструменти. По-високата износоустойчивост на аморфните покрития е потвърдена и от резултатите в работите [5,6]

Описаният по-горе процес се отнася за покритията от електроди ***ВК*** и ***Р25***. При нанесените с електроди ***ТН*** и ***ТНМ*** покрития разширението на струкрурните максимуми е по-слабо изразено, даже и при режимите с най-висока енергия.

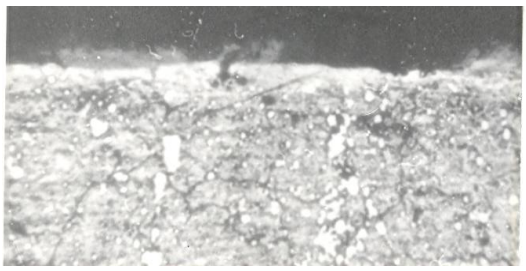
На ***Фиг.4.*** е показано изменението микротвърдостта на покритията нанесени с електрод ***ВК*** за различни режими за ***ЕН*** и температури на отгряване. От фигурата се вижда, че с увеличение на ***Ее*** нараства и микротвърдостта на белия слой. С увеличение на температурата на отгряване се появява слаба тенденция към нарастване на микротвърдостта на белия слой и на границата слой-основа. Разликите в микротвърдостта на покритията нанесени с използваните два електрода са малки и не съответстват на разликите в изходната им твърдост. Причина за това са промените, които анодните материали претърпяват в процеса на преноса.

По аналогичен начин се изменят дифракционната картина и микротвърдостта на покритията, нанесени с останалите три електрода с тази разлика, че с увеличение на температурата на отгряване микротвърдостта на покритията, нанесени с ***ТН*** и ***ТНМ*** нараства по-слабо, а по-интензивно расте твърдостта на границата слой-основа, като стойностите се стабилизират и размахът намалява. От снимките на микрошлифове на покритията при 20, 400 и 600^{0}C - ***Фиг.5***. се установява, че след нагряване термоповлияната зона се заличава, а други структурни промени не се забелязват.

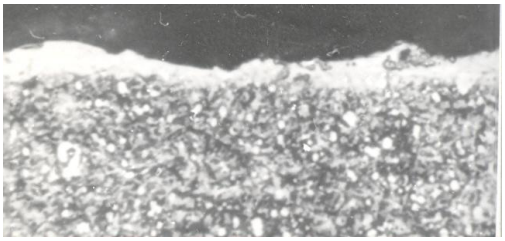
Бързото нагряване и охлаждане в процеса на преноса и бързата кристализация на материалите на ***НЕ*** и основата водят до изменение на структурата и състава на нанесеното покритие. Кратковременното течно състояние е предпоставка за протичане на изравняваща дифузия и формиране на слой с усреднен химически състав, а охлаждането с висока скорост



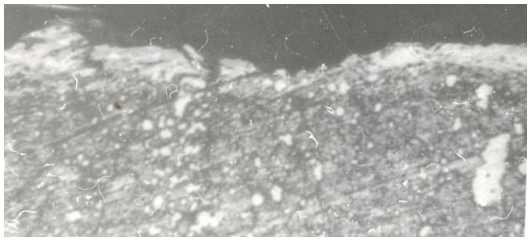
1. ВК/P6M5–I16A,C0,2μF,Ti3μs–t20^{0}C



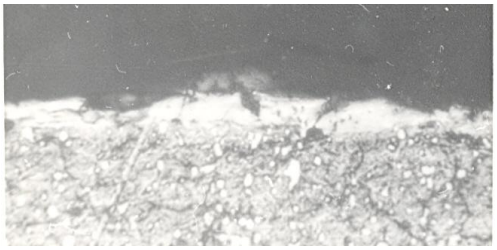
1. ВК/P6M5 –I16A, C0,2 μ F, Ti 3 μs – t600^{0}C



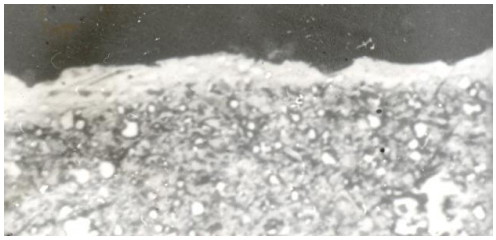
3. ВК/P6M5 –I16A,C0,2μF,Ti12μs–t20^{0}C



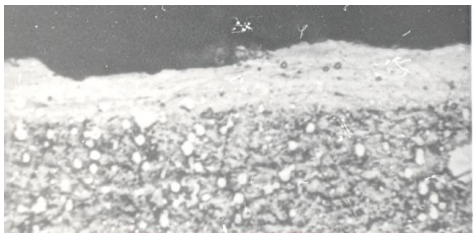
3.ВК/P6M5–I16A,C0,2μF,Ti12μs–t600^{0}C



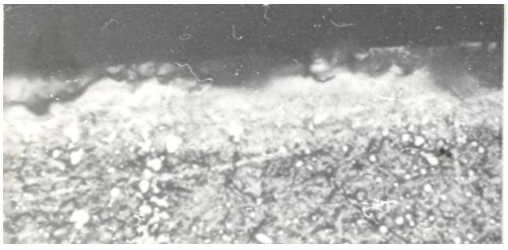
5.ВК/P6M5–I16A,C1μF,Ti12μs–20^{0}C



5.ВК/P6M5–16AqC1μF,Ti12μs– t600^{0}C



7.ВК/P6M5–I60A,C1μF,Ti20μs–t20^{0}C



7. ВК/P6M5–I60A,C0,2μF,Ti20μs–t600^{0}C

Фигура 5. Микроструктура на електроискрови покрития след отгряване при температура 600^{0}C

Figure 5. Electrical discharge coatings microstructure after annealing at 600^{0}C

променя механизма на кристализацията. В резултат структурата постепенно издребнява до появата на ултрадисперсното аморфно състояние, устойчиво до 600^{0}C. Горните изменения в значителна степен определят макро свойствата и експлоатационните характеристики на покритията при различни условия на работа. Познаването на тези изменения има важно значение, тъй като дава възможност за различни условия на работа да се подбират най-подходящите за конкретния случай режими и материал на напластяващия електрод определящи вида и структурата на покритието, което ще обезпечи възможната максимална износоустойчивост на напластеното изделие.

ИЗВОДИ:

1. Установено е че при електроискрово напластяване с електрод ***P25*** повърхностният слой се обогатява с карбиди в по- голяма степен отколкото при електроди ***ВК***.
2. Използването на режими с по-висока енергия води до по-дълго съхранение на

неравновесните ултрадисперсни и аморфни структури и твърдите разтвори на анодните материали в желязото, което е предпоставка за по-висока износоустойчивост на покритията.

3. По-високата степен на дисперсност на покритията от електроди на основа WC , при режимите с висока енергия създават предпоставки за ро-добра адхезия и по-високи якостни характеристики на този вид покрития. Следователно, при ***ЕН*** на изделия, работещи в условия на високи температури и ударни натоварвания е необходимо покритията да се нанасят с електроди на основа WC при режими с възможната за случая най-висока енергия.

ЛИТЕРАТУРА

1. Кузнецов, И.С.”Электроискровая обработка электродами из аморфных и нанокристаллических сплавов режущих деталей” Сб. Докл. ГОСТНИТИ 2011, т.108, стр.230
2. Гитлевич.,А.Е., В.В. Михайлов и др.: “Электроискровое легирование металлических поверхностей”, Кишинев, Штиница, 1985г.,196стр.
3. Верхотуров,А.Д. И.М.Муха. Технология электроискрового легирования металлических поверхностей. Наукова думка. Киев.1976.
4. Пеняшки, Т.Г ”Изследване на качествените характеристики на електроискрово напластени покрития с псевдоаморфен строеж” – Сб. Доклади “БУЛТРИБ”- 2004
5. Пеняшки Т. , И. Ликов, „ Изследване на износването на режещи инструменти с електроискрови покрития от високоенергиен източник” сб. Доклади АМО 2009, т.1.
6. Пеняшки Т.Г. Изследване износването на инструменти с електроискрови покрития от високоенергиен източник при прекъснато рязане Сб. Доклади “БУЛТРИБ”- 2013
7. Миркин Л.С. Рентгеноструктурный контрол машиностроительных материалов. Справочник. Машиностроение., 1979

Резюме: *В настоящата работа е проведено изследване на фазовия състав и микротвърдостта на електроискрово нанесени покрития с псевдоаморфен строеж след отгряването им при температури 200, 400 и 600°C. Покритията са нанесени от твърдосплавни композиционни материали на основа WC върху бързорежеща стомана Р6М5. Установен е характера на изменение на фазовия състав и микротвърдостта на покритията в зависимост от материала на напластяващия електрод, параметрите на режима за напластяване и температурата на отгряване. Получените резултати дават възможнаст за различни условия на експлоатация на напластените изделия да се подбират режими и материали за напластяване, които да обезпечават максимално възможната износоустойчивост на покритията.*

КОНТАКТИ :

Тодор Пеняшки

Институт по почвознание, агротехнологии и защита на растенията към Селскостопанска академия - гр. София, 1331, ул. „Шосе Банкя” 3
Jsm +359 879-29-39-13, e-mail tpeniashki@abv.bg

Tribological Journal BULTRIB, **Vol. IV, 2014**
Papers from the International Conference **BULTRIB '13**
October 24-26, 2013, Sofia
Society of Bulgarian Tribologists
Technical University of Sofia

3D SURFACE LAYER CHARACTERIZATION FOR HYDROGENATED X 65 STEEL SAMPLES

Claudiu TELETIN, Constantin SPÂNU, Iulian Gabriel BÎRSAN and Sorin CIORTAN

Abstract: *The paper studies the influence of hydrogen embrittlement on the surface roughness of samples collected from slabs of steel X 65 obtained by continuous casting. It was considered same parameters of the roughness:* S_a *(average roughness),* S_{ku} *(kurtosis) and* S_{sk} *(skewness). For the determination of these parameters it was used a universal microtribometer (UMT).*

Key Words: *hydrogen embrittlement, 3D roughness.*

1. INTRODUCTION

Hydrogen is the element with the simplest structure. Its reactivity and rate of diffusion is very large. Hydrogen can reach into steel in several ways: through steelmaking and casting (so called internal or metallurgical hydrogen) and through the surface of the steel, at the manufacture of metal parts and then, due to environmental conditions and mechanical stresses. After adsorption of atomic hydrogen in metal, it diffuses [1] and accumulates in the crystalline structure defects (nonmetallic inclusions, voids, grain joints, interfaces etc.). These defects are traps for it. Here the hydrogen recombination takes place, resulting in molecular hydrogen, with volume greater than the atomic hydrogen. Thus, in the traps, it creates high pressure (>0.5 MPa), which can lead to embrittlement of the steel, if a critical threshold is reached. Numerous damages due to the presence into petroleum products of harmful substances, particularly hydrogen sulphide, which favors the penetration of hydrogen into steel and the resulting embrittlement has led to the need to study the influence of hydrogen on steels used in the construction of pipelines and oil facilities. The X 65 PSL 2 steel (according standard API 5 L) studied in this paper is used in construction of oil pipelines.

During the hydrogen embrittlement in a H_2S medium, atomic hydrogen is produced by hydrogen sulphide dissociation, while the corrosion process in hydrated environment. The final reaction is [2, 3] :

$$Fe + H_2S = FeS + 2H_{ads} \quad (1)$$

2. EXPERIMENTS

2.1. The test specimens

The samples were taken from the surface of a slab obtained through continuous casting. They have form and size like in Fig.1 and were grinded on a horizontal grinding machine.

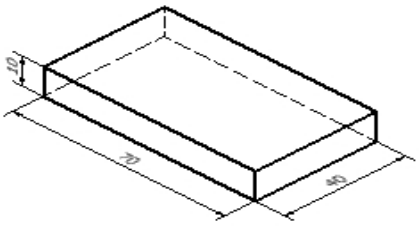


Fig. 1. The test specimen form and dimensions.

To simulate environmental conditions caused by hydrogen sulphide in the oil industry installations using X 65 steel, sets of samples were treated in hydrogen sulphide environment, for different periods of time.

Samples treatment was made under similar conditions of the test HIC (NACE Standard TM 0284 [4]), using a saline solution, acidified, in which was bubbled H_2S. The hydrogen sulphide is prepared in a Kipp bows from sodium sulphide and sulphuric acid according to reaction:

$$Na_2S + H_2SO_4 = Na_2SO_4 + H_2S \quad (2)$$

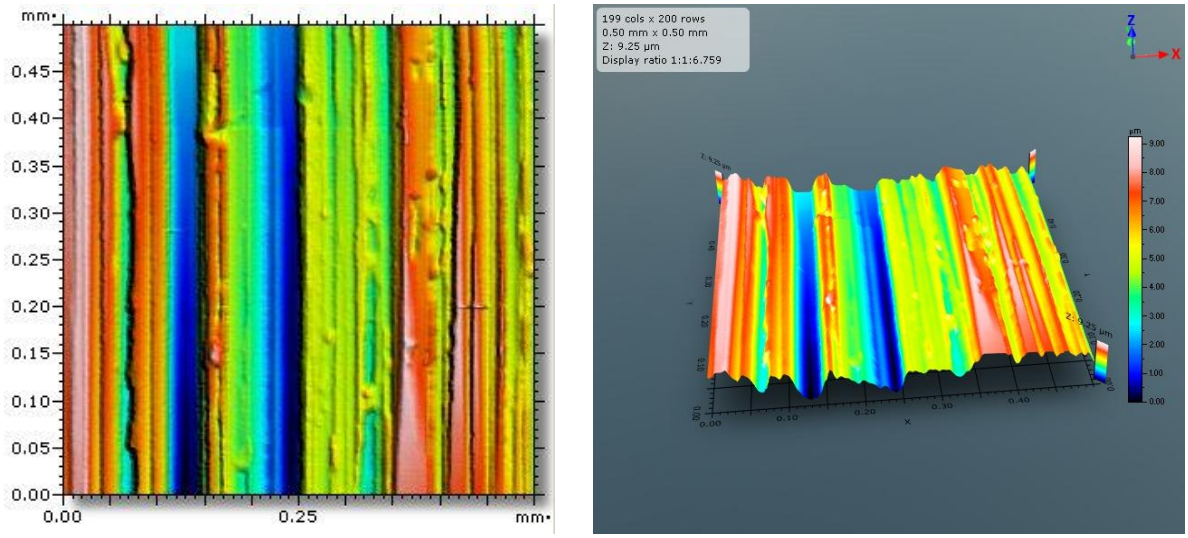
Same of the test specimens where hydrogenated for 96 hours and 192 hours, while others do not [5]. Hydrogenation was done by bubbling sulphured hydrogen into acidulate salt solution.

2.2. 3 D roughness measurement

The characterization of 2D roughness is usually done using among others the R_a parameter. This is easy to define, easy to measure giving a general description of surface amplitude. The parameter is insensitive to small variations in the profile [6]. However, the 2D surface roughness characterization has inherent limitations, as non indication of functional aspects of the surface. The three dimensional techniques give a better understanding of the surface in its functional state [7]. So a 3D roughness study was necessary. This was made with a universal microtribometer (UMT). The results can bee seen in the Figs. 2 – 4 where are presented the aspects of the investigated surfaces.

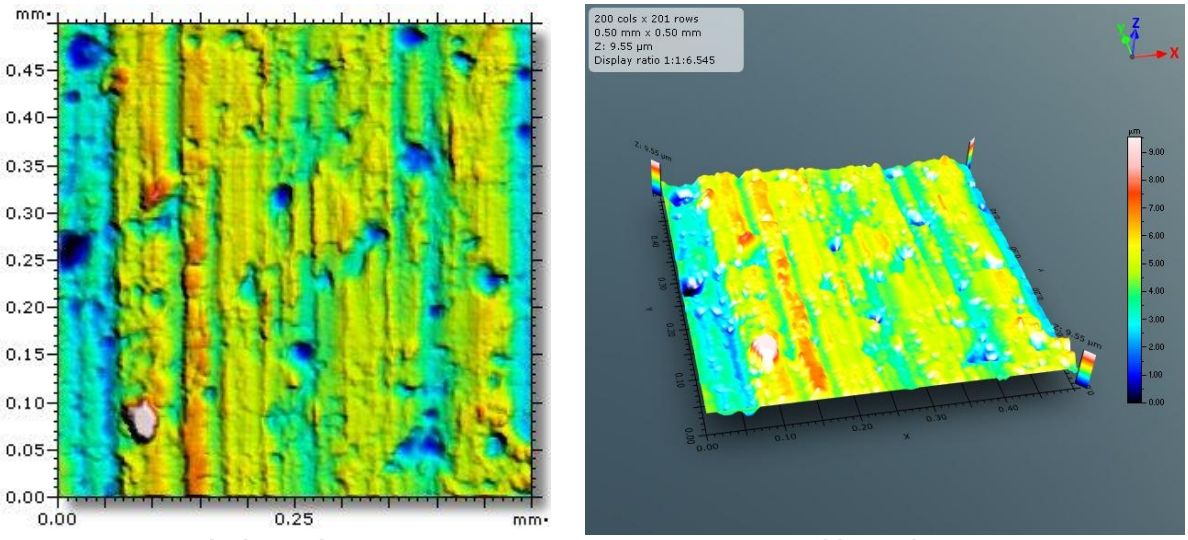
To analyze the surface condition of nonydrogenated and hydrogenated samples was chosen to follow the development of quality parameters at surface irregularities that describe both the height and shape of the surface [8].

The considered surface parameters are: S_a surface average roughness (eq.3), S_{sk} - surface skewness (eq.4) and S_{ku} - surface kurtosis (eq.5).



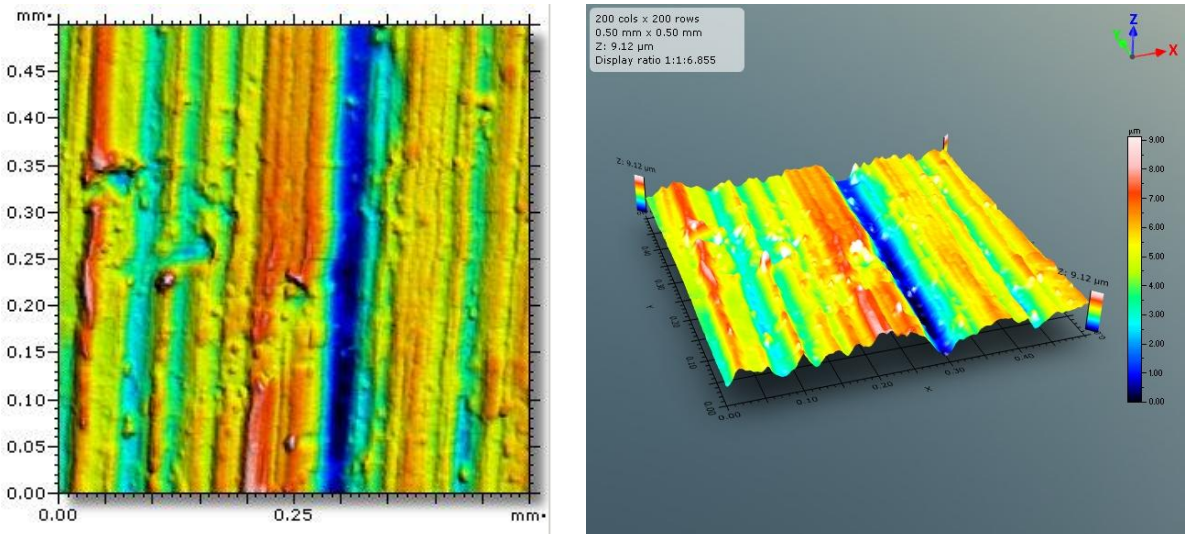
a) plane view ***b) 3D view***

Fig. 2. Non-hydrogenated sample



a) plane view ***b) 3D view***

Fig. 3. 96 hours hydrogenated sample



a) plane view ***b) 3D view***

Fig. 4. 192 hours hydrogenated sample

$$S_a = \frac{1}{MN}\sum_{j=1}^{N}\sum_{i=1}^{M}|z|(x_i, y_j) \tag{3}$$

$$S_{sk} = \frac{1}{MNS_q^3}\sum_{j=1}^{N}\sum_{i=1}^{M} z^3(x_i, y_j) \tag{4}$$

were: S_q root mean square, that is calculated with (5a)

$$S_q = \sqrt{\frac{1}{MN}\sum_{j=1}^{N}\sum_{i=1}^{M} z^2(x_i, y_j)} \tag{4a}$$

$$S_{ku} = \frac{1}{MNS_q^4}\sum_{j=1}^{N}\sum_{i=1}^{M} z^4(x_i, y_j) \tag{5}$$

In equations 3, 4, 5: M is the number of columns on the surface and N the is the number of rows on the surface. Their vales can be seen in Figs. 2 – 4.

As concerning S_a, it is considered not to be a significant parameter in surface characterization. *Sq* instead is a much more statistically significant parameter.

The S_{sk} parameter is the measure of the profile symmetry about the mean plane. The direction of the skew is dependent on whether the bulk of the material is above the mean plane (negative skew) or below the mean plane (positive skew). This parameter is very useful because make a difference between two surfaces having the same S_a value.

As an example a good bearing surface have a negative skew. A positive skew is obtained because of the lack of deep valleys. Surfaces with a positive skewness can be turned surfaces that have high spikes above the mean plane. For a Gaussian surface that has symmetrical topography, the skewness is zero. The S_{sk} parameter correlates well with load carrying ability and porosity.

The correlation between the value of S_{sk} and the surface shape is shown in Fig. 5 [9].

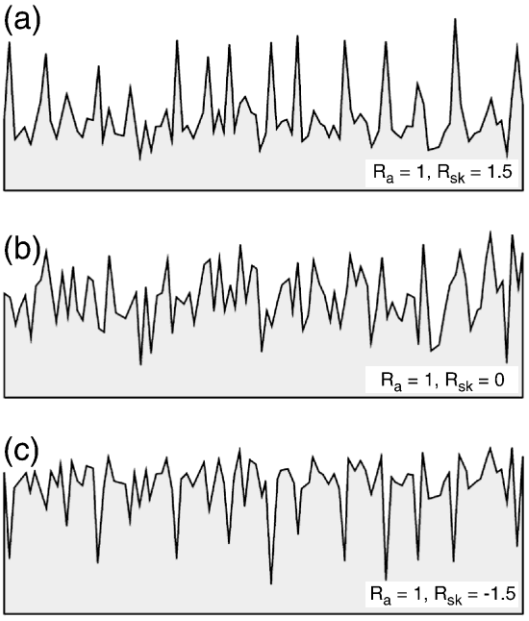


Fig. 5. Three surface with different skewness parameters and equal R_a roughness [9]

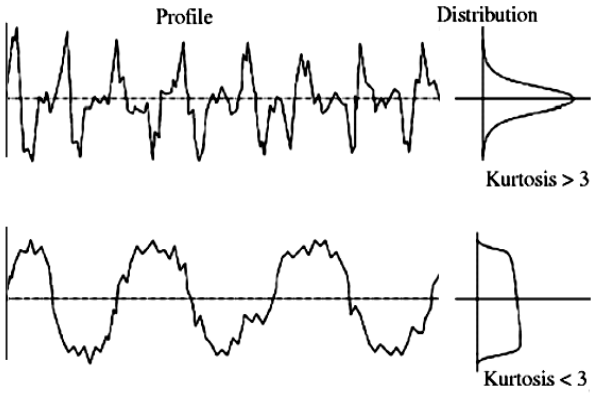


Fig. .6. Two surface with different kurtosis parameters [6]

The *Sku* parameter is a measure of the sharpness of the surface height distribution and characterized the spread of the height distribution. A Gaussian surface has a kurtosis value around three as in Fig. 6. In opposition with *Ssk* this parameter, the *Sku* parameter can indicates of the spikiness of the area: high kurtosis value signify a spiky surface and a low kurtosis value a bumpy surface. This parameter is very useful in predicting the wear behavior and the retention of lubricant. As an important observation that kurtosis cannot differentiate between a picks and a valley [6].

The calculated values of the: S_a, S_{sk} and S_{ku} parameters are presented in table 1. With the results were obtained the graphs shown in Figs. 7-9.

Table 1 The surface parameters values vs. hydrogenation time

Surface parameter	Hydrogenation time [h]		
	0	96	192
Sa	1.6	0.89	1.12
Ssk	-0.432	-0.214	-0.823
Sku	2.618	4.043	3.76

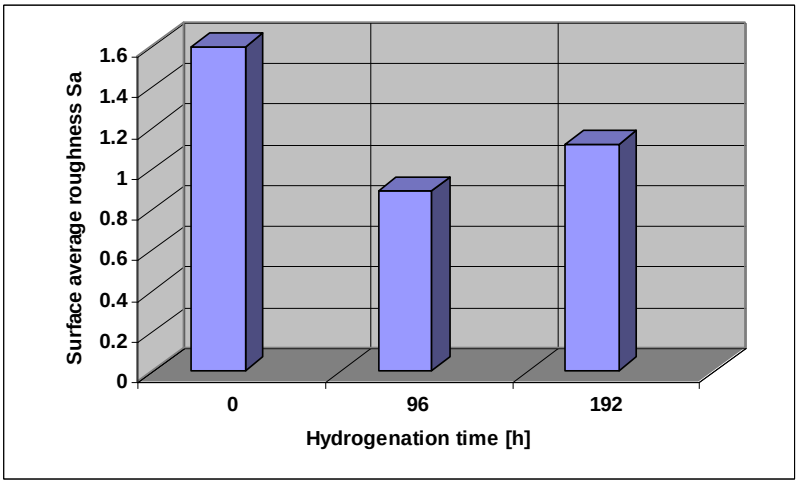


Fig. 7. The surface average roughness S_a values vs. hydrogenation time

Looking at the graph in Fig. 7 it can be seen that hydrogenation leads to lower S_a roughness values.

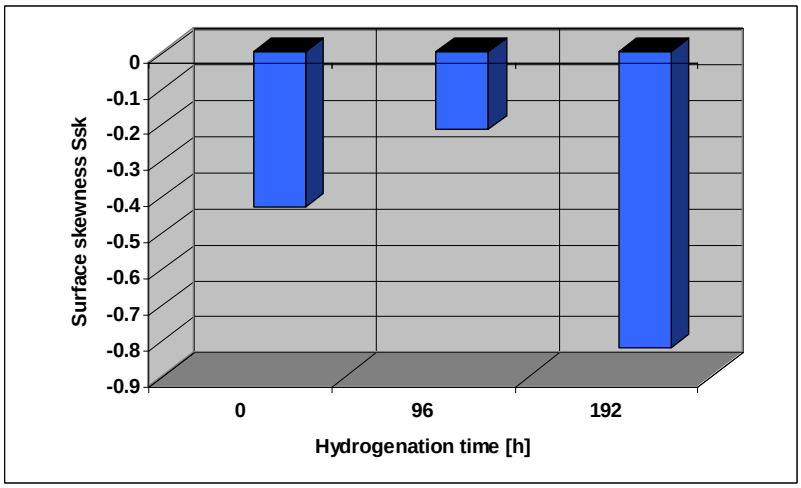


Fig. 8. The surface skewness S_{sk} values vs. hydrogenation time

The graph in Fig. 8 by negative values of the skewness suggests that the roughness profile is intermediate to those shown in Figs. 5b and 5c.

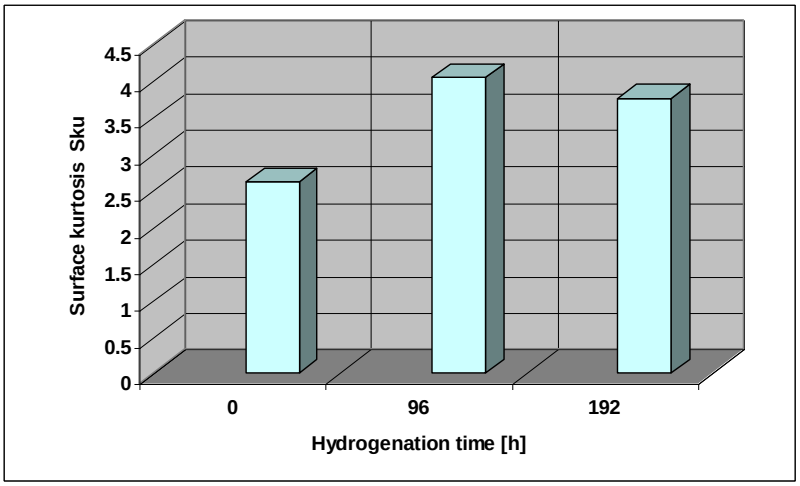


Fig. 9. The surface kurtosis S_{ku} values vs. hydrogenation time

Values of the surface kurtosis in Fig. 9 shows that for nonhydrogenated sample the roughness has a non-Gaussian distribution, while for the hydrogenated samples is a Gaussian one, as shown in Fig. 6.

3. CONCLUSIONS

From the measurements of 3D roughness is noted that for nonhydrogenated samples, the surface profile is net, obvious and continuous edged, whereas hydrogenated samples presenting a softer surface profile, edges being interrupted by numerous discontinuities.

The presence of surface discontinuities may be attributed to the contamination of the sample surface with various compounds (particularly oxides) which characterizes the corrosion generated by the hydrogenation process.

The surface parameters like: average surface roughness**,** surface skewness and surface kurtosis are very useful for characterizing the roughness profile and its distribution.

REFERENCES

1. GIBALA, R., HEHEMANN, R. F.(eds), Hydrogen embrittlement and stress corrosion cracking, Metals Park, Ohio : American Society for Metals, ©1984.
2. MILLION, A., MILLION, C., L'hydrogène dans les aciers et dans les joints soudés, Les Editions Dunod, Paris, 1971.
3. RYTIROVA, L., Étude de la dégradation par l'hydrogène des aciers microalliés et duplex. Influence de la microstructure, École Centrale, Paris, Ph.D. Thesis, 2006, (http://thesis.sangoru.com/these_docs/table_matieres_LR_these.pdf).
4. ***, NACE Standard TM0284, Evaluation of Pipeline and Pressure Vessel Steels for Resistance to Hydrogen-Induced Cracking, 2003.
5. TELETIN, C., Studies and researches on the presence of hydrogen in the steel continuous casting process, Ph.D. Thesis, Galaţi, 2009.
6. DAVIM, J.P. (ed), Surface Integrity in Machining, Springer-Verlag, London Limited, 2010.
7. ***,Guide for the Measurement of Smooth Surface Topography using Coherence Scanning Interferometry, (http://publications.npl.co.uk/npl_web/pdf/mgpg108.pdf, August 2013).
8. ***, Surface Texture (Surface Roughness, Waviness and Lay) ASME B46.1-2002.
9. PATEL, K., DOYLE, C.S., YONEKURA, D., JAMES, B.J., Effect of surface roughness parameters on thermally sprayed PEEK coatings, Surface and Coatings Technology **204** (21-22), 2010, pp. 3567-3572.

CORRESPONDENCE

Constantin SPÂNU
"Dunărea de Jos" University of Galați, Str. Domnească, nr. 47, 800008 – Galaţi, ROMANIA
e-mail: constantin.spanu@ugal.ro

Tribological Journal BULTRIB, **Vol. IV, 2014**
Papers from the International Conference **BULTRIB '13**
October 24-26, 2013, Sofia
Society of Bulgarian Tribologists
Technical University of Sofia

QUALITY OF ELECTRON BEAM WELDED CHARPY SPECIMENS

Ina YANKOVA

Abstract: *This paper reports results connected with the quality of electron beam welded joints. reconstitution of the Charpy specimens by electron beam welding technology. Material used in this study is reactor pressure vessel steel with thickness 10mm. Visual inspection, radiographic testing and metallographic analysis were conducted.*

Key Words: *EBW, imperfections, Charpy specimen*

ОЦЕНКА НА КАЧЕСТВОТО НА ЗАВАРЕНИ ЧРЕЗ ЕЛЕКТРОННО ЛЪЧЕВО ЗАВАРЯВАНЕ ШАРПИ ОБРАЗЦИ

Ина ЯНКОВА

Резюме: *В настоящата работа е оценено качеството на заварени съединения, чрез електронно лъчево заваряване. За изследването е използвана ниско въглеродна реакторно корпусна стомана с дебелина 10mm. Проведени са визуален радиографичен безразрушителен контрол и металографски анализ.*

Ключови думи: *ЕЛЗ, несъвършенства, образци тип "Шарпи"*

1. ВЪВЕДЕНИЕ

Развитието на ядрената енергетика поставя на преден план въпросите, свързани с осигуряването на безопасна и надеждна експлоатация на ядрените реактори. Ресурсът на всеки енергоблок на АЕЦ, се определя от ресурса на корпуса на реактора, защото неговата подмяна е технически много сложна и икономически неоправдана. За оценка степента на окрехкостяване на метала на корпуса на реактора се провеждат серия от динамични изследвания на образци тип Шарпи. Количество образци-свидетели, предварително заложени в реакторите ограничено, за увеличаване на информацията от тях се прилага възстановяване след първоначалното им разрушаване. Важността на проблема на възстановяване на образци за динамични изпитания тип “Шарпи” е наложило разработването на специален стандарт на ASTM E1253-07 A Standard Guide for Reconstitution of Irradied Charpy Specimens [1]. В стандарта са заложени основните изискания свързани, както с подготовката, така и със самият технологичен процес на заваряване при възстановяване на образци тип “Шарпи”. Съгласно ASTM E1253-07, при възстановяване на образци - свидетели, чрез електроннолъчево заваряване трябва да се осигури пълно проваряване на образеца (т.е. дълбочина на шева не трябва да бъде по малка от 10mm), като температурата в централна му част, на разстояние 2mm от повърхността (точка С, на фиг.1) на надреза не трябва да превишаваща 300°С, през целият процес на заваряване. В заваръчния шев и зоната на термично влияние не е допустимо наличието на несъвършенства, нарушаващи хомогенността на завареното съединение.

При ЕЛЗ, както и при другите методи се наблюдават несъвършенства при формиране на шева и отклонения от формата му. Наред с тях, при ЕЛЗ възникват типични за процеса несъвършенства [2, 3]: несъвършенства в корена на шева, непостоянна дълбочина на провара, продълговати кухини в обема на шева, пукнатини в средата на заваръчния шев, отклонение на геометрията на шева от типичната ‘’кинжална” форма.

Несъвършенствата в завареното съединение могат да бъдат установени чрез различни безразрушителни изпитвания. Радиографичният и ултразвуковият методи са най-подходящи за установяване на наличие на пори и пукнатини [3, 4, 5].

Целта на тази работа е да бъде оценено качеството на заварените съединения във възстановени чрез електронно лъчево заваряване (ЕЛЗ) образци.

2. ЕКСПЕРИМЕНТАЛНА ПРОЦЕДУРА

2.1. Изследван материал и апаратура

За изследванията е използвана реакторно корпусна стомана 15Х2НМФА от системата Cr-Ni-Mo-V. Това са топлоустойчиви, нисколегирани стомани с повишена механическа якост при високи температури и продължителни постоянни натоварвания.

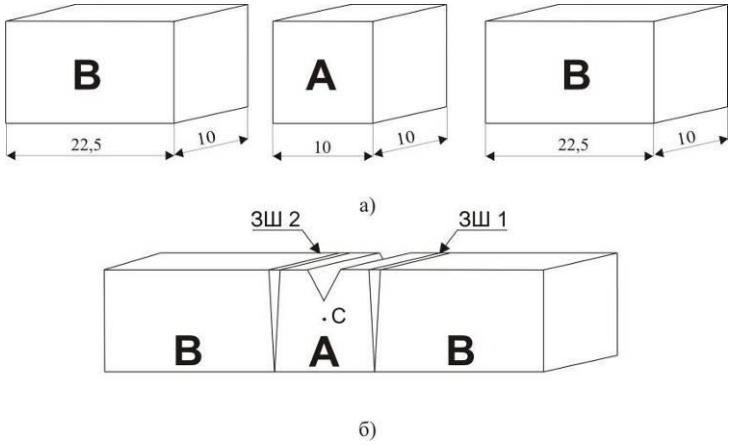
Заваряването е проведен на инсталация за електроннолъчево заваряване тип ESW300/60-15 произведена от фирмата Leybold – Heraeus в Института по електроника при БАН при следния технологичен режими: ток на електронния сноп – I =50mA, мощност на електронния сноп - в диапазон от 3-15kW при ускоряващо напрежение 60kV; (P=U.I); скорост на преместване на XY координатна маса V = 10mm/s; ток на фокусиращата система If= 497mA [8].

За безразрушителния контрол е използвано следното оборудване: Рентгенов дефектоскоп, мод.”Eresco 200/8” – Seifert – Germany; Система за дигитална радиография с детектор полугъвкави плаки (CR) - Това е нова технология за радиографичен контрол. Детекторът е фосфорен слой, нанесен на полугъвкава основа – плака. Подобно на филмовата радиография, изображението не се създава директно, а чрез междинна фаза – скрито (латентно) изображение. Преимуществата на дигиталната радиография са: по-малки експозиции, по-малки разходи за консумативи, възможност за подобряване на изображението и условията за архивиране [5].

След провеждане на експериментите на възстановените образци, са изготвени металографски шлифове. За проявяване на макроструктурата е използване 4% разтвор на HNO_3 в етанол. Геометричните характеристики са измерени с помощта на оптичен металографски микроскоп Neophot–2, Olympus GX41 и софтуер за анализ на изображението.

2.2. Схема на опитната постановка

На Фиг.1 е показана схема на съставен образец тип “Шарпи”, състоящ се от централна част А и две допълнителни части /вставки/ В, съединени чрез ЕЛЗ, съответно (ЗШ) 1 и 2. Централната част на образеца е с размери 10x10x10mm, а двете допълнителни части 22,5x10x10mm.



Фиг.1 Схема на възстановен “Шарпи “ образец

При оценка на качеството на заваръчните шевове от един образец, трябва да се има предвид, че за да се оцени качеството на целия образец е необходимо и двата шева да покриват качеството за най висок клас В, съгласно БДС EN ISO 13919-1 [6].

3. РЕЗУЛТАТИ И АНАЛИЗ

За целта на изследването са възстановени дванадесет образци тип “Шарпи”, чрез електронно лъчево заваряване. На образците е направен визуален и радиографичен безразрушителен контрол. Радиографичният контрол е направен съгласно БДС EN ISO 17636-1:2013 по технология отговаряща на клас В – подобрена технология [5, 9]. При пролъчвана дебелина 10mm е използвано рентгеново лъчение с напрежение 170kW. Избраната за

технология клас В филмова система, е клас С4. Оптическата плътност на радиограмите е по-голяма от 2,3, а стойността на качеството на полученото изображение определено със жичков ИКИ е над W14, което покрива условията на подобрена технология - клас В. С цел увеличаване на информацията е направено и пролъчване по дължина на шевовете.

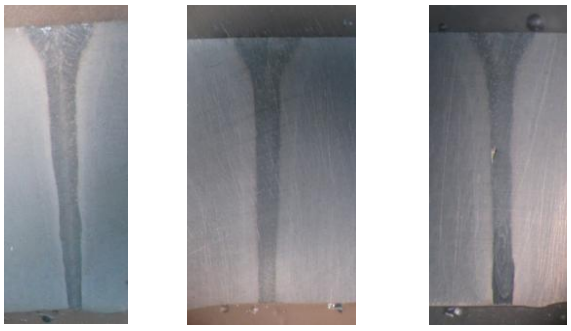
За оценка на качеството на заварени съединения при електроннолъчево заваряване има отделен стандарт: БДС EN ISO 13919-1 „Заваряване. Електроннолъчево и лазерно заварване на съединения. Ръководство за нивата на качество според несъвършенствата. Част 1: Стомана" [6]. Несъвършенствата които са обект на оценка в БДС EN ISO 13919-1 [6], както и означенията им по БДС EN ISO 6520-1 [7] са дадени в табл.1.

Табл.1 Групи несъвършенства при ЕЛЗ обект на оценка в БДС EN ISO 13919-1

Означение по БДС EN ISO 6520-1	Несъвършенства при ЕЛЗ, които се оценяват по БДС EN ISO 13919-1	Означение по БДС EN ISO 6520-1	Несъвършенства при ЕЛЗ, които се оценяват по БДС EN ISO 13919-1
100	Пукнатина	**500**	Несъвършена форма и размери
104	Кратерна пукнатина	501	Подрез
200	Кухина	5011	Подрез -непрекъснат
2013	Групирана пористост	5012	Подрез -прекъснат
2014	Линейна пористост	502	Излишен метал на шева
202	Всмукнатина	504	Прокапване
2024	Кратер (кратерна лула)	507	Линейно изместване
300	Твърдо включване	509	Хлътване на шева
400	Несплавяване и непълен провар	511	Недозапълване на шева
401	Несплавяване	515	Вдлъбнатост на корена
402	Непълен провар (непровар)	602	Заваръчни пръски

Представени са резултатите от дванадесет образеца с по два заваръчни шева. Образците са изследвани след проведена механична обработка – шлифоване и изработване на надрез, т.е. изработване на образец тип „Шарпи". Нивото на качество съгласно БДС EN ISO 13919-1 и нивото на приемане съгласно БДС EN ISO 10675-1 на заваръчните шевове е представено в табл.2.

При образци №1, 2, 3, 6, 7, 9 ,12 не се наблюдава наличието на несъвършенсва, както на радиограмите, така и на металографските образци (фиг. 2).



Фиг.2 Макроструктура на напречно сечение на ЗШ №1.1, ЗШ №2.1 и ЗШ №3.1



Фиг.3 Макроструктура на напречно сечение на ЗШ №4.1

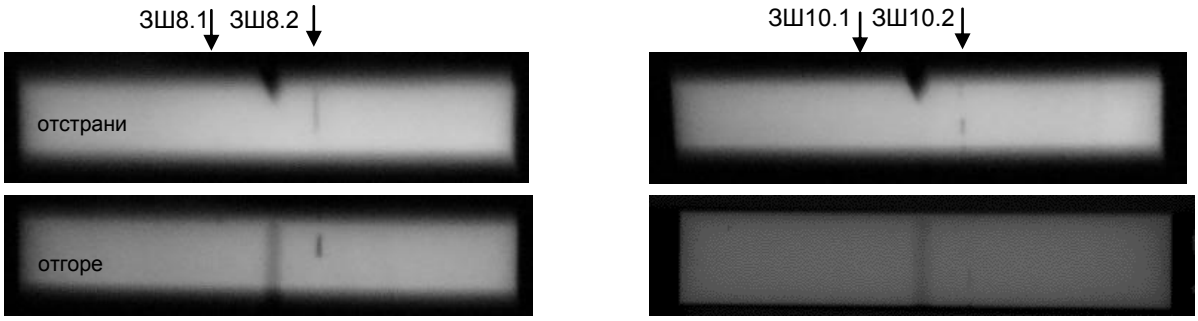
При ЗШ 4.1 на образец №4 се наблюдава несъвършенство в корена на шева – непостоянна дълбочина на провара; по дължината си корена на шева има иглообразна форма. Това се дължи на особеностите на пренос на метала в заваръчната вана, а именно периодичното заливане на парогазовия канал по височината му, което възпрепятства транспортирането на метал през корена на шева (фиг. 3 и фиг. 4). Несъвършенството е с дължина 3,5mm, което според стандарта отговаря на ний-ниско ниво на приемане, което не удовлетворява поставените изисквания.

При образец №5 се наблюдава същото несъвършенство, като дължината му е 5,5mm, което според стандарта не отговаря на никое ниво на приемане. Може да се счита за недопустимо според размерите си несъвършенство (фиг. 4 и фиг. 7).



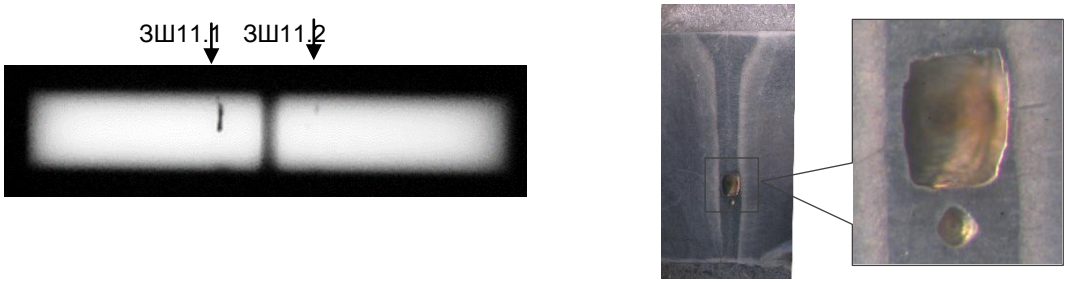
Фиг.4 Радиограми на образци №4и №5

При образци №8 и №10 се наблюдават продълговати кухини в обема на шева, като размерите им отговарят на ниво на качество - С, съгласно БДС EN ISO 13919-1 (фиг.5).



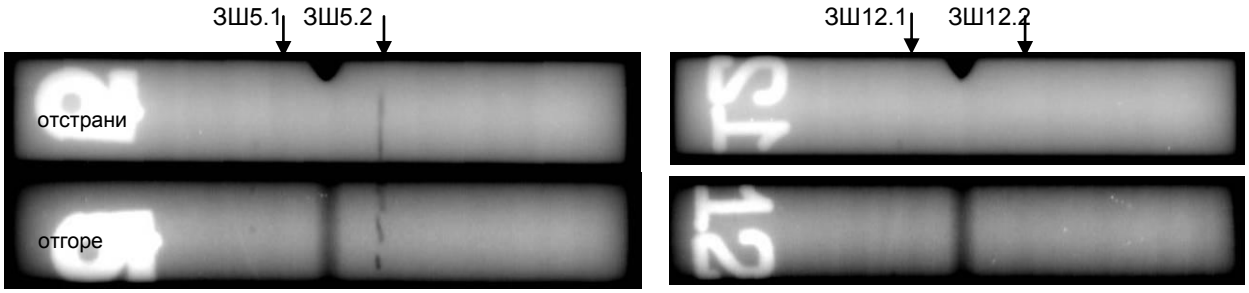
Фиг.5 Радиограми на образци №8 и №10

При образец №11 се наблюдава в ЗШ11.1 продължената кухина в обема на шева. Дължината на несъвършенството обхваща почти половината от ЗШ, което го определя като недопустим.



Фиг.6 Радиограма на образец №11 и Макроструктура на напречно сечение на ЗШ №11.1

Резултатите от металографския анализ в зоната на шева на заварените съединения потвърждават оценката на радиограмите. Показват и съществуването на несъвършенства , които не се виждат добре на радиограмите, като малки пори. С подобряване на качеството на изображението и улесняване на оценката е приложен и дигитален радиографичен контрол на образци №5 и №12. Дигиталните радиограми (фиг.7) са с много по - добър контраст и качество на изображението.



Фиг.7 Радиограми на образци №5 и №12

С проведените изследвания с конвенционални и специализирани технически средства се потвърди оценката от радиографията. Установи се, че за разгледаните заварени съединения с дебелина 10mm, за по прецизно определяне на геометрията на шева и несъвършенствата е необходимо да се прилагат специализирани технически средства.

Табл.2 Нива на качество и приемане на наблюдаваните несъвършенства

№	Наблюдавани несъвършенства съгласно БДС EN ISO 6520-1	Ниво на качество съгласно БДС EN ISO 13919-1	Ниво на приемане съгласно БДС EN ISO 10675-1	№	Наблюдавани несъвършенства с означение по БДС EN ISO 6520-1	Ниво на качество съгласно БДС EN ISO 13919-1	Ниво на приемане съгласно БДС EN ISO 10675-1
1.1	-	B	1	**7.1**	-	B	1
1.2	-	B	1	**7.2**	-	B	1
2.1	-	B	1	**8.1**	-	B	1
2.2	-	B	1	**8.2**	2015	C	2
3.1	-	B	1	**9.1**	-	B	1
3.2	-	B	1	**9.2**	-	B	1
4.1	2011	B	1	**10.1**	-	B	1
4.2	2015	D	3	**10.2**	2015	C	2
5.1	2015	D	3	**11.1**	2015	D	3
5.2	2011	B	1	**11.2**	2011	B	1
6.1	-	B	1	**12.1**	-	B	1
6.2	-	B	1	**12.2**	-	B	1

4. ЗАКЛЮЧЕНИЕ

Анализирани са дефектите в ЗШ и ЗТВ при ЕЛЗ на стомана 15Х2НМФА с дебелина 10mm. Експериментално са потвърдени данните за получаване на типични за електроннолъчево заваряване несъвършенства. От направената оценка на ниво на качество съгласно БДС EN ISO 13919-1 и нивото на приемане съгласно БДС EN ISO 10675-1 се вижда, че по-голяма част от образците отговарят на поставеното изискване за не наличие на несъвършенства във възстановените образци. Заваръчните шевове, при които се наблюдават недопустими несъвършенства принадлежат на един образец и причината за тяхното съществуване може да се търси в неправилно изпълнена технология на заваръчния процес.

БЛАГОДАРНОСТИ

Настоящите изследвания са свързани с проект № BG051PO 001-3.3.06-0046 “Подкрепа за развитието на докторанти, постдокторанти и млади учени в областта на виртуалното инженерство и индустриалните технологии”. Проектът се осъществява с финансовата подкрепа на Оперативна програма „Развитие на човешките ресурси”, съфинансирана от Европейския социален фонд на Европейския съюз.

ЛИТЕРАТУРА

1. ASTM E 1253-07, Standard Guide for Reconstitution of Irradiated Charpy-Sized Specimens, 2007 Annual book of ASTM Standards, Section 12: Nuclear energy (II), Solar and Geothermal Energy, vol. 12.02, pp. 634–637.
2. Назаренко О. К., Кайдалов А. А., Кавбасенко С. Н. И др.; под ред. Б. Е. Патона , Электронно-лучевая сварка – Киев: Наук. думка, 1987
3. ASM Handbook Volume 17: Nondestructive Evaluation and Quality Control, Nondestructive Inspection of Weldments, Brazed Assemblies, and Soldered Joints
4. Radhakrishnan, W.M., Welding Technology And Design, New Age International Ltd., 2007
5. Бъчваров, И., Радиационни методи за неразрушаващ контрол, Контролтест”ООД, София 2010
6. БДС EN ISO 13919-1: Welding - Electrons and laser beam welded joints - Guidance on quality levels for imperfections - Part 1: Steel.
7. БДС EN ISO 6520-1:2007 Заваряване и сродни процеси. Класификация на геометричните несъвършенства в метални материали. Част 1: Заваряване чрез стопяване.

8. Tabakova B., I. Yankova, P. Petrov, Statistical modeling of electron beam welding process for reconstruction of charpy spesimens, Machines Technologies Materials, Issue 8-9, pp.33-36, 2007, (ISSN 1313-0226).
9. БДС EN ISO 17636-1:2013: Non-destructive testing of welds -- Radiographic testing -- Part 1: X- and gamma-ray techniques with film.
10. БДС EN ISO 10675-1:2013: Non-destructive testing of welds - Acceptance levels for radiographic testing - Part 1: Steel, nickel, titanium and their alloys

КОРЕСПОНДЕНЦИЯ

Ина Янкова
Технически Университет –София
Машинни-технологичен факултет, катедра Материалознание и технология на материалите
iyankova@tu-sofia.bg

Tribological Journal BULTRIB, **Vol. IV, 2014**
Papers from the International Conference **BULTRIB '13**
October 24-26, 2013, Sofia
Society of Bulgarian Tribologists
Technical University of Sofia

CHARACTERIZATION OF CERAMIC LAYERS PRODUCED BY PLASMA TRANSFERRED ARC PROCESS

Tatiana SIMEONOVA
Department of Materials Science and Technology, Technical University – Sofia, Bulgaria

Abstract: *Oxide ceramic coatings on S275JR non-alloy structural steel substrate were produced using plasma transferred arc (PTA) scanning process. Coatings were carried out by preplaced powder method using pure ceramic powders (Al_2O_3 and Cr_2O_3) and a mixture of Ni-Al_2O_3 and Ni-Cr_2O_3 powders and a binder, painted over the substrate. Microstructural characterization studies were carried out by optical and scanning electron microscopy (SEM) with energy dispersive X-ray energy spectrometer (EDS). Wear resistance experiments were conducted using pin on disk wear test apparatus.*

Key Words: *ceramic, layers, PTA process, microstructure, wear*

1. INTRODUCTION

In the recent years a lot of investigations, considering different surfacing techniques were carried out in order to improve surface properties of the materials. Most of these techniques involve high concentrated energy sources for producing coatings with fine microstructure and enhanced mechanical and tribological properties without affecting seriously the properties of the substrate material. Ceramics, such as alumina, zirconia, cordierite, etc., offer cost-effective alternative to modify the component surface properties and are used in a wide range of industrial applications, primarily for wear resistance, thermal barrier and corrosive environment [1]. In this respect there has been considerable interest in the use of ceramic powders with different overlaying methods such as plasma spraying [2-8], laser cladding and remelting [9-11] and plasma transferred arc processing [12-13] for their extremely high temperature, which is essential for dealing with feedstock like oxide and carbide ceramics, whose melting temperature is very high [2]. Hou et al. showed the beneficial effect of nano-Al_2O_3 particles on the microstructure and wear resistance of a nickel-based alloy coating deposited by plasma transferred arc (PTA) [12]. Wang et al. investigated the effect of three nano-particles additions (Al_2O_3, SiC, CeO_2) on the high temperature wear behavior of a Ni-based alloy coatings produced by laser cladding technique and reported that the addition of these nanoparticles increased the wear resistance of the coatings [9]. The effect of incorporation of nano-ZrO_2 particles in a Ni matrix has been studied by Fernandes et al. and the results show that hardness and wear behavior of coatings was improved with nanostructure zirconia additions while the friction coefficient is decreased [2].

Among these processes PTA surfacing process is characterized by extremely high temperature, excellent arc stability, low thermal distortion of the part, and high coating speeds and so it is widely used for the surface treatment of materials. Although, there is a lack of investigations taking in consideration the use of PTA process for production of alumina and chromia layers. And since these are ceramic materials of high level of hardness, wear and oxidation resistance, its use as reinforcement material in nickel-based coatings deposited by PTA processes should be investigated.

In this context the aim of present work is to study the possibility of obtaining oxide ceramic coatings on S275JR non-alloy structural steel substrate using preplaced powder method and subsequent plasma transferred arc (PTA) scanning process.

2. EXPERIMENTAL PROCEDURE

2.1. Materials and PTA overlaying

The analyzed ceramic coatings were carried out by preplaced powder method, where the filler material is pasted as slurry over the substrate and subsequent plasma transferred arc scanning. S275JR non-alloy structural steel plates of 100x100x4 mm in dimension were used as substrate

material. The filler material slurry was made by mixing pure oxide ceramic powders (Al_2O_3 and Cr_2O_3) and a mixture of Ni-Al_2O_3 and Ni-Cr_2O_3 powders with a 20% sodium silicate solution in water as a binder. Chemical composition of coating materials and substrate are presented in table 1 and table 2, respectively.

Table 1. Composition of coating materials

Coating material	***PA***	***PAN***	***PC***	***PCN***
Al_2O_3	100 wt%	50 wt%	-	-
Cr_2O_3	-	-	100 wt%	50 wt%
Ni	-	50 wt%	-	50 wt%

Table 2. Composition of substrate materials

	C	***Mn***	***P***	***S***	***N***	***Cu***
S275JR non-alloy structural steel	0.22	1.5	0.04	0.04	0.012	0.55

The plates were then covered with so prepared slurry and heated up to 90°C for 30 min in order to dry out the moisture. The resulting thickness of pasted filler material was about 1.3-1.5 mm. The specimens were then mounted on a cooper plate and scanned with the plasma arc to melt the coating layer and the upper surface of the substrate forming metallurgical bond between them. Schematic drawing of the plasma transferred arc scanning process is presented in previous investigations [15]. Four different sets of experiments were done with varying the composition of coating material (refer to table 1). Main PTA overlaying parameters used for layer preparation are: Scanning current I=85 A, Scanning speed V=85 mm/min, Plasma gas flow rate (Ar) – 8.0 l/min, Shield gas flow rate (Ar) – 5 l/min. The parameters of the PTA process were chosen so as to provide sufficient thickness and formation of the coating layers. Overlays were produced and cooled under Ar atmosphere. All analyzed coatings were deposited in one pass.

2.2. Layer characterization

Metallographic preparation of coated surfaces for examination involved preparing transverse sections by grinding and polishing up to 1 μm diamond paste and then etching the specimens with 2% HNO_3 solution in ethanol. Overlay characterization included microstructural analysis on the transverse section of specimens by optical (OM) and scanning electron microscopy (SEM), using the secondary electron and backscattered imaging mode. Chemical composition identification of a certain points of overlaid coatings was performed in SEM by energy dispersive X-ray microanalysis (EDS).

2.3. Pin on disk testing

Wear resistance experiments were conducted using pin on disk wear test apparatus with parameters, listed in table 3. The pin-on-disk testing machine consists of rotating disk whereon the abrasive paper (cloth) is fixed. The tested specimen is fixed in the holder and pressed against the abrasive cloth. Schematic drawing of the testing process is presented in a previous investigation [16]. The weight loss was measured by the WPS 180/C/2 electronic balance with the precision of 0.01 mg.

Table 3. Wear testing parameters

Parameter	***Value***	***Units***
Nominal contact are, A_a	2.5	cm^2
Specimen shape	square 158x158	mm
Nominal contact pressure, p_a	4.12	N/cm^2
Average sliding velocity, V	22	cm/s
Sliding distance, S	110	m

3. RESULTS AND DISCUSSIONS

3.1. Microstructural characterization

Four different layers were produced by changing the coating material from using pure ceramic powders (Al_2O_3 and Cr_2O_3) and a mixture of Ni-Al_2O_3 and Ni-Cr_2O_3 powders. Visual inspection of Al_2O_3 and Cr_2O_3 coatings showed poor formation of the layers with a lot of welding defect, such as pores, cracks and even zones without layer formation. These defects led to the exclusion of these specimens

(PA and PC) from further characterization. Addition of Ni to form a mixture of Ni-Al_2O_3 and Ni-Cr_2O_3 powders, led to the formation of better coatings with much smaller amount of welding defects.

Fig. 1 and 2 shows the optical micrograph of Ni-Al_2O_3 and Ni-Cr_2O_3 respectively. It can be seen that the cross section of the obtained samples can be generally divided into deposited coating and substrate. Microstructural analysis on the transverse section of specimens by optical (OM) microscopy revealed the presence of Widmanstätten-like morphology formed in the fusion zone between substrate and coating layer for both specimens. The coating layer is well bonded to the substrate without cracks and porosities in the interface zones, as can be seen in fig. 1 and fig. 2.

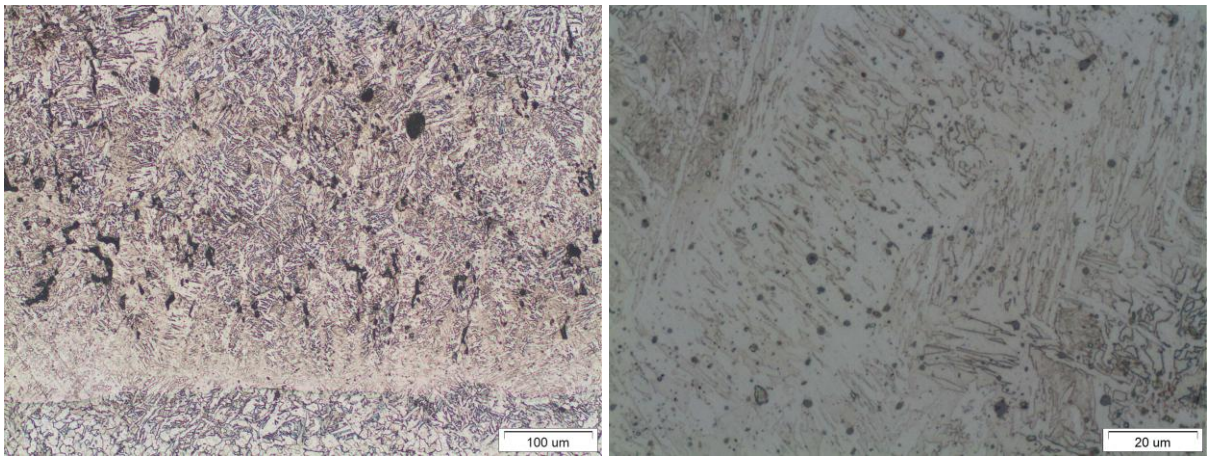


Fig. 1. Microstructure of PCN layer

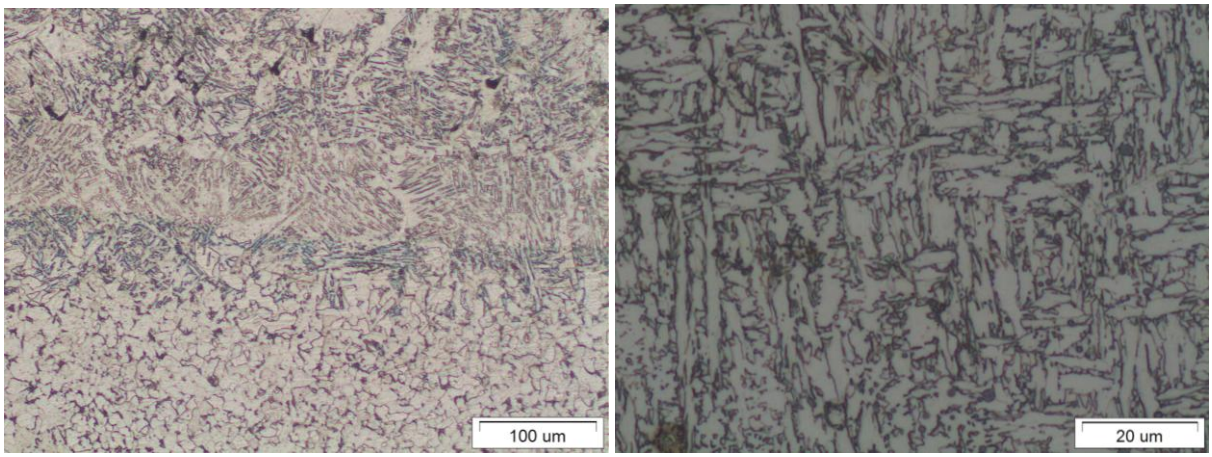


Fig. 2. Microstructure of PCN layer

More details about the microstructure of the deposited coatings can be obtained by SEM analysis. Scanning electron microscopy (SEM), using backscattered imaging mode revealed the formation of (Fe,Ni) solid solution dendritic phase and interdendritic precipitates, which are considered to be Al_2O_3 (for PAN layer) and Cr_2O_3 (for PCN layer). Chemical composition identification of a certain areas of overlaid coatings which was performed in SEM by energy dispersive x-ray microanalysis (EDS) revealed also the presence of some silicium oxides, formed in the upper surface zones of the layers. It was also cleared that a high dense concentration of ceramic particles are situated mainly in the upper layer of the coatings, where some pores and micro cracking are also observed (fig 3 and fig.4).

Because of the high temperature of the plasma transferred arc some of the Al_2O_3 and Cr_2O_3 particles are expected to be decomposed into Al, Cr and O atoms. Nevertheless, the other particles could not be decomposed and are expected to be found preserved in the deposited coatings because the cooling rate of the PTA treatment was quick [12, 13]. This is proved by EDS analysis in SEM, which revealed particles rich in Cr and O for PCN coating and in Al and O for PAN coating. Therefore, the Al_2O_3 and Cr_2O_3 phases could be indexed more precisely by XRD analysis, which will be part of a future investigation. Though some Cr atoms exist in the Ni-Cr_2O_3 coating, carbides could not be formed in this coating, because the tested substrate contained low carbon [13].

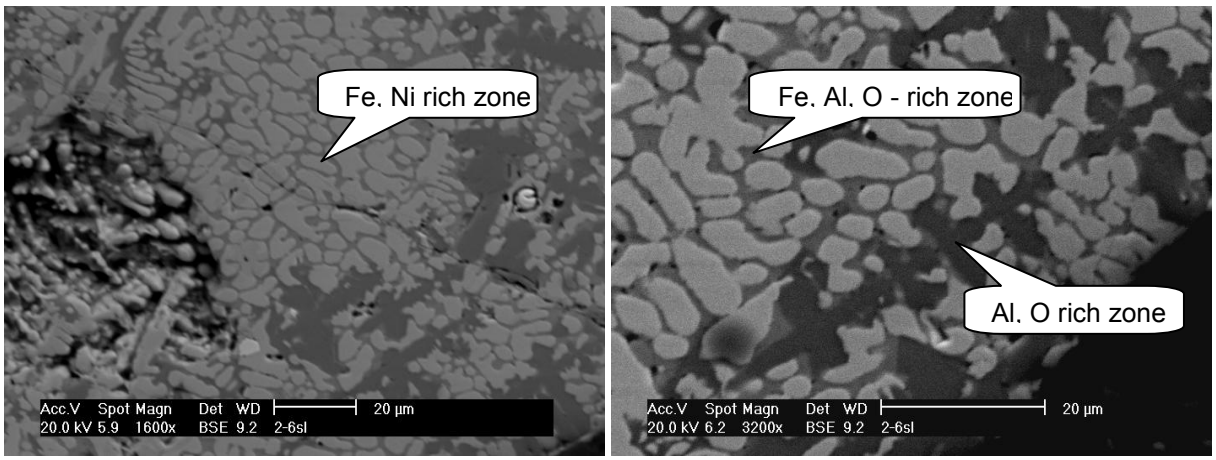


Fig. 3. SEM images of PAN layer

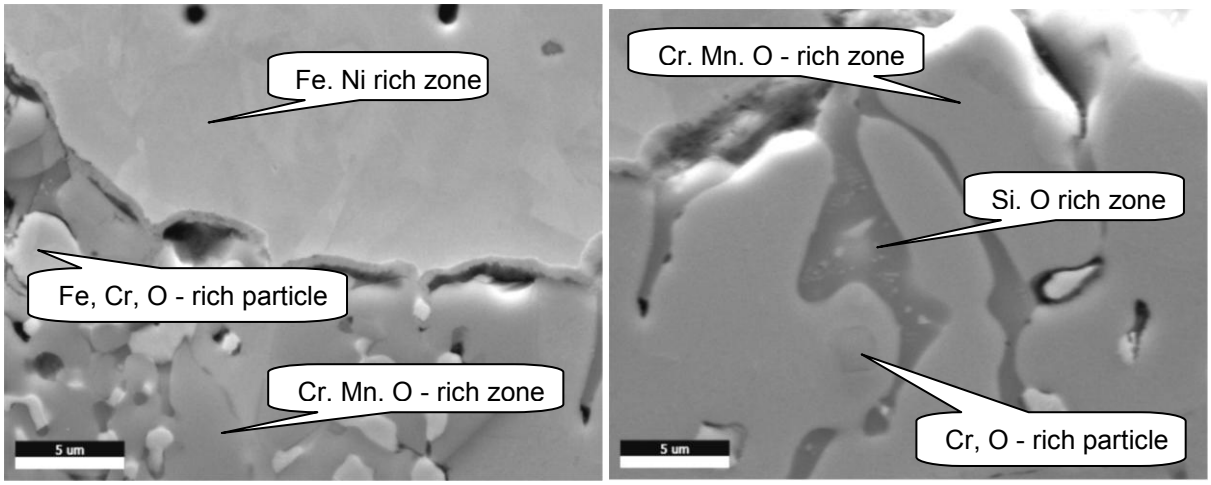


Fig. 4. SEM images of PCN layer

The spinel compound $NiAl_2O_4$ could be expected based on a previous investigations [11]. Also both α and γ phases of Al_2O_3 are suspected to be present in PAN coating [14].

EDS analysis in SEM has shown that high density concentration of the alloying elements is observed in a thin surface layer on the top of a specimens which decreases in the fusion zone direction. In this respect the formation of a kind of an intermediate Ni based layer between steel substrate and high dense oxide surface layer of the ceramic coatings is observed. And the elemental mapping has proven homogenous distribution of aluminum and oxygen (PAN specimen) and chromium and oxygen (PCN specimen) through the dept of that intermediate layer.

3.2. Wear characterization

Pin on disk test results are listed in table 4. As it could be seen Ni-Al_2O_3 layer shows less mass loss and wear loss rate than Ni-Cr_2O_3 layer. This could be due to the higher hardness of alumina compared to the chromia. It is also obvious that the mass loss of PAN coating is more than two times lower than the substrate material (fig.5).

Table 4. Abrasive wear results

Coating material	***PAN***	***PCN***	***Substrate***
Mass loss, mg	28.2	37.4	64.1
Wear loss rate, mg/min	12	15.6	27.5

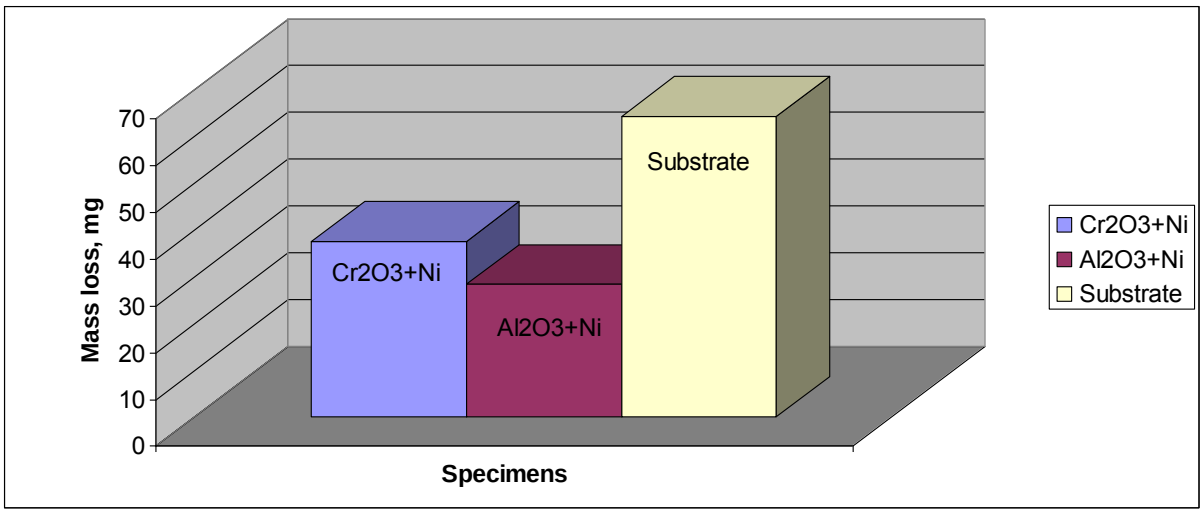


Fig. 5. Mass loss results

Fig. 6 shows the abrasive wear resistance of the deposited coatings. It can be seen that abrasive wear resistance of Ni-Al_2O_3 coatings is higher than Ni-Cr_2O_3 coating. Both coatings have higher wear resistance than the substrate material. This could be due to the fact that undecomposed oxide particles blocked dislocation movement and contributed to the increase of wear resistance [13].

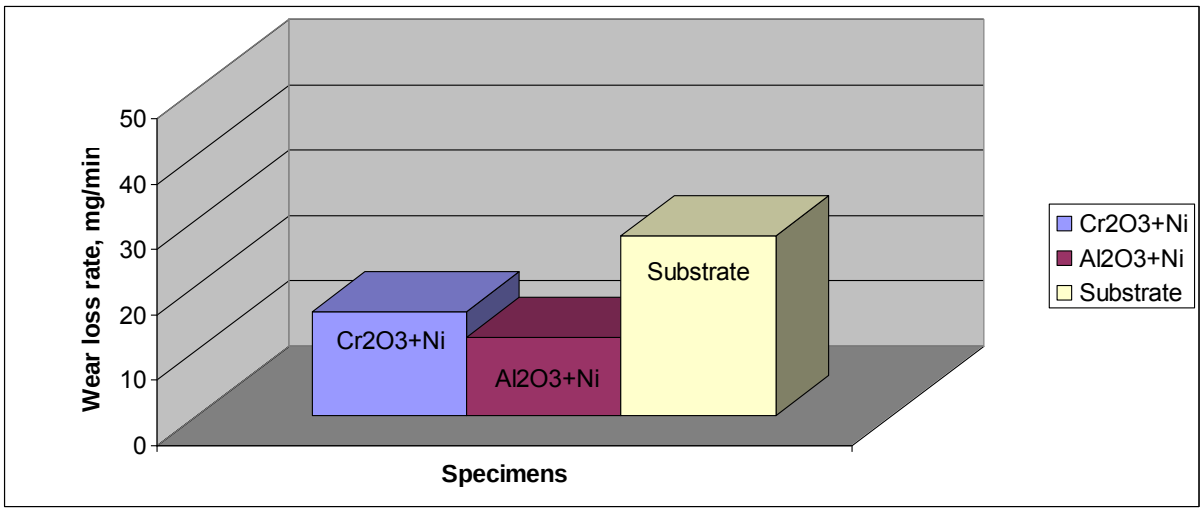


Fig. 6. Wear loss rate results

Among the investigated Ni-Al_2O_3 and Ni-Cr_2O_3 coatings, a maximum resistance against abrasion was provided by the Ni-Al_2O_3 coating. Although none of the coatings could improve significantly the abrasive resistance of steel for the given sliding distance of 110m. However, the outcome of the study would help in designing and developing ceramic coatings for abrasive wear applications.

4. CONCLUSION

Described plasma transferred arc technology is a promising technique for producing ceramic layers on plain carbon steel

A typical solidification structure for PTA overlaying is obtained, consisting of (Fe,Ni) solid solution dendritic phase and interdendritic precipitates, based on oxides.

The investigation has revealed that a high dense concentration of ceramic particles are situated mainly in the upper layer of the coatings, where some pores and micro cracking are also observed

Al_2O_3 based layer showed slightly higher wear resistance, than Cr_2O_3 based coating, which is considered to be due to higher hardness of Al_2O_3 particles

ACKNOWLEDGMENTS

The author wish to express special thanks to Prof. Rumen Petrov for assistance in SEM observation and Prof. Mara Kandeva for abrasive wear resistance tests.

REFERENCES

1. GAO, Y., XU, X., YAN, Z., XIN, G., High hardness alumina coatings prepared by low power plasma spraying, Surface and Coating Technology, **154** (2002), pp.189–193.
2. FERNANDES, F., RAMALHO, A., LOUREIRO, A., GUILEMANY, J.M., TORRELL, M., CAVALEIRO, A., Influence of nanostructured ZrO_2 additions on the wear resistance of Ni-based alloy coatings deposited by APS process, Wear, http://dx.doi.org/10.1016/j.wear.2013.04.012
3. WANG, C., FAN, L., FAN, J., ZHANG, D., WANG, H., Effect of spraying power on microstructure and properties of supersonic plasma sprayed Al_2O_3 coating on porous Si_3N_4 substrate, Journal of Alloys and Compounds, **559** (2013), 152–157
4. YINA, Z., TAOA, S., ZHOUA, X., Effect of the thickness on properties of Al_2O_3 coatings deposited by plasma spraying, Materials characterization, **62** (2011) 90–93
5. MATTHEWS, S., TALIANA, F., JAMES, B., Heat treatment of plasma-sprayed Al_2O_3 and Al_2O_3–WO_3 coatings between 500 and 1000 °C, Surface & Coatings Technology, **212** (2012) 109–118
6. SARAFOGLOU, CH., PANTELIS, D., BEAUVAIS, S., JEANDIN, M., Study of Al_2O_3 coatings on AISI 316 stainless steel obtained by controlled atmosphere plasma spraying (CAPS), Surface & Coatings Technology, **202** (2007) 155–161
7. TAO, S., YIN, Z., ZHOU, X., DING, C., Sliding wear characteristics of plasma-sprayed Al_2O_3 and Cr_2O_3 coatings against copper alloy under severe conditions, Tribology International, **43** (2010), 69–75
8. YANG, K., ZHOU, X., ZHAO, H., TAO, S., Microstructure and mechanical properties of Al_2O_3–Cr_2O_3 composite coatings produced by atmospheric plasma spraying, Surface & Coatings Technology, **206** (2011) 1362–1371
9. WANG, H., ZUO, D., WANG, M., SUN, G., MIAO, H., SUN, Y., High temperature frictional wear behaviors of nano-particle reinforced NiCoCrAlY cladded coatings, Trans. Nonferrous Met. Soc. China, **21** (2011), 1322-1328.
10. GAO Y., WANG C., YAO M., LIU H., The resistance to wear and corrosion of laser-cladding Al_2O_3 ceramic coating on Mg alloy, Applied Surface Science, **253** (2007), 5306–5311
11. GAO, X., TIAN, Z., LIU, Z., SHEN L., Interface characteristics of Al_2O_3-13%TiO2 ceramic coatings prepared by laser cladding, Trans. Nonferrous Met. Soc. China, **22** (2012), pp. 2498-2503
12. HOU, Q.Y., HUANG, Z., WANG, J.T., Influence of nano-Al_2O_3 particles on the microstructure and wear resistance of the nickel-based alloy coating deposited by plasma transferred arc overlay welding, Surface and Coating Technology, **205** (2011), 2806-2812.
13. HOU, Q.Y., WANG, J.T., Influence of CeO2 on the microstructure and wear resistance of iron-based alloy coating studied by Rietveld refinement method, Surface & Coatings Technology, **204** (2010), 2677–2682
14. GREWAL, H.S., SINGH, H., AGRAWAL, A., Understanding Liquid Impingement erosion behavior of nickel–alumina based thermal spray coatings, Wear, **301** (2013) 424–433
15. TONGOV, M., SIMEONOVA, T., "Study of the formation of layers produced by high concentrated energy", 11-th International Scientific Conference of the Association Of Machine Technology Faculties in Bulgaria "AMTEH'2012", PROCEEDINGS, ISBN 978-954-438-994-9, pp.156-165
16. TONGOV, M., SIMEONOVA, T., Study of the wear-resistance of layers, obtained by plasma melting, IX National Conference on Tribology with International Participation "BULTRIB'2012", Tribological Journal BULTRIB , ISSN 1313-9878, vol.III, № 3,2013, pp.358

CORRESPONDENCE

Department of Materials Science and Technology, Technical University – Sofia, Kliment Ohridski № 8 Street, 1000 Sofia, Bulgaria
E-mail: terra_sim@abv.bg (MSc. Eng. Tatiana Simeonova)

Tribological Journal BULTRIB, **Vol. IV, 2014**
Papers from the International Conference **BULTRIB '13**
October 24-26, 2013, Sofia
Society of Bulgarian Tribologists
Technical University of Sofia

TRIBOLOGICAL PROPERTIES OF Ni DOPED TiO_2 COATINGS

Mara KANDEVA, Vladimir BLASKOV, Irina STAMBOLOVA, Nina G. KOSTOVA, Sasho VASSILEV, Konstantin BALASHEV, Maria SHIPOCHKA

Abstract: *Titania (TiO_2) thin films doped with Ni are obtained by spray pyrolysis. Aluminum foils are applied as substrates. The obtained samples contain 2, 5, 10 and 15 at % Ni. The films are investigated by X-ray diffraction (XRD) and X-ray photoelectron spectroscopy (XPS). The tribological properties of the films are investigated. The samples with 2 and 15 at% Ni revealed the higher wear resistance.*

Key Words: *tribology, titanium dioxide, nickel doped, solid lubricant, abrasive wear resistance, spray pyrolysis*

ТРИБОЛОГИЧНИ СВОЙСТВА НА СЛОЕВЕ ОТ TiO_2 ДОТИРАНИ С НИКЕЛ

Мара КАНДЕВА, Владимир БЛЪСКОВ, Ирина СТАМБОЛОВА, Нина Г. КОСТОВА, Сашо ВАСИЛЕВ, Константин БАЛАШЕВ, Мария ШИПОЧКА

Резюме: *С помощта на метода спрей пиролиза са получени слове от TiO_2 дотирани с Ni. Като подложки са използвани алуминиеви листове.Образците съдържат 2, 5, 10 и 15 ат % Ni.Слоевете са изследвани с рентгенов фазов анализ (XRD) и рентгенова фотоелектронна спектроскопия (XPS). Изследвани са трибологичните свойства на образците. Най–висока износоустойчивост показаха образците съдържащи 2 и15 ат % Ni.*

Ключови думи: *трибология, титанов диоксид, допант никел, твърда смазка, абразивна износоустойчивост, спрей пиролиза*

1. УВОД

Титановият диоксид намира широко приложение в медицината; за получаването на различни хетерогенни катализатори, сензори,слънчеви батерии и т.н. [1,2]. В последните години се засилва интересът на учените към изследване на неговите трибологични и механични свойства. Оказва се че покритията от TiO_2 имат добра износо- и корозионна устойчивост [3,4]. Слоевете от титанов диоксид с добри трибологични свойства са получавани предимно чрез физични методи [3,5]. Тези методи обаче изискват да се използва скъпа и сложна апаратура. Данните за получаването на слове от TiO_2 с помощта на евтините и лесно достъпни химични методи (зол - гел и спрей пиролиза) са оскъдни [6,7].Още по-оскъдни са данните за получаването на слоеве от титанов диоксид дотирани с различни метали и неметали [5-8]. Затова в настоящата работа се насочихме към получаването на слоеве от дотиран с никел TiO_2 върху алуминиева подложка чрез спрей пиролиза и изследване на някои техни трибологични свойства.

2. ЕКСПЕРИМЕНТАЛНА ЧАСТ

2.1. Получаване и охарактеризиране на слоевете

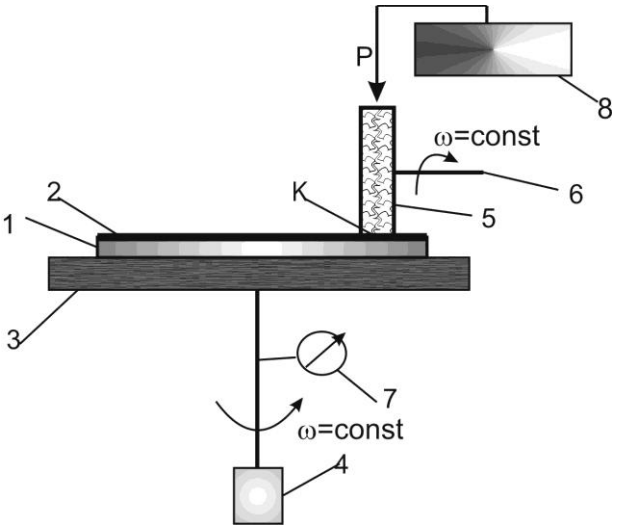
Титановият хлорид ($TiCl_4$) се разтваря в етанол (разтвор А). Полученият разтвор се смесва с изопропанол и бутил карбитол ($C_4H_9OC_2H_4OC_2H_4OH$) при интензивно разбъркване, след което се смесва с разтвор на $NiCl_2$ така че да се получи концентрация на никел между 2 и 15 at%.

Изпръсква се върху нагрята алуминиева подложка. Една част от слоевете са отложени върху полираната страна на подложката, а другата – върху неполираната страна. Полученият образец се нагрява изотермично при температура 400°C за 1 час. Фазовият състав на пробите е определен чрез рентгенов фазов анализ (XRD) при CuK_α лъчение. Химичният състав на повърхността е изследван с помощта на рентгенова фотоелектронна спектроскопия (XPS).

2.2. Методика и устройство за изследване на износването в условия на закрепени абразивни частици

Експерименталното изследване се осъществява по методика, разработена в научно-приложната лаборатория „Трибология" към катедра „МТМ" – МТФ-ТУ-София под ръководството на доц. д-р М. Кандева. Методиката се реализира с устройство по кинематичната схема „диск-ролка" на TABER ABRASER, който е модифициран към разработената методика. Методиката е съобразена с изискванията на действащия стандарт, хармонизиран с европейските стандарти.

Функционалната схема на устройството е представена на фиг. 1.



Фиг. 1: Функционална схема на устройството за износване при триене с абразивно противотяло

Образецът 1 (тялото) с нанесено покритие 2 с форма на кръгла пластина е подходящо закрепен върху хоризонтален диск 3, който се задвижва от електродвигател 4 с постоянна ъглова скорост ω при брой на оборотите $n = 60\ tr/\min$.

Противотялото 5 представлява диск (ролка) от специален абразивен материал *CS 10*, монтиран върху хоризонталната ос 6 в устройството 8, чрез което се задава желаното нормално натоварване P в центъра на контактната зона K. По този начин тялото 1 и противотялото 5 се намират на две кръстосани оси и при постоянната ъглова скорост на образеца 1 и постоянно номинално контактно налягане p_a триенето в контактната зона K поддържа постоянна скорост на ротация на противотялото 5.

Методиката на изследване включва следната последователност:

1. Всички образци се подготвят с еднаква форма и размери преди и след нанасяне на покритието. Това е задължително условие, което гарантира достоверността резултатите от изследването.

2. Измерва се масата на всеки образец преди и след определен път L на триене (брой цикли N). Масата на образците се измерва с помощта на електронна везна тип WPS 180/C/2 с точност до 0,1 mg.

Преди всяко измерване с везната образците се почистват с разтвор, неутрализиращ статичното електричество.

3. Образецът 1 се закрепва върху носещия хоризонтален диск 3 и чрез лостова система в устройството 8 се задава желаното нормално натоварване P. Пътят на триене L се пресмята чрез броя цикли N, които се отчитат с оборотомера 8.

Основните параметри на изследването са:

- *абсолютно масово износване* m, $[mg]$ - разрушената маса от покритието в процеса на износване, която се определя като разлика между масите на образеца преди и след определен път на триене.
- *скорост на масовото износване* dm/dt $\left[mg/\min\right]$ - разрушената маса от покритието за определено време, в случая за време една минута.

- *интензивност на линейното износване* i - намалената височина (линейно износване) на покритието за единица път на триене. Това е бездименсионно число, което изразено чрез измереното масово износване, се определя по формулата:

$$i = \frac{m}{\rho.A_a.L} \tag{1}$$

където:

ρ е плътността на покритието. В случая $\rho(TiO_2) = 3{,}89 g/cm^3$; $\rho(Al) = 2{,}7 g/cm^3$

A_a е номиналната контактна площ на взаимодействие.

L е пътят на триене, който се пресмята чрез броя цикли N на триене по формулата:

$$L = 2\pi.R.N \tag{2}$$

Параметърът R представлява разстоянието между оста на въртене на носещия диск и масовия център на контактната площадка между образеца 1 и контратялото 5.

- *абсолютна линейна износоустойчивост* I - бездименсионно число, което се пресмята като реципрочна стойност на интензивността на износване, т.е.

$$I = \frac{1}{i} = \frac{\rho.A_a.L}{m} \tag{3}$$

- *номинално контактно налягане* p_a, $[N/cm^2]$ - нормалното натоварване, което се разпределя на единица номинална контактна площ на взаимодействие A_a, т.е.

$$p_a = \frac{P}{A_a} \tag{4}$$

- *средна скорост на плъзгане* V, $[cm/s]$ - линейната скорост на центъра на тежестта на контактната площадка, определена по формулата:

$$V = \omega.R = \frac{\pi.n}{30} R \tag{5}$$

В таблица 1 са представени данни за образците.

Таблица 1: ***Описание на образците***

Код на образец	Концентрация на Ni [ат. %]	Страна на нанасяне
К 9	2	полирана
К10	5	полирана
К11	10	полирана
К12	15	полирана
К13	2	неполирана
К14	5	неполирана
К15	10	неполирана
К16	15	неполирана

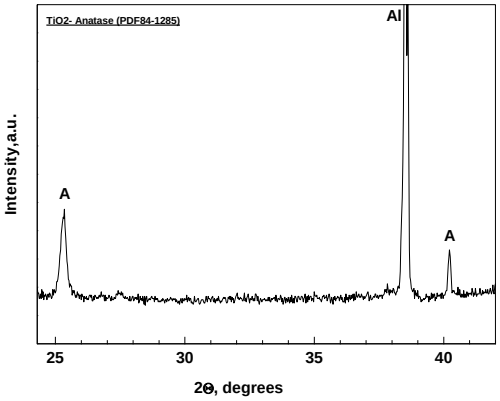
В таблица 2 са представени параметрите на контактното взаимодействие, при които е проведено експерименталното изследване.

Таблица 2: ***Параметри на експеримента:***

Номинална контактна площ, A_a	$26.10^{-6}\,[m^2]$
Средна скорост на плъзгане, V	$17{,}90\ [cm/s]$

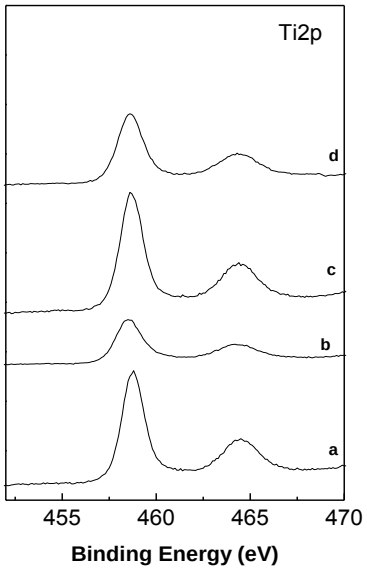
3. ЕКСПЕРИМЕНТАЛНИ РЕЗУЛТАТИ

На фигура 2 е представена рентгенова дифрактограма на слой от титанов диоксид дотиран с никел, получен чрез спрей пиролиза.

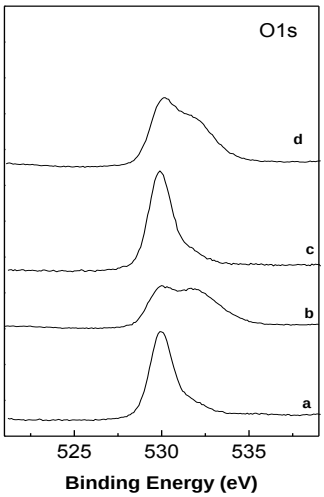


Фиг. 2 Типичен рентгенов дифракционен спектър на слой от TiO_2, дотиран с 5 ат % Ni.

От рентгеновите дифрактограми на слоевете се установи че анатазната фаза (A) е основна за всички изследвани образци, като не се наблюдават пикове, принадлежащи на никелови фази.Наблюдава се и интензивен пик (Al) от подложката.



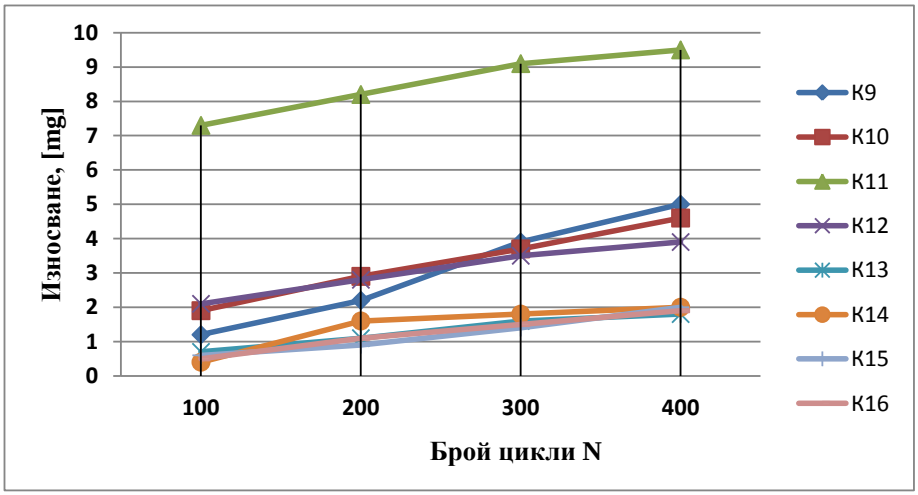
Фиг. 3 Рентгенови фотоелектронни спектри на Ti2p електронно състояние на слоеве от TiO_2 дотирани с 5 ат. % преди и след абразивните тестове (a и b, респ.) и 15 ат. % никел преди и след абразивни тестове (c и d , респ.)



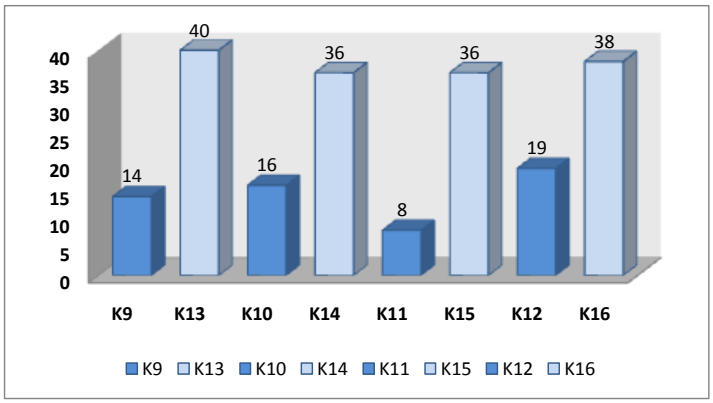
Фиг. 4 Рентгенови фотоелектронни спектри на O1s електронно състояние на слоеве от TiO_2 дотирани с 5 ат. % преди и след абразивните тестове (a и b, респ.) и 15 ат. % никел преди и след абразивни тестове (c и d , респ.)

Фигури 3 и 4 показват рентгеновите фотоелектронни (XPS) спектри на Ti2p и O1s електронни състояния за образци дотирани с 5 и 15 ат % Ni. За Ti2p състояние (Фиг.3), спектърът съдържа два пика със свързващи енергии 464.4 eV and 458.8 eV за Ti $2p_{1/2}$ and Ti $2p_{3/2}$ състояния, съответно. Тези енергии съответстват на Ti^{4+} състояние. XPS спектърът на кислородното състояние O1s (Фиг. 4) е слабо асиметричен и съдържа два пика, като пика при по-висока свързваща енергия съответства на кислороден атом (O^{2-}) в решетката на TiO_2, докато по ниско енергийния пик съответства на кислороден йон (O^{2-}) във водни молекули, адсорбирани на повърхността.Вижда се също, че интензитета на втория пик нараства след абразивните тестове.

Експерименталните резултати за износването на всеки образец са представени във фигури 5 и 6.



Фиг.5 Зависимост на масовото износване от брой цикли на триене



Фиг.6. Диаграма на износоустойчивостта I_m на покрития, нанесени върху полирана и неполирана част на подложката за път на триене N=400 cI (L=72 m)

4. ЗАКЛЮЧЕНИЕ

Чрез спрей пиролиза са получени тънки слоеве от TiO_2 дотирани с никел. Концентрацията на Ni варира от 2 до 15 ат %. Според рентгенофазовия анализ анатазната фаза е основна за дотираните образци преди и след абразивните тестове.

Най-висока износоустойчивост показват образците, нанесени върху неполираната страна на подложката и дотирани с 2 и 15 ат % Ni.

БЛАГОДАРНОСТИ

Авторите изказват благодарности за финансовата подкрепа на Фонд Научни изследвания по дог. N ДВУ 02/36 (2010) и ДНТС/СЛОВАКИЯ 01/3

ЛИТЕРАТУРА

1. Koo H.-J.,Kim Y.J.,Lee Y.H., Lee W.I., Kim K.,Park N.-G., Nano-embossed hollow spherical TiO_2 as bifunctional material for high –efficiency dye-sensitized solar cells, Adv.Mater., **20,** 2008, 195-199.
2. Tang H., Prasad R., Sanjines R., Levy F., TiO_2 anatase thin films as gas sensors, Sens. Actuators, **B 71 ,**1995**,** 26-27.
3. Sun Y.**,** Tribological rutile - TiO_2 coating on aluminium alloy, Appl. Surf. Sci., **233**, 2004, 328-335.
4. Shen G.X., Chen Y.C., Lin C.J., Corrosion protection of 316L stainless steel of TiO_2 nanoparticle coating prepared by sol gel method, Thin Solid Coatings, **489,** 1996 130-134.
5. Wang H-F., Tang
6. W., Li H-Y., Microstructure and wear resistance of N-doped TiO_2 coatings grown on stainless steel by plasma surface alloying technology, J. Iron Steel Res. Int. **18,** 2011, 73-78.
7. Wan Y., Zhen XU.,Chao W., Zhang Ju. Sol-gel derived nickel – doped TiO_2 films as wear protection coating, J. Exper. Nanosci. **8**, 2013, 618-623.
8. Jia Q., Zhang Yu., Wu Zh., Zhang P., Tribological properties of anatase TiO_2 sol-gel films controlled by mutually soluble dopants, Tribology Letters, **26**, 2007, 19-24.
9. Kandeva M., Blaskov V., Stambolova I., Kostova N., Vasilev S., Tribological Properties Of Sprayed TiO_2 Coatings Deposited On Al Substrate, Tribological Journal BULTRIB, **Vol. III, № 3**, 2013, 216-225.

КОРЕСПОНДЕНЦИЯ

Мара КАНДЕВА
Технически университет-София, бул. Кл. Охридски” № 8, блок 3, лаб. 3125
e-mail:kandeva@tu-sofia.bg

Tribological Journal BULTRIB, **Vol. IV, 2014**
Papers from the International Conference **BULTRIB '13**
October 24-26, 2013, Sofia
Society of Bulgarian Tribologists
Technical University of Sofia

MECHANOCHEMICAL PREPARATION OF PEROVSKITE TYPE MATERIALS

I. Yordanova, Z. Cherkezova-Zheleva, D. Paneva, B. Kunev and I. Mitov

Institute of Catalysis, Bulgarian Academy of Sciences, Acad. G. Bonchev Str., Bld. 11, Sofia 1113, Bulgaria

Abstract: *The perovskite materials $LaFeO_3$ and $LaCoO_3$, were prepared by co-precipitation and mechanochemical activation. They have nanometric size and cubic crystal structure. These properties were found by X-ray diffraction (XRD).*

Keywords: *co-precipitation, mechanochemical synthesis, perovskite, $LaFeO_3$ and $LaCoO_3$*

1. INTRODUCTION

Perovskite-type oxides having general formula ABO_3 (where A is cation of larger size than B) are very good oxidative catalysts and cheaper than noble metal supported catalysts. The redox properties of the transition cation, the availability of weakly bonded oxygen at the surface and the presence of lattice defects make perovskites such as $LaFeO_3$ and $LaCoO_3$ be suitable for the total oxidation of volatile organic compoundsVOCs[1-3].

Perovskite materials are stabile to high temperature but often their limit in catalysis is presented by low surface area. Synthetic methods produce perovskites to be crystalline and defect in different forms. Co-precipitation and mechanochemical activation have been studied due to their simplicity and low temperature synthesis. Moreover these methods produce pure phase and homogeneous powder. The effects of crystalline and defect forms in perovskites are key factors in determining the catalytic activity besides the surface area. Both synthetic methods should provide appropriate conditions in producing high catalytic performance perovskites. In this regard one of the key factors is the preparation of ultradispersedperovskites. Physicochemical properties of nanosize materials strongly depend on the preparation conditions. There are many different methods for preparation of nanosize powders that are described in the literature. It is very important particle size and particle size distribution to be controlled during the synthesis [4]. Mechanochemistry is the subject that deals with the chemical and physicochemical changes of substances induced by mechanical force [5]. In the last decade, mechanochemistry was frequently used to produce different nanosize compounds. Depending on the system and the applied conditions, solid state reactions could be done at room temperature or at reduced temperatures, because the mechanochemical treatment already induced structural changes [4]. Several mixed oxides of perovskite structure have been recognized as active catalysis for a variety of reactions f some significance in environmental catalysis such as the catalytic combustion of hydrocarbons [5-7] and other volatile organic compounds (VOC) [7-8], NOxdecomposition [9-10] and NOxselectivecatalyticreduction [11-12].

The aim of this study is the mechanochemical synthesis of monophase $LaFeO_3$ and $LaCoO_3$perovskiteswith high dispersion avoiding high temperature treatments and to study their physicochemical properties (composition, structure, crystallite size and dispersity).

2. EXPERIMENTAL

2.1. Samples preparation

Materials: $LaCoO_3$ and $LaFeO_3$ were prepared by combination of co- precipitation and mechanochemical activation methods.

Aqueous solution of $Co(NO_3)_2.6H_2O$ or $Fe(NO_3)_3.9H_2O$ we precipitated with aqueous solution of NaOH (2 mol/l) added slowly with continuous stirring. The final pH of solution was 10. After that we washed the solution to neutral pH during filtering and at last the sample was dried 12 hours at 60ºC.

Highenergy planetary ball mill type PM 100, Retsch, Germany is used for mechanochemical treatments. Mechanochemical milling of the Fe- or Co-hydroxide precursor materials is done for 10h and rotation speed 600 rpm for preparation of single phase materials. The stoichiometric ratios of obtained materials and $La_2O_3$are taken for the next milling activation process. La_2O_3 (Alfa Aesar 99,9%(REO) was added to Co_3O_4 orferrihydrite materials in triboreactor. It is carried out for 6 hours and rotation speed 600 rpm. The weight ratio between balls and powder is 12:1.

2.2. Samples characterization

Powder X-ray diffraction (XRD) patterns were collected using a TUR-M62 apparatus (Germany) with Co-Kα radiation. This method is for use in the study of crystalline substances which use X-ray diffraction. The process is fundamental to the diagnosis and determines a point of the structure and the symmetry of the crystal body. Data interpretation was carried out using the JCPDS database. Average crystallite sizes were determined from the XRD peaks using Scherrer'sequation[13].

3. RESULTS AND DISCUSSION

3.1. Characterization of Fe sample

The investigated samples were characterized using the XRD to monitor the process of preparation of the aimed systems and the presence of crystalline phases.

Figure 1(left) shows the XRD pattern of precipitated $Fe(NO_3).9H_2O$ with aqueous solution of NaOH.It can be seen that the synthesized phase is amorphous because the observed lines are very wide and X-ray amorphous halo is registered. It can be supposed that XRD spectrum of the iron precursor corresponds to the two-line ferrihydrite. Figure1 (right) shows the XRD pattern of precipitated $Fe(NO_3).9H_2O$ with aqueous solution of NaOH, milled for 3 hours. Again the spectrum shows an amorphous halo. Comparative analysis showed that the mechanochemical activation does not lead to a significantly improved crystallinity. There is no occurrence of a crystal phase.

Increaseof themilling time results inappearsof thecrystalphase. The low intensive peakscorrespond to $5Fe_2O_3•9H_2O$.

Figure 3 shows the spectrum of a sample obtained by mechanochemical processing mixture and $La_2O_3$and iron oxide precursor milled 10 hours.The resulting spectrum haswell-pronounced peaks corresponding to $LaFeO_3$ with cubic crystal structure. Already visible crystal structure indicates that the aim of our synthesis is achieved and $LaFeO_3$perovskite is obtained. On the bases of the recorded spectrum some calculations were done. From the equation of D.Sherer (D = k λ / β cosQ) the average size of the crystallite which is 15nm is to be defined. Obtained sample has cubic crystal structure and unite cell parameter a= 0,390nm. Calculated values of microstrains were determined from XRD data are $e=3,2.10^{-3}$.

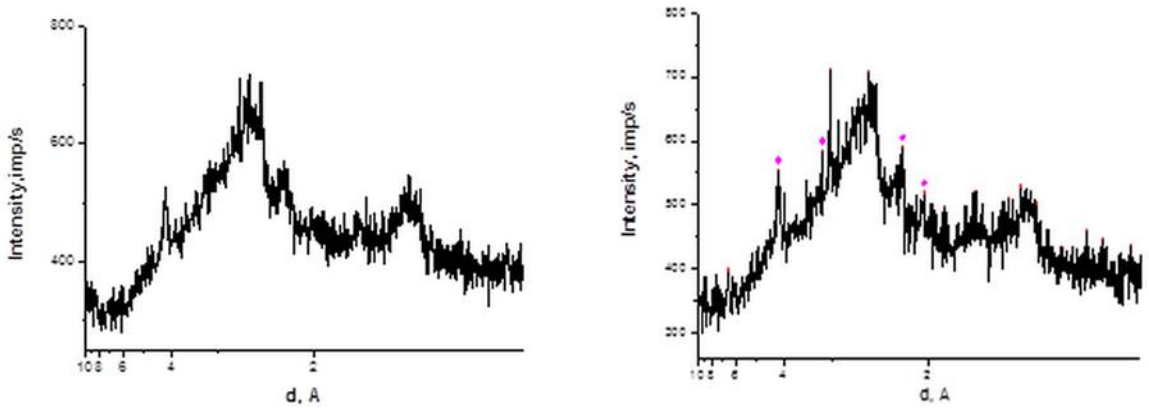


Fig.1.XRD patterns of precipitated $Fe(NO_3)_3.9H_2O$ with aqueous solution of NaOH(left) and mechanochemically activated 3 hours (right)

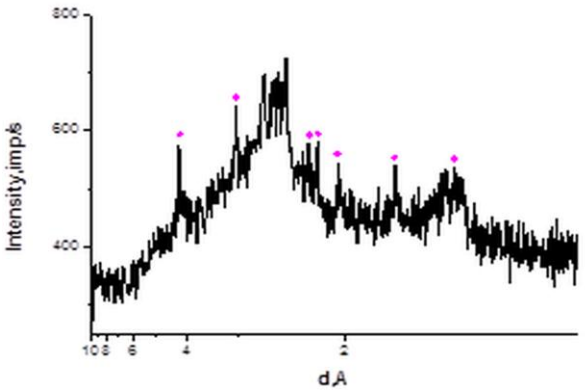


Fig. 2. XRD pattern of precipitated $Fe(NO_3).9H_2O$ with aqueous solution of NaOHmechanochemically activated 10 hours

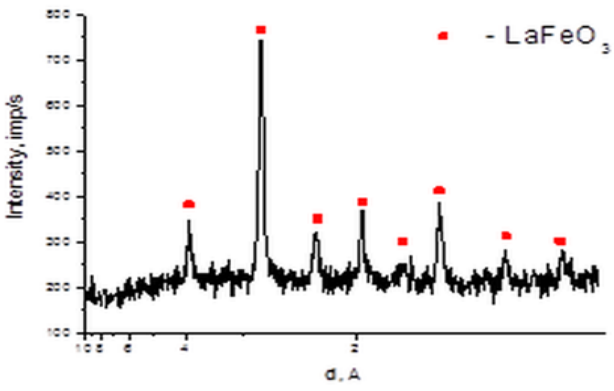


Fig. 3. XRD pattern of sample obtained after 6 hours milling of mixture of La_2O_3 powder and iron oxide precursor

3.2. Characterization of Co sample

In order to make our work more complete and to explore differences in catalytic behavior between the two materials, in our future work,we also synthesized $LaCoO_3$.

In Figure 4 we can see the presence of the crystal phase of $Co(OH)_2$ after precipitation of $Co(NO_3)_2.6H_2O$ with aqueous solution of NaOH. In order to improve synthesis procedure the precursor material was mechanochemically activated.

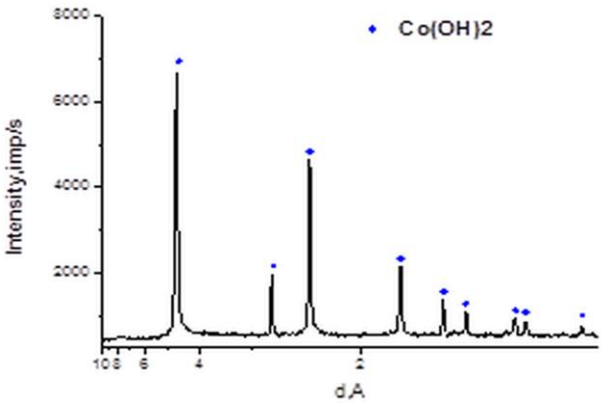


Fig. 4.XRD pattern of precipitated $Co(NO_3)_2.6H_2O$ with aqueous solution of NaOH.

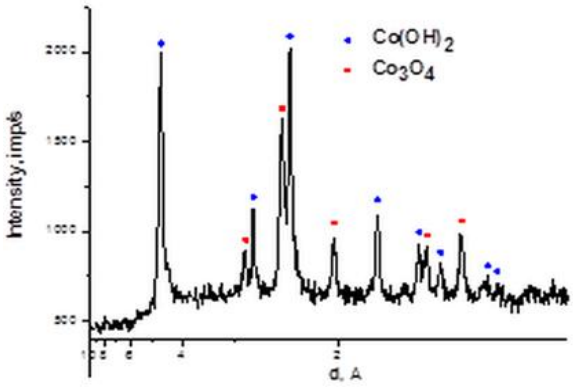


Fig. 5. XRD spectrum of precipitated cobalt precursor after 3 hours mechanochemical activation.

After 3 hours of mechanochemical activation which results in the formation of a new phase of Co_3O_4.Prolonged mechanical treatment leads to increase of spinel cobalt oxide phase and decrease of hydroxide phase as it can be seen in figures 5 and 6. La_2O_3 was added to this precursor material in triboreactor. Mechanochemical milling of this mixture for 6 h leads to the formation of single phase material $LaCoO_3$.We can see the final spectrum of obtained perovskite materials in Fig. 7. The obtained sample has cubic crystal structure and unite cell parameter a = 0,386 nm. Calculated values of mean crystallite size and microstrains were determined from XRD data: D = 14nm and e = $3{,}2.10^{-3}$.

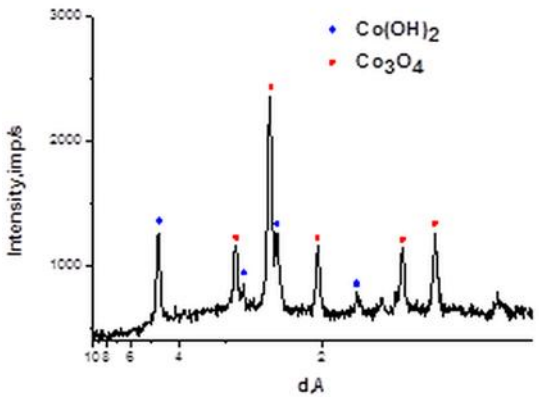


Fig. 6. XRD spectrum of precipitated $Co(NO_3).6H_2O$ with aqueous solition of NaOHmechanochemically activated 3 hours and additionally milled 7 hours.

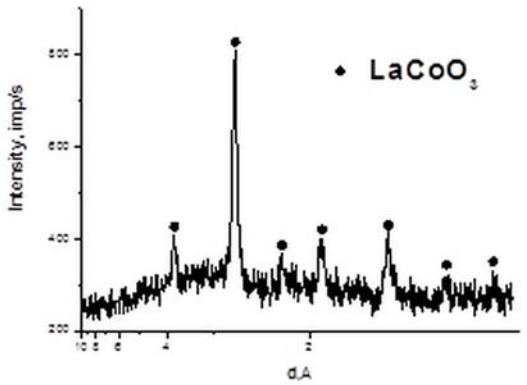


Fig. 7.XRD pattern of sample obtained after 6 hours milling of mixture of La_2O_3 powder and cobalt oxide precipitate previously milled for 10 hours

4. CONCLUSIONS

Precursor materials were prepared by combination of co-precipitation and mechanical milling. Nano-sized single phase perovskite type materials$LaFeO_3$ and $LaCoO_3$were successfully synthesized by mechnochemical activation method. The prepared materials have nano-metric size which is of great importance of their catalytic behavior.

ACKNOWLEDGEMENTS *The authors are grateful for the financial support of National Science Fund of Bulgaria under Project DFNI-E 01/7/2012.*

REFERENCES

1. J. HEREMANS, J. Phys. **D 26**, 1993, 1149.
2. C. N. R. RAO, B. RAVEAU, C.N.R. RAO and B. RAVEAU, Editors, Colossal Magnetoresistance, Charge Ordering and Related Properties and Manganese Oxides, World Scientific, Singapore, 1998.
3. K. DORR, J. Phys. **D 39**, 2006, R 125.
4. Z. CVETIC, S. RAKIC, A. KREMENOVIC, B. ANTIC, C. JOVALEKIC, P. COLOMBAN, Nanosize ferrites obtained by ballmilling: Crystalstructure, cationdistribution, size-strain analysis and Raman investigations, Solid State Sciences, **8**, 2006, 908–915.
5. Z.ZHAO, O. KINGSAM, W.MING, Structural macrokinetics of synthesizing $ZnFe_2O_4$ bymechanical ball milling, Trans. NonferrousMet. Soc. China, **20**, 2010, 1131-1135.
6. H. ARAI, T. YAMADA, K. EGUCHI, T. Seiyama, Appl. Catal. 26,1986, 265.
7 L. G. TEJUCA, J. L. G. FIERRO (Eds.), Properties and Application of Perovskite-Type Oxides, Marcel Dekker, New York,1992.
8 H. G. LINTZ, K. WITTSTOCK, Catal. Today, **29,** 1996 457
9. Z. ZHAO, X. YANG, Y. WU, Appl. Catal. B: Environmental**8,**1996, 281.
10. J. WANG, H. YASUDA, K. INUMARU, M. MISONO, Bull. Chem.Soc. Jpn. **68,** 1995, 1226.]
11. M. SKOGLUNDH, L. LÖWENDHAL, K. JANSSON, L. DAHLAND, M. NYGREN, Appl. Catal. B: Environmental,**3**,1994, 259.
12. M. ÖCAL, R. OUKACI, G. MARCELIN, Ind. Eng. Chem. Res. **33**,1994, 2930.
13. B. D. CULLITY, S. R. STOCK, Elements of X-ray Diffraction, Prentice Hall, Englewood Cliffs, **3rd**, 2001.

CORRESPONDENCE

IliyanaYordanova
Institute of Catalysis, Bulgarian Academy of Sciences, “Acad. G. Bonchev” St., Block 11, 1113 Sofia, Bulgaria
e-mail:yordanova@ic.bas.bg

Tribological Journal BULTRIB, **Vol. IV, 2014**
Papers from the International Conference **BULTRIB '13**
October 24-26, 2013, Sofia
Society of Bulgarian Tribologists
Technical University of Sofia

ADVANCED TECHNOLOGIES USED IN EDUCATION AND TRAINING FOR LUBRICATION PROCESSES

Alexandru RADULESCU, Irina RADULESCU

Abstract: *The paper presents a wear degree and durability modeling and simulation tool for oils, by developing a fast diagnostic device for liquid lubricants, with minimum investment, with a high precision degree and easy to use. Significant benefits are made by the proposed procedure: the small amount of lubricant required for a determination, the short time measurement and the possibility of adapting the method according to concrete conditions. This is used as a method of educating and training students and specialists in the lubricating process.*

Key Words: *lubricant, wear, durability, modeling, simulation*

1. INTRODUCTION

The paper aims to present an integrated tool for the lubricants wear degree and durability modeling and simulation, which was made during a partnership project.

Researches basic idea consider the current fabrication conditions by developing a fast diagnostic method for liquid lubricants, able to be used in automotive domain. The actual need for rapid and adaptive design in industry requires the use of advanced technologies, the namely tools for modeling, simulation and integrated products.

Based on current practice of exchanging oil from cars, the proposed idea was to make the change when the oil is completely worn out and not according to the manufacturer's theoretical recommendations. Using advanced technologies by making a modeling and simulation tool for lubricants behavior involved minimal investment, a high degree precision and an easy to use way. The procedure has as advantages a small amount of lubricant required for a determination, a short time measurement and the possibility of adapting the method according to specific conditions.

1.1. The current state of research in the field

At current stage, in western europe, usa or japan - the oil from equipment is changed according to manufacturer's recommendations, considering the minimum number of operation hours or of miles traveled. in romania these instructions are almost not followed, the oil is changed faster because the engine oil market was invaded by pirate products. the oil replacement timing is difficult to establish, there are many factors to control, that is why the oil changing is more frequently than necessary, being an harmless technical process, but expensive.

The replacement of used oil can not be established by a common term for all engines, to define the vehicle distance covered or the timing. oil degradation during service depends on the engine life, oxidation and contamination. the oil degrees of contamination and utilization time depend on operating conditions, on oil quality, engine construction and technical condition. the assessment of degradation state and changing time are made considering a periodical analysis of its physical and chemical characteristics; there are established acceptable limit values for each type of engine, by the manufacturer.

At international level, the main directions and guidelines are channeled in predictive maintenance, which is applicable to any closed loop lubrication system. to be effective, it is necessary to adopt a modern program for oil analysis, monitoring the wear residues for the qualitative determination of the wear particles nature, which are carried by working lubricant and monitoring lubricant estate, which is based on physical-chemical tests, to determine if the lubricant is fit for exploitation [1], [2].

1.2. The proposed method for the achievement of the integrated instrument

The new method for the lubricants diagnosis is based on the expulsion process of lubricant film (squeeze-film). It is a fast one; determinations for lubricants behavior are made during 5-10 minutes on a small amount of lubricant (about 100 ml).

By collecting and comparative test of oil samples at different times and varying wear degrees, there are assigned viscometric curves for each lubricant. Using an appropriate mathematical apparatus, it can be determined the variation law of the wear degree according to time, which is required in order to establish the lubricant "reserve life" considered. It is an objective criterion for assessing the oil degradation and the optimal timing of replacement. The accuracy and precision of the method are provided by the determinations comparative character, by using two parallel measurement systems, one in original conception and the other – the viscometric reference one.

LabVIEW software facilities were used among the advanced technologies to create the modeling and simulation tool for evaluating and quantifying the lubricant wear degree. It represents one of the most modern management tools, used for processing and data acquisition, also being a device for the education and training for lubrication processes, in this case [3].

The device has a multidisciplinary character, by combining its centralized type architecture, which manages a set of four main working modules: the theoretical module, the rheological experimental module, the validation viscometric module and the spectrometric analysis module.

2. ADVANCED TECHNOLOGIES OF INTEGRATED INFORMATICS DEVICE USED FOR EDUCATION AND TRAINING IN LUBRICATION PROCESSES

Among the advanced technologies used in education and training for lubrication processes a special one is represented by the Lab VIEW software - Laboratory Virtual Instrument Engineering Workbench, a graphical programming environment developed by National Instruments Corporation. The software is useful in data acquisition, processing and presentation, also for control and industrial process control, for the systems dynamic behavior analysis.

The specialists are using a graphical programming language; in this environment they can run applications, which are called virtual instruments. There are used block diagrams (Figure 1), which are then compiled into machine code. Virtual instruments are made up of a front panel, which simulates the mask of the meter and a block diagram, which represents the executable software. The front panel contains icons representing various buttons, switches, screens and other elements that might enter into the meter composition, [3].

The integrated informatic device uses advanced technologies, which are present in the four working component modules, in order to realize the lubricants behavior modeling and simulation. Their core functions are described here:

1. **The theoretical module** role is to analyze the phenomena which are based the lubricant film extrusion process. Also it generates theoretical curves specific to the interstitial fluid flow, which are necessary for the experimental results correlation and interpretation, [7]. This module is based on LabVIEW software.

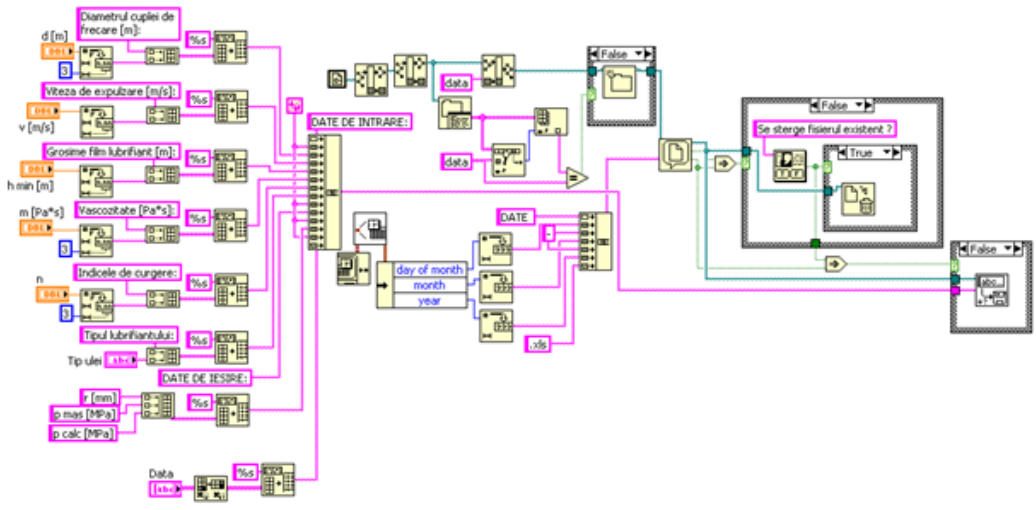


Fig. 1. The block diagram of LabVIEW application

2. **The rheological experimental module** is a modern one, containing an original measurement device, which is coupled with a data acquisition and data processing system. By using a small amount of lubricant for the diagnose (100 ml) and two semi - coupling, it is registered the time variation function lubricant pressure and thickness.

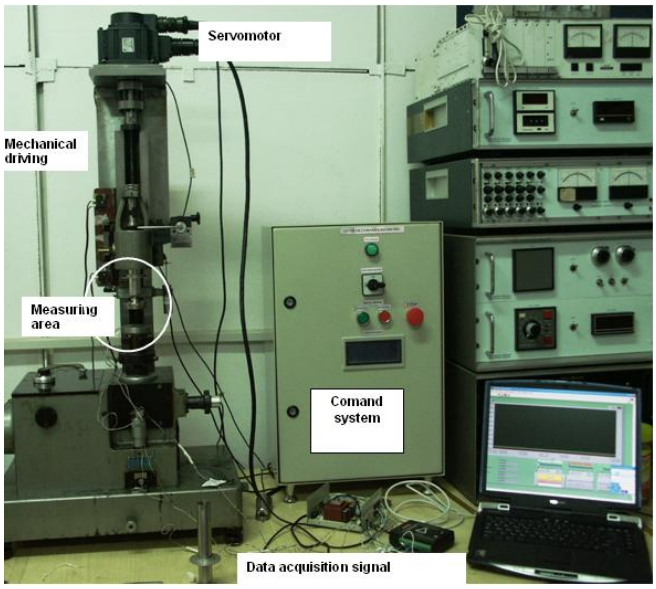


Fig. 2. Experimental stand for lubricants testing in "squeezing" movement

It is important to work with qualified staff or to educate students and specialists to work with the three presure transducers and one proximity sensor, while the oil film is expelled under the wight of the upper coupling (Figure 2). Squeeze-film curve is recorded as the „fingerprint" of the used lubricant, that depends on many factors, including the lubricant wear degree, [4].

3. Considering **the viscometric validation module**, this one is based on a PHYSICA rheometer (Figure 3) and it is composed of a mechanical unit and an electronic one. The components of mechanical unit are represented by the measurement system, thermostat installation, training system and additional installations.

The electronic unit is composed of a transfer system for the measured parameters, the data processing system and the central control and command unit. The module role is to validate the experimental results which are supplied by the experimental rheological module and to establish the necessary correlations [5], [6].



Fig. 3. PHYSICA Rheometer – general view

4. **The spectrometric analysis module** is based on the use of transmission electron microscopy by obtaining information concerning the wear particles which can be identified in samples of worn off lubricants (Figure 4). By comparing two microscopic structures of the same lubricant, in various stages of use, it may reveal the wear particles, their shape and their size [8].



Fig. 4. Transmission electron microscopy – general view

3. RESULTS

The experimental research was monitored for 10W40 oil, used for internal combustion engines, during its working time, until the complete degradation. The theoretical LabVIEW simulation of the flow process (variation of the pressure versus radius and load versus film thickness), is presented in Fig. 5.

The rheological and structural tests were conducted, over the entire service time of the four lubricants; finally there was obtained the following characteristics:

- the "fingerprint" of the lubricant, which is expressed by the experimental variation of the pressure versus film thickness (Fig. 6);
- the reference rheological lubricant feature, obtained with the viscometer validation module, which is expressed by the variation of the shear stress versus shear rate (Fig. 7);
- the structural (microscopic) lubricant feature, obtained with the wear particles analysis module, which is done by the solid particles type which are identified in the fresh and worn lubricant Fig. 8).

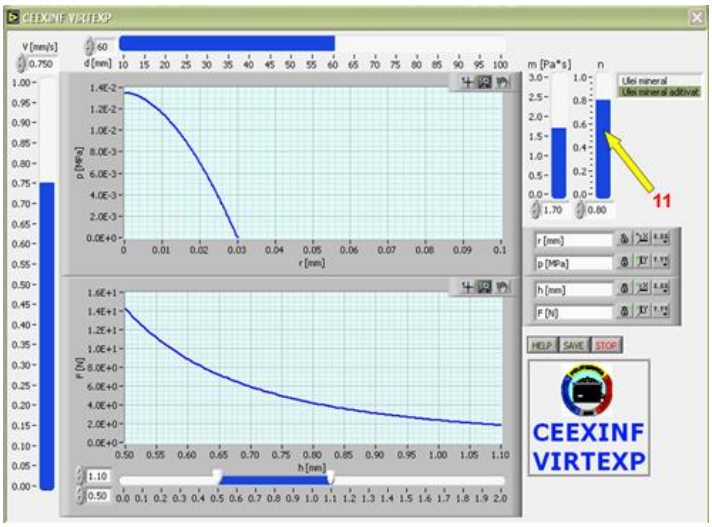


Fig. 5. Theoretical simulation with LabVIEW

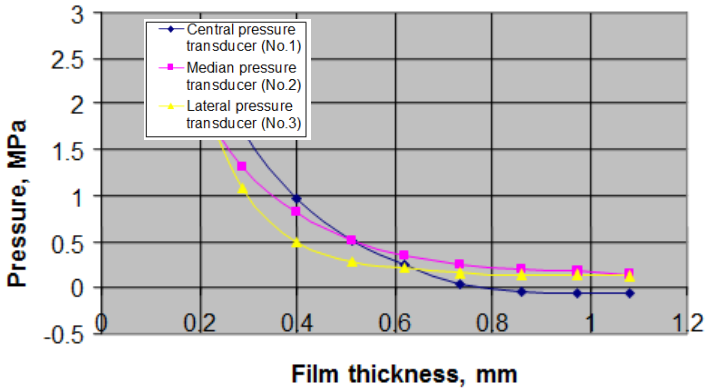


Fig. 6. "Fingerprint" of the lubricant

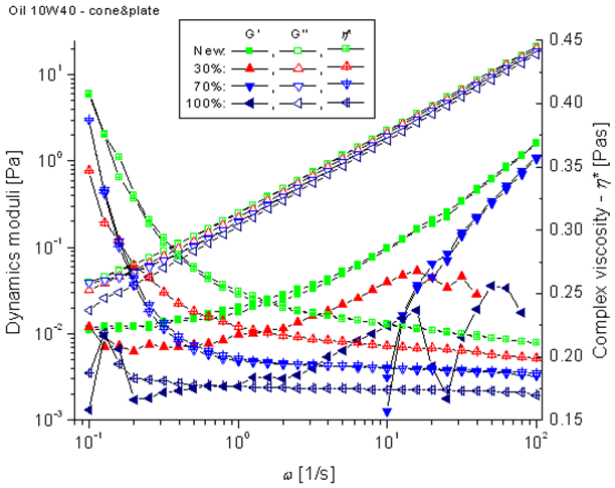
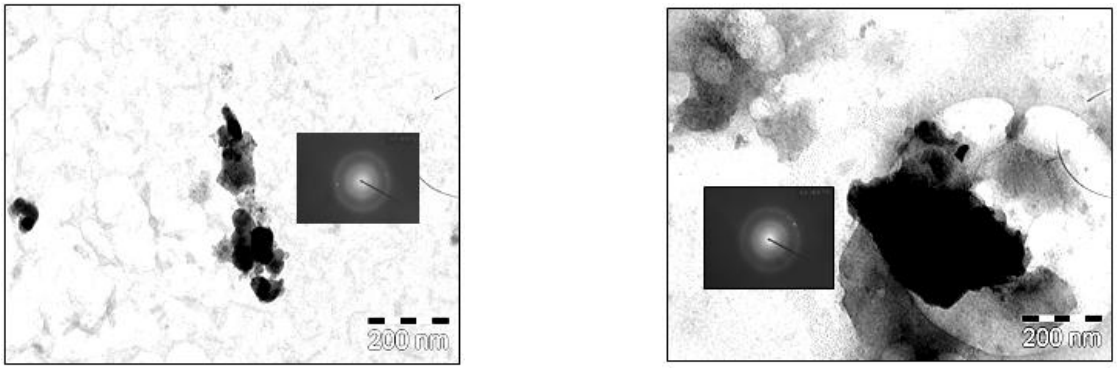


Fig. 7. Rheogram of the lubricant



a. $Mn_{0,9}V_{0,1}P$ orthorombic (ASTM 78-0802) *b. ZnO hexagonal (ASTM 79-0255)*

Fig. 8. Wear particles in the lubricant

4. CONCLUSIONS

By using advanced technologies it was obtained a new, modern and efficient methodology. By developing research in this area it was assured the modernization of existing laboratories and there were created premises for new ways for lubricants sustainability development. Modern technologies used to achieve the integrated informatics instrument have contributed to obtain a "friendly" environment device, also friendly with its users. It can be used by a large number of beneficiaries, both in research, educational and training laboratories and in production units with small financial possibilities.

The high level of performance and quality parameters of developed system is outlined by the main characteristics and performance:

The system is fully integrated. All modules are interlinked, the users can work simultaneously and they can process the same network data. Data flows are fast and well organized, which is an important support for information management.

The system is flexible and scalable. It is easy to adapt the system to each specific beneficiary potential, with a minimal cost. It is possible to achieve an optimal configuration for each user, by the selection of components and services required.

The system uses top information technology. It is well adapted for network work. There are achieved quality and performance, ensured by the processing system and Lab VIEW data acquisition use.

The system is open. The access to inner system data is free, for the use in analysis program or other systems. It is capable of operate on multiple hardware platforms, with latest technologies (Web / Intranet / Internet). There are facilities which allow integration with existing applications and a smooth transition, with minimal efforts, from other applications to the developed software system.

REFERENCES

1. *** The rheology of lubricating greases, ELGI, Amsterdam, 2000.
2. ALLISTON-GREINER A.F., Test methods in tribology, Proc.**1 st** World Tribology Congress, London, 1997.
3. ARSENOIU, L., SAVU, T., SZUDER, A., Bazele programării în LabVIEW, Ed. Printech, Bucureşti, 1999 (in Roumanian).
4. BRIANT, J. ş.a., Propriétés rhéologiques des lubrifiants, Ed. Technique, Paris, 1985.
5. CROCKER, D.C., How to use regression analysis in quality control, **Vol. IX**, American Society for Quality Control, 1983.
6. SALVENDY, G., Handbook of Industrial Engineering, **Sect.13.6**, John Wiley &Sons, Inc., New York, 1982.
7. VODĂ, Gh.V., Noi modele statistice în studiul durabilităţii produselor, Ed. Academiei R.S.R., Bucureşti, 1980 (in Romanian).
8. M. BORN et al., Relationship between Chemical Structure and Effectiveness of Some Dialkyl-Diaryldithiophosphates in Lubricated Mech., Lubrication Science, **4-2**, pp. 97-100.

CORRESPONDENCE

Alexandru RADULESCU
Organisation: POLITEHNICA University Bucharest, Romania
Address: 313 Spl. Independentei, Sect. 6, 060042, Bucharest, Romania
e-mail: varrav2000@yahoo.com
Irina RADULESCU
Organisation: POLITEHNICA University Bucharest, Romania
Address: 313 Spl. Independentei, Sect. 6, 060042, Bucharest, Romania
e-mail: irena_sandu@yahoo.com

Tribological Journal BULTRIB, **Vol. IV, 2014**
Papers from the International Conference **BULTRIB '13**
October 24-26, 2013, Sofia
Society of Bulgarian Tribologists
Technical University of Sofia

FUNCTIONALLY GRADED MATERIALS IN TRIBOLOGY

Adelina MITEVA

Abstract: *This paper is motivated by the tremendous interest in the functionally graded materials (FGMs). Here we present a brief review of the main principals in the FGMs with an emphasis on the connection with tribology. It includes stress, stability and dynamic analyses, testing and fracture. The need to focus more research effort on an extensive studies on material characterization of FGMs is discussed in order to bring down the manufacturing cost of FGM and increase productivity and applicability in this regard.*

Key Words: *Functionally graded material, Applications of FGM, Material characterization of FGMs*

1. INTRODUCTION

The present work is motivated by the nowadays tremendous interest in the functionally graded materials (FGMs) [1-20]. The information contained in this study has been compiled from the literature and it may be considered as a brief introduction to the subject mentioned above. Functionally graded material (FGM) is an advanced material characterized by variation in properties as the dimension varies. In a FGM the properties change gradually with the position. The property gradient in the material is caused by a position-dependent chemical composition, microstructure or atomic order. The overall properties of FMG are unique and different from any of the individual material that forms it. There is a wide range of applications for FGM and it is expected to increase. In this paper, an overview of the most promising properties of FGM is presented. The emphasis is made on the connection of FGMs with tribology, as they are a distinguished area in the field of material tribology.

2. A LITTLE HISTORY ABOUT FGM

In the case of a position-dependent chemical composition in FGMs the gradient can be defined by the so-called transition function which describes the concentration of the component as a function of position. Already in 1972, the usefulness for applicability of functionally graded composites with a graded structure was recognized in theoretical papers by Bever and Duwez [2], and Shen and Bever [3]. However, their work had only limited impact, probably due to a lack of suitable production methods and technologies for FGMs at that time. It took 15 more years until systematic research on manufacturing processes for functionally graded materials was carried out in the framework of a national research program on FGMs in Japan. Today many countries have their own research programs on FGMs. In [4] an overview of the achievements of the German priority program on FGMs in the field of processing techniques is given (see Fig. 1).

There is a substantial difference between FGM and composite material (CM). CM is a class of advanced material, made up of one or more materials combined in solid states with distinct physical and chemical properties. CM offers an excellent combination of properties which are different from the individual parent materials. Wood is a CM from nature. CMs will fail under extreme working conditions through a process called delamination (separation of reinforcement from the matrix) [5]. To solve this problem, researchers in Japan in the mid 1980s, confronted with this challenge and came up with a novel material called FGM.

FGM, a revolutionary material, belongs to a class of advanced materials with varying properties over a changing dimension. The gradation of properties in an FGM reduces the thermal stresses, residual stresses, and stress concentrations found in traditional composites. FGMs occur in nature as bones, teeth etc. Nature designed these materials to meet their expected service requirements. This idea is emulated from nature to solve engineering problem, the same way artificial neural

network is used to emulate human brain. FGM may include more than two constituent phases (as CM) (see Fig. 2).

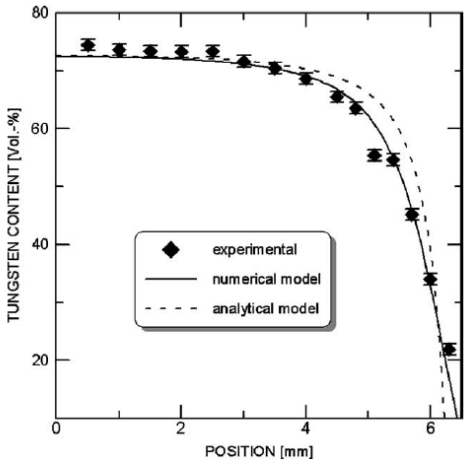


Fig. 1. Comparison of the predicted and observed tungsten content in an electrochemically graded W/Cu composite, (- - -) analytical model; (—) numerical model. The numerical model includes the effects of structural changes on the current distribution in the porous electrode. Initial tungsten content was 75 vol.%, current density 12.2 mA/cm^2 and NaOH concentration 2 mol/l (see Fig. 20 [4]).

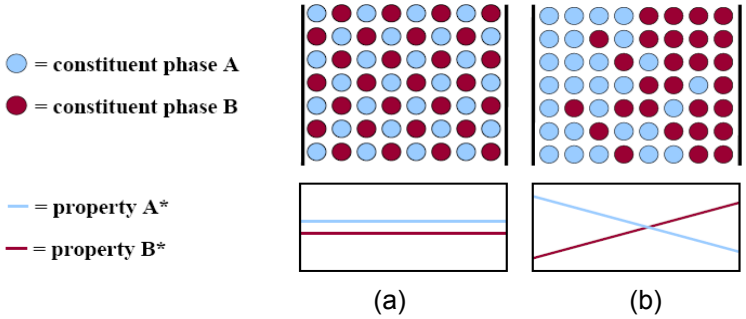


Fig. 2. Material of two phases. (a) constant composition and properties; (b) FGM – gradual change in composition and microstructure gives a gradient in properties [6]

FGM eliminates the sharp interfaces existing in CM which is where failure is initiated [7]. It replaces this sharp interface with a gradient interface which produces smooth transition from one material to the next. One unique characteristic of FGM is the ability to tailor a material for specific application. Such unique characteristics possess also semiconductor superlattices and quantum wells, which electronic structure may tailor for specific applications.

An FGM's gradation in material properties allows the designer to tailor material response to meet design criteria. For example, the Space Shuttle utilizes ceramic tiles as thermal protection from heat generated during re-entry into the Earth's atmosphere. However, these tiles are prone to cracking at the tile / superstructure interface due to differences in thermal expansion coefficients. An FGM made of ceramic and metal can provide the thermal protection and load carrying capability in one material thus eliminating the problem of cracked tiles found on the Space Shuttle.

There are different methods for producing FGMs. FGMs can be divided into two broad groups namely: thin and bulk FGM. Thin FGM are relatively thin sections or thin surface coating, while the bulk FGM are volume of materials which require more labour intensive processes. Thin section or surface coating FGM are produced by Physical or Chemical Vapour Deposition (PVD/CVD), Plasma Spraying, Self-propagating Hightemperature Synthesis (SHS) etc [8]. Bulk FGM is produced using powder metallurgy technique, centrifugal casting method, solid freeform technology etc [9].

3. APPLICATION AREAS OF FGMS

FGMs find various applications in aerospace, automobile, medicine, sport, energy, sensors, optoelectronic etc [10]. Owing to the importance of FGM applications, there are lots of research efforts at improving the material processing, fabrication processing and properties of the FGM. Here we present a brief overview of application areas of FGMs:

3.1. Aerospace

FGMs possess very high thermal gradient resistivity, which makes them suitable for use in structures and materials for space plane body, rocket engine component and are promising in wider areas of aerospace industry [11].

3.2. Medicine

FGMs have find a wide range of applications mostly in dental [12] and orthopedic applications for teeth and bone replacement [13].

3.3. Defense

FGMs have the strong ability to inhibit crack propagation. This property makes them useful in defense applications, as a penetration resistant materials used for armour plates and bullet-proof vests [14].

3.4. Energy

FGMs are used in energy industry as energy conversion devices. They also provide thermal barrier and are used as protective coating on turbine blades in gas turbine engine [5].

3.5. Optoelectronics

FGMs are used in optoelectronics as graded refractive index materials and in audio-video discs magnetic storage media.

Other areas of application are: cutting tool insert coating, automobile engine components, nuclear reactor components, turbine blade, heat exchanger, tribology, sensors, fire retardant doors, etc [5]. The list is endless and more application is springing up as the processing technology, cost of production and properties of FMGs improve [5].

4. RECENT RESEARCH ACTIVITIES IN FGM

A lot of studies have been made on the subject of the properties, manufacturing and behavour of FGMs [5], and the literature is very rich on this because of the wide areas of application of this novel and useful materials. Performance of FGM under localized transverse loading was investigated by Woodward and Kashtalyan [15]. A comprehensive review on performance of FGM was published in 2007 by Birman and Byrd, [16]. An overview on fracture behaviour of FGM was conducted by Shanmugavel et al., [17]. Other reviews on FGMs available in the literature are: review study on research and development by Cherradi et al., [18], Tilbrook et al., also conducted review study on crack propagation in functionally graded materials [19]. A number of researches have also been conducted in the areas of analysis and modeling work on functionally graded material; some of these work can be found in [5]. There are still more to be done in terms of research to improve the performance of manufacturing processes of FGM.

5. MODELING OF FGM PROCESSING

In the field of FGMs computer simulations and modeling (which are an important component of modern science) are particularly useful. They complement, develop and connect theory and experiment and technology. Today modeling can predict many of the properties of substances from their composition. Here we also examine the possibilities for the application of computer modeling and numerical simulations tools for the design of parts and for the optimization of manufacturing processes. Process modeling may be especially important in connection with functionally graded

materials, since gradients often cause special problems. In some cases the simulation can help to establish the desired gradient, and to maintain it throughout the entire process by an appropriate process control. In other cases, process modeling may help to circumvent or at least minimize problems such as warpage or cracking during the fabrication of a component.

The theses [20] show the accuracy of modeling FGMs using ABAQUS software. Conclusions drawn from FGM characterization are used to develop a patch to retrofit a cracked aircraft exhaust wash structure and reduce thermally induced cracking.

In [6] were reported several simulations on FGMs. Here are some of them:

- In order to account for the gradient, several SEM images were assembled and used to build the FEM grids;
- Thermal residual stresses were simulated and experimentally measured on samples obtained by percolation in alumina substrates (see Fig. 2);
- The hydrostatic stress in the alumina was calculated as a function of depth along the glass infiltration direction. The simulated values were compared with the experimental ones, obtained by means of apiezo-spectroscopic technique (see Fig. 3);
- Elastic properties - OOF allowed to evaluate the elastic properties as a function of depth. The so obtained values could be compared with the results of the Rule of Mixture and with the experimental data obtained via a depth-sensing Vickers micro-indentation test performed on the cross section;
- In the plasma sprayed systems, the predicted values were slightly overestimated with respect to the experimental ones. The discrepancies were likely to be caused bymicrocracksand other defects which, due to their thinness, could be hardly seen in SEM images (see Fig. 4);
- Crack propagation - in FGM specimens obtained via percolation, cracks mainly started from residual pores and then propagated through glass domains. The system failure was substantially governed by microstructural defects (pores) and glass spatial distribution. No delamination was predicted;
- In the plasma sprayed sample, the weakest link –as far as the adhesion was concerned –was represented by the graded coating-substrate interface; the coating broke off from the substrate when the (simulated) applied strain was just 0.2%.

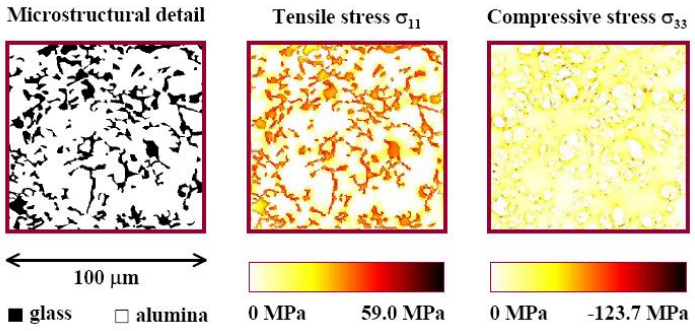


Fig. 2. Simulations –Thermal residual stresses [6]

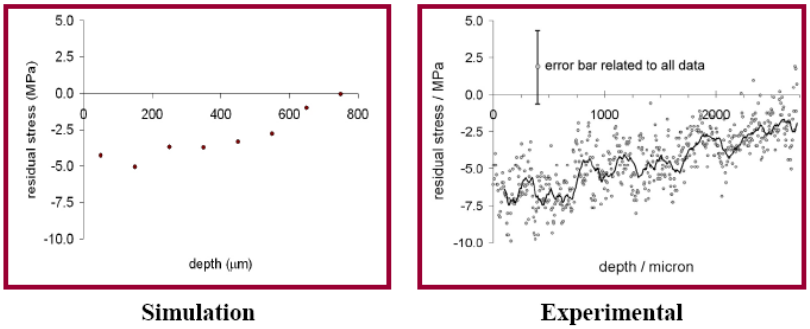


Fig. 3. Simulations –Thermal residual stresses. Hydrostatic stress in alumina [6]

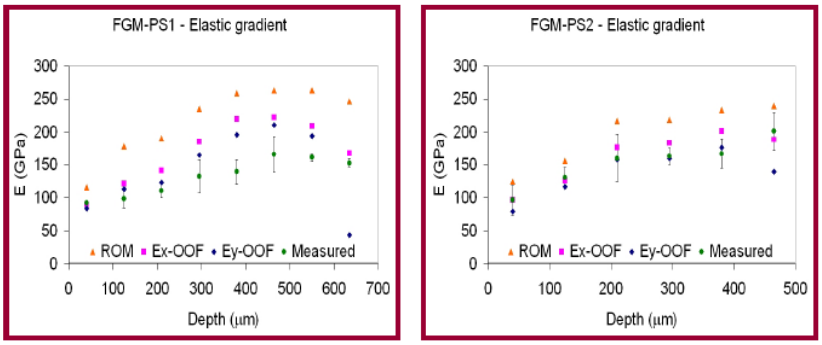


Fig. 4. Simulations –Elastic properties [6]

6. FINAL REMARKS AND FUTURE RESEARCH DIRECTION

FGMs are really complex systems: they are multi-phase materials, with a peculiar compositional and microstructural variation in space. FGMs represent a rapidly developing area of science and engineering with numerous practical and potential applications. The research needs in this area are uniquely numerous and diverse, but FGMs promise significant potential benefits that fully justify the necessary effort.

By exploiting the possibilities in the FGM concept, it is anticipated that scientists and engineers will optimize the properties of material systems and new and novel multifunctionalities, and applications will be created.

The recent progress in the characterization, modeling, and analysis of FGM has been briefly reviewed in this paper. Due to the broad and rapidly developing field of FGM, these conclusions cannot encompass all significant directions, trends, and needs. Nevertheless, they reflect some of the observations based on the published research.

To faithfully predict the properties and performances of FGMs, a suitable computational tool is required, which is able to account for the microstructural features of such graded systems (distribution of the constituent phases; pores; interfaces; etc.). This field of activity is now widely open to every scientist.

REFERENCES

1. 13th International Symposium on Multiscale, Multifunctional and Functionally Graded Materials October 19-22, 2014, Taua Resort, SP, Brazil.
2. Bever, M.B., P.F. Duwez, Mater. Sci. Eng., Vol. 10, 1972, 1–8.
3. Shen, M., M.B. Bever, J. Mater. Sci., Vol. 7, 1972, 741–746.
4. Kieback, B., A. Neubrand, H. Riedel, Processing techniques for functionally graded materials, Mater. Sci. Eng., Vol. A362, 2003, 81–105.
5. Rasheedat M. Mahamood, Esther T. Akinlabi Member, IAENG, Mukul Shukla and Sisa Pityana
6. Rasheedat M. Mahamood, Esther T. Akinlabi Member, IAENG, Mukul Shukla and Sisa Pityana
5. Mahamood, R. M., E. T. Akinlabi, M. Shukla, S. Pityana, Functionally Graded Material: An Overview, Proceedings of the World Congress on Engineering, Vol III, 2012, London, U.K.
6. Cannillo, V., L. Lusvarghi, T. Manfredini, M. Montorsi, C. Siligardi, A. Sola , Functionally Graded Materials: prevision of properties and performances, OOF Workshop–24, 25 August 2006, Dipartimento di Ingegneria dei Materiali e dell'Ambiente University of Modena and Reggio Emilia – Italy.
7. Miteva, A., On the microstructure and the strengthening of aliminium alloys, Tribological Journal BULTRIB, Papers from the 9-th International Conference BULTRIB '12, October 18-20 2012 Sofia, ISSN: 1313-9878, Publ. House TU-Sofia, Sofia 2013, vol. 3, 2013, 367-370.
8. Ivosevic, M., R. Knight, S. R. Kalidindi, G. R. Palmese, J. K. Sutter, Solid particle erosion resistance of thermally sprayed functionally graded coatings for polymer matrix composites, Surface Coat Tech, 2005.
9. Knoppers, R., J. W. Gunnink, J. Van den Hout, W. Van Vliet, The reality of functionally graded material products, TNO Science and Industry, The Netherlands, 38-43.
10. Functionally Graded Material by European virtual institute of knowledge-based multifunctional material, Accessed on 10th of January 2012, Available at http://www.kmmvin.eu/Research/FunctionallyGradedMaterials/tabid/68/Default.aspx

11. Marin, L., Numerical solution of the Cauchy problem for steady-state heat transfer in two dimensional functionally graded materials, Int. J. Solids Struct, Vol. 42, 2005, 4338-4351.
12. Matsuo, S., F. Watari, N. Ohata, Fabrication of functionally graded dental composite resin post and core by laser lithography and finite element analysis of its stress relaxation effect on tooth root, Dental Mater J, Vol.20(4), 2001, 257–274.
13. Watari, F., A. Yokoyama, M. Omori, T. Hirai, H. Kondo, M. Uo, et al. Biocompatibility of materials and development to functionally graded implant for bio-medical application, Compos Sci Technol, Vol. 64, 2004, 893–908.
14. Lu, L., M. Chekroun, O. Abraham, V. Maupin, G. Villain, Mechanical properties estimation of functionally graded materials using surface waves recorded with a laser interferometer, NDT & E International, Vol. 44 (2), 2011, 169-177.
15. Malinina, M., T. Sammi, M. Gasik, Corrosion resistance of homogeneous and FGM coatings, Mater Sci Forum, vol.492–493, (2005), 305–310.
16. Birman, V., L.W. Byrd, Modeling and analysis of Functionally graded materials and structures, Appl Mech Rev, Vol. 60(1–6), 2007, 195–216.
17. Shanmugavel, P., G. B. Bhaskar, M. Chandrasekaran, P. S. Mani, S. P. Srinivasan, An overview of fracture analysis in functionally graded materials, Eur. J. Sci. Res., Vol.68 (3), 2012, 412-439.
18. Cherradi, N., A. Kawasaki, M. Gasik, Worldwide trends in functional gradient materials research and development, Compos Eng, Vol. 8, 1994, 883-894.
19. Tilbrook, M. T., R. J. Moon, M. Hoffman, Crack propagation in graded composites, Compo Sci Tech, Vol. 65, 2005, 201-220.
20. Cooley, W. G., Application of functionally graded materials in aircraft structures, Thesis, Dep. of the air force university, air force institute of technology, Wright-Patterson Air Force Base, Ohio, March 2005.

CORRESPONDENCE

Adelina MITEVA
Space Research and Technology Institute, Bulgarian Academy of Sciences,
“Acad. G. Bonchev” Street, Block 1, Sofia 1113, Bulgaria
e-mail: ad.miteva@gmail.com

Tribological Journal BULTRIB, **Vol. IV, 2014**
Papers from the International Conference **BULTRIB '13**
October 24-26, 2013, Sofia
Society of Bulgarian Tribologists
Technical University of Sofia

КОНЦЕПТУАЛНИ ТРИБОЛОГИЧНИ ПРОБЛЕМИ

Маг.инж. Цонка Костевска

Резюме:*Триенето, износването и смазването на телата в природата и в частност в техниката, са явления неизбежни при използването на механични връзки, машини и технически съоръжения. Докладът разглежда накратко развитието на трибологията в различни технически направления на човешката дейност.*

***Ключови думи**: трибология, триене, смазване, износване, нанотрибология.*

***Resume:** Friction, wear and lubrication of the bodies in nature, particularly in technology are inevitable phenomena in the use of mechanical joints, machinery and equipment. The report briefly discusses the development of tribology in various technical areas of human activity.*

***Keywords:** tribology, friction, lubrication, wear, nanotribology.*

КОНЦЕПТУАЛНИ ТРИБОЛОГИЧНИ ПРОБЛЕМИ

(по материали от световния печат)

Маг.инж. Цонка Костевска

Триенето, износването и смазването на телата в природата и в частност в техниката, са явления неизбежни при използването на механични връзки, машини и технически съоръжения. Те съпътстват развитието и упадъка на редица цивилизации на човечеството. Хората от една или друга епоха са прилагали различни начини и средства, например течности от разновиден характер, за да преодолеят критични прояви в съоръженията при наличие на триене, износване или смазване при контакт - статичен или от релативното преместване на една спрямо друга на минимум две допиращи се повърхности. Военната индустрия в съвременния свят, след Втората световна война и последващата я Студена война, се развива бурно. Вложените инвестиции изискват качество и съответно количество. Производството е главно в областите авиация, корабоплаване, автомобилостроене, военна техника, а оттам и в съпътстващите ги индустрии. Началото е през 1946 година в САЩ, Великобритания, Франция, СССР, а в последствие във Федерална Република Германия /ФРГ/ и Япония. Производители на техническите изделия в тези страни отчитат през 1960 година големи загуби по отношение на машини, съоръжения и съставните им части поради износване, липса на достатъчно резервни количества и финансови загуби, причинени от тези ситуации. Решаването на част от проблемите е съпътствано от развитието на нови интер дисциплинарни науки като екологията, кибернетика, трибология.

Триенето е явление, отрицателно за продуктите на тези производства. Намалява коефициента на полезно действие, създава обстоятелства за загуба на енергия и износване на съответните допирни тела, последвани от загуби на материали, съответно на детайли. Загубите са огромни

в световен мащаб. Тези факти стават база за възникване на науката трибология през 1966 г. Неин основател е проф. Питър Джост

/ Peter Jost /. Днес, страни като Германия, САЩ, Канада, Китай, Великобритания и Япония са изчислили, че спестяванията, от инвестиране в решаването на проблеми, свързани с триенето, отговарят на 1,4% от БВП.

Съществуват две главни теми в екологичния аспект на трибологията и те са свързани с това да бъдат сведени до минимум съответно:

- Износването на материалите и консумацията на енергия /основно електрическа и физическа/ като се прилагат знанията за процеса на триенето.
- Страничните ефекти или нежеланите последици от практическото приложение на триенето.

Трибологията прави първи стъпки в производството с основната цел да подобри работата и удължи жизнения цикъл на машините в редица индустрии.
Биват насърчавани икономическите и екологичните ползи от контрола на триенето и намаляването на износването в процесите на експлоатацията на изделията.Трибологията е част от образованието на висшите технически кадри. Учени от редица страни изследват и разработват нови нови методи и технологии, чието приложение в практиката позволява икономия на материали и дълготрайност при експлоатация на изделията.
Науката трибология ще намира все повече практическо приложение в областите хуманна и дентална медицина, нанотехнологии, алтернативни източници на енергия, вятърни турбини, екология.

Нанотрибологията изучава процесите, характерни за ултра ниско налягане на контакт на приплъзването и зацепването при повърхностите на контактуващи тела,.

Развитието на микроелектрониката, системите за магнитно съхранение на информацията и разработването на нови материали с дебелини от порядъка на нано размери през 90-те години на 20 век, развиват трибологията и нейното приложение в нова област - нанотрибология или молекулярна трибология.Това направление е свързано с теоретичното и експерименталното изучаване на процесите на триене, износване, взаимодействие на повърхностите, адхезия, износване на контактните повърхности в атомни и молекулярни размери.

Появяват се нови технологии в изчислителната техника и това изисква нанотрибология да изследва различни процеси на атомно, молекулно и микроскопично ниво.Тези изследвания подпомагат развитието на знанията относно микро- и наноструктури на различни видове повъхности и/или маси. Намират приложение в областта на химията, системите за производства на лекарства, създаване на наночастици с различни приложения в техниката, чип системи, ново поколение лазери.

Биотрибологията е всъщност трибология, която намира приложение в медико-биологични системи.Включва гама от изделия и материали заместващи увредени части от човешкото и/ или животинското тяло.Те са разработени от синтетични или естествени тъкани подходяши за приложението им в сложни интерактивни биологични среди. Изделията са съобразени с процеса на триене в жизнената среда, вида, дизайна и начина на работа на съответния орган или кости, износването и/или смазването съответно на биологични повърхности. Това помага за тяхното безпроблемно приложение при различни нарушения на функциите на органи или кости.

Изделията заместват или подпомагат функциите на кожата, кръвоносните съдове, ставните връзки, хрущялите, дейността на сърцет и други.

Биомиметиката като дума има гръцки произход.Терминът „биомиметика“ свързва две думи - гръцката дума βίος , BIOS - "живот" и наставката „ немиметично ", изразяващо „ мимикрия

".Последната дума, първоначално е използвана още от 1630-те и произлиза от гръцката μιμητικός , mimetikos, което означава „ подражателни " . Биомиметиката е създадена от американския биофизик и енциклопедист Ото Шмит през 1950 г., по време на разработването на неговата докторска дисертация.Тогава той я развива, като изучава нервите в сепия и се опитва да конструира устройство, което да възпроизвежда биологичната система на разпространение на нервите . Продължава да се фокусира върху устройства , които имитират естествените системи от природата.Създава новата наука биомиметика през 1957 г като приема обратно на биофизиката виждане.Смята, че биофизика не е предмет, а е гледна точка. Този подход към проблемите на биологичната наука използва теорията и технологията на физическите науки . Обратно, биомиметиката е подход на биологията към проблемите на физическата наука и инженерство. Измислени и изработени от човешката дейност процеси, устройства, вещества, и системи, които имитират пиродата се наричат биомиметични. Изкуството и науката да бъдат проектирани и изработени биомиметични апарати се нарича биомиметика. Тя намира приложение в областта на нанотехнологиите, роботиката, медицинската и военната промишлености, изкуствения интелект. Някои биомиметични процеси са употребявани при синтеза на витамини и антибиотици. Биомиметиката намира приложение при разработването на системи за машинно зрение, сигнални усилватели, машини за системи за слуха, навигационни системи. Невронната мрежа е хипотетичен биомиметичен компютър, тъй като работи чрез асоциации и предположения. Биомиметиката намира приложение днес при разработването на изкуствани органи и крайница от човешкото тяло, както и в различни електронни устройства. Биочипът, микропроцесорът и оплодената яйцеклетка се считат за най-интересни изобретения в тази област.

Зелената трибология съпътства ежедневието на човека и неговата здеъйност, независимо от характера на последната. Концепцията за зелена трибология е въведена от г-н Питър Жост. Той я определя като „наука и технология относно трибологичните аспекти на екологичното равновесие, екологичните и биологични въздействия“. Учените са убедени, че редица проблеми могат да бъдат решени от зелената трибология. Те разглеждат проблемите на взаимодействащи повърхности в относителна скорост на движение, които имат значение за енергията, устойчивостта на околната среда и/или характера на влияние върху околната среда.

Учените Носоновски /Nosonovsky/ и Бушан / Bhushan/ са предложили, а може би по-точно казано са установили, 12-те принципа на зелената трибология. Те са :

1. Намаляване на триенето;
2. Износване;
3. Намаляване или пълно премахване на смазването, включително самостоятелно смазване /колкото и парадоксално да звучи/;
4. Физическите смазвания
5. Биоразградиа смазвания;
6. Използването на устойчива химия и инженерни принципи;
7. Биомиметични подходи;
8. Повърхностно текстуриране;
9. Екологичните последици от покритията;
10. Мониторинг в реално време;
11. Дизайн за разграждане /Например:Предвиден е начина на разграждане на повърхностното покритие и откриване на повърхността под него./
12. Устойчиви енергийни приложения.

    Същите учени определят и три основни областти на зелената трибология:
    1.Биомиметиката за трибологични приложения;
    2.Смазки, щадящи околната среда;
    3.Трибологията на възобновяема енергия .

Вятърни турбини са едно от големите технически решения на човечеството.Те намират днес приложение като алтернативен източник на енергия.Те са трудни за поддържане и скъпи за ремонт. Възникват проблеми от трибологичен характер в скоростните кутии и смазването на турбината.Тези фактори могат да намалят тяхната надеждност и жизнен цикъл. редица проучвания и изследвания в областта на смазочните материали, лагерите и скоростните кутии са правени, а вероятно и ще съпътстват винаги употребата на тези технически съоръжения, с основна цел да се подобри надеждността на турбината в екстремни ситуации.

Трибологията в Космоса е най-новата и най-непозната област на контакта наука – природа. Първите стъпки в това направление са свързани с техниката, която човечеството отправя в дълбините на Вселената. Спътниците и изграждащите ги механични системи са изградени от редица механични части. Има редица изисквания за тяхната надеждност при движение, която е силно ограничена от износването и влошаване на състоянието на смазочните материали. Системите са изложени на различни влияния, характерни за заобикалящото ги космическо пространство - атомен кислород, различни електростаттични частици, слънчева радиация, температурен диапазон - от криогенно до 400^0C. Ниски /криогенни/ температури са тези, които са под 120 К до температура 0,7 К, т.е от температурата на кондензация на природния газ до температурата на хелия във вакуум. Температури под 0,3 К са в областта на свръх ниските температури. Те се получават при използване на специални методи на охлаждане. Горепосочените системи понякога остават в Космоса за години в порядъка от 10 до 30 , а от друга страна се изпитват и съхраняват при земни условия за дълъг период от време.

Нано-композитни и нано-структурирани покрития се прилагат чрез технологиите при които имаме вакуумно отлагане. Техните механични и трибологични свойства зависят от граничните ефекти/възможности на зърната на покритието и съответно синергичните съставки на покритието. Тези покрития предлагат от друга страна изключителна възможност да бъдат произвеждани адаптивни или смарт трибологични покрития. Последните са наречени „хамелеон“ поради способността им да предпазват от триене и износване съответните повърхност, чрез промяна на химическата повърхност и микроструктура при различните въздействия на околната среда, т.е както животинката хамелеон си променя цвета на кожата при възникнала опастност от хищник. Концепцията за мазилни вещества - покрития „хамелеон“ е разработена да отговори на тези предизвикателства. Подходът разчита покритието да промени повърхността, върху която е положено, като химия и като структура т.е. да се самонастройва към околната среда и да постига по този начин съответната дълготрайност. Първото поколение „хамелеон “ покрития са направени от диамантен въглерод /DLC/ , второто - от итрий стабилизиран цирконий /YSZ/ в златни матрици с капсулирани резервоари с наночастици на MoS2 и DLS. Покритията „хамелеон“ с разновиден химически състав се изработват с различни характерни аналитични, механични и трибологични методи.Най – често използваните смазочни материали в космическата индустрия са прахове, разработени на базата на MoS2 , WS2 , NbSe2 и смесени с различни органични и неорганични вещества.

ЛИТЕРАТУРА:

1.Nanocomposite and nanostructured tribological materials for space application, A.A.Voevodin, J.S. Zabinski.

2.MLBT, Air Force Research Laboratory, Materials and Manufacturing Directorate, Wright–Patterson Air Force Base, OH 45433-7750, USA.

3. Bharat B. Nanotribology and Nanomechanics: An Introduction. 2nd ed. — Springer, 2008.— 1516 p.

4. Tom Ricci, ASME.org

5. Engineering Tribology (Fourth Edition) 2014

6. Source:2012 Journal Citation Reports® (Thomson Reuters, 2013)

7.Bio-tribology and bio-mimetics in the operating environment, D. Dowson, A. Neville,School of Mechanical Engineering, The University of Leeds, Leeds, UK

8. "Mimetic". Online Etymological Dictionary.

9. Vincent, Julian F.V.; Bogatyreva, Olga A., Bogatyrev, Nikolaj R., Bowyer, Adrian, Pahl, Anja-Karina (21 August 2006). "Biomimetics: its practice and theory". Journal of The Royal Society Interface 3 (9): 471–482. doi:10.1098/rsif.2006.0127.

10. "Otto H. Schmitt, Como People of the Past". Connie Sullivan, Como History Article.

11. Vincent, Julian F. V. (November 2009). "Biomimetics -- a review". Journal of Engineering in Medicine. Proceedings of the Institution of Mechanical Engineers. Part H 223 (8): 919–939. doi:10.1243/09544119JEIM561.

12. Schmitt O. Third Int. Biophysics Congress. 1969. Some interesting and useful biomimetic transforms. p. 297.

(по материали от световния печат)

КОРЕСПОНДЕНЦИЯ:

Костевска Цонка, 0895586129

„Креди Йес София“ ЕООД,

Гр. София 1000, ул. Славянска № 29

tzkosti@abv.bg

Tribological Journal BULTRIB, **Vol. IV, 2014**
Papers from the International Conference **BULTRIB '13**
October 24-26, 2013, Sofia
Society of Bulgarian Tribologists
Technical University of Sofia

STUDY OF MATERIALS AND COATINGS THAT WORK UNDER CONDITIONS OF IMPACT-ABRASION

Kristina ILIEVA-STOYCHEVA

Abstract: *The object of this paper is the wear of elements that work under conditions of impact-abrasion wear. For the needs of the study it has been elaborated a bench for testing the impact-abrasion wear of materials and coatings. In this paper are given the methods for conducting of bench tests in accordance with the international.*

Key Words*: tribology, impact-abrasion wear, bench, construction, methods*

ИЗСЛЕДВАНЕ НА МАТЕРИАЛИ И ПОКРИТИЯ, РАБОТЕЩИ В УСЛОВИЯТА НА УДАРНО-АБРАЗИВНО НАТОВАРВАНЕ

Кристина ИЛИЕВА-СТОЙЧЕВА

Резюме: *В статията са разгледани въпроси за износването на елементи, работещи в условията на ударно-абразивно износване. За нуждите на изследването е разработен стенд за изследване на ударно-абразивно износване на материали и покрития. Показана е методиката за провеждане на изследвания със стенда съгласно международни стандарти.*

Ключови думи**:** *трибология, ударно-абразивно износване, стенд, конструкция, методика*

1. ВЪВЕДЕНИЕ

Основна причина за намаляване на дълготрайността на детайлите на машините, механизмите и инструментите в машиностроенето е износването. В следствие на износването се съкръщава ефективното време за работа на машините и усилията се насочват към ремонт, възстановяване и замяна на износените детайли.

Видовете износвания са различни и се определят в зависимост от условия на работа на конкретните обекти. По-голямата част от минната механизация е подложена на ударно натоварване във връзка със спецификата на технологичните процеси /трошене, смилане, копаене/. Контактът със силно абразивна среда също е предпоставка за износване.

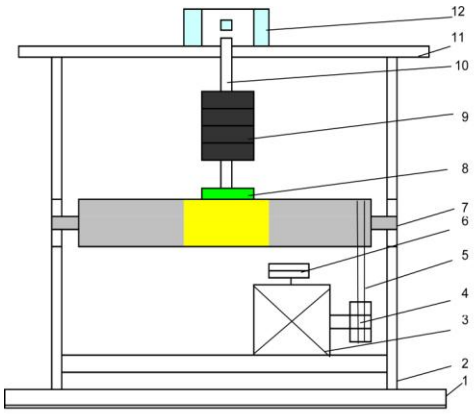
Ударно-абразивното износване протича при удар по твърди частици, които могат да повреждат контактната повърхност от прякото им динамично внедряване [1]. Механизмът на ударно-абразивното износване са състои във внедряването на твърдата частица в метала и предизвикването на деформация, водеща до разрушаване на микрообеми в метала и образуване на частици от износването.

2. УСТРОЙСТВО И МЕТОДИКА НА СТЕНД ЗА УДАРНО-АБРАЗИВНО ИЗНОСВАНЕ

Изследванията на ударно-абразивно износване на материали и покрития се осъществяват със стенд, разработен в катедра „Машинознание” на МГУ „Св.Иван Рилски” – София [2, 3].

2.1. Устройство

Функционалната схема на стенда е показана на Фиг. 1, а стенда – на Фиг 2.



Фиг. 1. Схема на стенд за ударно-абразивно износване



Фиг. 2. Стенд за ударно-абразивно износване

Стендът представлява метална конструкция, състояща се от носещи греди 2, на които е монтирана ролка 7 с абразивно покритие под зоната на образеца и хоризонтална греда 11, върху която е монтиран електромагнит 12. Изследваният образец 8 е закрепен неподвижно към захващащото приспособление на прът 10. Върху подложения на изследване образец се създава натоварване с помощта на тежести 9 и ударни импулси, създавани с електромагнит 12. На ролката 7 се предава въртящ момент от двигателя 3 чрез ремъчна шайба 4 и ремък 5. Образецът 8 се трие в абразива на въртящата се ролка 7 и успоредно с това му се предава ударен импулс от електромагнита 12 посредством пръта 10. Предаваният на образеца удар е централен с ъглово отклонение до 5^0 .

Енергията на удара по образеца може да варира в диапазон от 3 до 30 J, което се постига с набор от различни по мощност електромагнити.

Опитите са проведени при изпитания с енергия на удара 4.9 J и скорост на удар 1 m/s с честота на ударите 50 Hz и абразив - шкурка № E-28-P80.

Отчитането на масата на образците е с електронна везна WPS180/C/2 с точност до 0.1 mg.

Изпитанията са проведени при еднакви за образците условия /време на изпитване, енергия на удара и физически обем на образеца/.

2.2. Методика на изчисляване на ударно-абразивно износване

Методиката на изчисляване на ударно-абразивно износване включва определяне на следните параметри: средна загуба на тегло и относителна износоустойчивост.

Средната загуба на тегло на образците от изследвания материал се определя по формулата:

$$g_u = \frac{\sum_1^3 g_{ui}}{3}, \qquad (1)$$

където:

g_{ui} - маса на изследвания материал при отделните опити, [g],

Относителната износоустойчивост на изследвания материал се определя по формулата:

$$i = \frac{\rho_u}{g_u}.V_e \,, \qquad (2)$$

където:

V_e - обем на изследвания материал, [sm^3],

ρ_u - плътност на изследвания материал, [g/sm^3],

2.3. Резултати

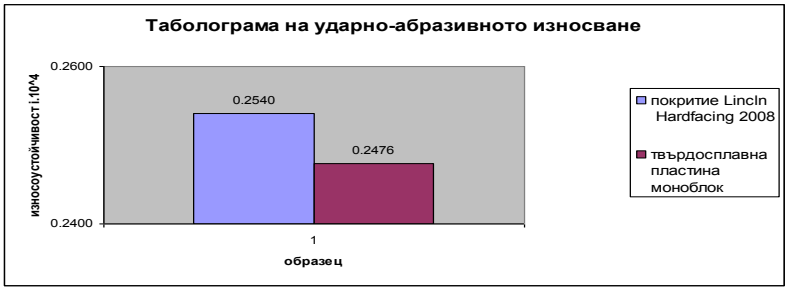
Опитите протичат с три тела от изпитвания образец и три тела от еталонния образец. Резултатите се нанасят в протокол и се определя относителната износоустойчивост по методиката.

Изследваните образци са: 1 – електродно покритие Lincoln Hardfacing 2008 и 2 – твърдосплавна пластина моноблок и в таблица 1 са показани резултатите от опитите за ударно-абразивно износване.

Таблица 1. Резултати от ударно-абразивното износване

Обра-зец	наиме-нование	плът-ност [g/m^3]	обем [sm^3]	опит	маса преди удара [g]	маса след удара [g]	загуба на масата [g]	средна загуба на масата [g]	износо-устой-чивост
1	Покритие Lincln Hardfacing 2008	7.61	5.44	1 2 3	41.4510 41.4349 41.4182	41.4350 41.4183 41.4018	0.0160 0.0166 0.0164	0.0163	0.2540.10^4
2	Твърдо-сплавна пластина моноблок	13.748	5.44	1 2 3	74.8794 74.8491 74.8191	74.8491 74.8190 74.7891	0.0303 0.0301 0.0300	0.3020	0.2476.10^4

На Фиг. 3 е представена диаграма на относителната износоустойчивост на изследваните образци при ударно-абразивно износване.



Фиг. 3. Износоустойчивост на образците при ударно-абразивно износване

След анализ на направените експериментални резултати се констатират сходни резултати на относителната износоустойчивост на изследваното покритие и материала.

3. ЗАКЛЮЧЕНИЕ

Създаването на инженерни методи за определяне на интензивността на износване при удар и прогнозирането му е свързано с установяване на зависимостта между износването и физико-механичните свойства, силовите характеристики и микрогеометрията на контактните повърхности.

Ударно-абразивното износване е широко разпространено в много отрасли на машиностроенето и определянето на основните му признаци е с научно и практическо приложение.

ЛИТЕРАТУРА

1. ВИНОГРАДОВ, В. Н., СОРОКИН, Г. М., АЛБАГЧИЕВ, А. Ю., Изнашивание при ударе, Машиностроене, Москва, 1982.
2. ГОСТ 23.207-79, Обеспечение износостойкости изделий. Метод испытаний машиностроительных материалов на ударно-абразивное изнашивание.
3. ИЛИЕВА-СТОЙЧЕВА, К. К., Изследване на износоустойчивостта на пробивен инструмент от минната механизация, Дисертация, София, 2014.

КОРЕСПОНДЕНЦИЯ

Кристина ИЛИЕВА-СТОЙЧЕВА
Филиал на МГУ „Св. Иван Рилски” София – Кърджали,
Кърджали, 6600, ул.Георги Кондолов 24, ст.100
e-mail: *ilievakrisi@gmail.com*

Tribological Journal BULTRIB, Vol. IV, 2014
Papers from the International Conference BULTRIB '13
October 24-26, 2013, Sofia
Society of Bulgarian Tribologists
Technical University of Sofia

ИЗСЛЕДВАНЕ НА СТРУКТУРАТА И МИКРОТВЪРДОСТТА НА ЗАВАРЕНИ ОБРАЗЦИ ОТ СТОМАНА WELDOX 700

гл.ас. д-р Елисавета Ташева, гл.ас. Валентин Гайдаров, доц. д-р Пламен Ташев,
доц. д-р Галина Замфирова, доц. д-р Серьожа Вълканов

***Резюме:**. Проведено е металографско и микроиндентационно изследване на образци от високояка стомана Weldox 700. Изследването е направено на образци от ръчно електродъгово заварени съединения. Изследването включва и определяне на редица характеристики: микротвърдост по Викерс и Оливер-Фаар, Динамична и Мартенсова микротвърдост, модул на еластичност и др. и дава възможност за оценка на механичните свойства на материала в различни характерни зони в и около заваръчния шев. Направен е анализ на получените резултати от гледна точка на връзката между микроиндентационните характеристики и структурата на материала.*

***Ключови думи:** заваряване, стомани, ъглови заварени съединения, високояки стомани, микротвърдост, динамична и мартенсова микротвърдост, модул на еластичност, Weldox 700*

1. Въведение

Weldox 700 е конструкционна стомана с висока якост и широко приложение за изработването на носещи конструкции. Характеризира се с повтаряемост на свойствата, и добра заваряемост. Weldox 700 отговаря на изискванията на EN 10025. Изследователи на съвремените високояки стомани са установили.[2]

Анализ на структурата на тези стомани е затруднено, поради известна свобода при избора на химичен състав и технология на производство от производителите. [4].

За да се постигане необходимото високо качество на заварени съединения от тази стомана е необходимо да се даде оценка на заваряемостта на стоманата.

2. Същност на изследването.

Проведени са серия експерименти с метод и устройство за изпитване и оценяване склонността към образуване на студени пукнатини на ъглови заварени съединения от високояки стомани. [1]

Изпитваните образци са изработени от листов материал с дебелина 5 mm.

Химическият състав и механичните свойства на стоманата според приложеният сертификат са показани в таблици 1 и 2.

Експериментите са проведени с метод ръчно електродъгово заваряване с обмазани електроди. Тип на обмазката на електода – базична.

Таблица 1. Химически състав в %

C	Si	Mn	Cr	Mo	Ni	Cu	V	Nb	Ti	N
0,13	0,32	1,2	0,24	0,136	0,04	0,01	0,12	0,02	0,014	0,004
Al	B	P	S	EW						
0,042	0,001	0,01	0,002	0,41						

Таблица 2. Механични свойства

Re_{02} [N/mm^2]	Rm [N/mm^2]	A_5 [%]	ISO-V/ -40ºC [J]
828	864	17	50

Използвани са два режима заваряване (табл.3), единият е с линейна енергия Q=0,67 [kJ/mm], която е близка до препоръчваната от фирмата производител за дебелини до 5 [mm], другият режим е с близо два пъти по-висока стойност от препоръчваната - Q=1,24 [kJ/mm].

Таблица 3. Режим на заваряване

Режим к=0,8	d_{el} [mm]	I, [A]	U [V]	$V_{зав.}$ [mm/min]	Q [kJ/mm]
I	4	180	24	167	1,24
II	3,2	100	22	214	0,67

Получените резултати от изпитванията са показани в таблица 4.

Таблица 4 . Резултати от изпитването

Q [kJ/mm]	$T_{8/5}$ [s]	Обр. №	$\sigma_{ог}$ [MPa]	Разрушаване	Дефор. [mm]
1,24	14	1	630	○	x
		2	700	○	x
		3	960	○	3,3
		5	1600	∟	-
0,67	10	6	630	○	x
		7	960	○	2,0
		8	700	○	x

○ – не разрушен образец в продължение на 24 часа

∟ - огънат на 90º и не разрушен образец в продължение на 24 часа

X – няма остатъчна деформация

При първият режим при натоварвания на огъване равни на 630 и на 700 [MPa] не се наблюдава остатъчна деформация и няма разрушаване в продължение на 24 часа. При натоварване от 960 [MPa] се наблюдава остатъчна деформация от 3,3 [mm], без разрушаване, което показва, че е достигната границата на провлачване за тази стомана. Проведено е натоварване с $\sigma_{ог}$ 1600 [MPa], образеца се огъва под 90º без да се разруши.

При вторият режим при натоварвания на огъване равни съответно на 630 и на 700 [MPa] не се наблюдава остатъчна деформация и няма разрушаване в продължение на 24 часа. При натоварване от 960 [MPa] се наблюдава остатъчна деформация от 2,0 [mm], без разрушаване, което показва, че и тук е достигната границата на провлачване на стоманата.

3. Изследване на структурата и микротвърдостта на заварени образци от стомана Weldox 700

За изследване бяха определени образци - № 2, 5, 7 и 8 (съгласно табл.4). Образците бяха разрязани надлъжно по оста на симетрия и от тях бяха изработени металографски шлифове. Характерно за изследваните образци е, че независимо от стойността на натоварването те не са разрушени.

Металографският анализ е направен с микроскоп Olympus BX41 за установяване общия вид на съединението, структурата и евентуални дефекти.

Твърдостта беше измерена в четири зони -1 – метал на шева, 2 – зона на термично влияние, по-близо до линията на сплавяване, 3- зона на термично влияние, по-близо до основния материал, 4 - основен метал (фиг. 1).

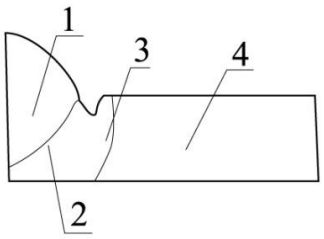
На фигура 2 е показан отпечатък от измерване в зоната на термично влияние на образец №8, при увеличение x500.

Измерванията са проведени с Динамичен ултрамикротвърдомер DUH-211S (Shimatzu-Япония) Условията за изпитанията са:

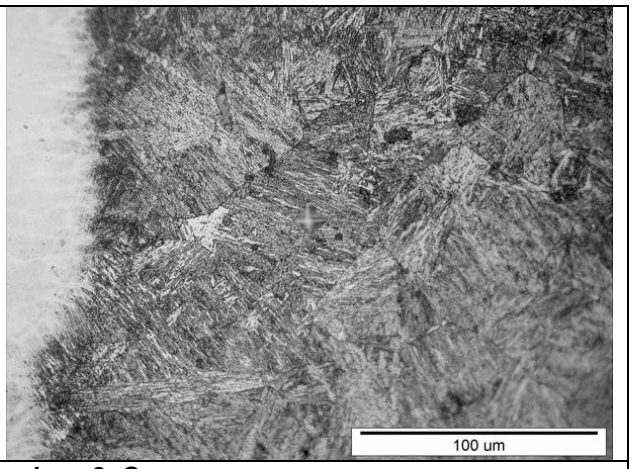
- Режим - натоварване-разтоварване
- Инденторът е Викерсова пирамида (правилна четириъгълна пирамида с ъгъл между срещулежащите страни 136º)
- Скорост на натоварване– 14 mN/s;
- Максимална стойност на натоварването - 500 mN;
- Всички измервания са извършени при стайна температура.

Методите са известни като “depth-sensing indentation“(DSI) или “instrumented indentation testing” (IIT). На фиг. 3 е показана типична индентационна крива. За високо еластични материали тази зависимост не е линейна.

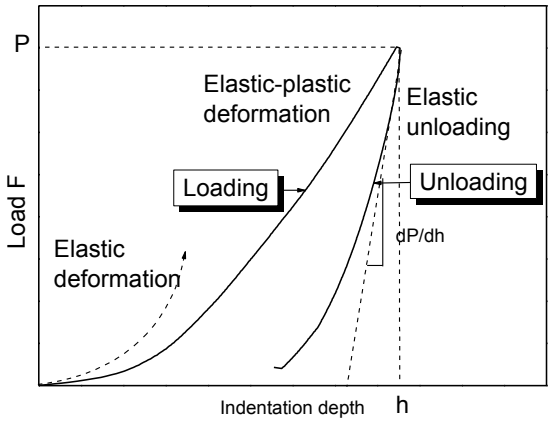
Чрез индентационните криви, могат да се определят следните микротвърдостни характеристики (стандарт ISO 14577-1):



Фиг.1. Твърдост измерена в зони
-1 – метал на шева,
2 – зона на термично влияние, по-близо до линията на сплавяване,
3- зона на термично влияние, по-близо до основния материал,
4 - основен метал



Фиг. 2. Отпечатък в зоната на термично влияние на образец №8 (x500)



Фиг. 3. Зависимост на дълбочината на проникване на индентора, h, като функция на приложеното натоварване, F, при постоянна скорост на натоварването.

1. Динамична твърдост (HMV) [3]:

$$HMV = \frac{a.F}{h^2}$$

където a е константа, определена от вида на индентора, F и h са съответно приложената сила и дълбочина на проникване на индентора. Тази характеристика е свързана с пластичната, еластичната и вискоеластична деформация по време на теста.

2. Мартенсова твърдост (HMs) [3]:

$$HMs = \frac{1}{26{,}43.m^2} \ ,$$

където m е наклона на индентационната крива при натоварване в интервала (0,5-0,9)F_{max}

3. Индентационна твърдост (Hit) [3], определена съгласно модела на Оливер-Фаар:

$$Hit = \frac{P}{24{,}50.h_c^2} \ ,$$

Където h_c е дълбочината на контакта на индентора с повърхността на изследвания образец.

4. Индентационен модул на еластичност (Eit), определящ се от кривата на разтоварване:

$$\frac{1}{E_r} = \frac{\left(1-\nu_s^2\right)}{Eit} + \frac{\left(1-\nu_i^2\right)}{E_i} ,$$

където E_r е модула на еластичност базиран на индентационния контакт, E_i модула на еластичност на индентора, а v_s и v_i са коефициентите на Поасон за образеца и индентора.

5. Еластичната част от работата в процеса на индентация, определена от площта под натоварващата и разтоварващата част на индентационната крива ($W = \int Pdh$), изразена в проценти:

$$\eta it = W_{el}/(W_{el} + W_{pl})$$

6. Микротвърдост по Викерс (HV):

$$HV = \frac{k.F}{d^2} \ ,$$

където к е константа, определена от геометрията на пирамидата, F е приложеното натоварване върху индентора и d е средноаритметичната стойност на двата диагонала на отпечатъка. Микротвърдостта по Викерс характеризира локалното съпротивление срещу пластична деформация.

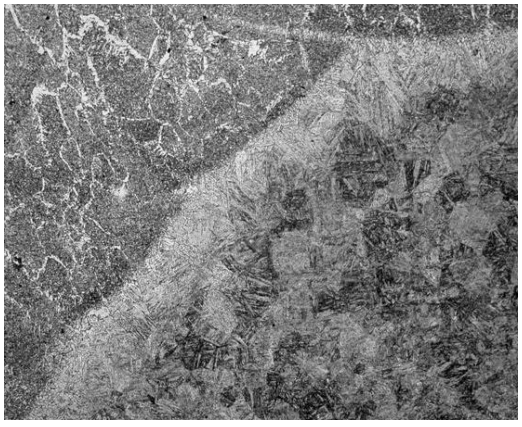
ОБРАЗЕЦ №2

Образецът е натоварен на огъване с 700 [MPa], не се наблюдава остатъчна деформация и няма разрушаване в продължение на 24 часа.

На фиг.4 се виждат трите структури характерни за трите зони на заварени съединения, зоната на метала на шева (МШ), зона на термично влияние (ЗТВ) и основен метал (ОМ). На фиг.5 ясно се вижда линията на сплавяване.



Фиг.4 Структури характерни за трите зони за заварени съединения

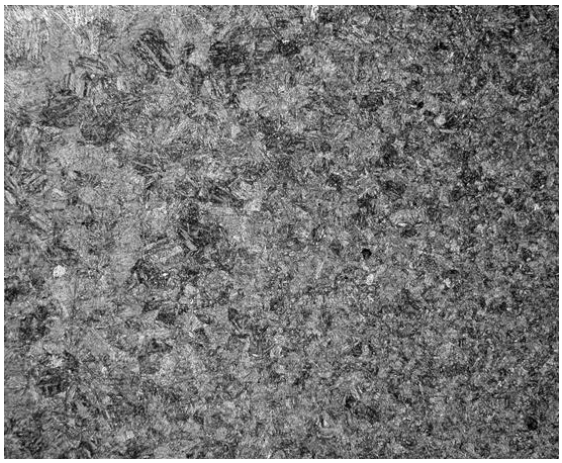


Фиг. 5 Линия на сплавяване

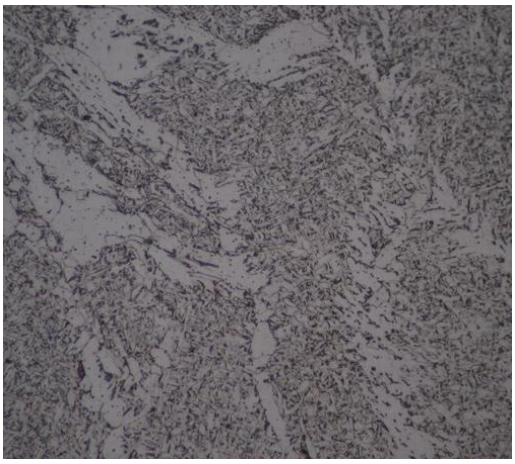
На фиг.6 се наблюдава нисковъглеродна мартензитна структура на зоната на термично влияние (ЗТВ).

На фиг. 7 се вижда феритна структура с нисковъглеродни мартензитни участъци, което е характерно за високояки стомани.

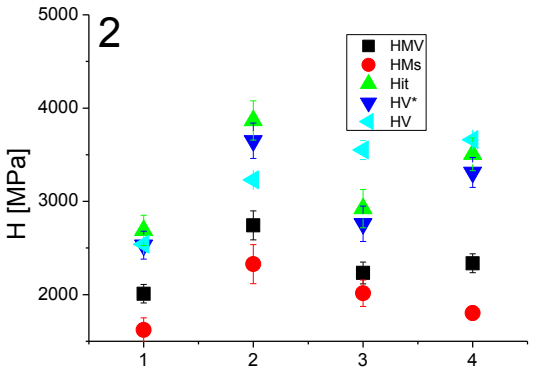
На фиг. 8 е показано изменението на микротвърдостта на образец 2. Стойността ѝ в зона 2 е по-висока, което може да се дължи на образуването на нисковъглероден мартензит.



Фиг. 6. Нисковъглеродна мартензитна структура на зоната на термично влияние (ЗТВ)



Фиг. 7 Феритна структура с нисковъглеродни мартензитни участъци



Фиг.8. Изменение на микротвърдостта на образец 2 в зависимост от зоната на измерване.

ОБРАЗЕЦ №5

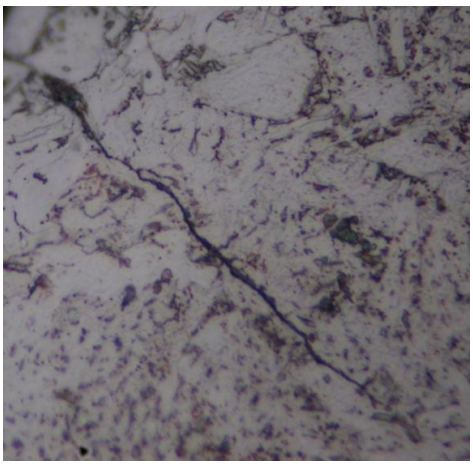
При натоварване с $\sigma_{ог}$ 1600 [MPa], образеца се огъва под 90º и не се разрушава в продължение на 24 часа.

На фиг.9 отново се виждат трите структури характерни за трите зони характерни за заварени съединения, зоната на метала на шева (МШ), зона на термично влияние (ЗТВ) и основен метал (ОМ), както и линията на сплавяване. Въпреки, че няма разрушаване на фиг. 10 ясно се вижда пукнатина.

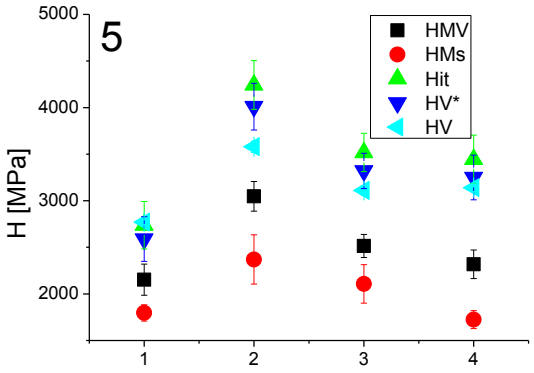
При натоварване с $\sigma_{ог}$ 1600 [MPa], образец №5 се огъва под 90º и не се разрушава в продължение на 24 часа. Отново имаме по-високи стойности на микротвърдост в зона 2 (фиг.11), в резултат и на протеклата пластичната деформация



Фиг.9 Структури на метала на шева (МШ), зона на термично влияние (ЗТВ), основен метал (ОМ)



Фиг. 10. Пукнатина образувала се при огъване на образеца



Фиг.11. Изменение на микротвърдостта на образец 5 в зависимост от зоната на измерване

ОБРАЗЕЦ №7

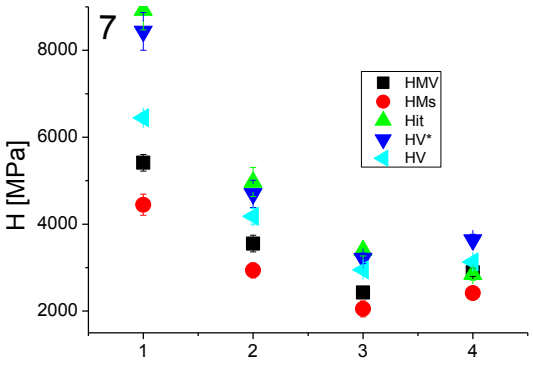
При натоварване от 960 [MPa] се наблюдава остатъчна деформация от 2,0 [mm], без разрушаване, което показва, че е достигната границата на провлачване на стоманата. На фиг.12 се виждат линиите на валцуване.



Фиг.12 Линии на валцуване



Фиг.13 Игловидна микроструктура на нисковъглероден мартензит



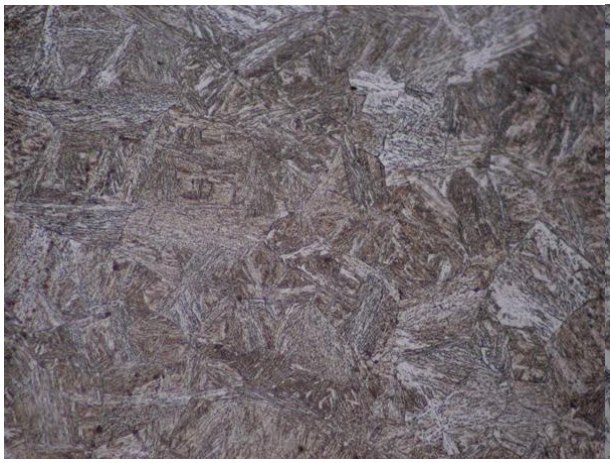
Фиг.14. Изменение на микротвърдостта на образец 7 в зависимост от зоната на измерване

На фиг.13 се вижда игловидния характер на микроструктурата на нисковъглеродния мартензит. На фиг. 14 е дадено изменението на микротвърдостта в зависимост от зоната на измерване.

ОБРАЗЕЦ № 8

При натоварване с σ_{oz}700 [MPa] не се наблюдава остатъчна деформация и няма разрушаване в продължение на 24 часа. Отново се наблюдава нисковъглеродна мартензитна структура на зоната на термично влияние (ЗТВ) (фиг.15). На фиг. 16 се виждат много фини зърна на ферит и титанови нитриди.

На фиг. 17 се вижда изменението на микротвърдостта на образец 8 в зависимост от зоната на измерване

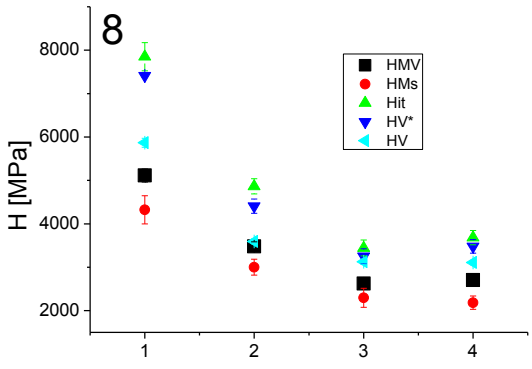


Фиг.15. Нисковъглеродна мартензитна структура (ЗТВ)

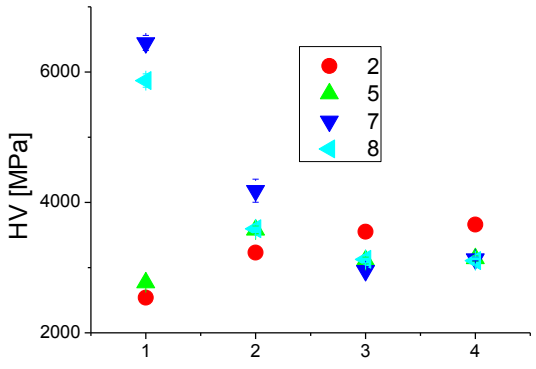


Фиг.16. Фини зърна на ферит и титанови нитриди

Микротвърдостта по Викерс HV е показана на фиг. 18, вижда се че стойностите й в зони 2,3 и 4, и на четирите образеца са от един порядък, разликата в зона 1 може да се обясни с попадане на индикатора в области с по-високо съдържание на карбиди.

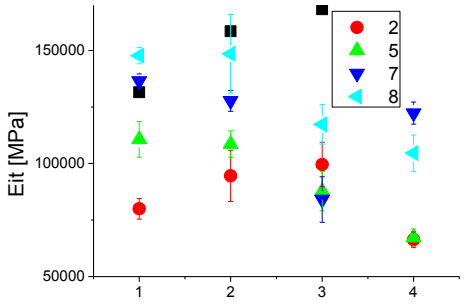


Фиг.17. Изменение на микротвърдостта на образец 8 в зависимост от зоната на измерване

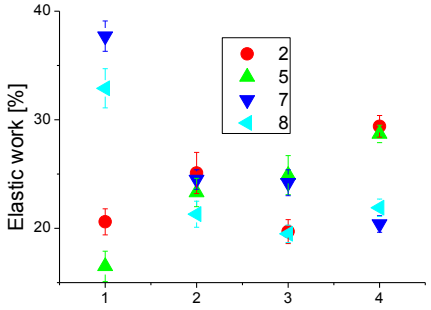


Фиг.18. Микротвърдост по Викерс HV

Индентационен модул на еластичност (Eit), определящ се от кривата на разтоварване на четирите образеца е даден на фиг. 18.



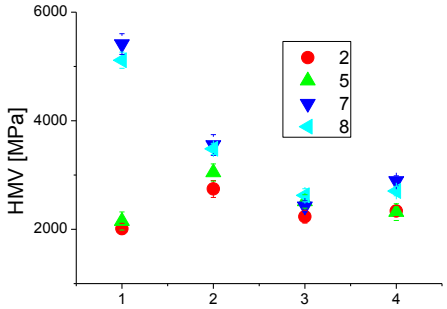
Фиг.19. Индентационен модул на еластичност (Eit), в зоните на измерване



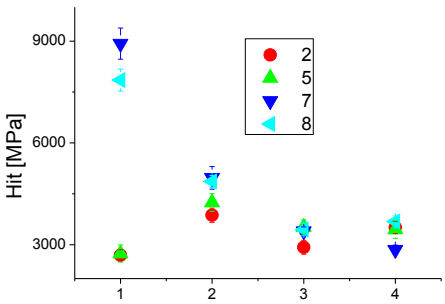
Фиг.20. Еластичната част от работата в процеса на индентация в зоните на измерван

Еластичната част от работата в процеса на индентация, определена от площта под натоварващата и разтоварващата част на индентационната крива е дадена на фиг. 19.

На фиг.21 е показано изменението на Динамична твърдост (HMV) в зоните на измерване на четирите образеца.



Фиг.21. Динамична твърдост (HMV)



Фиг.22. Индентационна твърдост (Hit) на Оливер-Фаар

Изменението на индентационна твърдост (Hit) на Оливер-Фаар е показано на фиг. 22

4. Анализ на резултатите:

Тези резултати са валидни за изследваната дебелина, плавка, метод на заваряване и електрод.

Получената микроструктурата е нисковъглероден мартензит с игловиден характер или феритна структура с нисковъглеродни мартензитни участъци, характерни за стомани с повишена якост, подложени на нагряване съпроводено с определена скорост на охлаждане.

Измерената микротвърдост в зоната на термично влияние зависи от структура, която се получава при получаване на нисковъглероден мартензит се наблюдават по-високи стойности на твърдостта.

При образците, с натоварване довело до преминаване на границата на провлачване се наблюдават по-високи стойностти на микротвърдостта в резултат на пластична деформация.

ЛИТЕРАТУРА

1. Ташева Е, „Оценяване на съпротивлението на високо яка стомана към образуването на студени пукнатини с помощта на специализирана за ъглови съединения от листов материал проба" БулТранс-2011 - Третата конференция с международно участие по авиационна, автомобилна и железопътна техника и технологии, България, Созопол, 27-30 септември 2011, стр. 279-283

2. www.weldox.com

3. http://www.ssi.shimadzu.com/products/literature/Testing/DUH-211_211S.pdf

4. Lachowicz M., Nosko W., Spawanie stali konstrukcyjnej Weldox 700, Przegląd Spawalnictwa 1/2010, 13-18

КОРЕНСПОДЕНЦИЯ

Елисавета Ташева
Висше ТранспортноУчилище "Тодор Каблешков",
ул. "Гео Милев" 158, София 1574, България,
e-mail: elitasheva@abv.bg
Валентин Гайдаров
Висше ТранспортноУчилище "Тодор Каблешков",
ул. "Гео Милев" 158, София 1574, България,
e-mail: v_gaydarov@yahoo.com
Пламен Ташев
ИМСТЦХ - БАН „Акад. А. Балевски",
ул. " Шипченски проход" 67, София 1574, България,
e-mails: weld@abv.bg
Галина Замфирова
Висше ТранспортноУчилище "Тодор Каблешков",
ул. "Гео Милев" 158, София 1574, България,
e-mail:gzamfirova@mail.bg,
Серьожа Вълканов
ИМТЦХ - БАН „Акад. А. Балевски",
ул. " Шипченски проход" 67, София 1574, България,
e-mails: svalkanov@mail.bg;

Tribological Journal BULTRIB, Vol. IV, 2014
Papers from the International Conference BULTRIB '13
October 24-26, 2013, Sofia
Society of Bulgarian Tribologists
Technical University of Sofia

STUDY OF LAYER BUILT-UP WITH ADDING TiN NANOPARTICLES

Assoc. Prof. Dr. Plamen Tashev, Assoc. Prof. Dr. Rumyana Lazarova

Annotation: *On plates of low carbon steel, there layers with nano modifier TiN + Cr are overlaid by TIG method using additional wire. Metallographic examinations on the structures of specimens from surfaced welds with and without introduction of nano modifier are conducted; the microhardness is measured in the base zone, heat affected zone and weld seam metal. Conclusions are made about the influence of the nano modifier on structure and microhardness.*

Key words: *nanomaterials, nano modifiers, nano technology, TiN, overlay welding, TIG, modification, metallography, micro hardness*

Introduction

Recently, with the development of nanotechnology, the ability occurs to modify the metal of the seam with nanometre-scale particles during the processes of welding or overlay welding. The introduction of nano dispersed materials with unique physical chemical and mechanical properties in the fused steel furthers the modification of the metal, steers the redistribution of harmful impurities, decreases the grain size, and leads to formation of a zone or a layer with increased strength, micro hardness, and wear resistance [1, 2]. The influence of the iron cladded nano modifiers TiCN, TiCN and Y2O3 in welding of low carbon steel is examined [3]. It is found that the employment of nano modifier alters the micro structure of the welded joint and improved strength properties and Vickers micro hardness in width and height of the weld are registered.

Nano modifiers used

An alternative to the presently used modifiers are some high-melting compounds (nitrides, carbides, carbonitrides, borides, etc.) as nanopowders obtained through plasma-chemical synthesis and having a small particle size (4-100 nm). The IMSETCH-BAS is conducting research on the impact of various types of nano modifiers on the performance properties of steels and cast irons. The following nano modifiers are used in the experiments: TiC, TiN, TiCN, SiC, etc. [4,5]. The nano powders TiCN, TiC, TiN are manufactured by the company Neomat CO, Latvia and the Institute of Theoretic and Applied Mechanics CO PAH. The powders are passivized with oleic acid for prevention of atmospheric influence. In order to facilitate the wettability, the powders are cladded with Ni, Cr, Fe, Al, Cu, etc. in advance. The cladding is carried out through mechanochemical processing in planetary mills or in special tanks by electroless method [6, 7]

The nanomaterial used for the present development is TiN cladded with Cr.

Preparation of the specimens

The specimens used are plates with thickness 4[mm] made of steel S235JR according to DIN17100/Rst 37-2; EN10025/ S235JR. The chemical content is shown in Table 1.

Table 1. Chemical content of steel S235JR

C max	Mn max	S max	P max	Si	N max
0.17	1.40	0.040	0.040	0.15 – 0.25	0.012

The surfaced of the plates are abrasively cleaned (Fig. 1) and degreased.

Method of overlaying

According to the technology developed, the TIG method is applied for overlay welding, i.e. arc overlay welding in inert gas with unmeltable electrode, using welding wire coated with nano material. The test specimens are overlaid in position PA.

Shielding gas

The inert shielding gas used is argon according to BSS EN ISO 14175 designated as I 1.

Welding wire

The welding wire selected for TIG welding is DT-SGMo according to DIN 8576 with nominal diameter 1.6mm, which is appropriate for overlay welding of specimens of the steel used.

A new and original technology for cladding nano- and ultra-dispersed powders on the welding wire is created [8]. The cladding consists of several operations that ensure uniform distribution of the powders upon the wire's surface. Herein the selected welding wire is used coated with a layer containing nano-modifier TiN +Cr and binding agent.

Equipment and mode of surfacing

The experiments are carried out using equipment Fronius Magic Wave 2500 (Fig. 1). That is designated for TIG welding and surfacing.



Fig. 1. Impulse equipment Fronius Magic Wave 2500 designated for TIG welding and surfacing.



Fig. 2. Surfacing of test specimen

The following welding mode is used:

Welding current I = 90A; voltage U = 12V.

Technique of welding

The equipment used for surface welding is shown in Fig. 2. The additional wire is fed in the zone of the weld bath at a certain distance out of the arc. The wire is fed at angle 30 - 45° to the surface of the welded workpiece. The welding torch and wire move from left to right (for right hand working welder).

Experiments

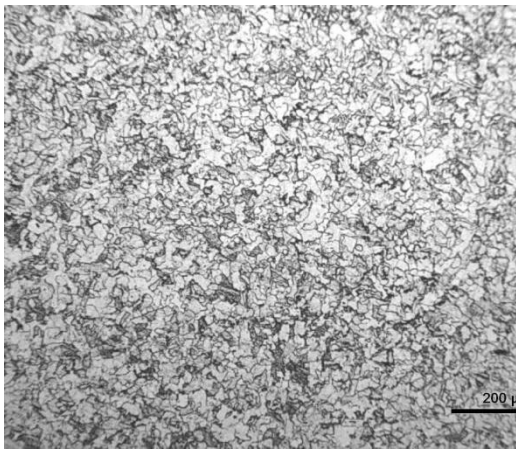
Two types of test specimens of the following designations are surfaced:
Specimen No 1: Reference, made with welding wire without coating.
Specimen No 2: Made using welding wire coated with a layer containing nano-modifier TiN +Cr and bonding compound.

Metallographic analysis

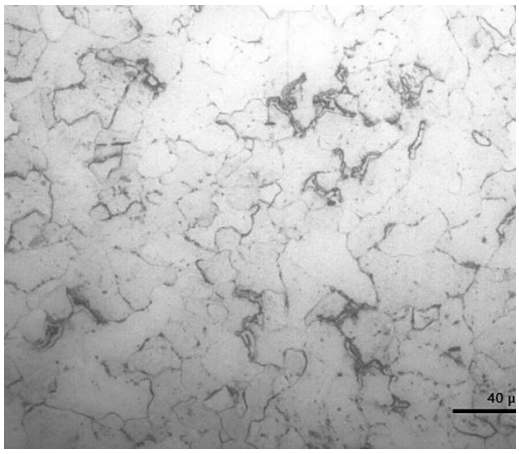
The specimens from overlaid welds are prepared for metallographic examinations according to the methodology developed. The micro-structure is observed using metallographic microscope PolyvarMet from ReichertJung Co. with maximum magnification 1000 x provided with digital camera and computer with display.

In Figures 3 and 4 the metallographic images of the different zones are shown in different magnifications: No 1 without nano-modifier, and No 2 with nano-modifier. The structures of the different zones in two magnifications are shown.

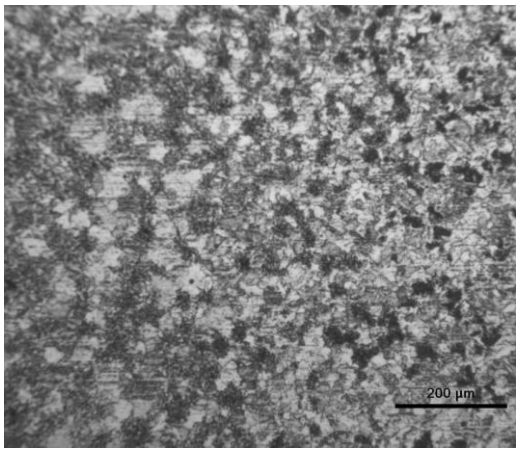
The examinations indicate that the micro-structure of the base metal zone in both specimens is ferrite-perlite (with a small amount of perlite) and does not vary substantially. In both specimens there perlite clusters are observed within the transition zone between the base metal and heat affected zone. The microstructure in the heat affected zone consists of ferrite with beynitic sectors. The microstructure in the heat affected zone of both specimens is beynitic; however in specimen No 1 it is rough beynitic with precipitations of Widmanstatten ferrite, and in specimen No 2 it is fine ferritic.



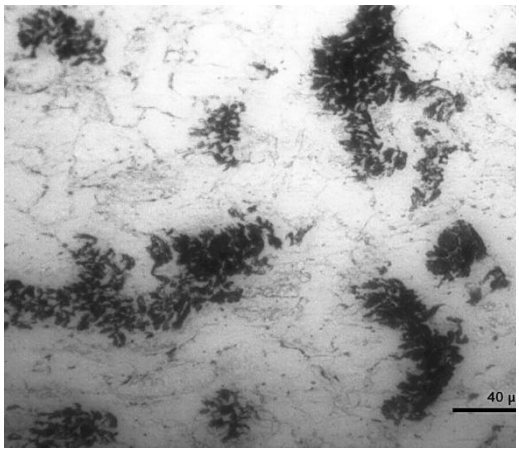
Base metal



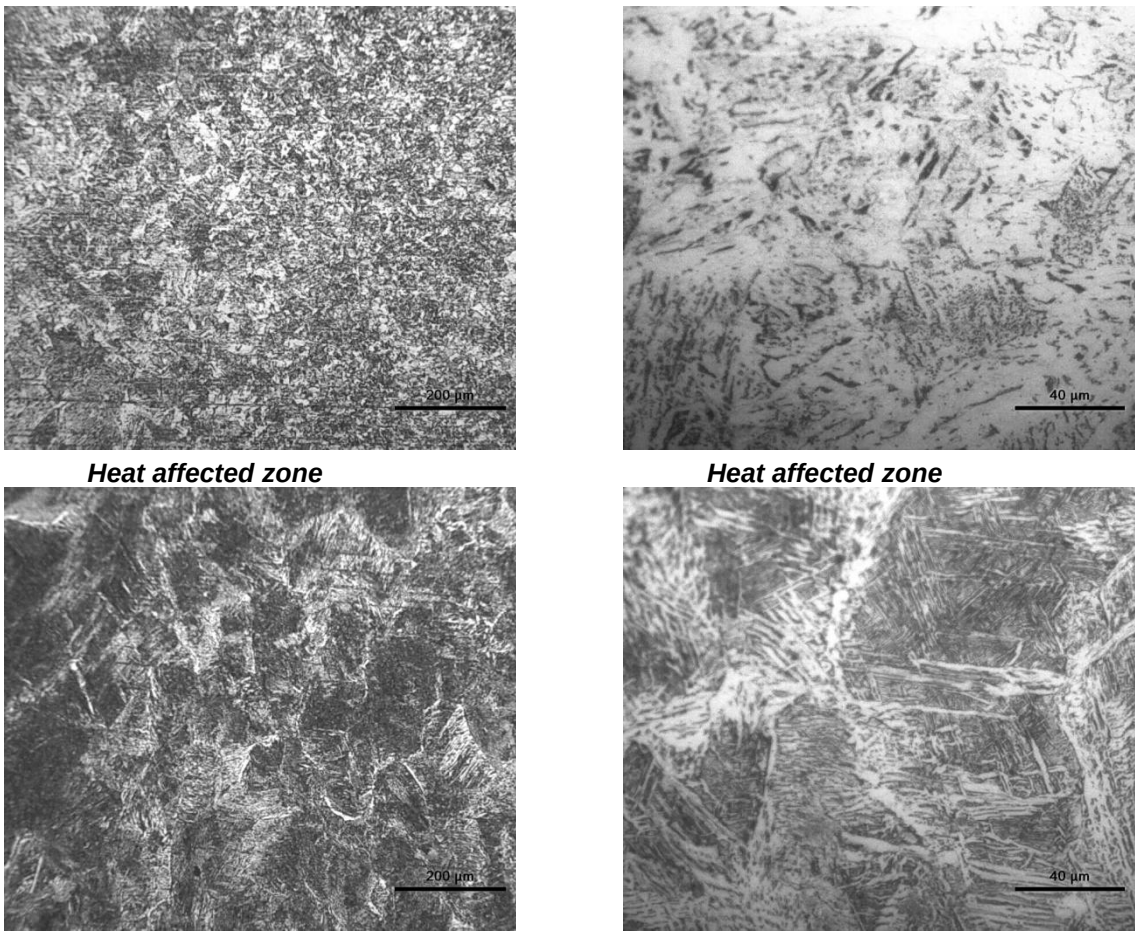
Base metal



Heat affected zone – base metal



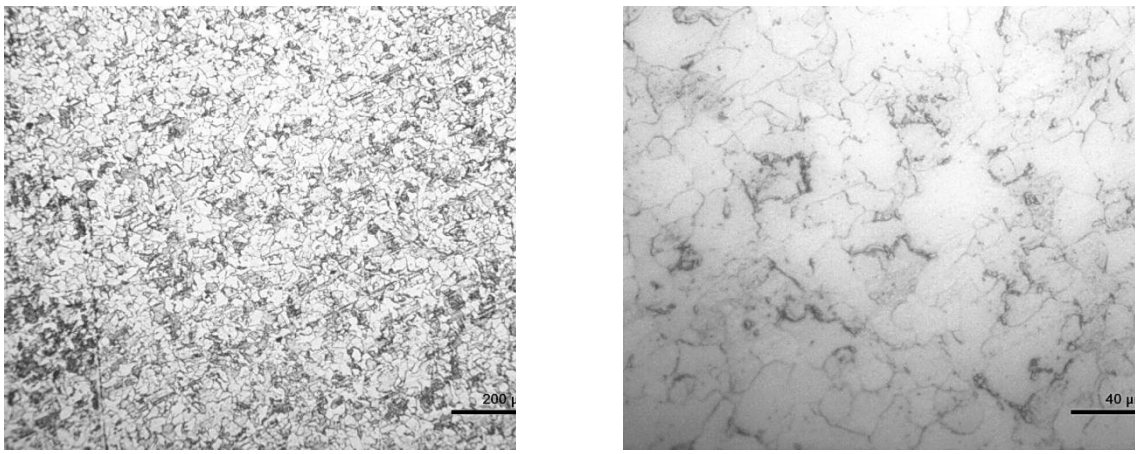
Heat affected zone – base metal



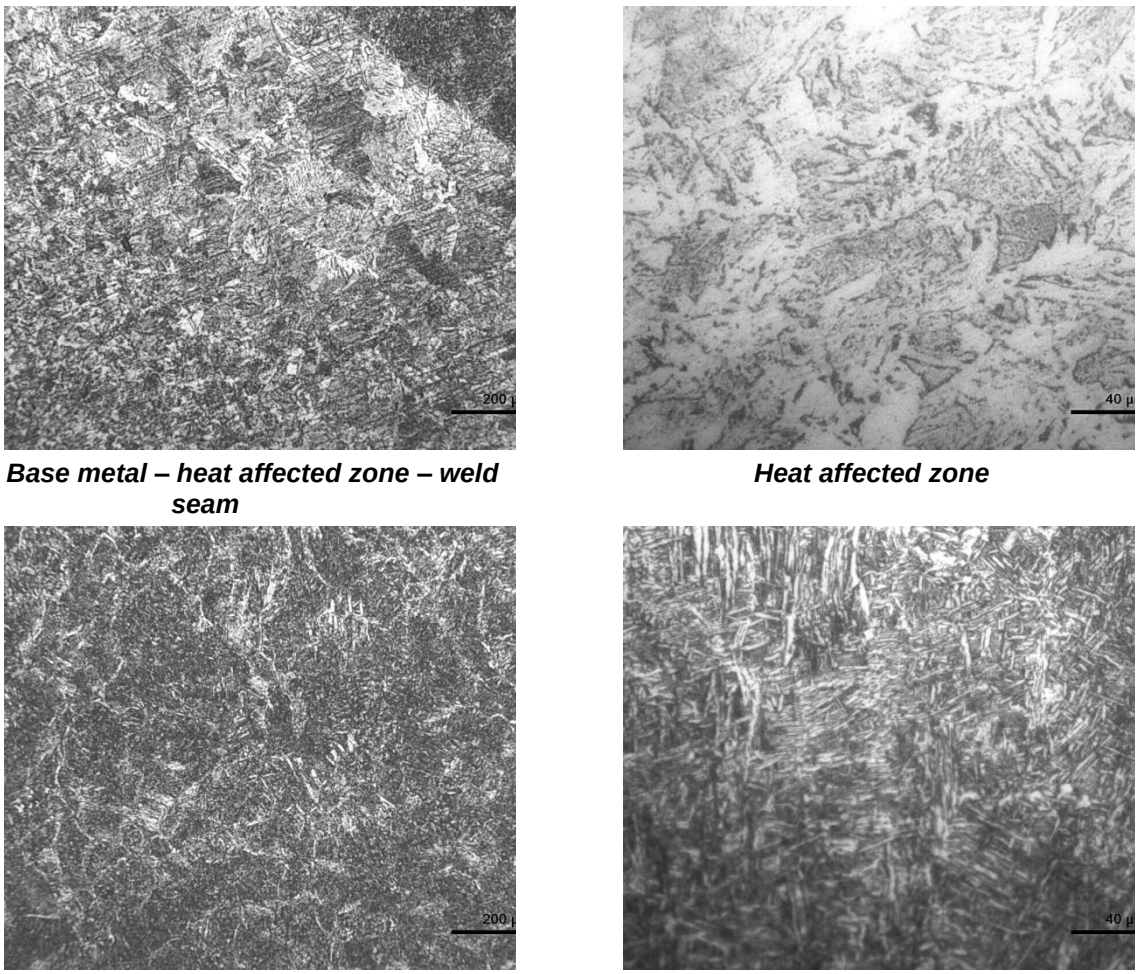
Heat affected zone ***Heat affected zone***

Weld seam ***Weld seam***

Fig. 3. Micro structure of Specimen No 1 without nano-modifier. Zones of the surfaced joint in two magnifications.



Base metal ***Base metal***



Base metal – heat affected zone – weld seam

Heat affected zone

Weld seam

Weld seam

Fig. 4. Micro-structure of Specimen No 2 with nano-modifier. Zones of the surfaced joint in two magnifications.

Measurement of Vickers micro hardness

The micro hardness is measured using micro hardness measuring device MicroDuromat 4000 according to Vickers' method with loading 50 g and duration 10s.

The measurements of the micro hardness in the weld zone from the surface to the inside indicate that in specimen No 1 without nano modifier (Fig. 5) there the hardness is almost unchanged with value around 276 kg/mm2; and in Specimen No 2 with nano modifier (Fig. 6) it decreases from the surface to the inside from 368 kg/mm2 to 295 kg/mm2, as the average value in the core is 295 kg/mm2. The average value of the core is achieved at depth about 450 from the surface.

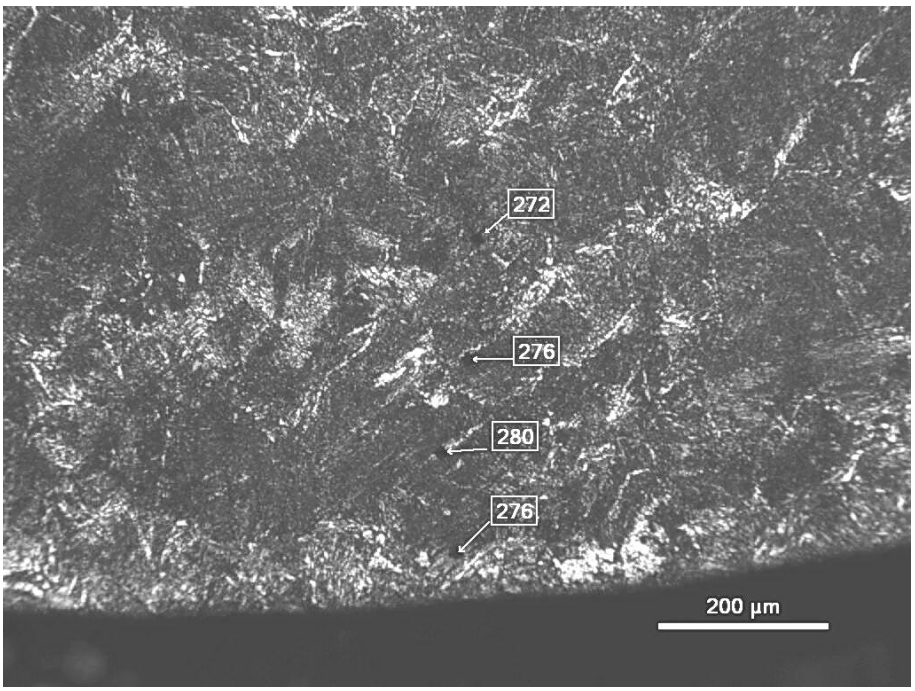


Fig. 5. Specimen No 1. Recesses from micro hardness measurements.

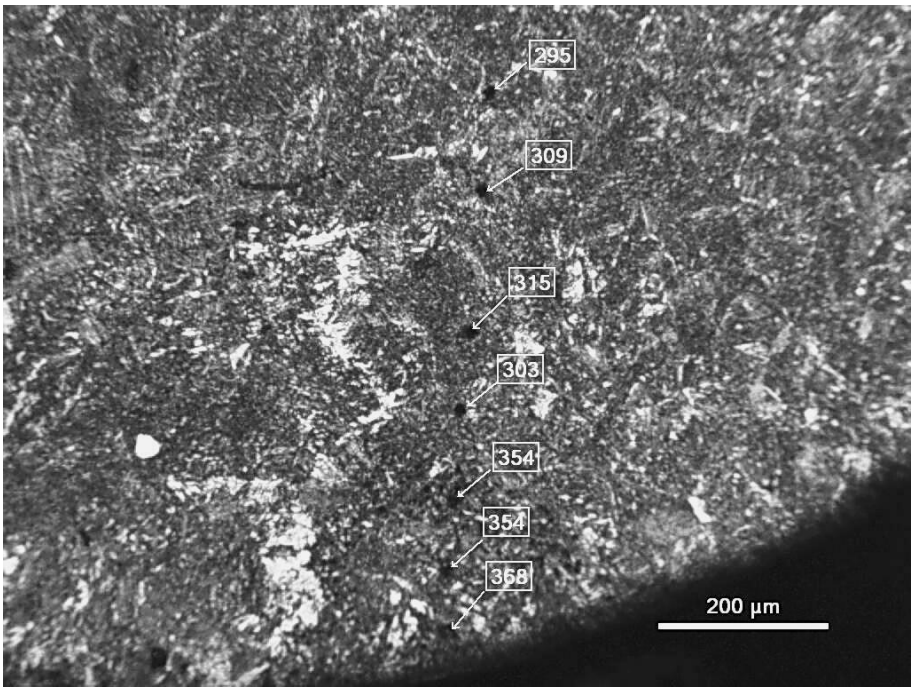


Fig. 6. Specimen No 2. Recesses from micro hardness measurements.

Conclusions

The introduction of nano modifier TiN + Cr through coated additional wire in the process of TIG overlay welding of specimens with thickness 4 [mm] of low carbon steel S235JR results in:

- Grain refinement of the structure in the weld zone; and

- Increasing the microhardness of the surface layer of the weld seam with 23%.

The examination indicates that the zone of influence of nano particles is about 400-450μm extending from the surface to the core of the overlaid specimens. The micro structure in the rest zones remains unchanged.

References

1. Черепанов А.Н. и др. „О применении нанопорошков тугоплавких соединений при сварке и обработке металлов и сплавов", Тяжелое машиностроение. №4/2. 2008. С. 25-26
2. Трошков А.С. „Модифицирование структуры наплавленного металла нанодисперсными карбидами вольфрама", Ползуновский альманах №2 2009
3. Дроздов, В. О., А. Г. Маликов и др. Зкспериментално исследование лазерной сварки металлов с применением нанопорошковых добавок. Докл. V Всеросийской конференций „Взаимодействивие высококонцентрированных потоков знергии с материалами в перспективных технологиях и медицине". Новосибисирск, 26-29 марта, 2013, с. 97-101.
4. Лазарова, Р., П.Кузманов и др. Исследование свойств стали 110ГЛ13 и чугуна СЧ25, модифицированных нанопорошковыми иникуляторами. Доклады IV Всеросийской конференции,22-25 марта, 2011, Новосибирск, Россия.
5. Кузманов, П., В.Манолов и др. Износоустойчивост на модифицирани с наномодификатори чугун GG 25 и стомана GX120MN12. Tribological Journal BULTRIB, Papers of Conference BULTRIB'11, Oct. 28, 2011, Sofia.
6. Низкотемпературная плазма. Том 12. Плазмохимический синтез ультрадисперсных порошков и их применение для модифицирования металлов и сплавов (отв. ред. В. М. Фомин, А. Н. Черепанов). Новосибирск, Наука, Сибирская издательская фирма РАН, 1995, с. 339.
7. Karaguiozova Zdravka, Manolov Valentin and Tarasov Michael, Elektroless iron coating on nanosized particles, BULTRIB'11 - 8th National Conference on Tribology with International Participation, Sofia, 28.10.2011, изнесен доклад и публикация в Tribological Journal BULTRIB Vol. 2, 2012, pp. 73-79
8. Tashev P., T. Petrov, Y. Lukarski, G. Stefanov, „Technologies for introduction of nano-sized particles in the weld seam during processes of overlay welding", Engineer Sciences, year L, 2013, № 3, journal of Department Engineer Sciences to BAS, pp. 82-93.

CORRESPONDENCE
Assoc. Prof. Dr. PLAMEN TASHEV
IMSETCH "Acad. A. Balevski" - BAS,67q Shipchenski prohod str., 1574 Sofia, BULGARIA
e-mail: weld@abv.bg

Assoc. Prof. Dr. RUMYANA LAZAROVA
IMSETCH "Acad. A. Balevski" - BAS,67q Shipchenski prohod str., 1574 Sofia, BULGARIA
e-mail: r.lazarova@ims.bas.bg